OCTOBER 1987
ENVIRONMENTAL SCIENCE & TECHNOLOGY

ES&T

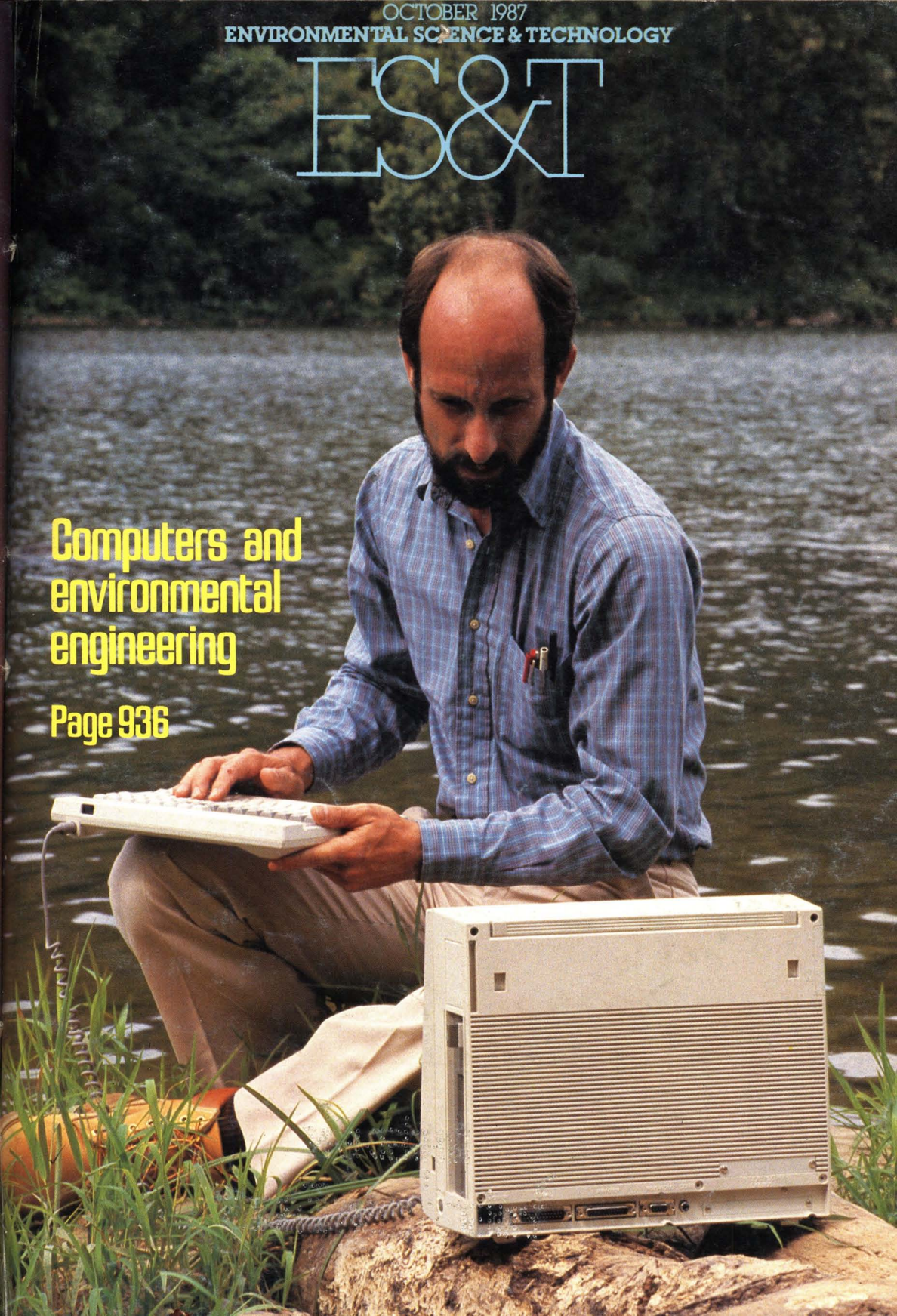

Computers and environmental engineering

Page 936

HP offers you more ways to do organic analysis than the EPA has methods.

And your analytical options keep growing.

For example, we've just added an infrared detector, an FPD, 601/602 water analyzer, and MS software specifically tailored to the newest EPA-reporting requirements. These further expand what is already one of the broadest selections of analytical instruments and automation systems available for organic analysis. They reflect, too, HP's continuing commitment to provide the application solutions you need for your organic environmental analysis methods—and the EPA's.

Our support of your environmental laboratory needs includes a full range of automated systems for data analysis, management and EPA-approved reporting. Whether you need general or application specific instrumentation, GC/MS, GC/FTIR, or LC, HP has a data system to fit.

Breadth of line also means HP can give you the bonus of one-source support. You know the value of that if you've ever had to track down and coordinate multiple vendor support teams! Contrast those complexities and frustrations with the comprehensive across-the-board response that a single phone call to HP can provide.

Plus, there's HP's time-proven quality and reliability. It's reflected in tens of thousands of HP analytical instruments that are working day-in, day-out around the world. You also see it in the 99% uptime guarantee available for our industry standard HP 5890A GC.

Quality, breadth of line and support are all a result of our "What If..." approach that sets your needs, always, as our starting point. See for yourself. Call the HP office listed in your telephone directory white pages and ask for an analytical products representative. Or write to Hewlett-Packard Analytical Group, 1820 Embarcadero Rd., Palo Alto, CA 94303.

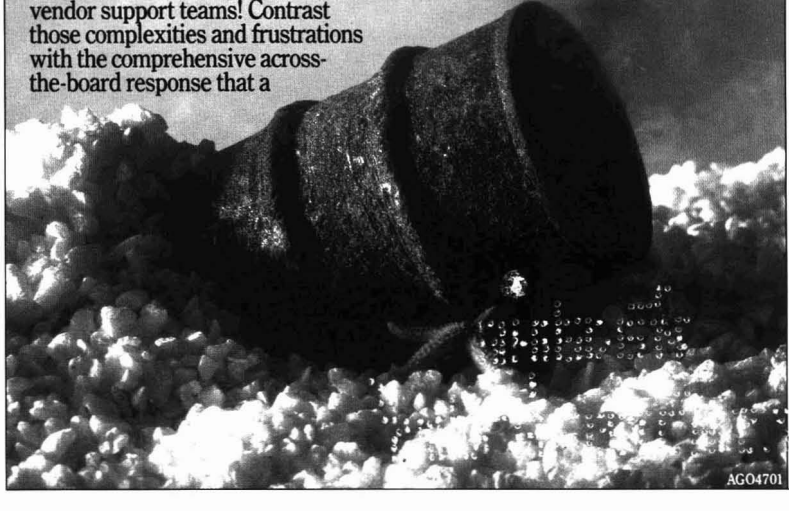

AGO4701

HEWLETT PACKARD

Environmental Science & Technology

Please send *research* manuscripts to Manuscript Reviewing, *feature* manuscripts to Managing Editor. For editorial policy, author's guide, and peer review policy, see the January 1987 issue, page 27, or write Monica Creamer, Manuscript Reviewing Office, *ES&T.* A sample copyright transfer form, which may be copied, appears on the inside back cover of the January 1987 issue.

Environmental Science & Technology, ES&T (ISSN 0013-936X), is published monthly by the American Chemical Society at 1155 16th Street, N.W., Washington, D.C. 20036. Second-class postage paid at Washington, D.C., and at additional mailing offices. POSTMASTER: Send address changes to *Environmental Science & Technology,* Membership & Subscription Services, P.O. Box 3337, Columbus, Ohio 43210.

SUBSCRIPTION PRICES 1987: Members, $30 per year; nonmembers (for personal use), $45 per year; institutions, $176 per year. Foreign postage, $8 additional for Canada and Mexico, $16 additional for Europe including air service, and $24 additional for all other countries including air service. Single issues, $15 for current year; $19 for prior years. Back volumes, $219 each. For foreign rates add $2 for single issues and $10 for back volumes. Rates above do not apply to nonmember subscribers in Japan, who must enter subscription orders with Maruzen Company Ltd., 3-10 Nihon bashi 2 chome, Chuo-ku, Tokyo 103, Japan. Tel: (03) 272-7211.

SUBSCRIPTION SERVICE: Orders for new subscriptions, single issues, back volumes, and microform editions should be sent with payment to Office of the Treasurer, Financial Operations, ACS, 1155 16th St., N.W., Washington, D.C. 20036. Phone orders may be placed, using Visa, Master Card, or American Express, by calling the ACS Sales Office toll free (800) ACS-5558 from anywhere in the continental U.S. (In the Washington, D.C., area call 872-4600.) Changes of address, subscription renewals, claims for missing issues, and inquiries concerning records and accounts should be directed to Manager, Membership and Subscription Services, ACS, P.O. Box 3337, Columbus, Ohio 43210. Changes of address should allow six weeks and be accompanied by old and new addresses and a recent mailing label. Claims for missing issues will not be allowed if loss was due to insufficient notice of change of address, if claim is dated more than 90 days after the issue date for North American subscribers or more than one year for foreign subscribers, or if the reason given is "missing from files."

ES&T CONTENTS

Volume 21, Number 10, October 1987

FEATURES

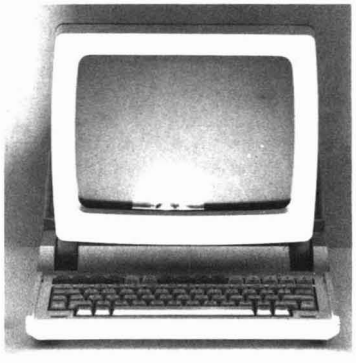

REGULATORY FOCUS

VIEWS

DEPARTMENTS

UPCOMING

Cancer risk series, Part III—cancer dose–response extrapolations

Simulation and design models for adsorption processes

RESEARCH

ESTHAG 21(10)929–1024 (1987)
ISSN 0013 936X

Cover: Amy J. Hayes
Credits: p. 936, Julian Josephson

964
Polychlorinated dibenzofurans and dibenzo-*p*-dioxins and other chlorinated contaminants in cow milk from various locations in Switzerland. Christoffer Rappe,* Martin Nygren, Gunilla Lindström, Hans Rudolf Buser, Otto Blaser, and Claude Wüthrich

This study focuses on the occurrence and distribution of chlorinated dioxins and dibenzofurans in cow milk.

971
Isomer-specific determination of polychlorinated dibenzo-*p*-dioxins and dibenzofurans in incinerator-related environmental samples. Akio Yasuhara,* Hiroyasu Ito, and Masatoshi Morita

PCDDs and PCDFs in water, soil, sediment, incinerator ash, and fly ash are determined by high-resolution gas chromatography–low-resolution mass spectrometry.

979
Reductive dissolution of manganese(III/IV) oxides by substituted phenols. Alan T. Stone

Effects of pH, ring substituents, phenol concentration, and oxide composition on rates of reaction between manganese oxides and substituted phenols are examined.

988
Comparison of terrestrial and hypolimnetic generation of acid neutralizing capacity for an acidic Adirondack lake. Gary C. Schafran* and Charles T. Driscoll

In the Adirondack region of New York, terrestrial sources of acid neutralizing capacity appear to be more significant in neutralizing acidic deposition than processes occurring within lakes.

994
Estimation of effect of environmental tobacco smoke on air quality within passenger cabins of commercial aircraft. Guy B. Oldaker III* and Fred C. Conrad, Jr.

Vapor-phase nicotine is sampled in aircraft passenger cabins to measure environmental tobacco smoke (ETS) levels and to determine if smoker segregation reduces exposure to ETS.

999
Oligomerization of 4-chloroaniline by oxidoreductases. Kathleen E. Simmons, Robert D. Minard, and Jean-Marc Bollag*

HPLC is used to monitor substrate and products following enzymatic oxidation of 4-chloroaniline. Based on the results, mechanisms for formation of oligomers are proposed.

1003
Mixed-substrate utilization by acclimated activated sludge in batch and continuous-flow stirred tank reactors. Sarvottam D. Deshpande, Tapan Chakrabarti,* and P. V. R. Subrahmanyam

The degradation of substituted benzenes in a multisubstrate environment is studied in batch and continuous-flow stirred tank reactors.

1009
Prediction of algal bioaccumulation and uptake rate of nine organic compounds by 10 physicochemical properties. Hélène Mailhot

Quantitative structure–activity relationships are studied to predict the time course of uptake for different organic compounds.

■ 1014
Kinetics and products of the gas-phase reactions of OH radicals and N_2O_5 with naphthalene and biphenyl. Roger Atkinson,* Janet Arey, Barbara Zielinska, and Sara M. Aschmann

The nitroarene products and yields are consistent with ambient air measurements and suggest that many, if not most, of the nitroarenes observed in ambient air are formed from their parent PAH via atmospheric reactions.

NOTES

1022
Soil-gas measurements for detection of groundwater contamination by volatile organic compounds. Henry B. Kerfoot

The field evaluation of a soil-gas measurement technique designed to locate groundwater contamination by volatile organic compounds is described.

*To whom correspondence should be addressed.

■ This article contains supplementary material in microform. See ordering instructions at end of paper.

ES&T
GUEST EDITORIAL

Environmental cancer and prevention

Although control of chemical carcinogenic hazards in the workplace was widely recognized during the post-World War II era, much of the research effort of that time was directed to the identification of cancer viruses and possible vaccines. The discovery of the causal role of cigarette smoking in lung cancer was a milestone that led to expanded research on cancer causes—including chemical carcinogens and life-style factors—as a base for prevention.

Later, Rachel Carson's *Silent Spring,* which described ecological damage caused by misuse of commercial chemicals, had a major impact on the public, who equated ecological hazards and environmental pollution with ill health, especially cancer. The politically and intellectually attractive view became widespread that human cancer could predominantly be controlled through elimination of the many potential carcinogenic chemicals in the ambient environment. Further, "cancerphobia" proved a useful adjunct to obtaining political support for the control of ecological hazards.

In retrospect, it is clear that these views resulted from a misunderstanding of the major causes of human cancer, notably cigarettes. The tobacco industry continually emphasized ambient air pollution as the cause of lung cancer. Further, when the public accepted the view that 80-90% of cancers were attributable to the environment, the term "environment" was misinterpreted as applying only to chemicals.

Chris Wilkinson's review (*ES&T,* September 1987, pp. 843–47) on the existing knowledge of the environmental causes of cancer is timely and places known and potential cancer hazards, including cultural and dietary factors, in perspective. Unfortunately, investigations of the latter are difficult because definitive control methods do not yet exist for most dietary factors. Apart from drugs, occupation, and certain point source exposures, there is no evidence that the vast majority of chemical carcinogens individually or in toto (synthetic and natural) in the ambient environment at the usual levels of human exposure have had a detectable impact on the cancer burden. Wilkinson outlines the need to distinguish between trivial and significant risks in developing effective cancer prevention policies.

In 1980 Isaac Berenblum, professor emeritus at the Weizmann Institute in Rehovoth, Israel, concluded that only a slight reduction of the cancer burden was possible through the traditional eliminatory approach, apart from recognized public health procedures. He anticipated future efforts on preventative research that would focus on developing methods for active intervention to carcinogenic mechanisms through chemoprevention and chemotherapy. According to Berenblum, such preventative research represents the logical outcome of current basic research.

Nonetheless, this view has received little attention in the regulatory circles that confuse stringent chemical controls, irrespective of effectiveness, with cancer prevention. The misdirection of preventative efforts may not only distort public health strategies and research efforts, but also divert national resources from more useful social goals. Prudent control of carcinogens should be based on scientific data, judgment, and common sense—not political and regulatory conveniences.

John Higginson *is senior fellow at the Institute for Health Policy Analysis at the Georgetown University Medical Center and professor in the Departments of Community Medicine and Pathology. He is also a research professor in pathology and epidemiology at the University of North Carolina. He was founding director of the International Agency on Cancer Research in Lyon, France (1966–81).*

0013-936X/87/0921-0932$01.50/0

INTERNATIONAL

The Inter-American Development Bank announced Aug. 5 that, unless Brazil complies with the environmental protection provisions of a $58.5 million loan for a road-building project, disbursement of the money will be stopped. These provisions encompass the protection of tropical forests and the demarcation of land for indigenous Indian tribes. Nevertheless, Sens. Daniel Inouye (D-Hawaii) and Bob Kasten (R-Wis.) said that the bank acted "only after we threatened to cut off all U.S. aid to the bank." If Brazil does not assure compliance with the environmental protection provisions, funding for the project will end Oct. 4.

FEDERAL

EPA administrator Lee Thomas has criticized the Clean Air Act reauthorization bill, under consideration by the Senate, as too costly. He told a Senate committee that the bill (S. 1351), if enacted, could cost as much as $30 billion/yr, would impose controls in areas that do not need them, and would diminish the role of states in controlling air pollution. Thomas especially criticized controls on acid deposition that S. 1351 would mandate, stating that these requirements have no firm scientific basis. The bill would require electric utilities to reduce sulfur dioxide emissions to 0.9 lb/10^6 Btu and would tighten restrictions on toxic emissions to the air, as well as standards for air quality. The bill also would extend the deadline for certain areas to meet air quality standards if certain actions set forth in the bill are undertaken.

Sens. John Rockefeller (D-W. Va.), John Danforth (R-Mo.), and Pete Wilson (R-Calif.) want to see more methanol-powered cars. They have introduced legislation that would give American car makers incentives to manufacture cars powered by methanol and other alternative fuels. Car makers would get additional credits if they met fuel efficiency standards,

Rockefeller: Wants methanol cars

effective with 1993 models, for vehicles using alcohol fuels or natural gas. These fuels, especially methanol, are considered desirable because they produce lower emissions of nitrogen oxides and hydrocarbons, both of which are ozone precursors. Moreover, the use of these fuels can lower the demand for imported petroleum. Rockefeller predicted that Japanese car makers will become interested in selling alternate fuel vehicles, particularly in the California market.

EPA has proposed rules requiring new cars to be equipped with canisters to recover vapors when the cars are refueled. These regulations are expected to reduce emissions of hydrocarbon ozone precursors by 10%, EPA administrator Lee Thomas said at a press conference July 22. The replacement of old cars with new ones would result in a further reduction of 20% in precursor emissions, he estimated. A 30% total reduction in precursor emissions would bring into compliance about 35 of the 70 cities that do not now meet ozone standards, Thomas said. In most parts of the United States, the vapor pressure of gasoline escaping from cars being refueled would have to be reduced from the current recommended level of 11.5 lb/in.^{2} to 10.5 lb/in.^{2} in 1989 and 9 lb/in.^{2} in 1992. In the Southwest, the 1989 and 1992 levels would have to be 8.2 lb/in.^{2} and 7 lb/in.^{2}, respectively.

The U.S. Court of Appeals for the District of Columbia Circuit has ruled that materials reused in manufacturing processes are not subject to regulation by EPA under the Resource Conservation and Recovery Act (RCRA). The July 31 decision overturns regulations EPA promulgated in January 1985. The court found that Congress did not intend that EPA regulate "spent" materials that are recycled and reused in an ongoing manufacturing or industrial process. The judges explained that the solid waste that EPA has the authority to regulate under RCRA is defined as discarded material. The suit challenging EPA's 1985 regulation was brought by the American Mining Congress and several other plaintiffs.

EPA released results Aug. 4 of the largest indoor radon survey it has conducted to date. Results of the 10-state survey, carried out during the winter of 1986–87, show that radon levels exceeded EPA's guideline of 4 pCi/L of air in 21% of the 11,600 homes tested. The 10 states surveyed were Alabama, Colorado, Connecticut, Kansas, Kentucky, Michigan, Rhode Island, Tennessee, Wisconsin, and Wyoming. More than 25% of the homes tested in Colorado, Wisconsin, and Wyoming had radon levels above 4 pCi/L, with a maximum level of 84 pCi/L found in Wisconsin. Paradoxically, although only 6% of homes tested in Alabama had radon levels above 4 pCi/L, the highest concentration—180 pCi/L—was found in northern Alabama. Local geology is one explanation proposed for high radon levels in a given area. EPA plans a six-state survey during the winter of 1987–88.

EPA has cancelled all uses of cadmium-containing pesticides on golf course fairways and home lawns and has restricted their application on golf course tees and greens. Cadmium-containing compounds, which have been registered since the late 1940s as fungicides, are suspected of causing cancer and adverse kidney effects. About 13,640 kg/yr of cadmium-containing pesticides are used;

0013-936X/87/0921-0933$01.50/0

this comprises less than 0.1% of total cadmium use in the United States. Under the new EPA guidelines, these pesticides may be applied in golf tee and green areas only by certified applicators wearing protective clothing and using only power boom-spraying equipment. EPA will require additional applicator exposure data by July 1988.

STATES

The Louisiana Board of Regents has awarded Louisiana State University (LSU) $270,000 to develop a method of using electricity to clean up contaminated soil. Yalcin Acar of LSU is directing a project to investigate how electroosmosis can be used to immobilize hazardous wastes in soils in situ and possibly to remove these materials. Acar believes the technique can be used to force water into normally impermeable soils. The water would wash the wastes into specific areas where the offending materials could either be removed or be subjected to enough electricity to change the soil into a ceramic substance that immobilizes the wastes. Acar estimates that the method could cost from $3.90 to $39 per cubic meter, compared with $65 to $650 per cubic meter for excavating and hauling the soil and washing it elsewhere.

The New York State Assembly has passed a bill limiting the liability of contractors who clean up hazardous-waste sites in the state under Superfund. Contractors would be liable for damages only in cases in which "negligence, gross negligence, or reckless, wanton, or intentional misconduct" could be proved. The bill also limits joint and several liability by strictly apportioning damages related to property and to a person's injury-related noneconomic losses. Strict apportionment pertains to contractors less than 50% liable and not guilty of reckless disregard for the safety of others or of misconduct. The bill also applies to firms cleaning up petroleum spills or removing asbestos.

Virginia Gov. Gerald Baliles forecasts that aquaculture (fish farming) could become a $20 million industry in his state and plans to offer incentives to Virginia farmers interested in entering the industry. He especially wants to promote the farming of hybrid rockfish, a type of bass. Aquaculture is said to be one of the few industries that profits from measures that curb water pollution.

Baliles: Favors fish farms

Entrepreneurs who hope to promote aquaculture in portions of Puget Sound, Wash., say their industry would be the first to suffer if the water became polluted. This argument, however, has not convinced residents of islands in Puget Sound who claim that their recreational fishing areas would be harmed and that local waters would be severely polluted by wastes from salmon raised in underwater pens.

SCIENCE

Chromosome analysis can reveal stress even from low levels of radiation, according to scientists at the Gesellschaft für Strahlen- und Umweltforschung (GSF, Neuherberg, West Germany). The chromosomes used for tests are human lymphocytic chromosomes so modified in the laboratory that they are able to produce metaphase filaments (this normally cannot occur within the human body). The filaments join at a single point, in a manner resembling the letter X. If the chromosomes are exposed to even weak radiation, filaments can join at several points rather than at one central point. The more of these extra meeting points there are, the stronger the radiation to which the chromosomes have been exposed. This method now is being used at GSF to calibrate dosimeters. GSF scientists also are investigating chromosomal analysis as a means to evaluate stress from exposure to toxic chemicals.

Active communities of microorganisms exist much farther below the earth's surface than previously believed, says James Fredrickson of Battelle Northwest (Richland, Wash.). He hopes that these organisms may be used to create biological barriers that prevent the movement of subsurface contaminants and mitigate groundwater contamination. Fredrickson also believes that an understanding of the subsurface environment may allow the use of these microbes to degrade organic contaminants of groundwater and to reduce the corrosion of waste containers placed deep underground. Samples of groundwater from depths of 262 m contained microbe populations ranging from nondetectable to 107 cells/g of sediment. Previously, knowledge of microorganisms existing below 50 m has been very limited, according to Fredrickson.

Radioactive fallout from Chernobyl has been found in the Greenland icecap and can help scientists track global weather patterns, says Mark Monaghan of the University of Chicago. He and Cliff Davidson of Carnegie-Mellon University have found well-defined traces of cesium-134 and cesium-137 at depths of 10–20 cm below the icecap's surface. Monaghan observes that the cesium layer pinpoints events of the spring of 1986 and will enable scientists to compute the accumulation of snowfall for the next 80 years very accurately. He adds that the amount of Chernobyl fallout in the icecap is insignificant in terms of public health and can be detected only with the most sensitive equipment.

TECHNOLOGY

Emissions of dioxins and furans from garbage-burning incinerators can be minimized by good combustion practices, according to the American Society of Mechanical Engineers (ASME). One step is to maintain incinerator temperatures above 815 °C; emissions of dioxins and furans have been found to increase when temperatures fall below this level. Another step is to monitor carbon monoxide (CO) and keep its levels below 100 ppm, because dioxin and furan emissions are found to increase when CO levels exceed 100 ppm. It also has been found that if proper combustion practices are carried out, the amount of polyvinyl chloride and moisture in refuse does not increase the emission of dioxins and furans. Research that led to recommending these practices was sponsored by ASME, the New York State Energy Authority, and other cosponsors.

A slagging coal combustor developed by TRW (Redondo Beach, Calif.) has completed 4000 hours of commercial operation with combustor availability of at least 99% and carbon conversion of more than 99.5%. The combustor's output is

40 million Btu/h; it burns 20,000 lb/h of coal and has produced 35,000 lb/h of steam. NO_x emissions (30% excess oxygen input) did not exceed 450 ppm and were recorded as low as 200 ppm during many operations. Reductions of NO_x to 180 ppm are considered possible with over-fire air. With Ohio No. 6 coal, which contains 1.8% sulfur, SO_2 emissions as low as 0.4–1.2 lb/10^6 Btu have been achieved, thus meeting environmental requirements, according to TRW spokesmen. They also say that tests of limestone injection in systems that simulate the combustor have achieved 70–90% SO_2 capture with a broad range of eastern and western coals. According to TRW, the combustor can replace oil- and gas-fired boilers with no power plant rating penalty.

The toxicity of chlorinated organic wastes can be eliminated by on-site scrubbing with methane, according to Sidney Benson and Maia Weissman of the University of Southern California. In the absence of air, methane is added to the wastes, which then are heated to about 1000 °C. All of the chlorine is converted to hydrogen chloride which may, in turn, be reacted with sodium hydroxide to form sodium chloride. According to Benson, the process can be carried out in small, mobile units. The volume of the sodium chloride produced would be about 1% of the volume of the original waste. Moreover, he says, the cost and risk involved in hauling the waste to a landfill or incineration site would be eliminated. Benson estimates that his method could reduce costs of toxic waste management by as much as 90%.

The emission of oxides of nitrogen (NO_x) can be reduced noncatalytically to less than 100 ppm. The process limits NO_x at municipal incineration plants and uses ammonia gas or ammonia water injection at 750–950 °C. The NO_x is converted into water and nitrogen gas, according to a spokesman for Nippon Kokan (Japan), developer of the process. Unreacted ammonia used to be a major problem for noncatalytic destruction of NO_x, but this has been eliminated through microcomputer control of the operation. The system now is in use at three refuse incineration plants in Japan and is being installed at a fourth plant. It has received the 14th Environmental Research Center Superior Award in Japan.

BUSINESS

The Halogenated Solvents Industry Alliance (HSIA, Washington, D.C.) strongly objects to an EPA recommendation that perchloroethylene (PCE) be reclassified and regulated as a probable human carcinogen. Currently PCE, which is used by 75% of the nation's dry cleaners, is listed as a possible carcinogen. HSIA president Paul Cammer told a press conference July 28 that scientific evidence does not support the proposed reclassification of PCE and that EPA's science advisory board shares his view. He acknowledged that PCE was found to induce liver tumors in mice, but he noted that results of cancer research show that the mechanism of this type of tumor induction in mice does not apply to humans. Cammer said that an epidemiological study of 615 dry cleaner workers exposed to PCE showed no evidence of an increased cancer mortality rate. He added that if PCE were reclassified, resulting occupational safety and liability costs would drive most dry cleaners out of business.

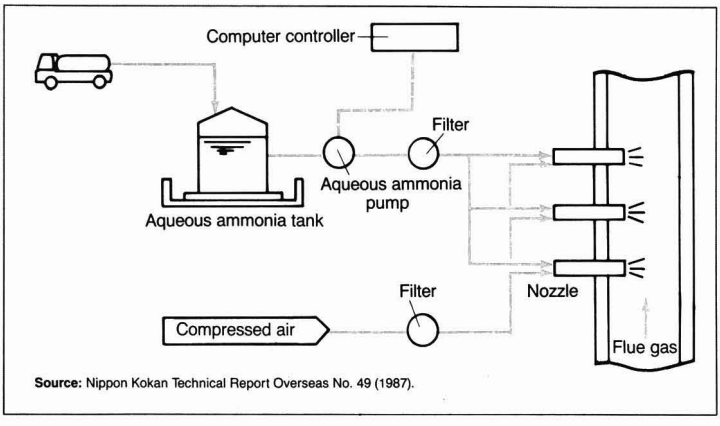

Source: Nippon Kokan Technical Report Overseas No. 49 (1987).

The American Council for an Energy-Efficient Economy (ACE^3, Washington, D.C.) recommends electricity conservation as an approach to curbing sulfur oxide emissions and acid deposition. Its report, "Acid Rain and Electricity Conservation," identifies energy efficiency improvements that can reduce electricity consumption in the Midwest by 26% (the Midwest often is cited as the major source of sulfate precursors of acid rain). The report suggests that this, in turn, would lead to reduced coal use and a direct 7–11% reduction in SO_2 emissions during the 1990s. Also, substantial cost savings would be realized because the construction of power plants could be postponed. ACE^3 suggests that the savings will offset costs of cleaning up "dirty" coal-fired power plants, thereby reducing SO_2 emissions even more.

An EPA report issued Aug. 10 lists 277 laboratories and businesses that measure indoor radon levels. Of these, 124 offer their measurement services nationally. In addition to private firms, the list includes 10 state-operated laboratories, 10 university laboratories, and EPA's two radiation laboratories. The report also describes the agency's Radon/Radon Progeny Measurement Proficiency Program by which laboratories may have their radon measuring devices evaluated by EPA. One aim of the program is to provide homeowners wishing to assess radon levels in their homes with names and locations of organizations qualified to make the necessary measurements. Those interested in the program should call 919-541-7131.

ERT (Concord, Mass.) is conducting a $13.5 million acid deposition measurement program for the Electric Power Research Institute (Palo Alto, Calif.). The five-year program calls for high-quality aerometric, meteorological, and precipitation measurements at up to 40 locations nationwide. Known as the Operational Evaluation Network, the program is being coordinated with networks operated by EPA and by Canadian federal and provincial agencies. The data base developed will serve to construct acid deposition models for the United States, Canada, and West Germany. The program, which began in July 1986 and will end in 1990, involves taking daily precipitation and air samples. Values from continuous-flow gas analyzers and meteorological instruments are averaged hourly.

ES&T FEATURE

Personal computers and environmental engineering

Part II - Applications

Raymond P. Canale
University of Michigan
Ann Arbor, Mich. 48109

Martin T. Auer
Michigan Technological University
Houghton, Mich. 49931

Dramatic advances have been made in micro or personal computer technology in recent years (*1*). Most environmental engineers now have direct access to such computers and are using them increasingly because of their low cost and ever-expanding capabilities. Personal computers also are portable and easily programmable for graphic and animated displays.

There are, however, significant questions regarding the role of personal computers for large-scale water quality management applications. For example, mathematical operations and data handling processes are slower on personal computers than on traditional mainframe computer systems. If this limitation of the personal computer is not too serious, we may be able to increase significantly our ability to communicate the results of technical analyses to decision makers. However, if the characteristics of personal computers prove too limiting, we may be unable to perform calculations efficiently.

The objective of this paper is to provide an example of the application of personal computers for water quality management in Green Bay, Wis. The capabilities of the personal computer can help decision makers determine the level of remediation necessary to meet specified water quality goals through

- development and use of complex mathematical models for water quality parameters, such as phosphorus and oxygen,
- organization and manipulation of the large amounts of field data required for model calibration and verification,
- simulation of a variety of management options aimed at cost-effective improvement of water quality, and
- effective communication of technical concepts and management recommendations to decision makers and public interest groups.

The Green Bay system

Green Bay, a large gulf on the northwest corner of Lake Michigan, has been cited as one of the major problem areas for water quality in the Great Lakes. The bay's length along its major northeast-southwest axis is 160 km, its mean width is 22 km, its mean depth is 15.8 m, and its mean hydraulic residence time is six years (*2*). The four major tributaries to the bay are the Fox, Oconto, Peshtigo, and Menominee rivers. The Fox River, which is the largest source of water and pollutants, contributes 45% of the major tributary flow and 63% of the tributary biochemical oxygen demand to Green Bay. It also discharges 78% of the total phosphorus and 87% of the suspended solids loads into the bay.

Marked longitudinal gradients in water quality and trophic state occur along the major axis of the bay in response to pollutant loadings from the Fox River. The southern end of Green Bay is hypereutrophic: It contains high levels of turbidity, chlorophyll, and phosphorus and is not saturated with dis-

0013-936X/87/0921-0936$01.50/0

solved oxygen, despite its shallow depth. Water quality improves with distance from the mouth of the Fox River, approaching an oligotrophic state approximately 100 km to the north, near the bay's junction with Lake Michigan.

Historically, industrial (pulp and paper), municipal, and agricultural discharges of oxygen-demanding substances and nutrients that stimulate algal growth have contributed to severe depletion of dissolved oxygen during the summer in the lower Fox River and southern Green Bay. In winter, oxygen depletion has occurred under the ice to a distance of 25 km along the east shore of the bay (*3*). Reductions in point source loads of oxygen-demanding substances during the past decade have led to some improvement in water quality in the Fox River and southern Green Bay (*4*).

Nevertheless, significant residual water quality problems remain. These problems are related to point and nonpoint sources of phosphorus and sediment as well as internal production of oxygen-demanding materials. Green Bay waters exhibit poor transparency because of excessive levels of phytoplankton and abiotic particulate matter. Severe hypolimnetic oxygen depletion has been observed at eutrophic and mesotrophic mid-bay sites far from discharges of organic material, apparently in response to nutrient enrichment (manmade eutrophication). Remediation efforts are hindered by both the severity and the complexity of the problem.

In this article, we will describe a mathematical model designed to clarify cause–effect relationships between pollutant loads and environmental conditions in Green Bay. The model is used to simulate the impact of remedial actions on water quality.

Purpose of the computer program

The computer program was designed to:
- orient the user and communicate the overall features of the study site and approach;
- provide the capability to store and retrieve large amounts of information, including field data, model coefficients, and forcing functions;
- compute interactively pollutant concentrations on both a steady-state and dynamic basis in all parts of the bay; and
- provide an interactive management analysis tool for decision makers to permit convenient evaluation of alternative pollution abatement plans.

Definitions of symbols in Equation 1

A_i = area of the interface between i and the adjacent cell j
C_i = the oxygen concentration in cell i
C_j = the oxygen concentration in adjacent cell j
C_s = the saturation oxygen concentration
E_i = the coefficient for dispersion across the boundary of cell i
K_i = the atmospheric oxygen exchange coefficient for cell i
L_i = the distance between the centers of cells i and j
P_i = photosynthetic production of oxygen in cell i
Q_i = the flow leaving cell i
Q_j = the flow entering from cell j
R_i = water column respiration in cell i
S_i = sediment respiration in cell i
t = time
V_i = the volume of cell i
W_i = the tributary oxygen loading to cell i

TABLE 1
Source and sink terms for the water quality mass balance model

Variable	Source	Sinks
Chloride	Tributary loads	None (conservative)
Total phosphorus	Tributary loads	Settling
	Atmospheric loads	
	Sediment release	
Total organic carbon	Tributary loads	Settling
	Primary production	Water column respiration
Dissolved oxygen	Atmospheric exchange	Atmospheric exchange
	Photosynthesis	Water column respiration
		Sediment respiration

The mass balance model

Water quality conditions in Green Bay are simulated using a mass balance model. The bay is divided into 19 control volumes or model cells (12 surface cells—one for each surface cell that exhibits thermal stratification—and 7 bottom cells). A mass balance computation is performed on each model cell for all the variables of interest, such as chloride, total phosphorus, total organic carbon, and dissolved oxygen. The mass balance includes exchange among adjacent model cells (horizontal and vertical mass transport) and all sources and sinks of material (Table 1). The last three variables in Table 1, phosphorus, organic carbon, and oxygen, are closely related. The phosphorus concentration controls algal activity and the internal production of organic carbon. The breakdown of organic carbon in the water column and in sediment has an impact on the dissolved oxygen mass balance.

The general form of the mass balance equation for oxygen in each model cell is given in Equation 1:

$$V_i \frac{dC_i}{dt} = \sum_j \left[\frac{E_i A_i}{L_i} (C_j - C_i) + Q_j C_j \right] + W_i - Q_i C_i + K_i(C_s - C_i) + P_i - S_i - R_i$$

The terms that appear in Equation 1 are defined in the box. Similar equations are developed for all of the other dependent variables, such as chloride, total phosphorus, and total organic carbon. Variable-specific source and sink characteristics of these materials are accounted for in the equations. The equations are solved either as a function of time or at steady state ($dC_i/dt = 0$).

The geometry of each cell (A, L, V) was calculated using data for the shape and depth of the water body obtained from National Ocean Survey charts. Sources, sinks, and mass transport characteristics were quantified through an extensive program of field-monitoring and laboratory experimentation. Tributary loads (W) were calculated from river water chemistry data and U.S. Geological Survey (USGS) flow records. Algal production of oxygen and organic carbon was calculated by relating photosynthesis (P) to light, temperature, and phosphorus concentration (*5, 6*).

Water column respiration (R) was found to be a linear function of the total organic carbon concentration. Sedi-

ment respiration (S) was calculated from surficial sediment characteristics and laboratory measurements of sediment oxygen demand (*7*). Re-aeration was calculated as the product of the atmospheric exchange coefficient (K) and the surface water oxygen deficit (*8, 9*). Net horizontal advective mass transport (Q) was calculated as throughput using tributary flow data (USGS). Dispersive mass transport (E) was estimated from chloride profiles (horizontally) and from temperature profiles (vertically) (*10*). Data for overall model development were collected weekly at 34 bay and tributary stations from May to September 1982.

The model of the Green Bay system has several components and includes complex nonlinear interactions and processes. The overall model contains 114 differential equations with time-variable forcing functions. These equations must be solved numerically. The field data set for model calibration contains approximately 8000 individual items of information. We need to be able to manipulate these data easily and quickly. Finally, we would like to perform simulations rapidly and interactively to encourage application of the model for decision making. Computer software that meets all of these needs has been developed for this study and is described below.

Applying the models

The complexity of the water quality problems and the management issues facing decision makers in Green Bay must be addressed through the development and application of mathematical models. The models described here are based on an extensive field-monitoring program and analyses of the key physical and biochemical processes that influence water quality. The potential of the personal computer for communicating results and facilitating the decision making process was examined using a comprehensive computer program written for the IBM PC in the BASIC language.

The program is menu-driven to facilitate use and provide flexibility of operation. The main menu for the model software is shown in Screen 1. This, along with other color figures in this paper, are photographic images of the actual computer screen.

The main menu allows the user to select any of 10 options, ranging from an orientation and outline of the study approach to management applications. Thus all of the components of a comprehensive water quality management tool are at the fingertips of the user in a single personal computer program.

System familiarization. The first five options from the main menu

SCREEN 1
Main menu for Green Bay ecosystem model software

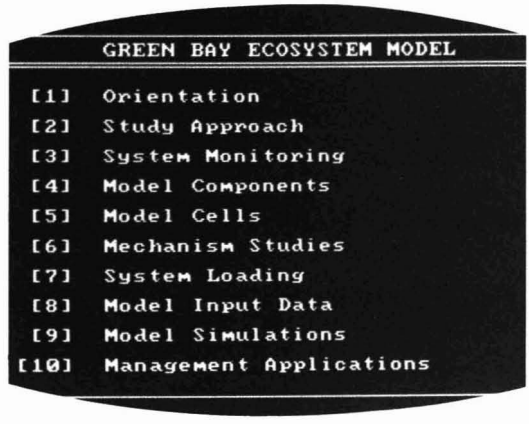

SCREEN 2
Listing of some water quality problems and site location for Green Bay and Lake Michigan

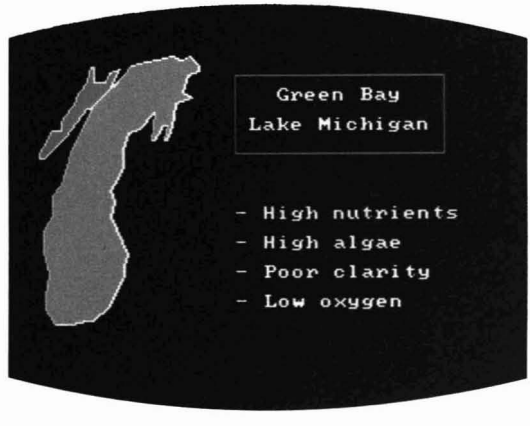

SCREEN 3
Key components and processes in the model[a]

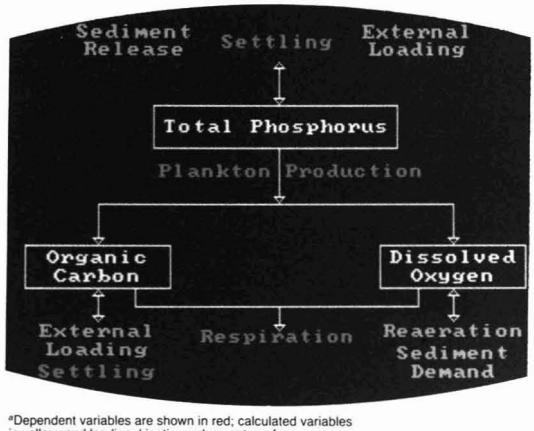

[a]Dependent variables are shown in red; calculated variables in yellow; and loading, kinetic, and mass-transfer processes in green.

(Screen 1) are concerned with system familiarization. They provide the user with an idea of the general nature of water quality problems in Green Bay, the structure and components of the model, and the location of monitoring stations. Screen 2 shows a computer-drawn map of Lake Michigan and Green Bay and a list of some important water quality problems. Color graphics enhance communication and increase the interest of users. This is one of the chief advantages of using personal rather than mainframe computers.

Option 4 from the main menu (Screen 1) gives a submenu that allows the user to view the overall interactions among the model components and examine the details of any single variable in the model. Screen 3 shows a computer-generated color graphic representation of the key components and interactions in the model. Different colors are used to distinguish between dependent variables, internally computed variables, forcing functions, kinetic processes, and mass transfer mechanisms. Dependent variables are shown in red; calculated variables in yellow; and loading, kinetic, and mass transfer processes in green.

This illustration is constructed piece by piece as the user displays each component of the model using keyboard commands. Thus the presentation of these ideas is comparable to an artist's dynamically painting a scene rather than a photographer's snapping a static picture. We believe the ability to construct such a graphic rather than simply to show a completed illustration leads to more effective communication. The personal computer and the color graphic screen provide an ideal means of using this approach.

Screen 4 shows the processes that occur in a single model cell. This figure is constructed by the computer with color graphics and uses animation to illustrate turbulent exchange among model cells. Animation is accomplished by slowly revolving the concentric circles that represent the exchange process. This simple technique helps communicate complex ideas to decision makers who may not always be familiar with the technical concepts. Screen 5 expands these ideas to show how cells in a network interact. The circles and arrows move to represent the mass transport process.

Screen 6 shows a computer graphic of the model cells superimposed on a map of the Green Bay, along with sampling stations in the bay and in its tributaries. These types of illustrations facilitate rapid and effective communication between the engineer and the decision maker.

Data management. The previous

SCREEN 4
Physical, chemical, and biological processes in each model cell[a]

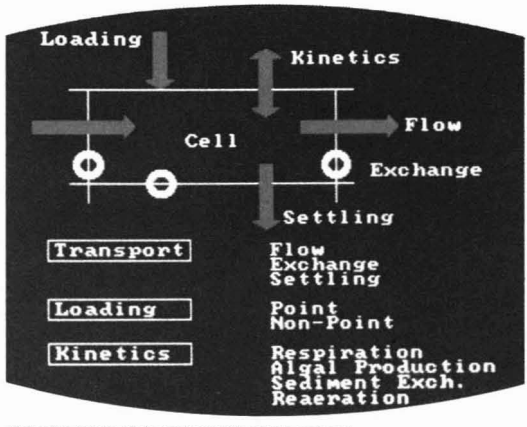

[a]Animation (moving circles and arrows) is used to represent flow and exchange processes.

SCREEN 5
A network of model cells[a]

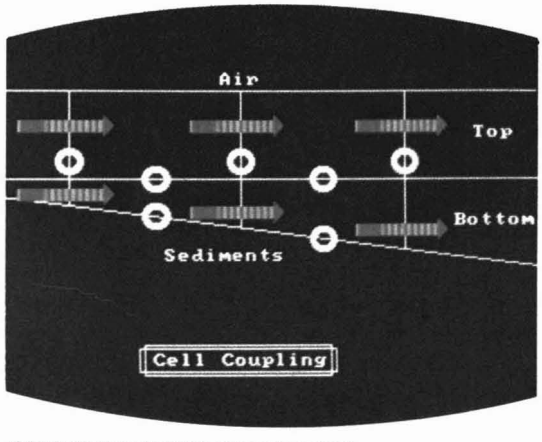

[a]Animation (moving circles and arrows) is used to represent cell transfer processes.

SCREEN 6
Map of Green Bay[a,b]

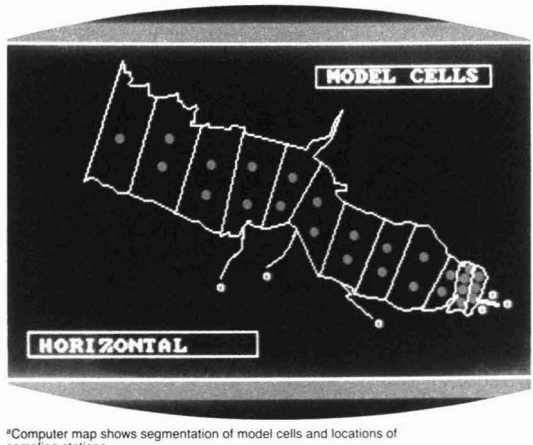

[a]Computer map shows segmentation of model cells and locations of sampling stations.
[b]Fox River is shown at far right, not to scale.

discussion explains how the personal computer can be used to organize and illustrate the components of a large-scale water quality management project. The personal computer also can be used to store, display, and retrieve data on an interactive basis. *Option 6* from the main menu (Screen 1) contains data from experiments that define the major kinetic mechanisms in the model. *Option 7* allows the user to display system-loading data in a convenient manner. As an example, Screen 7 shows a pie chart for the total phosphorus loading into the bay from the four major tributaries. It summarizes vast quantities of data regarding the magnitude of phosphorus loading from each tributary. Such illustrations are easy to develop with BASIC and color graphics commands available on many personal computers.

Option 8 from the main menu (Screen 1) presents the user with a submenu for model input data. All of the model coefficients, forcing functions, and calibration data can be interactively input, retained, and later retrieved from the computer using this submenu. The ability to handle data in an interactive manner is an important advantage of the personal computer in large-scale water quality management projects.

Model simulations. The personal computer can be used to compute the steady-state or time-variable concentration of pollutants in various sections of Green Bay. The steady-state concentrations are computed by solving a system of linear algebraic equations. In our case, 19 equations represent the concentrations of each variable in each model cell. There are six model variables for a total of 114 equations. These equations can be solved by a number of standard numerical techniques. We have found that the Gauss–Seidel iterative technique (*11*) is well suited for our equations when measured concentrations are used as initial guesses. Convergence to within 0.1% is usually obtained in 20–40 iterations and takes less than one min of execution time when compiled BASIC programs are run with a standard IBM PC.

Option 9 from the main menu (Screen 1) gives a model simulation submenu. The submenu allows the user to select the variable to be computed, steady-state or time-variable concentrations, and graphic or tabular output. Screen 8 shows a computer-generated plot of measured summer average phosphorus data (represented by the small boxes) versus concentrations calculated by the model (shown as the line).

Time-variable concentrations are computed by solving a system of differential rather than algebraic equations.

SCREEN 7

Computer-drawn pie chart showing contribution by tributaries to total phosphorus load

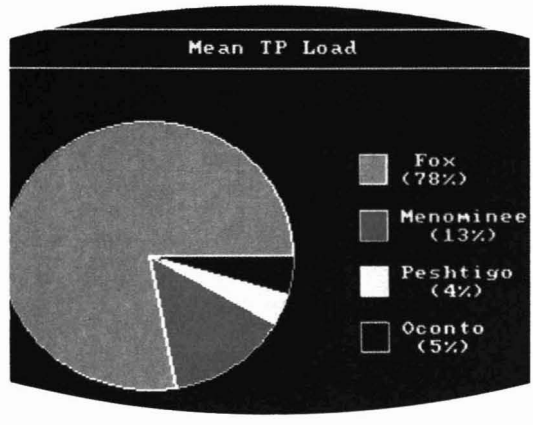

SCREEN 8

Total phosphorus concentrations[a,b,c,d]

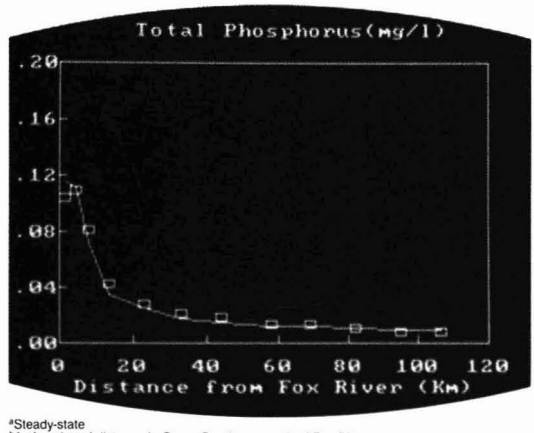

[a]Steady-state.
[b]As function of distance in Green Bay from mouth of Fox River.
[c]Small boxes represent measured summer average total of phosphorus concentration for each model cell.
[d]Line represents concentration calculated from model.

SCREEN 9

Time-variable total phosphorus concentrations[a,b]

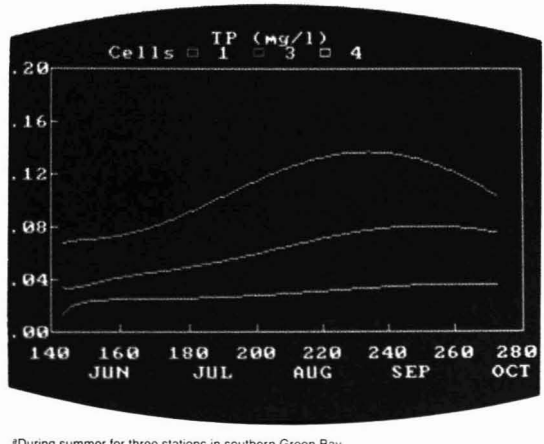

[a]During summer for three stations in southern Green Bay.
[b]Horizontal axis represents day of the year.

The equations have time-variable coefficients and forcing functions because temperature and tributary loading vary throughout the season. The differential equations can be solved using various numerical techniques. We have found that a second-order Ralston technique (*11*) is simple to program and is sufficiently accurate when using a step-size of 0.5 day.

Screen 9 shows a computer-generated plot of the seasonal variation of phosphorus for the first three model cells lakeward from the mouth of the Fox River. The vertical axis represents phosphorus concentrations in mg/L; the horizontal axis represents the day of the year. We are able to compute the seasonal variation of all model variables in about 6 min using compiled BASIC programs and a standard IBM PC. Although this is satisfactory for most applications, the computation time could be reduced considerably by using a math-processing chip, a more efficient language, or more powerful hardware. Higher order mathematical techniques then may be employed with a larger step size, but these are more difficult to program. We elected to use the most basic approach because of its simplicity and widespread availability.

Management applications. *Option 10* from the main menu (Screen 1) concerns management applications. This selection allows the user to employ the personal computer to investigate interactively various management strategies or pollution abatement alternatives. The user defines new loads for the variables of interest and then returns to the main menu (Screen 1) to recompute the resultant concentration profiles. New profiles can be compared with profiles computed under current conditions to evaluate the impact of changes in system loading. For example, using *Option 10,* the total phosphorus loading from the upper Fox River was substantially reduced, simulating a hypothetical phosphorus management program; the software allowed new concentrations to be computed and compared with old concentrations.

Screen 10 shows the comparison on a plot constructed by the personal computer. The top curve represents a profile of phosphorus concentrations before a major phosphorus management program was undertaken; the bottom curve shows this profile after the program came into being.

The model also may be used to evaluate the relative importance of individual biochemical rate processes by omitting the contribution of specific components in the mass balance equations. For example, when *Option 8* is chosen from the main menu, the impact of sediment oxygen demand on dissolved oxygen concentration can be examined by changing the appropriate coefficient values.

SCREEN 10

Profile of steady-state total phosphorus concentrations[a,b]

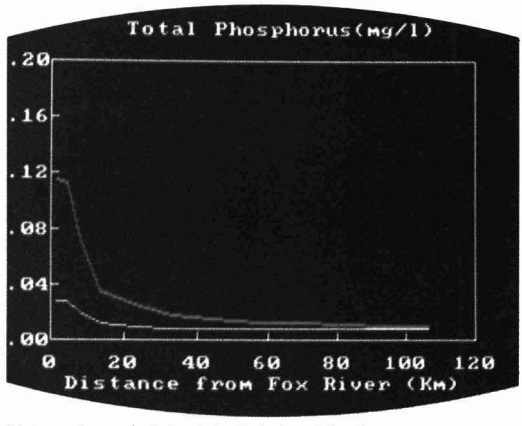

[a]Red curve shows concentrations before the implementation of a major phosphorus management program in the Fox River basin. [b]Yellow curve shows concentrations after program was implemented.

SCREEN 11

Profile of steady-state dissolved oxygen concentration[a,b]

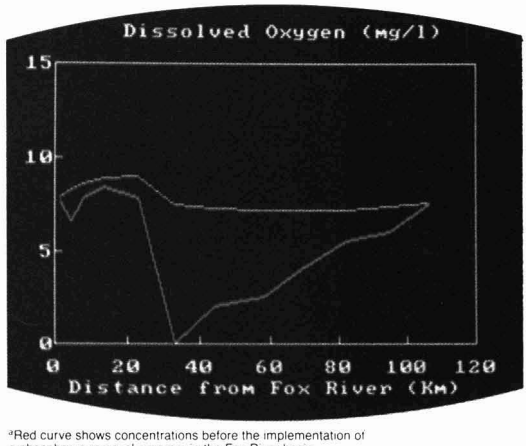

[a]Red curve shows concentrations before the implementation of a phosphorus removal program in the Fox River basin. [b]Yellow curve shows concentration after program was implemented.

Screen 11 shows the calculated increase in dissolved oxygen (top curve) following a significant reduction in Fox River total phosphorus loads and the attendant reduction of the sediment oxygen demand to zero. The bottom curve shows the oxygen concentrations prior to the improvements.

Historically, oxygen depletion problems in Green Bay have been linked to tributary loads of oxygen-demanding substances. The simulations presented here strongly suggest that internally produced organic matter and sediment oxygen demand are the primary causes of dissolved oxygen depletion in Green Bay. They indicate that remedial measures to control total phosphorus discharges and reduce eutrophication offer the greatest opportunity for significant improvements in water quality.

These computations can be performed easily with the personal computer and the program developed for this project. The personal computer facilitates the consideration of many management alternatives on an interactive basis and enables decision makers to evaluate readily the impact of various abatement strategies on water quality.

New applications

The personal computer is becoming increasingly advantageous for modeling large systems such as Green Bay. More research will be devoted to the development of natural system models that have fewer computational demands and are more accurate and reliable. Simple models may be more reliable than needlessly complex ones, because of the uncertainties introduced with an excessive number of model coeffi-

cients. Monte Carlo techniques can be used to evaluate the performance and reliability of models of different complexity (*1*).

The convenience of personal computers and the use of simple but elegant models will facilitate the consideration of more alternatives during the design and evaluation phases of large-scale modeling projects. This will encourage more creative and holistic analysis and management activities. We will be able to communicate the results of our analyses to decision makers and to the public more effectively using graphics, animation, and the portability features of personal computers.

Overall, our experience with Green Bay and the personal computer strongly suggests that water quality modeling will play a greater role in decision making and management. In the long run, we expect to see these applications expand to larger systems as computer hardware becomes more powerful and as we become more sophisticated in our approach to model design.

Acknowledgments

Field studies and model development were supported by grants from EPA's Office of Grants and Centers, Washington, D.C. (Grant No. R809521) and EPA's Environmental Research Laboratory, Duluth, Minn. (Grant No. R810076). Tad Slawecki of LimnoTech (Ann Arbor, Mich.) assisted with the graphics programming.

This article was reviewed for suitability as an ES&T feature by Bill Batchelor, Texas A&M University, College Station, Tex. 77843.

References

(1) Chapra, S. C.; Canale, R. P. *Environ. Sci. Technol.* **1987,** *21,* 832-37.
(2) Mortimer, C. H. In *Green Bay Workshop Proceedings;* Harris, H. J.; Garsow, V., Eds.; University of Wisconsin Sea Grant Publication No. WIS-SG-78-234; University of Wisconsin: Madison, 1978, pp. 10-56.
(3) Epstein, E. et al. "Lower Green Bay: An Evaluation of Existing and Historical Conditions," EPA-905/9-74-006; EPA: Chicago, 1974; p. 95.
(4) Day, H. J. et al. *Civ. Eng. (N.Y.)* **1980,** 78-81.
(5) Barth, A. K. M.S. Thesis, Michigan Technological University, May 1984.
(6) Auer, M. T.; Kieser, M. S.; Canale, R. P. *J. Canadian Fisheries and Aquatic Science* **1986,** *43*(2), 379-88.
(7) Gardiner, R. D.; Auer, M. T.; Canale, R. P. In *Environmental Engineering: Proceedings of the 1984 Specialty Conference;* Pirbazari, M.; Divinny, J. S., Eds.; American Society of Civil Engineers: New York, 1984; pp. 514-29.
(8) DiToro, D. M.; Connolly, J. P. "Mathematical Models of Water Quality in Large Lakes. Part 2. Lake Erie," EPA-600/3-80-065; EPA: Duluth, Minn., 1980; pp. 124-25.
(9) Chapra, S. C.; Reckhow, K. H. *Engineering Approaches for Lake Management, Vol. 2;* Butterworth: Woburn, Mass., 1983; p. 177.
(10) Thibodeaux, L. J. *Chemodynamics;* Wiley: New York, 1979; pp. 368-73.
(11) Chapra, S. C.; Canale, R. P. *Numerical Methods for Engineers with Personal Computer Applications;* McGraw-Hill: New York, 1985, pp. 241, 542.

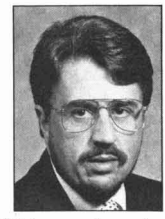

Raymond P. Canale *(l.) is a professor in the Department of Civil Engineering at the University of Michigan. He has published extensively on subjects related to mathematical modeling of water quality in natural systems. He is also the author of several books and software packages on computer applications in engineering.*

Martin T. Auer *(r.) is an associate professor of civil engineering and an adjunct associate professor of biological sciences at Michigan Technological University. He received his B.S. in zoology from the State University of New York College of Environmental Science and Forestry, his M.S. in civil engineering from Syracuse University, and his Ph.D. in water resources science from the University of Michigan. Auer has published widely on a variety of topics relating to lakes, including algal ecology, nutrient dynamics, and eutrophication.*

THE AMERICAN CHEMICAL SOCIETY ANNOUNCES A NEW JOURNAL PUBLISHED BIMONTHLY BEGINNING JANUARY/FEBRUARY 1988

CALL FOR PAPERS

Chemical Research in Toxicology

EDITED BY LAWRENCE J. MARNETT, WAYNE STATE UNIVERSITY
ASSOCIATE EDITOR, PAUL HOLLENBERG, WAYNE STATE UNIVERSITY

An all new international journal for scientists needing the most current chemical research in the highly active field of toxicology.

CHEMICAL RESEARCH IN TOXICOLOGY, the latest ACS journal, promises comprehensive reports in the field. A prestigious editorial advisory board, headed by Lawrence J. Marnett of Wayne State University, will assure expert coverage of all aspects of the molecular basis of toxicology.

Each bimonthly issue will publish full papers, rapid communications, and invited reviews on structural, mechanistic, and technological advances in research concerned with the toxicological effects of chemical agents.

SPECIFICALLY, *CHEMICAL RESEARCH IN TOXICOLOGY* WILL ADDRESS THESE IMPORTANT AREAS OF THE FIELD:

- Structure elucidation of novel toxic agents
- Chemical and physical studies on chemical agents that provide insight into their mode or mechanism of action
- Experimental and theoretical investigations of the interaction of toxic chemicals with biological macromolecules and other biological targets
- And much more!

CHEMICAL RESEARCH IN TOXICOLOGY will emphasize rigorous standards for characterization of compounds and the description of the methods used.

Toxic effects are broadly defined to include toxicity, mutagenicity, carcinogenicity, teratogenicity, neurotoxicity, immunotoxicity, and other related areas.

LOOK TO *CHEMICAL RESEARCH IN TOXICOLOGY* FOR RAPID PUBLICATION OF MANUSCRIPTS

The editors are working toward a timely turnaround from submission to publication. Contributors and subscribers will be at the forefront of developments in the field or toxicological research.

CHEMICAL RESEARCH IN TOXICOLOGY published bimonthly by American Chemical Society. One volume per year. Volume 1 (1988) ISSN 0893-228X

	U.S.	Canada and Mexico	Europe Air Service Included	All Other Countries Air Service Included
ACS Members				
One year	$ 46	$ 50	$ 54	$ 59
Two years	$ 82	$ 90	$ 98	$108
Nonmembers	$269	$273	$277	$282

Call TOLL FREE: (800) 277-5558 (U.S. only). In D.C. or outside the U.S. call (202) 872-4363, **or write:** American Chemical Society, Marketing Communications Department, 1155 Sixteenth Street, NW, Washington, DC 20036.

GUIDING *CHEMICAL RESEARCH IN TOXICOLOGY* IN ITS FIRST YEAR 1988 EDITORIAL ADVISORY BOARD

ES&T
SERIES

Physiological pharmacokinetic modeling

Second of a five-part series on cancer risk assessment

Daniel B. Menzel
Duke Comprehensive Cancer Center
Durham, N.C. 27710

Risk assessment is the necessary process of determining human health risks from exposure to chemicals and physical agents that precedes the implementation of governmental action. Risk assessment has been divided into four steps: hazard identification, dose–response assessment, exposure assessment, and risk characterization (*1*).

Each step is complex and related to the next. Because of the importance of this process to government regulation, data collection for risk assessment has consumed, and continues to consume, many of the resources devoted to toxicology. The purpose of toxicology is to predict health risks. Thus refinement of risk assessment is a worthy endeavor for toxicologists.

Because risk assessment often defines the approach and the degree of regulation, decisions in risk assessment often have major regulatory impacts. Chemicals that have economic value or that were byproducts of the chemical industry are common subjects of such decisions. Regrettably, decisions related to risk assessment, science, or regulatory matters will frequently be made with incomplete information and on the basis of intuitive reasoning.

Statistical fits to experimental data have been used to estimate risks in humans from experimental data in animals. These treatments have not taken into account the obvious differences in physiology, biochemistry, and size be-

0013-936X/87/0921-0944$01.50/0

FIGURE 1
Relationship between humans and experimental animals[a,b]

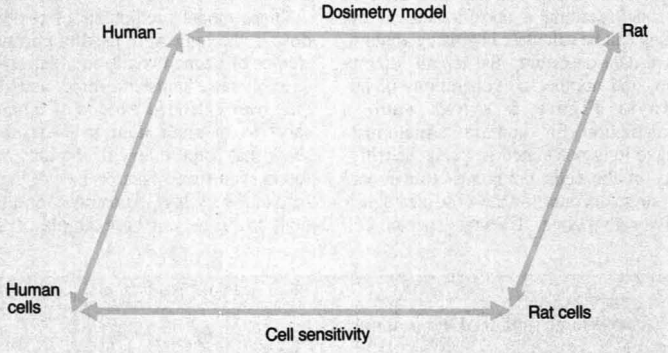

[a]Humans refers to individuals in the population; rats to animals exposed to chemicals as intact animals; human and rat cells represent cultured cells of the same type.
[b]Dosimetry modeling relates effects in rats to those in humans, while the relative sensitivity of human and rat cells corrects for species differences in sensitivity.

tween animals and humans. The next article in this series deals with ways to individualize and to improve the reliability of such data.

In this article the use of mathematical models based on continuous relationships, rather than quantal events, are discussed. The mathematical models can be used to adjust the dose in the quantal response model, but the emphasis will be on how these mathematical models are conceived and what implications their use holds for risk assessment. The general utility of these models is best shown in the parallelogram relationship of Figure 1. Experiments with humans that produce toxic effects cannot be done. Data for human toxicity will always be lacking.

As an alternative, human cells can be cultured and used to measure the intracellular or molecular dose of a chemical producing a toxic effect. The relation between a biochemical marker of toxicity, for example, and the intracellular concentration of a toxic chemical or a metabolite of the toxic chemical can now be studied in a wide variety of human cells under physiological conditions. Similarly, the same cell type from rodents used in toxicological experiments can be cultured and exposed to the toxic chemical under equally physiological conditions.

The intracellular concentration of the toxic chemical may or may not be identical for the same toxic effect in the animal and human cell; for example, the human cell may be less or more sensitive than the rodent cell at the same intracellular concentration of the toxic chemical. The relative sensitivity of human to rat cells can be found experimentally. This ratio of inherent sensitivity forms the base of the parallelogram relationship. In animal experiments, toxic effects of chemicals can be measured at several levels of exposure concentrations of the chemical.

By using physiologically based mathematical models of the transport, distribution, and metabolism of toxic chemicals, scientists can predict and confirm the organ or intracellular dose of the chemical by experimental analysis in exposed animals. By this process the exposure concentration is converted to a tissue dose.

The tissue dose in humans also can be predicted by the same mathematical model once it is adjusted for differences in organ size, blood flow, and other physiological parameters. This forms the top of the parallelogram relationship in Figure 1. When the relative sensitivity of human and rat cells to the toxic chemical has been determined in culture and the organ dose for both has been calculated, the toxic effect in humans can be predicted from the toxic effects measured in animals. When the organ dose is known, the mathematical model can then be used to calculate the equivalent exposure needed for humans to experience the same toxic effect as measured experimentally in animals. Such estimates of effects on human health can be adjusted for genetic differences, disease processes, development and maturation, and a host of other factors common to humans; one need not resort to arbitrary judgments now used to justify "safety factors" or "uncertainty factors."

Two examples illustrate this type of mathematical modeling and how it can be applied to risk assessment.

Chemicals in the body

One of the most basic advances in toxicology has been the recognition that the dose determines the effect. This result seems obvious, but it implies that metabolism and distribution of chemicals determine much of their toxicity. Detecting adverse effects of chemicals on humans is often difficult because of the rarity of the events occurring at doses encountered in the environment. Although the incidence of toxicity in humans is rare, toxic effects such as cancer, birth defects, sterility, or chronic disease are individually devastating. Thus greater precision in predicting health effects is of practical importance.

To obtain the best chance for a positive result, most toxic effects are detected in experimental animals exposed to much higher doses than humans are likely to encounter. To exaggerate toxic effects, animals often are exposed for lifetimes, whereas humans generally are exposed during brief periods. Experiments with animals presume that animals are good surrogates for humans and that effects detected in animals also will occur in humans. It is difficult to prove this theory for all species, and it is even difficult to demonstrate for a limited number of species. So far, these assumptions have proven correct in a qualitative sense with rodents, but quantitative experiments are still needed. As more chemicals are studied, examples of species differences are more likely to be uncovered.

Consequently, extrapolations from high to low doses and from lifetime exposures to short-term exposures in rodents have been used to estimate risks to humans without validation and on theoretical grounds. Because rodents most often are used in these experiments, extrapolations between small animals and humans also have been undertaken with little or no direct validation in humans.

All of these extrapolations to date have been undertaken by fitting data to statistical models with little regard to the biochemical and physiological processes underlying the biological responses. Although such statistical fits were once the best approaches available, recent insights in toxicology based on mechanistic studies suggest new ways to approach such modeling. An alternative method is physiologically based models, which are ideally suited to mathematical modeling (*2, 3*).

Physiologically based models

Because the dose to the target tissue determines the response of the organism to the toxicant, one important application of mathematical models has been to define the dose at the presumed site of action of the chemical. Keeping in mind the need to extrapolate the results of any study in animals to hu-

mans, researchers should create models that capitalize on the similarities between animals and humans and that provide ways to recognize differences.

A detailed description of the respiratory tract of animals and humans has been used by Miller and his colleagues to calculate the dose of ozone reaching specific segments of the respiratory tract (*4*). Although differences clearly exist between humans and animals, mammals have similar respiratory tract anatomies that can be generalized by counting the number of bifurcations (generations) in the airways (Figure 2). A reactive chemical such as ozone is removed from the airways by reaction with the fluid lining the airways and underlying tissues.

The overall distribution of ozone in the lung is described in Equation 1:

Equation 1

$$\frac{\partial C}{\partial t} + U\frac{\partial C}{\partial X} = D\frac{\partial 2C}{\partial X} - \frac{2}{R}J_r$$

where t is the time and X is the distance from the trachea (top of the lung and toward the bottom), C is the average concentration of ozone in the lumen or airspace of the lung at the distance X and t, R is the radius of the airway, U is the average lumen air velocity, and D is the effective dispersion coefficient. J_r, which is the radial flux of ozone across the air-lung interface, accounts for the chemical reaction of ozone with cell or lung lining fluid.

The chemical kinetics of ozone reaction with biological molecules are incorporated into this term (*4*). Whereas the anatomy and physiology of the lung dictate the other terms in the dispersion of gases in the lung, the chemical and physical properties of the gas dictate the mass transfer into specific segments of the lung (e.g., the term J_r is dependent on the chemistry of the toxic gas).

The ozone dosimetry model is being enhanced for a variety of reactive chemical gases, including nitrogen dioxide and sulfur dioxide. A nonreactive gas is also accounted for by setting the chemical reaction term J_r to account for diffusional uptake in the lung lining fluid.

The chemical composition of the lung lining fluid varies between the upper and lower respiratory tracts. Mucous, a fluid containing glycoproteins and small amounts of lipids, provides a more effective barrier against the diffusion of gases of low water solubility than does the surfactant lining in the respiratory region of the lung.

Lung surfactant is composed mainly of lipid and is relatively anhydrous, allowing chemicals of lipid solubility or sparing solubility in water to reach the underlying tissues. The region receiving the greatest ozone dose is the zone where the mucous lining stops and the surfactant lining begins. The dose of ozone reaching a specific site in the lung can be calculated by using anatomical data describing the length, diameter, and number of generations of airways. Figure 3 shows such a calculation for humans. Anatomists have long postulated a special sensitivity of the cells lining this transitional zone to account for the observed sensitivity to ozone. Clearly, special cell sensitivity is not necessary to explain these effects, because these cells receive a greater dose of ozone (Figure 3).

These model predictions of regional dose in the lung were used to correlate studies of ozone toxicity in a variety of species (rats, hamsters, mice, and rabbits) over extended periods of time (as short as one-half hour to 7 days) to show that some injury to the lung was found even from short periods of exposure and very low exposure concentrations to ozone. As an example of this

FIGURE 2
A schematic model of the mammalian lung[a]

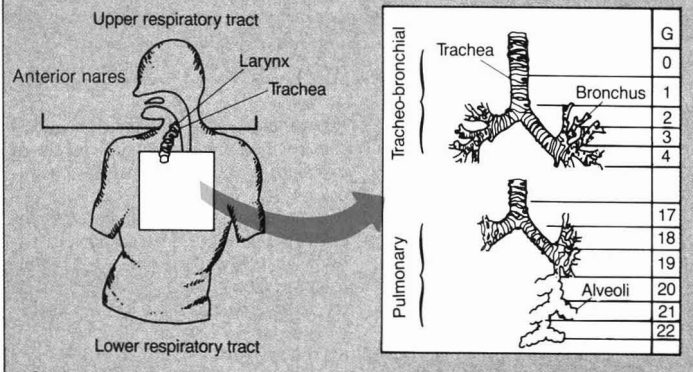

[a]Showing how the lung divides into smaller airways and eventual sacs or alveoli. Source: Reference 5.

FIGURE 3
Molecular doses of ozone reaching different regions of the human lung[a]

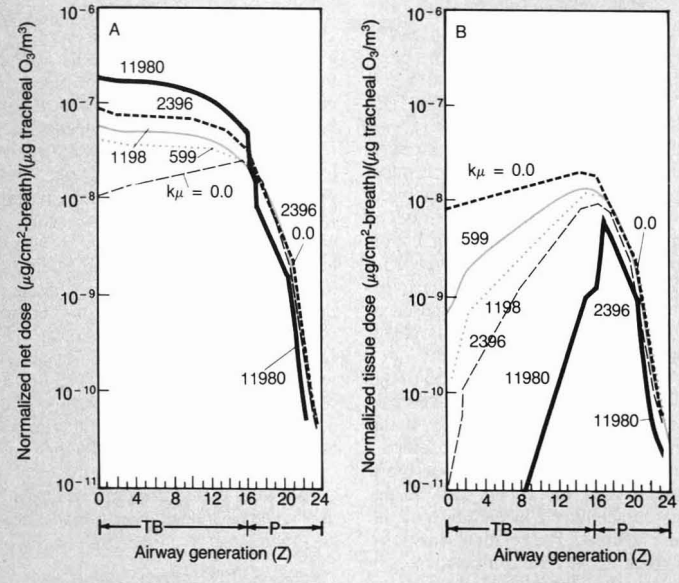

[a]As predicted by a physiologically based model incorporating chemical reactions. **Source:** Reference 4.

FIGURE 4
Construction of a dose–response curve for pulmonary edema[a,b]

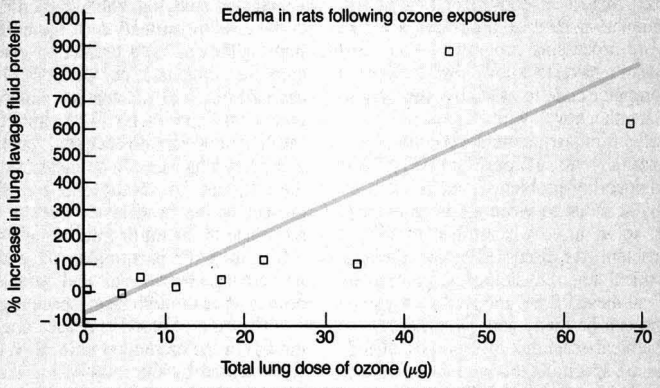

[a]Using multiple experiments reported by different laboratories and the mathematical model of ozone. [b]No dose of ozone occurs at which some biological effect is not found. **Source:** Reference 2.

type of analysis, Figure 4 shows that the extent of pulmonary edema occurring from exposure to ozone (characterized by the appearance of proteins in fluid removed from the lung) is a linear function of the dose of ozone reaching the lung.

Keep in mind that the curve represents the results of several laboratories using widely different exposure conditions. Yet for this index of toxicity, a simple relationship with dose was found. By using the physiologically based mathematical model of the dose of ozone reaching the lung, a threshold, or no effect dose, of ozone could not be found. Ozone may be an example of a reactive chemical that does not have a so-called threshold, as currently hypothesized for noncarcinogens. The linear relation between ozone dose and pulmonary edema suggests that current polluted air exposures may not be safe to humans.

Inhaled or ingested chemicals

Another type of model used for a large number of chemicals is the physiologically based pharmacokinetic (PB-PK) model. PB-PK models use the anatomically defined characteristics of organs to estimate the molecular dose of chemical reaching a particular organ during a certain time period. The organ volume, blood volume, blood flow, interorgan volume, and blood interconnections between organs are known and can be incorporated into PB-PK models.

Chemicals that have entered the body are distributed mostly by the blood. Figure 5 shows that the distribution of chemicals in the body then can be described using a schematic representation of the organs of the body and their interconnection by blood flow. Such descriptions were first introduced by Bischoff, Dedrick, and co-workers (*6*).

In this kind of scheme the organs are represented by boxes that have a defined blood volume and an interorgan volume.

In Figure 5 the blood volume is shown as separated from the internal volume by a dashed line. The uptake of chemicals in organs can be described by simple differential equations based on the idea that the blood concentration of chemicals is equilibrated with the interstitial and intracellular spaces of the organ (interorgan volume) on the passage of blood from the arterial blood supply to the venous blood removed from the organ.

The chemical is removed from the blood into the organ by diffusion, facilitated uptake, or active transport. Eventually the concentration of the chemical approaches a steady state in the organ if

FIGURE 5
Prediction of the distribution of chemicals in mammals[a,b]

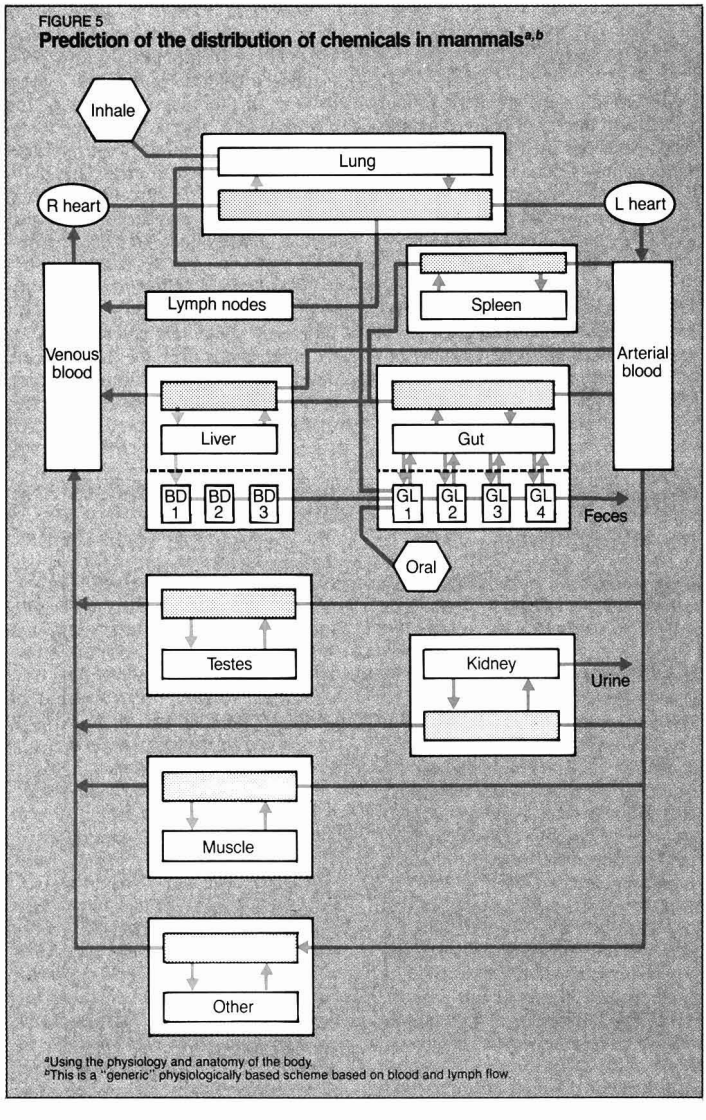

[a]Using the physiology and anatomy of the body. [b]This is a "generic" physiologically based scheme based on blood and lymph flow.

the chemical is not eliminated from the body or if the chemical is supplied to the body at a rate equal to or greater than the rate of elimination. The ratio of the concentration of the chemical in the blood to the concentration in the organ is referred to as the *extraction ratio.* Most toxic chemicals are taken up from the blood by diffusion, making the extraction ratio independent of the concentration of the chemical in the blood. A generalized form of these equations is given in Equation 2. Definitions of the symbols in Equation 2 are provided in the box.

Equation 2

$$dX_j(t)/dt = d_j(t) + \Sigma_i[X_i(t)/V_i]Q_{ij} - [X_j(t)/V_j]\{V_{MAXj}/[(X_j(t)/V_j) + K_{Mj}] + k_j\} - [X_j(t)/V_j]\ \Sigma_i Q_{ij}$$

Modern digital computers simplify solutions to the set of coupled simultaneous equations used to describe these relationships. Computer programs for solving these equations can be written in a number of ways. One way, which we used, is to develop an original computer code in a language such as C. Another way is to use a simulation control program, which writes computer codes to solve these equations. The investigator does not need to know how to write a computer code; he or she can follow a template or use special terms to assemble a complex program.

Two simulation control programs are SCoP, originated at Duke University, and ACSL, a commercial program. Simulation control programs are like word-processing programs. A novelist doesn't have to know how to write a computer code to assemble and manipulate the novel with a personal computer. Similarly, simulation control programs, developed mainly for engineering problems, can be used by any scientist to write a computer code to solve a very complex biological problem. As discussed below, the anatomical and physiological parameters of all these PB-PK models are the same and can be made generic, whereas the chemical reactions of the toxic chemical are specific. Generic PB-PK models are being made available through the Toxicology Information Network (TOXIN) described below.

Methylene chloride is one example of a chemical studied by PB-PK modeling. The carcinogenic potency of methylene chloride is of great interest because of the widespread use of the chemical as a solvent and a degreaser. A considerable number of workers have been exposed to methylene chloride. This chemical also has appeared in groundwater and drinking water; thus its toxicity and carcinogenesis aspects are of concern to the general population. Several animal cancer bioassays have been undertaken with apparently conflicting results. Some of the uncertainty over the carcinogenic potency of methylene chloride has been resolved by the use of PB-PK models.

Volatile chemicals are easily studied by inhalation but are difficult to study by drinking water exposure. One advantage in studying volatile chemicals is the ease of estimation of the extraction coefficient. The extraction coefficient for nonvolatile compounds is best estimated in vivo and requires complex biological experiments. The extraction coefficient of volatile chemicals such as methylene chloride can be measured by the amount of methylene chloride present in the head space over a homogenate of the rat or mice organs (*7*).

Similarly, the partitioning of methylene chloride between air and blood can be measured through head–space analysis. The ratio of blood to tissue concentration, or the extraction ratio, then can be estimated by the ratio of the air to blood and air to tissue homogenate measurements. Estimation of extraction ratios for nonvolatile chemicals is more complex and is best approached by measurement of the organ to blood concentrations in vivo at experimentally maintained steady-state conditions. Modeling of volatiles is appearing as the earliest example of the toxicological PB-PK model because of the ease of estimation of extraction ratios.

Methylene chloride is metabolized in humans and rodents by two pathways: an oxidative pathway dependent on the enzyme system cytochrome P450 (*8*) and a nonenzymatic pathway dependent on glutathione (GSH) (*9*). Both pathways could produce the ultimate potentially carcinogenic metabolite of methylene chloride (*7, 10, 11*). The GSH-dependent pathway has greater capacity than the cytochrome P450-dependent pathway, but the cytochrome P450 pathway has greater affinity for methylene chloride.

Chronic inhalation bioassays for tumorigenicity at 2000 or 4000 ppm produced increased lung and liver tumors (*12*), whereas a drinking water study in B6C3F1 mice failed to demonstrate any increase in tumors (*13*). In an attempt to resolve this conflict in data, dose surrogates (methylene chloride or metabolites) were compared with the tumor incidence data and the metabolite of the GSH-dependent pathway was found to correlate best with the tumor incidence.

Using the PB-PK model developed from the anatomical and biochemical relationships found experimentally for methylene chloride, the estimated values for the GSH metabolite in the liver were calculated. Figure 6 compares the PB-PK model and the current EPA method of linear dose extrapolation. A difference of some 200-fold exists between the PB-PK estimated target dose and the simple linear extrapolation of the dose. Such major differences in dose will have a great impact on decisions about what level of methylene

Definitions of symbols in Equation 2

Symbol	Units	Definition
i, j		Indices of particular compartments
t	(hr)	Time, starting at onset of exposure
$X_j(t)$	(ng)	Mass of chemical in *jth* compartment at time t
$X_i(t)$	(ng)	Mass of chemical in *ith* compartment at time t
$d_j(t)$	(ng hr^{-1})	Dosage rate into *jth* compartment at time t
V_j	(mL)	Effective volume of distribution, $(v_j + m_jR_j)$
v_j	(mL)	Capillary blood volume of *jth* compartment
m_j	(g)	Mass of *jth* compartment
R_j	(mL g^{-1})	Extraction ratio (ng g^{-1}/ng mL^{-1}) in *jth* compartment
Q_{ij}	(mL hr^{-1})	Flow rate of blood from *ith* to *jth* compartments
V_{MAXj}	(hr^{-1})	Michaelis–Menten maximum velocity for metabolic loss
K_{Mj}	(ng mL^{-1})	Michaelis–Menten concentration for half-maximal loss
k_j	(hr^{-1})	Linear clearance rate constant from *jth* compartment

chloride is acceptable for human exposure.

An important insight is gained in why exposure from drinking water failed to demonstrate tumorigenesis. Because of the limited intake of water, much lower doses of the methylene chloride metabolite were achieved in the liver from drinking water ingestion than from inhalation. For volatile chemicals of reasonable solubility in tissues, exposures from inhalation clearly are likely to result in higher organ doses than are exposures from drinking water. If the objective of the assay is to detect effects at the maximum possible dose, then inhalation is superior to ingestion even though ingestion is the more likely route of exposure to humans (as through drinking water). PB-PK modeling, however, is required to correct for target doses and to extrapolate between exposures from inhalation and ingestion.

PB-PK models are obviously a very useful means of comparing different routes of exposure. But their greatest power lies in comparisons between species in which the anatomical and physiological differences are incorporated into the model rather than estimated by crude parameters.

FIGURE 6
Prediction of the production of the carcinogenic metabolite in the liver[a,b]

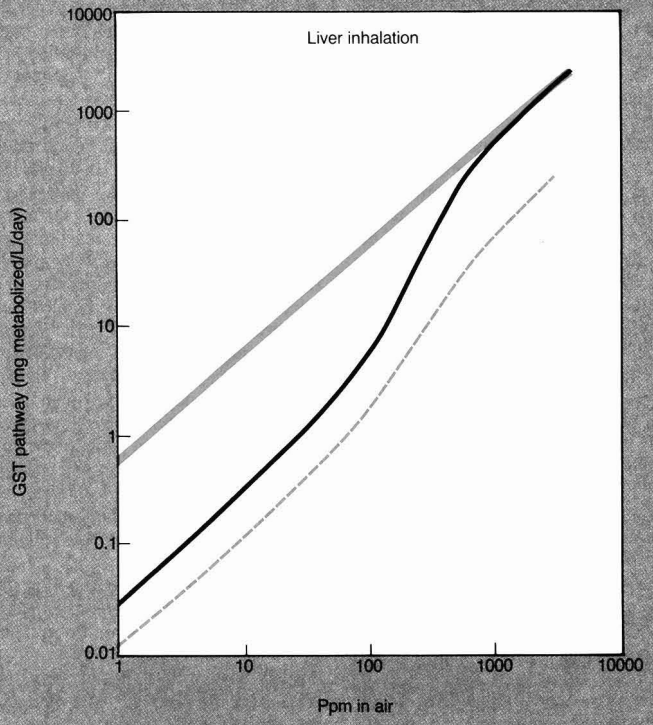

[a]Using a physiologically based model and comparing it to the prediction by linear extrapolation. [b]The equivalent prediction for humans is shown as the broken line. **Source:** Reference 6.

Availability of PB models

Development of PB models for simulation of toxic effects represents a considerable effort. Although differences in metabolism require that models be specific for a chemical, the anatomical, physiological, and biochemical aspects of such models are identical. It should be possible to create generic models of animals and humans. To encourage the use of mathematical models in general and to develop a consensus over critical aspects of mathematical models, the TOXIN has been established at Duke University Medical Center.

TOXIN consists of a computer-based storage of models, computational techniques, and communications through the National Biomedical Simulation Resource (Durham, N.C.) and is available to qualified scientists throughout the world. Generic models can be modified for specific cases and results computed through TOXIN. Specialized computing facilities also are available through the National Biomedical Simulation Resource.

Trends for risk assessment

Only two chemicals were examined here to illustrate the use of physiologically based mathematical models to estimate dose to target organs. Critical organs also could have been studied in place of the target organ. The two cases describe very different chemical situations. Ozone is highly reactive, but of low aqueous solubility. The toxicity of ozone is mostly confined to the lung, so that the anatomy and physiology of the lung dominate the processes leading to toxicity.

On the other hand, methylene chloride is metabolized to a carcinogenic intermediate in organs removed from the portal of entry. Distribution dictates the total parent compound reaching an organ, but metabolism determines how much of the methylene chloride is converted to a toxic compound. Thus the prediction of human health risks depends on a knowledge of the metabolism of methylene chloride as well as the processes by which it is distributed to the organs of the body. Saturation of metabolic steps leads to nonlinearity and complexity in extrapolation of the experimental results to human health risks.

Because these models use the anatomy of humans and animals, extrapolation from animals to humans can be done easily by substituting the characteristics of the organs of another species for the one studied, including human. Exposures by different routes can be accommodated into a single scheme to estimate the toxicity of a chemical.

In both cases, data deficiencies became clear. Research could be focused by studies of the available literature on the toxicity of the chemical. Because of the physiological, chemical, and anatomical bases of the models, they can be made more realistic as greater knowledge is acquired about the chemical reactions of the chemical or its metabolites.

The effects of human disease or development on toxicity can be predicted by alterations in the description of the organs to correspond to the developmental or disease stage. Experiments with children clearly are hazardous and unethical, but are we now providing enough or too much protection through the use of arbitrary safety factors that ignore the known differences in physiology and biochemistry of children? PB models provide a means of simulating the outcome of exposures to chemicals in children by using basic anatomical and biochemical data.

Humans are active animals. Work and exercise can modify the target dose received. Exercise, for example, increases the response of subjects to ozone. The increased response can be accounted for on the basis of a greater ozone dose reaching the distal portion of the lung on exercise (*4*). How human

activity affects toxicity can be studied in this manner.

Current theories of human disease are in a constant state of flux. The recognition of the potential role of oncogenes or cancer-causing genes in chemical carcinogenesis presents another challenge to the simple assumption that a single somatic mutation is sufficient for tumorigenesis. Similarly, cytotoxic chemicals as causes of chronic lung disease suggest that repair and remodeling of organs, particularly the lung, are vital to estimating the impact of the chemical on spontaneous lung disease rates. Does stimulation of cell turnover enhance the incidence of chronic respiratory disease including lung cancer?

The Clean Air Act introduced the concept that the government has a special responsibility to those individuals in the population with inherent sensitivities to chemicals. The populations at risk should be identified and protected. Populations at risk may be small fractions of the general population and difficult to detect by conventional clinical or epidemiological studies. A clear understanding of the potential extension of the problem and the means needed to detect such risks also can be had through the use of models of diseased individuals.

No one can now predict how the use of physiologically based modeling will affect risk estimation. Ozone may be far more hazardous than previously supposed, supporting an effort to maintain, if not lower, the present National Ambient Air Quality Standard. Methylene chloride apparently is less hazardous than previous assumptions suggest. How many chemicals might be liberalized versus restricted by the physiologically based approach compared with the present linearized dose approach simply is not now predictable.

An exciting prospect is the development of pharmacodynamic models or descriptions of the relation between the chemical reactions of a toxic chemical and its biological effect. For example, oncogene activation by chemicals may require translocation of pieces of genes. How such multiple chemical reactions will affect the relationship between target dose of chemical and tumor incidence is not known.

Behavioral modifications by drugs raise the possibility that chemicals also produce behavioral abnormalities. As the relation between neurochemicals and receptors becomes clearer, discovery of toxic reactions is likely. Teratogenesis may involve specific segments of genes or regulation of specific segments. How these relationships will affect the estimation of teratogenic risk from chemical exposure is still being explored.

From a chemical view, development of the details of the chemical reactions leading to toxicity is central to understanding the relation between molecular structure and toxicity. This step is badly needed to cope with the constellation of toxic chemicals naturally present in foods and toxic chemicals introduced by humans into the environment.

New chemical development continues at a rapid pace. It is not farfetched to expect major advances as the molecular reactions of toxic chemicals are characterized and the reactions critical to toxicity are identified by simulation of the pathways of metabolism in the body. Searching for desirable chemical structures and avoiding undesirable ones is coming closer at hand.

Only one class of models dealing with adjustment of dose, pharmacokinetic, was discussed here. Pharmacodynamic models are just developing. Both place risk assessment science on a firmer base by challenging the current wisdom of "safety factors" and linear treatments of dose-response relationships.

Although it may be good public policy to strive to reduce overall exposure to hazardous chemicals to a minimum, it is not good science policy to ignore available data or to fail to include plausible chemical, physical, and biochemical mechanisms in estimating human risks. Mathematical modeling also constrains the experimenter to be plausible. To describe the distribution of a chemical in the body, the experimenter must write down the chemical reaction or physical mechanism and then describe it mathematically. Vague thinking simply does not work.

Qualitative reasoning fails when quantitative differences produce different outcomes. When organ defenses are overwhelmed, toxicity in its myriad forms can occur that cannot be explained by qualitative interpretations. Most chemicals are metabolized simultaneously through two or more pathways. The outcome of exposure to the chemical may depend on the quantitative relations between pathways.

The drive for more credible and reliable estimates of risk from exposure to chemicals in the future also will demand better basic science and new visions of how chemicals produce their toxicities. By the very nature of the complexity of the reactions of chemicals with tissue components, and by the presence of multiple pathways operating simultaneously, intuitive reasoning no longer is acceptable. The methods now available for PB-PK modeling, crude though they are, must be used. Although risk assessment may be more complex, the process will be sounder for the use of mathematical models.

Acknowledgments

F. J. Miller, J. Overton, M. E. Anderson and R. Reitz have provided continuous encouragement and support. B. K. Bernard, D. L. Davis, and R. Thomas of the National Research Council provided the impetus for much of my thinking through their support of the activities of the Safe Drinking Water Committee. Research support on ozone modeling and heavy metal pharmacokinetics came from EPA, the National Institute of Environmental Health Sciences, and from the National Institutes of Health Division of Research Resources.

References

(1) *Risk Assessment in the Federal Government: Managing the Process;* National Academy Press: Washington, D.C., 1983.
(2) Miller, F. J.; Menzel, D. B. In *Fundamentals of Extrapolation Modeling of Inhaled Toxicants;* Miller, F. J.; Menzel, D. B., Eds.; Hemisphere-McGraw-Hill International: Washington, D.C., 1984; pp. 1–303.
(3) *Drinking Water and Health;* National Academy Press: Washington, D.C., 1986, p. 457.
(4) Miller, F. J. et al. *Toxicol. Appl. Pharmacol.* **1985,** *79,* 11–27.
(5) Menzel, D. B.; Smolko, E. D.; In *Assessment and Management of Risk;* Rodricks, J. V.; Tardiff, R. G., Eds.; American Chemical Society, Washington, D.C. 1984; pp. 23–35.
(6) Bischoff, K. B. et al. *J. Pharm. Sci.* **1971,** *60,* 1128–33.
(7) Andersen, M. E. et al. *Toxicol. Appl. Pharmacol.* **1987,** *87,* 185–205.
(8) Kubic, V. L. et al. *Drug Metab. Dispos.* **1977,** *2,* 53–57.
(9) Ahmed, A. E.; Anders, M. W. *Drug Metab. Dispos.* **1978,** *4,* 357–61.
(10) Angelo, M. J. et al. *J. Biopharmacol.* **1985,** *12,* 413–36.
(11) Reitz, R. H.; Smith, F. A.; Andersen, M. E. *The Toxicologist* **1986,** 6.
(12) National Toxicology Program. "Report on the toxicology and carcinogenesis studies of dichloromethane in F-344/N rats and B6C3Fl mice"; U.S. Department of Health and Human Services: Washington, D.C., 1985.
(13) Serota, D.; Ulland, B.; Carlborg, F. *Hazelton Chronic Oral Study in Mice,* Food Solvents Workshop: Methylene Chloride; Hazelton Labs: Bethesda, Md., March 8–9, 1984.

Daniel B. Menzel, *a graduate of the University of California, Berkeley, is professor of pharmacology and medicine at Duke Medical Center. A member of the EPA Science Advisory Board and of several National Research Council committees on toxicology and risk assessment, Menzel has been a leading advocate and researcher in the development and use of mathematical models in toxicology. His research has been primarily in air pollution and inhalation toxicology, emphasizing the chemical mechanisms of toxicity.*

ES&T VIEWS

Environmental service laboratories

Report shows strong growth ahead

By Nancy E. Pfund

The laboratories discussed in this article play a major role in the implementation of environmental regulations. For example, EPA uses competitive bidding to contract out analyses required by regulatory mandate. In fiscal 1985, EPA ordered about 100,000 gas chromatography–mass spectrometry tests for Superfund and dioxin programs alone.

Environmental service laboratories are increasingly useful to private sector clients, and they constitute the majority of a large laboratory's business. They act as environmental accountants by providing clients with objective, third-party chemical information. Often it is too expensive for companies to acquire data in a way that meets compliance standards. In addition, such company-derived data often are of questionable objectivity in the eyes of the court.

Last year, the market for environmental service laboratories in the United States was estimated to be $250 million (*1*). I predict that environmental service laboratories should be an active market in the next five years.

In the past, environmental service laboratories were usually small, private shops that drew their business from local or regional governments and corporations. Now environmental service laboratories are becoming an established industry (see box). This report looks at typical labs and points out that two of the companies have been public for a few years and that three went public in 1985. Many others have since followed suit, including TRC Companies, Inc. The six laboratories listed in the box have participated at various levels and times in the EPA contract laboratory program and in related federal or state contracts. The exacting standards of the EPA program give participating labs a kind of seal of approval that helps them in establishing reputations for providing quality service.

The largest stand-alone environmental service laboratory is Enseco. The company went public in June 1985, in 1986 it acquired two regional labs: California Analytical Laboratories, Inc. (Sacramento) and Rocky Mountain Analytical Laboratory (Denver). Enseco perhaps is exemplary of the business of environmental service laboratories. The company's business embraces the full range of analytical and consulting services related to hazardous-waste disposal. Clients include EPA, state and other federal regulators, engineering companies, and major corporations such as Allied, Du Pont, and General Electric.

One of the oldest companies that also provides environmental service laboratory capabilities is International Technology. This company went public in December 1983 and provides capabilities in four areas: analytical services; engineering services; decontamination and remedial services; and transportation, treatment, and disposal services. The first three services are provided nationwide for toxic substances and low-level nuclear–chemical waste areas; the fourth service is confined to the western United States and to chemical (not nuclear) wastes. Although International Technology is a larger corporation than Enseco, its business includes many nonlaboratory elements, as described above.

Thermo Analytical serves two markets: environmental analytical services and health physics, which monitors and protects against radioactive exposure. Its principal labs are in Albuquerque, N. M., and Richmond, Calif. Formerly this company was a subsidiary of Thermo Electron Corp.

The other two laboratories are CompuChem and Environmental Treatment and Technologies Corporation (ETTC). In addition to its environmental business, CompuChem also has an active business for testing drugs that are abused. ETTC began as an analytical laboratory, but following a 1986 merger with OH Materials the company has become a leader in testing and remediation services. Similarly, TRC Companies started out as an environmental engineering consulting firm but, through acquisitions and internal development, it is on its way to becoming a full-service analytical and remediation company.

Nancy E. Pfund

A sampling of publically held environmental service laboratories

CompuChem Corp. (Research Triangle Park, N.C.)
Enseco, Inc. (Berkeley Heights, N.J.)
Environmental Treatment and Technologies Corp. (Findlay, Ohio)
International Technology Corp. (Torrance, Calif.)
Thermo Analytical, Inc. (Waltham, Mass.)
TRC Companies, Inc. (East Hartford, Conn.)

Reference

(1) Pfund, N. E. "The Quiet Revolution: Analytical Instrumentation Extends Its Reach"; Hambrecht & Quist, Inc.: San Francisco, April 1986; Vols. I and II.

Nancy E. Pfund is a chemical technology analyst at Hambrecht & Quist and follows the environmental service industry. Previously she worked as a consultant to the California Department of Health Services in the toxic substance area and in governmental affairs at Intel Corporation. She holds B.A. and M.A. degrees from Stanford University and an MBA from the Yale School of Management.

0013-936X/87/0921-0951$01.50/0

Improving our regulatory tools

Douglas M. Costle

During the 1970s, the United States erected a massive, intricate structure of government institutions, laws, and regulations to control the discards of our industrialized society. In the past five years, major portions of that statutory base have been amended, and others are the subject of current public and Congressional debate.

Many of the hotly contested provisions of these laws were forged in the heat of confrontations among environmental, industrial, and administrative forces. Actual or alleged noncompliance and nonattainment of goals—demonstrated by persistent air and water pollution problems—have fueled efforts to tighten the laws. Legislative and regulatory changes have become increasingly specific in attempts to meld considerations of public policy, legal and economic equity, and scientific knowledge into effective programs. The result often resembles a regulatory fudge factory; concocted to cover every situation imaginable, it is too sticky to cover many actual situations very well.

When programs prove inadequate, stalemate ensues. The typical response to impasse is to decry the statutes and their implementation, excoriating agencies like EPA for real and apparent flaws such as cumbersome processes, shifting legal and technical policies, and plain bureaucratic inertia.

Acting as a scapegoat begs a subtle, more relevant issue: Have we identified and adopted the most effective tools to achieve our environmental and programmatic goals?

In answering this question, a look at the Superfund program, one year after Congress reauthorized and expanded it, is instructive. Friends and critics both see it mired in impasse. Negotiations and lawsuits drag as potentially responsible parties haggle over degrees of liability and apportionment of clean-up costs. Even settlement-minded participants become gridlocked over thorny questions of "How clean is clean?" Delay becomes an accepted tactic, and a glacial pace the norm. Predictably, the program is faulted for producing little in the way of real site clean-ups. Given this status, or a semblance of it, the answer to the question appears obvious: We have not identified effective clean-up mechanisms.

State actions

But the federal program is not the only game in town. Other approaches are being taken, with some promising successes. Several states (New Jersey, Connecticut, and Massachusetts) have enacted transfer laws requiring sellers of commercial real estate to notify buyers of any environmental problems associated with such property. While these state laws vary in their coverage and requirements, the compliance mechanism is built in: Property transfers are valid only with the required environmental certifications. These can range from simple negative declarations that no environmental liabilities exist to identification of known or suspected problems and remedial actions.

The value of a tool such as a real-estate certification program lies first in its self-enforcing, privately financed nature. The government does not have to investigate every real or suspected environmental hazard nor clean it up. The private market acts as policeman, more effectively than EPA ever could, even with an enforcer on every corner.

Private mechanisms

In addition, it produces self-reinforcing, ripple effects. Increasingly, for example, bankers, mortgage lenders, resellers, and buyers are evaluating such certification programs with an eye to their own financing practices. As these traditional private sector actors find their pocketbooks potentially affected by environmental liabilities, they are starting to modify their own policies and requirements to safeguard their interests.

I am not suggesting that such "private" mechanisms are cost- or trouble-free. Inevitably, there will be problems and associated expenses as new values and operating rules are devised and internalized. Procedural requirements can cause delays and bottlenecks. Some transactions are undoubtedly affected; potential buyers may walk away from a property rather than assume the environmental liabilities it may pose. But, as an ad says: "You can pay now, or you can pay later." And later, it should be noted, the price is higher.

There is precedent for expecting the marketplace to adjust to new requirements. A decade ago, new real-estate disclosure rules (on tax rates and sewer and water charges) were imposed and caused initial headaches for some home buyers and sellers. Today these procedures are routine.

It may overstate the case to claim that incorporating environmental certification provisions into state real-estate transfer laws is likely to encourage more site investigations, problem identifications and clean-ups than a massive federal investigation and enforcement program. But there is a kernel of truth in the claim. Wisely targeted private sector incentives may spur more environmental progress than conventional government remedies.

The next wave of environmental legislation and regulatory innovation may focus on inducing measurable results through increased reliance on nontraditional mechanisms. The business, environmental, and other interest communities could well serve the legislators and regulators by exploring and supporting improved implementation tools.

Douglas M. Costle, J.D., is dean of the Vermont Law School. He served as administrator of the EPA from 1977 to 1981.

0013-936X/87/0921-0952$01.50/0

Organic Carcinogens in Drinking Water: Detection, Treatment, and Risk Assessment. Neil M. Ram, Edward J. Calabrese, and Russell F. Christman, Eds. xvii + 542 pages. John Wiley & Sons, Inc., New York. 1986. $65, cloth.

Reviewed by George R. Hoffmann, Department of Biology, Holy Cross College, Worcester, Mass. 01610

Organic Carcinogens in Drinking Water: Detection, Treatment, and Risk Assessment is impressive because of the breadth of its coverage of this topic. Its logical organization provides a coherence that many multiauthored books lack, and most of the chapters strike a proper balance between technical content and general aspects. The sections on analytical chemistry and engineering practices are very readable, and the coverage of toxicology is straightforward and insightful.

The text is well documented with recent literature citations. It also is enhanced by tables on such diverse subjects as parameters for evaluating the organic content of water, federal regulations, germicidal treatments, sources of artifacts in analytical methods, toxicologic and epidemiologic studies, and lists of organic contaminants, including concentrations and risk assessment data. The straightforward presentation of the book's various topics makes its complex scientific and administrative issues understandable to anyone with a serious interest in organic carcinogens that contaminate drinking water.

There are a few thorns among the roses, however. The indexing of technical terms and concepts, as well as chemicals, is incomplete; a table discussed in the text has been omitted. The text itself generally is clear, but it suffers from occasional lapses into insufficiently defined technical terminology and cumbersome writing. The acronyms sometimes result in passages such as, "the proposed RMCLs for VOCs, and the MCL of 100 ppb for TTHMs defined as the arithmetic sum of the concentrations of THM compounds . . . ." Fortunately, the abbreviations are defined in the index and chapters, so, with some flipping of pages back and forth, one need not commit every ACL, MEPA, NIPDWR, CLSA, KUKLA, FRAN, and OLLIE to memory in order to read the book.

In the preface, the editors point out the interdisciplinary nature of the book's subject. They have done admirable work in assembling information on chemistry, engineering, toxicology, epidemiology, and public policy into a coherent treatment of organic carcinogens in drinking water.

Organic Carcinogens in Drinking Water consists of five parts: introductory papers, methods for identifying organic contaminants in water, processes for eliminating organic contaminants, assessment of toxicologic risks, and regulatory issues. N. M. Ram sets the tone of the book very well in Part 1 by defining the scope of the problem of organic carcinogens in drinking water from a scientific and regulatory point of view. The introduction is extended in excellent chapters on water chlorination and on dissolved and particulate organic contaminants in diverse water sources.

Part 2 covers methods for concentrating, isolating, and identifying organic compounds in water. Topics include sampling techniques, quality assurance and control, and analytical techniques both for a broad spectrum of compounds and for specific contaminants. Various chromatographic procedures (partitioning and adsorption), solvent extraction, distillation, membrane methods, lyophilization, and combined chromatographic and spectroscopic methods are summarized.

Part 3 concerns water treatment, including conventional processes (coagulation–flocculation, sedimentation, and filtration) and direct filtration methods. The generation of halogenated organic compounds is discussed, and the removal of total organic carbon and trihalomethane precursors is covered. Uses of activated carbon as an adsorbent for organic compounds in water are examined. The treatment of water with free chlorine is summarized, and its efficiency and practicality are compared with those of alternative disinfectants, including chloramines, chlorine dioxide, ozone, and hydrogen peroxide.

Part 4, the largest section of the book, focuses on toxicology. Short-term genetic tests for carcinogens, rodent cancer bioassays, epidemiologic methods, and risk assessment concepts are introduced, and guidance on their application and interpretation is offered.

The introduction to short-term tests was disappointing. Although useful information and references are presented, there are several errors and some potentially misleading interpretations. For example, specific figures quoted for the predictive value of short-term tests for carcinogens are debatable; so is the assertion that disagreements among test results involving a positive bacterial test and a negative animal cancer bioassay probably are explainable by flaws in the cancer bioassay.

The accuracy of short-term tests as predictors of carcinogenicity is far from clear, and the degree of this uncertainty has not been determined. Moreover, some relevant assays and modifications of the Ames test that have been used to study contaminants of drinking water have been overlooked.

Data from mutagenicity and carcinogenicity tests of compounds in drinking water are reviewed by R. J. Bull, and their implications are discussed clearly. Unfortunately, the review is restricted to pure compounds and does not cover tests of complex mixtures detected in drinking water. S. A. Beresford summarizes epidemiologic studies related to drinking water. Her careful analysis leads to the conclusion that there is sufficient evidence of an association between organic contaminants in drinking water and gastrointestinal and urinary tract cancers.

R. G. Tardiff and S. H. Youngren offer an insightful overview of applications of toxicologic data in risk assessment, in which they emphasize specific problems posed by organic compounds in water supplies. E. J. Calabrese and C. E. Younger explore unresolved issues and complications in risk assessment. Together, the chapters they have contributed provide an informative and balanced coverage of the toxicology of drinking water.

Part 5 extends the discussion into the realm of policy and examines regulatory philosophy, legislation, and practice pertaining to water supplies. Its chapters are somewhat uneven in quality, but they generally succeed in linking the other sections of the book that deal with regulatory issues.

In addition to providing technical information, *Organic Carcinogens in Drinking Water: Detection, Treatment, and Risk Assessment* offers practical guidance in the interpretation of complex scientific and regulatory issues. Although the book has shortcomings, the pluses outweigh the minuses. Consequently, it can be valuable to anyone interested in chemical contaminants in drinking water.

0013-936X/87/0921-0953$01.50/0

professional consulting services directory

CLASSIFIED SECTION

HAZARDOUS WASTE MANAGEMENT

Environmental Science and Engineering, Inc., an environmental consulting firm with offices nationwide, is seeking the following senior level staff members.

- **HYDROGEOLOGISTS**
- **CIVIL/ENVIRONMENTAL ENGINEERS**
- **PROJECT MANAGERS**

Individuals needed to manage projects in hazardous waste site investigations including RI/FS assignments, CERCLA oversight tasks, RCRA facility assessments and remedial designs at hazardous waste sites for both public and private clients. Positions require a minimum of 5 years related experience and BS/MS in Engineering or Geology. Prior experience in consulting and project management and professional registrations preferred. Positions available throughout regional offices; immediate needs in Gainesville, FL and Princeton, NJ.

- **TOXICOLOGIST RISK ASSESSMENT**

Individual needed to provide toxicological expertise to site-specific toxicity, exposure, risk and endangerment assessments. Candidates should be able to calculate contaminant intakes and acceptable daily doses. Position requires Ph.D. in Toxicology, Biochemistry or related degree, previous risk assessments experience, ability to write excellent proposals and technical reports. Position in the Gainesville, FL office.

- **INDUSTRIAL HYGIENIST**— (Dept. Manager) Gainesville, FL & St. Louis, MO
- **ANALYTICAL FIELD SERVICES**— (Dept. Manager) Gainesville, FL
- **CHEMISTS**— GC/GCMS Gainesville, FL & Denver, CO.

Joining ESE positions you as a capable professional within a growing 600+ person consulting firm; we are committed to working together within the corporation to provide high quality technical service to the client and to offer our staff a challenging environment in which to develop as individuals.

Interested candidates should submit resume, geographical preferences and salary requirements to:

ESE
ESE
ESE

Environmental Science & Engineering, Inc.
P.O. Box ESE Dept. EST-10
Gainesville, FL 32602

Or for immediate information contact:
Professional Recruiter
Leah Milio
1-800-874-7872

Equal Opportunity Employer M/F

Environmental Consulting – Several Positions

Interesting work involving hazardous waste/materials for a nationwide clientele. B.S. or M.S. with excellent grades in Environmental Chemistry or Engineering, strong technical skills and 0-5 years' experience. Projects are in the areas of environmental data management (PC-based) and chemical transport, fate and exposure modeling and data analysis.

Resumes to:

Gradient Corporation

44 Brattle Street
Cambridge, MA 02138

ENVIRONMENTAL COMPLIANCE NUCLEAR WASTE MANAGEMENT

Battelle's Office of Nuclear Waste Isolation has immediate needs for senior level Environmental Managers for our Salt Repository Project being conducted for the U.S. Department of Energy. Experience in the nuclear industry or the state of Texas is desirable but not required. All positions are in the Texas panhandle. Typical openings include:

- **COMPLIANCE SPECIALIST**
  MS and minimum of 10 years' in developing strategies for NEPA/NWPA compliance, obtaining permits or specifying/documenting the environmental, socioeconomic, and transportation assessment needed to meet state (Texas) and federal regulations.
- **SAFETY ANALYSIS ENGINEER**
  MS in Health Physics or equivalent and 5 years' in computer modeling of worker exposure/risk in a nuclear environment.
- **RADIOLOGICAL ENGINEER**
  MS and 5 years' experience in NRC licensing and regulatory compliance and design/operation of nuclear power plants.
- **TRANSPORTATION SPECIALIST**
  MS and 5 years' experience with regulations concerning transportation and handling nuclear materials.
- **NUCLEAR ENGINEER**
  MS and 5 years' experience conducting risk/safety assessment methodologies and experience with siting and NRC licensing/documentations.
- **SYSTEMS ANALYST**
  MS and 3 years' experience in verification and utilization of computerized predictive models.
- **ENVIRONMENTAL SCIENTISTS**
  BS/MS and 5 years' experience in planning, integration, and implementation of plans.
- **ENVIRONMENTAL HYDROLOGIST**
  MS/PhD and 9 years' experience in planning, integration, and implementation of water portion of plan.
- **ATTORNEY**
  J.D. and 10 years' experience in environmental law.
- **SOCIOECONOMIC MANAGER**
  MS/PhD and 15 years' experience of applied socioeconomic impact assessment/mitigation and community planning.
- **SOCIAL/SOCIOECONOMIC SCIENTIST**
  BS/MS and 5 years' in applied impact and assessment/mitigation and community planning.

Battelle is a world leader in R&D and we offer a comprehensive benefits program and a salary commensurate with your background. Send a resume in confidence to:

Battelle
Project Management Division

ONWI • Attention: Stu Pike
P.O. Box 2360 • Hereford, Texas 79045

An Equal Opportunity/Affirmative Action Employer M/F/H

CLASSIFIED SECTION

ENVIRONMENTAL SPECIALIST

The MBTA is seeking an Environmental Specialist to work on Authority-wide environmental issues. Applicants should possess a college degree in Environmental Engineering Science or a related field, and have working experience in the area of hazardous waste management. Applicants should also be familiar with state and federal environmental laws, and have the ability to communicate in written and graphic form. Salary range: low to mid $30's.

Interested persons meeting the criteria outlined above should send a cover letter and detailed resume, by October 23, 1987, to: Massachusetts Bay Transportation Authority, Personnel Department, 10 Park Plaza, Boston, MA 02116.

The MBTA is an affirmative action/equal opportunity employer (M/F/H/VEV).

Massachusetts Bay Transportation Authority

THE UNIVERSITY OF TEXAS-HOUSTON, SCHOOL OF PUBLIC HEALTH, is seeking applicants for a tenure-track position in Hazardous Waste Management. Applicants should have a Doctoral Degree with a strong background in Science or Engineering. Assistant or Associate level can be applied for depending on qualifications. Responsibilities consist of teaching M.S./PH.D./M.P.H./DR.P.H. programs and conducting research in a multidisciplinary setting. Applicants should send a detailed resume by November 1, 1987 to **Dr. E. M. Davis, Professor, Environmental Science, The University of Texas, School of Public Health, P.O. Box 20186, Houston, TX 77225.** An equal opportunity employer. Women and minorities are encouraged to apply.

Chemical Engineering and Public Policy. Tenure track faculty position for a candidate to teach and do research on technical and public policy problems. Topics of particular interest include mathematical modeling of chemical transport and transformation in environmental systems and problems in bioengineering. Send resume, references and sample publication to: **M. Granger Morgan, Head, Department of Engineering and Public Policy, Carnegie Mellon, Pittsburgh, PA 15213.**

ENVIRONMENTAL ENGINEERING/ INDUSTRIAL HYGIENE POSITIONS

Career opportunities are available for environmental engineers and industrial hygienists interested in management and technical-level positions. Opportunities exist nationwide for professionals with marketing/sales experience, management experience, strong technical skills, and a desire to grow both professionally and personally. Environmental Protection Systems, Inc. (EPS), is accepting applications for the following positions: Vice President, Technical Operations; Vice President, Analytical Services; Branch Managers; Analytical Department Managers; Engineering Department Managers; Industrial Hygiene Department Managers; and senior technical professionals. Salary range is variable depending upon position and experience. Key positions include stock option and bonus opportunities, and a comprehensive benefits program. Resumes including detailed history, salary history and references may be sent to Faye C. Byrd, Administrative Assistant, 1100 Kermit Drive, Suite 108, Nashville, Tennessee 37217. EOE

ENVIRONMENTAL ENGINEERS AND HYDROGEOLOGISTS

Kurz Associates, Inc. is a rapidly growing, progressive environmental, civil, hydrogeological and geotechnical consulting firm. With new offices located in Bridgewater, MA, we have immediate opportunities for an engineer with direct groundwater treatment technology experience and for a hydrogeologist with direct experience in groundwater supply and restoration studies. Advanced degrees and professional registration are all a plus. Qualified individuals should send their resumes to: Ralph J. Tella, Environmental Services Manager, Kurz Associates, Inc., Post Office Box 430, West Bridgewater, MA 02379.

Kurz Associates, Inc.

ENVIR. ENGR. SCIENTIST (water). Studies, designs, implements hazardous waste cleanup, water supply, & wastewater treatment/disposal. Req. M.S. Envir. Engr. (emphasis on aquatic chemistry). $17.88/hr. Place of employment & interviews in San Francisco, CA. Send this ad & your resume or letter stating your qualifications to **Job Order # NC 8214, P.O. Box 9560, Sacramento, CA 95823-0560,** *no later than* **10-30-87.**

INDEX TO THE ADVERTISERS IN THIS ISSUE

Advertising Management for the American Chemical Society Publications

CENTCOM, LTD.

President
Thomas N. J. Koerwer

Executive Vice President **James A. Byrne**
Senior Vice President **Benjamin W. Jones**
Clay S. Holden, *Vice President*
Robert L. Voepel, *Vice President*
Joseph P. Stenza, *Production Director*

500 Post Road East
P.O. Box 231
Westport, Connecticut 06880
(Area Code 203) 226-7131
Telex No. 643310

ADVERTISING SALES MANAGER
James A. Byrne, *VP*

ADVERTISING PRODUCTION MANAGER
Jay S. Francis

SALES REPRESENTATIVES

Philadelphia, Pa. . . . Patricia O'Donnell, CENTCOM, LTD., GSB Building, Suite 725, 1 Belmont Ave., Bala Cynwyd, Pa 19004 (Area Code 215) 667-9666

New York, N.Y. . . . Dean A. Baldwin, CENTCOM, LTD., 60 E. 42nd Street, New York 10165 (Area Code 212) 972-9660

Westport, Ct. . . . Edward M. Black, CENTCOM, LTD., 500 Post Road East, P.O. Box 231, Westport, Ct 06880 (Area Code 203) 226-7131

Cleveland, OH. . . .Bruce Poorman, John Guyot, CENTCOM, LTD., 325 Front St., Berea, OH 44017 (Area Code 312) 234-1333

Chicago, Ill. . . . Michael J. Pak, CENTCOM, LTD., 540 Frontage Rd., Northfield, Ill 60093 (Area Code 312) 441-6383

Houston, Tx. . . . Michael J. Pak, CENTCOM, LTD., (Area Code 312) 441-6383

San Francisco, Ca. . . . Paul M. Butts, CENTCOM, LTD., Suite 1070, 2672 Bayshore Frontage Road, Mountainview, CA 94043. (Area Code 415) 969-4604

Los Angeles, Ca. . . . Clay S. Holden, CENTCOM, LTD., 3142 Pacific Coast Highway, Suite 200, Torrance, CA 90505 (Area Code 213) 325-1903

Boston, Ma. . . . Edward M. Black, CENTCOM, LTD., (Area Code 203) 226-7131

Atlanta, Ga. . . . Edward M. Black, CENTCOM, LTD., (Area Code 203) 226-7131

Denver, Co. . . . Paul M. Butts, CENTCOM, LTD., (Area Code 415) 969-4604

ES&T RESEARCH

Sensitized Photooxidation of Phenols by Fulvic Acid and in Natural Waters

Bruce C. Faust and Jürg Hoigné*

Swiss Federal Institute for Water Resources and Water Pollution Control (EAWAG), CH-8600 Dübendorf, Switzerland

■ In addition to singlet oxygen, irradiation of fulvic acid solutions and lake water with UV and visible light ($\lambda >$ 315 nm) produces another transient oxidant species. This transient oxidant (probably an organic peroxy radical) is derived from natural dissolved organic material (DOM) and controls DOM-sensitized photooxidations of various alkylphenols. On the basis of kinetic data for the transient oxidant, DOM-sensitized photooxidation half-lives of alkylphenols are estimated to range from 1 day to several months in middle-latitude shallow surface waters.

Introduction

A quantitative assessment of the sensitized photooxidations of any compound of environmental interest is necessary for the accurate prediction of its fate in natural waters. It is now well established that some organic compounds [measured as dissolved organic carbon (DOC)] and inorganic compounds present in natural waters, when exposed to sunlight, sensitize the photoproduction of a variety of transient oxidants (OX) such as singlet oxygen (*1*, *2*), hydroxyl radical (*3–6*), and probably organic peroxy radicals (*7*, *8*). Singlet oxygen ($^1O_2$) is formed by energy transfer from dissolved organic material (DOM) triplets to molecular oxygen (*1*, *2*). Hydroxyl radical ($^\bullet$OH) is produced by photolysis of nitrate (*3–6*) and nitrite (*6*) and possibly in metal- (Cu, Fe, Mn) catalyzed decomposition of peroxides. Organic peroxy radicals are thought to be produced by photolysis of DOM (*7*, *8*).

In general, sensitized photooxidation kinetics can be interpreted in terms of the model given in reactions 1–4,

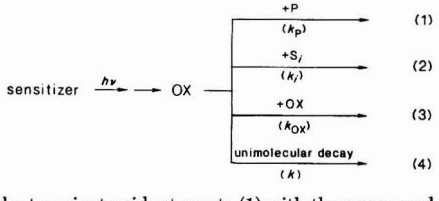

where the transient oxidant reacts (1) with the compound of interest (P) with second-order rate constant k_P, (2) with natural or added solutes (S_i) with second-order rate constant k_i, (3) with itself (OX) with second-order rate constant k_{OX}, and (4) by unimolecular decay (including solvent quenching) with first-order rate constant k. If the concentration of P is sufficiently small that $k_P[P] \ll k + k_{OX}[OX] + \sum k_i[S_i]$, then the lifetime of OX is controlled by reaction 2 [e.g., $^\bullet$OH (*3*, *4*)], reaction 4 [e.g., $^1O_2$ (*1*)], or reaction 3. With continuous irradiation of constant intensity, a steady-state concentration of the transient oxidant $[OX]_{ss}$ is attained rapidly and remains nearly constant, provided that the sensitizer concentration and $k + k_{OX}[OX] + \sum k_i[S_i]$ do not change appreciably during the irradiation period. As shown previously (*1–4*, *9*) for these conditions, the oxidation rate of P is first order with respect to [P]:

$$d[P]/dt = -k_{SENS}[P] \quad (5)$$

where the experimentally determined apparent first-order rate constant k_{SENS} is

$$k_{SENS} = k_P[OX]_{ss} \quad (6)$$

Therefore, $[OX]_{ss}$ is determined by measuring k_{SENS} with a compound of known k_P. This approach has worked very well for the determination of steady-state concentrations of transient oxidants, such as $^\bullet$OH and $^1O_2$, for which second-order rate constants with specific compounds (k_P) are known. However, second-order rate constants for reactions of DOM-derived radicals with specific compounds are not known because of the complicated and unknown speciation and structures of natural organic radicals. Collective steady-state concentrations ($\sum[OX_i]_{ss}$) of organic radicals in natural waters can be estimated but only by assuming that the type and reactivities of the DOM radicals are identical to those of a specific organic radical with known k_P. The validity of this assumption cannot be tested at present.

Phenols are present in natural waters as a consequence of natural decay processes (*10*), dry and wet deposition (*11*), industrial activities (*12–14*), and microbiological degradation of nonionic surfactants present in detergents (*15*). Many phenols present at low concentrations exhibit toxic effects on organisms (*16*, *17*) and form objectionable tastes and odors in drinking waters upon chlorination. Therefore, they are undesirable constituents of natural waters, particularly when these waters are sources for drinking water supplies. Quantitative rate information on all degradative pathways of phenols is therefore desired and required to accurately predict their persistence in natural waters. Consequently, their reactivity with various DOM-derived photoproduced transient oxidants is of interest. Some kinetic information on the reactivity of phenols with $^\bullet$OH and $^1O_2$ has been published (*18–20*); however, only limited kinetic information on their reactivity with other transient oxidants in water is available (*21–24*).

This study was therefore initiated with the objectives of (1) determining the relative reactivity of a series of alkylphenols with a photogenerated DOM-derived transient oxidant, (2) estimating DOM-sensitized "photooxidation half-lives" of a variety of alkylphenols in sunlit

0013-936X/87/0921-0957$01.50/0

natural waters, (3) tentatively identifying the transient oxidant on the basis of its relative reactivity with different phenols and by use of other diagnostic tests, and (4) identifying a probe molecule, which could be used in future studies, to determine steady-state concentrations of the transient oxidant and to operationally define absolute reaction rate constants.

Experimental Methods and Materials

Chemicals and Solutions. Except where noted, all chemicals were of reagent-grade quality and were used as received. All solutions were prepared from deionized/distilled water. Contech fulvic acid was obtained from Cooper H. Langford and has previously been characterized (*25*). A filtered (0.05 μm) fulvic acid stock solution was prepared and had the following chemical composition: [DOC] = 0.74 g/L, [Fe] = 50 μM, [Mn] = 0.2 μM, and [Cu] = 0.3 μM. It was stored in the dark at 4 °C. Decadic absorptivities [(g of carbon/L)$^{-1}$ cm^{-1}] of the fulvic acid at pH 8.1 as a function of wavelength (nm) are 32.5 (289), 28.0 (302), 25.0 (313), 19.9 (334), 12.9 (366), 7.5 (405), 5.29 (436), 1.65 (546), and 1.20 (578). Occasionally, filtered (0.45 μm) surface water from Greifensee (pH 8.4, [DOC] = 3.1 mg/L, [NO_3^-–N] = 1.4 mg/L), a polluted eutrophic prealpine Swiss lake, was used as a DOM source. Absorption spectra of Greifensee water are available elsewhere (*1*). Furfuryl alcohol was vacuum distilled under N_2(g) at ~80 °C and stored in the dark under N_2(g) at 4 °C. Isotope pure D_2O (99.8%) was obtained from the Swiss Federal Institute for Reactor Technology and was redistilled twice to remove most of the copper impurity. Technical-grade 4-nonylphenol, containing 10% 2-nonylphenol, was used as received (*15*). Superoxide dismutase (copper form, from bovine erythrocytes) was obtained from Sigma. The argon gas contained <5 ppm oxygen.

Analyses. All compounds, except for ascorbate, were analyzed by high-performance liquid chromatography (HPLC). In all cases the HPLC analyses were performed under isocratic conditions on an ODS-2 column with either acetonitrile/water or methanol/water mixtures as the mobile phase. Methanol/water mixtures, buffered with phosphate to pH 3, were used as the mobile phase for analyses of benzoic acid and hydroxybenzoic acids. Compounds were detected either by monitoring their UV absorbances [at 222 nm (phenols), 277 nm (4-dimethoxybenzene), and 235 nm (benzoic acid and hydroxybenzoic acids)], or (only for phenols) by monitoring their fluorescence emission at 300 nm (excitation λ = 277 nm). Sample aliquots of the reactant solution were stored in the dark at 20–25 °C and analyzed within 5 h of sampling. Immediately prior to analysis, 0.50 mL of an internal standard solution and 20 μL of 10% HCl were added to the 1.00-mL sample. Ascorbate was analyzed by a colorimetric method previously described (*26*).

Irradiations were performed in glass-stoppered quartz photolysis tubes (1.5-cm i.d.) either in a water-cooled merry-go-round reactor (MGRR) (*1*) or in sunlight. Except where noted, the output of the high-pressure Hanau TQ 718 Hg lamp (operated at 700 W) was filtered through solidex borosilicate glass and a 0.15 M $NaNO_3$ aqueous filter solution with an average light path length of approximately 2.8 cm. Total transmittances of the filter system (glass and $NaNO_3$) as a function of wavelength (nm) are <0.001 (λ < 303 nm), 0.008 (313), 0.5 (334), 0.7 (366), and >0.8 (λ > 405 nm). Sunlight photooxidations were performed during the 4-h period centered on solar noon, at EAWAG (Zürich, 47.5° N), with a rack that positioned the tubes about 30° from horizontal in a water-filled flat-bottom container. The water level inside the photolysis tubes was below the exterior cooling water level. The temperature was 20 ± 1 °C for MGRR experiments and 20 ± 4 °C for sunlight photooxidations. Sunlight intensity (in kW/m^2) was measured with a pyranometer that responds only to light of 400–1000 nm but is calibrated to give sunlight intensity over the range 280–2800 nm (*1*). Clear-sky, solar-noon, June sunlight intensity is ~1 kW/m^2, on the basis of this procedure.

Except where noted, all photolysis solutions were equilibrated with air prior to photolysis and had the following composition: 4.1 mg of carbon/L of fulvic acid, 20 μM initial total compound concentration, pH 8.0 ± 0.1, 0.010 M total orthophosphate buffer, and μ = 0.072 M ionic strength (adjusted with Na_2SO_4). Each compound was photooxidized in a separate photolysis tube. Direct photolysis and thermal (dark) reaction controls were performed under identical conditions except without sensitizer (DOM) and light, respectively. To internally normalize results of experiments performed with slightly different light intensities, a separate photooxidation of either 4-methylphenol or 4-ethylphenol was performed simultaneously with other photooxidations.

Deoxygenated solutions were prepared from argon-purged stock solutions and argon-purged deionized–distilled water. When necessary, solution preparations and transfers were performed inside an argon-purged glovebag, and the headspace of the photolysis tubes was purged with argon immediately prior to and following a sampling event.

When solution absorbances were not negligible, measured rate constants were converted to surface rate constants by dividing by the light screening factor (*27*) given in eq 7, where L is the average light path length (assumed

$$S_\lambda = (1 - 10^{-\alpha_\lambda L})/(2.3\alpha_\lambda L) \quad (7)$$

to be 1.5 cm for the photolysis tubes) and α_λ is the decadic absorption coefficient (cm^{-1}) of the water at wavelength λ. The choice of wavelength is not important for short path length corrections because, for the DOM concentrations used, the corrections were less than 16% for λ > 310 nm. All calculations were made with λ = 366 nm because the DOM-absorbed light intensity in the MGRR was greatest at this wavelength.

Results and Discussion

Kinetic Analyses and Controls. Oxidation rates of all compounds were first order in total compound concentration (see below), [P]. Therefore, kinetic results were analyzed with eq 8, where k_{DARK}, k_{DIRECT}, k_{SENS}, and k_{TOTAL}

$$\frac{d[P]}{dt} = -k_{TOTAL}[P] \equiv -(k_{DARK} + k_{DIRECT} + k_{SENS})[P] \quad (8)$$

are apparent first-order rate constants for dark reactions, direct photolysis, sensitized photooxidations, and the sum of all reactions, respectively. k_{SENS} is calculated by difference from independent measurements of k_{TOTAL}, k_{DIRECT}, and k_{DARK}. For sunlight irradiations, k_{SENS} may be expressed as an *exposure dose based* first-order rate constant [m^2/(kW·h)].

Direct solar photolyses of alkylphenols are slow because protonated forms of alkylphenols absorb weakly in the solar region (λ > 300 nm). For all phenols reported on here, except where noted, k_{DARK} and k_{DIRECT} (in the MGRR with the $NaNO_3$ filter solution) were less than 2% and 12% of k_{TOTAL}, respectively. For ascorbate, k_{DARK} + k_{DIRECT} was less than 10% of k_{TOTAL} in the MGRR. For 2,4,6-trimethylphenol (TMP), k_{DIRECT} was less than 5% of k_{TOTAL} in the MGRR and in sunlight. Smith et al. (*21*)

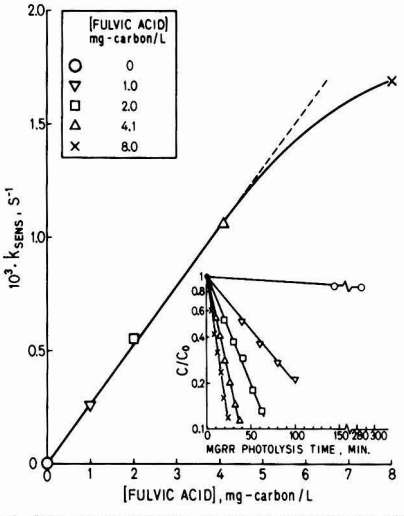

Figure 1. Rate constants for the sensitized photooxidation of 2,4,6-trimethylphenol (in the MGRR) as a function of fulvic acid concentration. (Insert) Kinetic data from which the rate constants were calculated. For all solutions: initial [TMP] = 20 μM, pH 7.9 (0.01 M orthophosphate), p_{O_2} = 0.21 atm, ionic strength = 0.072 M, and temperature = 20 °C.

found the rate of 4-methylphenol direct photolysis to be less than 10% of the total photooxidation rate in a solution containing 9.5 mg/L of humic acid, in sunlight. All results and discussions will focus on sensitized photooxidation pathways (k_{SENS}).

Values of k_{SENS} for fulvic acid (4.1 mg of carbon/L) sensitized photooxidations in the MGRR of TMP in argon-purged and air-equilibrated solutions (pH 7.9) were 1×10^{-5} and 1.1×10^{-3} s^{-1}, respectively, confirming the requirement of molecular oxygen in the reaction. The very small rate observed in the argon-purged solution was probably due to residual dissolved oxygen (5–10 μM), which is usually present in aqueous solutions even after vigorous argon purging.

Values of k_{SENS} for fulvic acid (4.1 mg of carbon/L) sensitized photooxidations in the MGRR of TMP at pH 7.9 were insensitive (<20% variability) to either the type of buffer (phosphate or bicarbonate) or the buffer concentration (1–10 mM). Therefore, $[OX]_{ss}$ is not altered either by higher buffer concentrations or by specific interactions with phosphate or bicarbonate.

[Fulvic Acid], [TMP], and pH Dependencies. As shown in Figure 1, k_{SENS} is linearly related to fulvic acid concentration, proving that some fulvic acid species sensitize the photooxidation. Figure 1 also proves that, at lower DOM concentrations ([DOC] < 5 mg/L), the transient oxidant lifetime is not controlled by scavenging reactions of the fulvic acid. However, Mill et al. (7) observed that organic materials in water with a high DOM concentration [Aucilla River, [DOC] ~ 18 mg/L (28)] compete efficiently with added 4-isopropylphenol for organic peroxy radicals. The departure from linearity of k_{SENS} vs. [fulvic acid] at higher fulvic acid concentrations (Figure 1) is consistent with their observations (7). This indicates that the lifetime of the transient oxidant is affected by scavenging reactions of the DOM (reaction 2 with $S_i \equiv$ DOM), but only at higher DOM concentrations ([DOC] > 5 mg/L).

Figure 2 demonstrates that the reaction is first order in TMP and that the apparent first-order rate constant

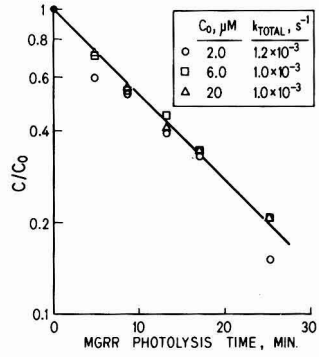

Figure 2. Photooxidation of 2,4,6-trimethylphenol (in the MGRR) for different initial concentrations of 2,4,6-trimethylphenol. Other experimental conditions are the same as for Figure 1 but with [fulvic acid] = 4.1 mg of carbon/L.

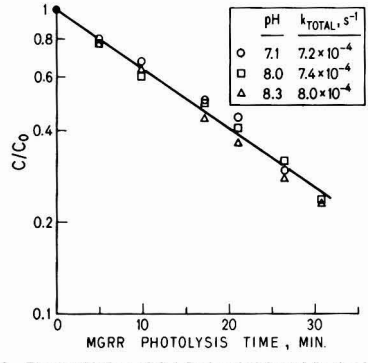

Figure 3. Photooxidation of 2,4,6-trimethylphenol (in the MGRR) at different pH values. For all solutions: initial [TMP] = 20 μM, [fulvic acid] = 4.1 mg of carbon/L, [orthophosphate] = 0.04 M, p_{O_2} = 0.21 atm, ionic strength = 0.47 M, and temperature = 20 °C.

(k_{TOTAL}) and therefore $[OX]_{ss}$ are independent of the TMP concentrations used in this study (<20 μM). Because TMP is the most reactive phenol used in this study and because it does not alter $[OX]_{ss}$ when [TMP] < 20 μM, rate constants determined from experiments with all phenols reported on here (concentration < 20 μM) can be used to reliably predict photooxidation half-lives of phenols present at lower concentrations typically found in natural waters.

The rate of TMP oxidation is independent of pH throughout the range 7.1 < pH < 8.3 (Figure 3). Since the concentration of TMP anion changes by about 1 order of magnitude over this pH range, this result indicates that sensitized photooxidation pathways involving undissociated TMP [pK_a > 9.8, that of phenol (29)] account for virtually all of the observed reaction rate in this pH range.

Relative Reactivities of Phenols and DOMs. All photooxidations of compounds reported on here exhibited apparent first-order kinetic behavior (Figure 4), indicating that the sensitization capacity of the fulvic acid is approximately constant for the time scales and illumination doses of these experiments.

Figure 4 also illustrates the wide range of reactivities of alkylphenols. Relative reactivities of the phenols reported on here vary by as much as a factor of 40 (Table I). Reactivity of the phenols increases with increasing ring substitution by electron-donating methyl groups. However, 4-alkylphenols exhibit an additional effect. The observed

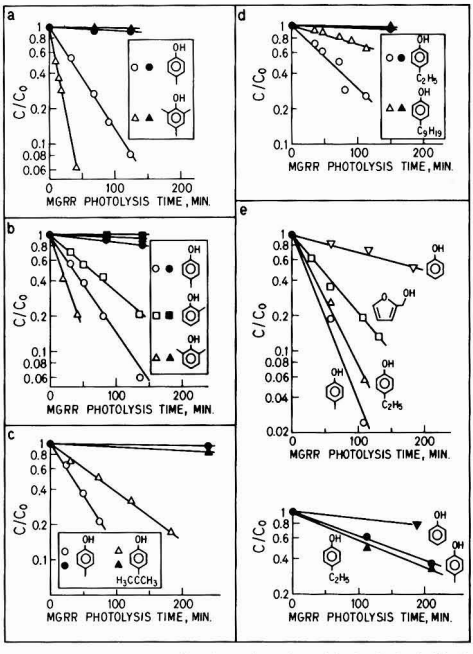

Figure 4. Photooxidation of various phenols and furfuryl alcohol in the MGRR. For all solutions: initial concentration = 20 μM for each phenol (25 μM for furfuryl alcohol), pH 8.0 (0.01 M orthophosphate), p_{O_2} = 0.21 atm, ionic strength = 0.072 M, and temperature = 20 °C. Solid symbols represent direct photolyses (no fulvic acid); open symbols represent photooxidations with [fulvic acid] = 4.1 mg of carbon/L. For experiments illustrated in part e, deionized water was substituted for the $NaNO_3$ filter solution to attain the higher light intensity required for the photooxidation of phenol.

relative reactivity sequence for 4-alkylphenols is methyl > ethyl > isopropyl > nonyl > H. The electron-donating character of alkyl groups, as measured by Hammett σ constants, is approximately constant or increases slightly with increasing size of the alkyl group. However, k_{SENS} decreases with increasing size of the alkyl group. Several interpretations of this behavior are possible. A large alkyl group may sterically hinder access of the phenol to some DOM radical sites. Alternatively, a large alkyl group might interact with hydrophobic parts of the DOM, which could inhibit attack of the phenol by the transient oxidant. Hyperconjugation effects of the alkyl group may also influence the reactivities of the 4-alkylphenols.

The reactivity of 4-dimethoxybenzene is much lower than that of 4-methoxyphenol (Table I), indicating the importance of the OH group in these DOM-sensitized photooxidations.

Benzoate anion and monohydroxybenzoate anions (ortho, meta, and para forms) were the least reactive compounds examined in this study (Table I). These compounds, reasonable models for some types of structures thought to be present in DOM, are rather resistant to oxidation by *all* transient oxidants generated in DOM-sensitized photooxidations.

Ascorbate anion reacts more rapidly than the phenolic compounds studied (Table I), in DOM-sensitized photooxidations, although not necessarily by the same mechanism as the phenols.

The relative reactivity (at pH 8.0) of TMP and 4-ethylphenol (EP) in the MGRR, compared for three different DOM sources, Contech fulvic acid (4.1 mg of carbon/L), Fluka "humic acid" (1.6 mg of carbon/L), and 91% Greifensee water, is k_{TMP}/k_{EP} = 4.1, 7.5, and 4.0, respectively. This demonstrates that relative reactivities of various alkylphenols are not strongly dependent on the DOM source.

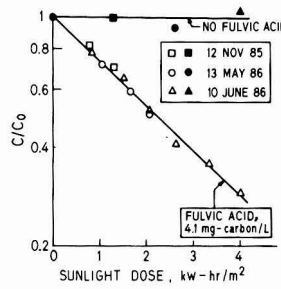

Figure 5. Sunlight photooxidation of 2,4,6-trimethylphenol at different times of the year. Symbol meanings (open or solid) and other experimental conditions are the same as for Figure 4. Average sunlight intensities were 0.35, 0.92, and 1.03 kW/m^2 for the November, May, and June experiments, respectively.

Light Source Effects and Sunlight Dosimetry. The relative reactivity of TMP and 4-methylphenol (MP) for fulvic acid (4.1 mg of carbon/L) sensitized photooxidations (pH 8.0) in the MGRR and in sunlight are k_{TMP}/k_{MP} = 3.3 (Table I) and 5.3, respectively.

Figure 5 presents first-order kinetic plots of the sunlight photooxidation of TMP, for different seasons, as a function of sunlight exposure dose. The linearity of the plots and their identical slopes demonstrate the validity of using polychromatic photometric dosimetry for calibrating kinetic data from DOM-sensitized sunlight photooxidations. Similar correlations have been observed by Haag and Hoigné (*1*) and suggested by Zepp et al. (*30*) for the formation of $^1O_2$. Figure 5 also shows that *exposure dose based* first-order rate constants [m^2/(kW·h)] exhibit <10% variability, although they are based on sunlight intensity measurements (400 nm < λ < 1100 nm) which do not reflect the greater seasonal fluctuations in UV light intensity.

$[OX]_{ss}$ and therefore k_{SENS} were proportional to the average light intensity (correlation coefficient > 0.998), which varied by a factor of 2.9, for experiments illustrated in Figure 5. This suggests that the lifetime of the transient oxidant is probably not controlled by reaction with itself (reaction 3), because this termination step would require k_{SENS} to be proportional to (light intensity)$^{0.5}$.

Primary Photophysical Step. Intersystem crossing (singlet to triplet) of molecules excited by π–π^* and n–π^* transitions is enhanced and unaffected, respectively, by heavy atoms (such as Cs^+) present in the solution (*31*, *32*). DOM triplets are likely precursors for many DOM-derived transient oxidants. Consequently, processes (such as Cs^+ quenching) that may alter $[DOM\ triplet]_{ss}$, and therefore alter photooxidation rates, could provide information about the primary photophysical transition. Rates of fulvic acid (4.1 mg of carbon/L) sensitized photooxidation of TMP in solutions (pH 7.9) containing different concentrations of Cs_2SO_4 (0, 0.010, 0.040, and 0.15 M), at a constant ionic strength of 0.47 M (adjusted with Na_2SO_4), differed by <10%. Therefore, if DOM triplets are precursors of the transient oxidant in these photooxidations, then n–π^* transitions are primarily responsible for DOM triplet production.

Transient Oxidant and Mechanism of Oxidation. Singlet oxygen is known to oxidize the anions of phenols (*20*). Consequently its potential role as the transient ox-

Emerging Developments in Environmental Science

ES&T

ENVIRONMENTAL SCIENCE & TECHNOLOGY

Enter your own monthly subscription to ES&T and be among the first to get the most authoritative technical and scientific information on environmental issues.

☐ **YES! I want my own one-year subscription to ENVIRONMENTAL SCIENCE & TECHNOLOGY at the rate checked below:**

1987 Published monthly	U.S.	Canada & Mexico	Europe	All Other Countries
ACS Members	☐ $ 30	☐ $38	☐ $46	☐ $54
Nonmembers—Personal	☐ $ 45	☐ $53	☐ $61	☐ $69
Nonmembers—Institutional	☐ $176	☐ $184	☐ $192	☐ $200

☐ Payment Enclosed (Payable to American Chemical Society)
☐ Bill Me ☐ Bill Company
Charge my ☐ VISA/MasterCard ☐ Access
☐ Diners Club/Carte Blanche ☐ Barclaycard

Card No. _____

Expires _____ Interbank No. _____
(M/C and Access)

Signature _____

Name _____

Title _____ Employer _____

Address ☐ Home
☐ Business _____

City, State, Zip _____

Employer's Business: ☐ Manufacturing ☐ Academic ☐ Government
☐ Other _____

Member rates are for personal use only.
Subscriptions outside the U.S., Canada, and Mexico are delivered via air service. Foreign payment must be made in U.S. currency by international money order, UNESCO coupons, U.S. bank draft, or order through your subscription agency. For nonmember rates in Japan, contact Maruzen Co., Ltd. Please allow 45 days for your first copy to be mailed. Redeem until December 31, 1987.

680 **MAIL THIS POSTAGE-PAID CARD TODAY!** 3847A

(800) 424-6747 (U.S. only)

NO POSTAGE
NECESSARY
IF MAILED
IN THE
UNITED STATES

BUSINESS REPLY MAIL

FIRST CLASS PERMIT NO. 10094 WASHINGTON, D.C.

POSTAGE WILL BE PAID BY ADDRESSEE

American Chemical Society
Marketing Communications Department
1155 Sixteenth Street, N.W.
Washington, D.C. 20036-9976

(800) 424-6747 (U.S. only)

NO POSTAGE
NECESSARY
IF MAILED
IN THE
UNITED STATES

BUSINESS REPLY MAIL

FIRST CLASS PERMIT NO. 10094 WASHINGTON, D.C.

POSTAGE WILL BE PAID BY ADDRESSEE

American Chemical Society
Marketing Communications Department
1155 Sixteenth Street, N.W.
Washington, D.C. 20036-9976

Table I. Relative Reactivity of Various Compounds, Normalized to Phenol, and Their Estimated Photooxidation Half-Lives in Greifensee Water

compound	reactivity relative to phenol[a]	photooxidation half-life,[b] hours of continuous sunlight		half-life in top meter of Greifensee,[d,e] days
		surface[c]	1-m depth average[d]	
phenol	1	176	455	72
4-nonylphenol	2.6	69	180	29
4-isopropylphenol	5.3	33	85	15
2-methylphenol	7.3	24	60	11
4-ethylphenol	8.9	20 (27)[f]	50	9
4-methylphenol	12.4	14 (46)[g]	35	4.4
4-methoxyphenol	23	7.7	20	2.0
2,6-dimethylphenol	24	7.4	19	1.9
2,4,6-trimethylphenol	41	4.3	11	0.9
benzoate and monohydroxybenzoates (o, m, and p forms)	<0.5	>350	>900	>250
4-dimethoxybenzene	~3	60	150	27
ascorbate	51	3.5	9.0	1.0

[a] [Fulvic acid] = 4.1 mg of carbon/L, pH 8.0, 20 μM initial compound concentration, 0.01 M orthophosphate, ionic strength = 0.072 M, p_{O_2} = 0.21 atm, and temperature = 20 °C in the MGRR. [b] Calculated for Greifensee water with adjusted pH 8.0 using 0.01 M orthophosphate, p_{O_2} = 0.21 atm, temperature = 20 °C, and adjusted ionic strength = 0.072 M, exposed continuously to clear-sky, solar-noon, June sunlight (~1 kW/m^2). [c] Values applicable only for the surface layer. [d] Depth-averaged values for a hypothetical well-mixed and isolated top meter, calculated from the surface values using eq 7 with α_{366} = 0.010 cm^{-1}. Calculations using α_{313} = 0.022 cm^{-1} predict values to be ~1.8 times the values given. [e] Half-life for DOM-sensitized photooxidations. Actual solar data beginning at 11:00 CET 2 June 1985 are used for the estimate. [f] Sunlight photooxidation (25 July 1985) with 7.6 mg of carbon/L of fulvic acid, temperature = 21 °C, pH 8.0, 0.01 M orthophosphate, μ = 0.072 M, and 1.0 μM 4-ethylphenol. The measured k_{SENS} was normalized to (1) 4.1 mg of carbon/L of fulvic acid by multiplying by 0.76 (based on Figure 1), (2) Greifensee water by multiplying by 0.46 (as reported in the text), and (3) June sunlight by multiplying by 1.04. [g] Sunlight photooxidation [calculated from the data of Smith et al. (*21*)] with 9.5 mg/L of humic acid (α_{366} = 0.02 cm^{-1}) from Menlo Park, CA (37.5° N). k_{SENS} was normalized to solar-noon, June, Zürich sunlight by multiplying by 1.15 and to Greifensee water (α_{366} = 0.01 cm^{-1}) by multiplying by 0.5.

idant in these sensitized photooxidations was examined with three independent tests: (1) D_2O solvent isotope effects, (2) azide quenching of $^1O_2$, and (3) kinetic analyses. As shown in previous studies (*1*, *20*), $[^1O_2]_{ss}$ and rates of $^1O_2$ oxidations are greater in D_2O/H_2O mixtures than in pure H_2O because the physical quenching of $^1O_2$ is slower in D_2O than in H_2O (*33*, *34*). Rates of TMP photooxidation ([fulvic acid] = 4.1 mg of carbon/L, pH 8.0) in pure H_2O and in a D_2O/H_2O mixture (90:10 v/v) are predicted to differ by a factor of 6.1 if $^1O_2$ is the oxidant; but in fact, they differ by <5%.

Azide anion physically quenches $^1O_2$ (*35*) and was used to control $[^1O_2]_{ss}$ in DOC-sensitized photooxidations of TMP. Rates of TMP photooxidation ([fulvic acid] = 4.1 mg of carbon/L, pH 8.0) with variable azide concentrations (0, 0.21, 0.50, 1.00 mM) are predicted to vary by up to a factor of 3.0 if $^1O_2$ is the oxidant; but in fact, they differ by <25%.

Furfuryl alcohol (FFA) is oxidized by $^1O_2$ (*36*) and was used to quantify a maximum $[^1O_2]_{ss}$ of 2.1×10^{-12} M for the experiments illustrated in Figure 4e. Maximum contributions of $^1O_2$ reactions to the photooxidations of 4-methylphenol and phenol were calculated from (1) measured $[^1O_2]_{ss}$, (2) published pK_a values of the phenols (*29*), and (3) reported rate constants for the reactions of $^1O_2$ with the phenols (*20*). On the basis of this information, maximum contributions of $^1O_2$ pathways to sensitized photooxidations of 4-methylphenol and phenol are ca. <4% and <22%, respectively, for the experiments performed at pH 8.0 presented in Figure 4e. From these results and from the negative results of the diagnostic $^1O_2$ tests (with D_2O and azide), we conclude that for the pH domain of most natural waters $^1O_2$ is not the oxidant responsible for DOM-sensitized photooxidations of alkylphenols.

Although the intermediacy of $^{\bullet}OH$ in these photooxidations was not examined experimentally, it can be eliminated as a possibility because many phenols are oxidized by $^{\bullet}OH$ at similar diffusion-controlled rates (*18*). This differs considerably from the wide range of phenol reactivities tabulated in Table I.

Tests for the intermediacy of superoxide radical anion ($^{\bullet}O_2^-$) in these photooxidations gave mixed results. Superoxide dismutase (SOD) concentrations of 10 and 100 mg/L, sufficient to scavenge most $^{\bullet}O_2^-$, decreased the rate of DOM-sensitized TMP photooxidation by up to 50% but increased the rate of 4-methylphenol photooxidation by a factor of 2.6, relative to controls without SOD. Although high SOD concentrations were used, these results could indicate that $^{\bullet}O_2^-$ may play different roles in reactions with phenols and possibly with intermediates generated in oxidations of phenols.

Organic oxy radicals (RO$^{\bullet}$) and excited-state humic acid triplets are probably not controlling DOM-sensitized photooxidation of alkylphenols. Das et al. (*37*) found that relative reactivities (normalized to phenol) of (1) 4-methylphenol, 2-methylphenol, 4-ethylphenol, and 4-isopropylphenol and (2) 4-methoxyphenol with *tert*-butoxy radicals range between 1.6 and 1.7 and between 4.8 and 6.4, respectively. They also found (*38*) that relative reactivities (normalized to phenol) of 4-methoxyphenol, 4-methylphenol, 4-ethylphenol, and 4-isopropylphenol with carbonyl triplets range between 1 and 3.5. In contrast, the relative reactivities of the same phenols determined in this study (Table I) are much larger and more variable. Although the other investigations (*37*, *38*) were performed in nonaqueous solvents, *relative* reactivities of 4-methoxyphenol and phenol with *tert*-butoxy radicals were remarkably similar for polar and nonpolar solvents (*37*). Observed rates of DOM-sensitized TMP photooxidation in sunlight (this work, Figure 5) are faster than upper bounds for rates of DOM triplet mediated reactions in sunlit natural waters, as reported by Zepp et al. (*39*).

Mill et al. (*7*) have reported that sunlit natural waters contain DOM-derived organic peroxy radicals (ROO$^{\bullet}$), and Smith et al. (*21*) have suggested that ROO$^{\bullet}$ are responsible for sensitized photooxidations of 4-methylphenol in natural

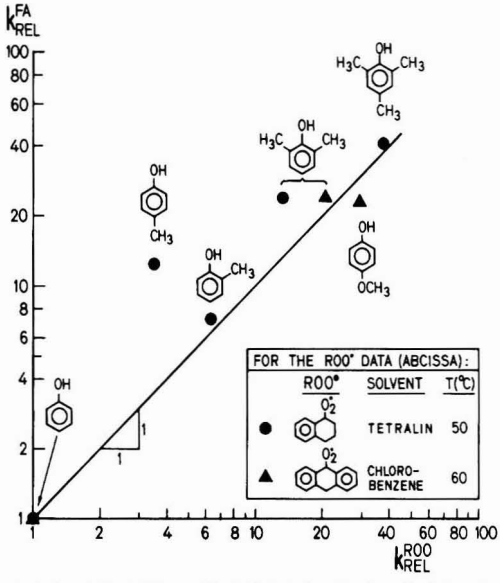

Figure 6. Relative rate constants (normalized to phenol) of phenols: (1) in fulvic acid sensitized photooxidations, k_{REL}^{FA} (this work); (2) toward organic peroxy radicals in organic solvents, k_{REL}^{ROO} [Howard and Scaiano (*41*)]. Experimental conditions for our studies are given in Figure 4.

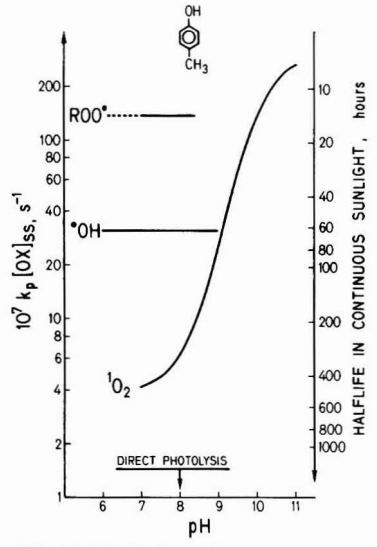

Figure 7. Calculated (for Greifensee) apparent first-order rate constants ($k_P[OX]_{ss}$) and corresponding half-lives for 4-methylphenol oxidation by the transient oxidant reported on here (proposed ROO•), by •OH, and by $^1O_2$ and the first-order rate constant for its direct photolysis. For ROO•, k_{SENS} ($=k_P[OX]_{ss}$) was measured and normalized to Greifensee with eq 9. Calculations for •OH and $^1O_2$ were based on their reported steady-state concentrations (*1*, *3*, *4*) and rate constants (*18*, *20*). All calculations apply to the surface layer of Greifensee (20 °C) in continuous clear-sky, solar-noon, June sunlight (~1 kW/m^2).

waters. In general, phenols are known to react with organic peroxy radicals (*40*, *41*). As illustrated in Figure 6, relative reactivities of phenols in DOM-sensitized photooxidations are similar to their relative reactivities in reactions with ROO•. This result and the requirement of oxygen for the photooxidation are also consistent with the idea that organic peroxy radicals control DOM-sensitized alkylphenol photooxidations. Molecular oxygen could possibly react with DOM triplet diradicals to produce organic peroxy radicals.

Sensitized Photooxidation Half-Lives of Phenols in Natural Waters. Table I presents estimates of half-lives for DOM-sensitized photooxidations of various compounds in the Greifensee. Surface rate constants, used for calculating surface half-lives, were determined from eq 9, where

$$k_{P,SUN}^{GREIF} = \frac{k_{P,MGRR}^{FA}}{k_{TMP,MGRR}^{FA}} \frac{k_{TMP,SUN}^{GREIF}}{k_{TMP,SUN}^{FA}} k_{TMP,SUN}^{FA} \qquad (9)$$

FA (4.1 mg of carbon/L of fulvic acid) and GREIF (Greifensee) specify the DOM sources, MGRR (merry-go-round reactor) and SUN (sunlight) specify the illumination conditions, and TMP and P (compound of interest) are the compounds being photooxidized. All rate constants in eq 9 are apparent first-order rate constants. The reactivity of a given compound relative to that of TMP in the MGRR ($k_{P,MGRR}^{FA}/k_{TMP,MGRR}^{FA}$) is assumed to be the same in sunlight, because the variability is <60% (see Light Source Effects and Sunlight Dosimetry). The reactivity of Greifensee water relative to that of the 4.1 mg of carbon/L of fulvic acid solution ($k_{TMP,SUN}^{GREIF}/k_{TMP,SUN}^{FA}$) was 0.46 when determined in sunlight (May 86) with TMP and 0.53 when determined in the MGRR with TMP and 4-ethylphenol. The former value was used to normalize the calculations to Greifensee water. $k_{TMP,SUN}^{FA}$ can be expressed as an exposure dose based rate constant for fulvic acid sensitized photooxidation of TMP in sunlight. An average value of $k_{TMP,SUN}^{FA} = 0.32$ m^2/(kW·h), determined from the results presented in Figure 5, was used for all calculations.

The last column of Table I illustrates that depth-averaged half-lives for DOM-sensitized photooxidations of alkylphenols in the top meter of Greifensee (assuming this to be well mixed and physically isolated) range between 1 day and several months. Because most photoactive light is absorbed in the top meter of Greifensee, depth-averaged half-lives for depths >1 m (assuming rapid mixing) are approximately proportional to depth.

General Comments and Environmental Significance

Figure 7 compares the rates of 4-methylphenol oxidation by different photochemical processes in the surface layer of Greifensee. Oxidation of 4-methylphenol by the transient oxidant reported on here (proposed ROO•) dominates all other photooxidation pathways throughout the pH range typical of most natural waters.

Alkylphenols are a subset of the compounds generally referred to as "antioxidants". Antioxidants such as aromatic amines, imines, and thiophenols are also known to react with organic peroxy radicals (*41*) and are expected to exhibit fairly high reactivity toward the transient oxidant reported on in this study. Additionally, electron-transfer reactions involving ROO• may represent a previously unrecognized pathway for the oxidation of some compounds in natural waters.

Biodegradation of phenols is the only mechanism that will effectively compete with DOM-sensitized photooxidations for controlling the degradation of alkylphenols in natural waters. Estimates of biodegradation half-lives for phenol in natural waters range between 0.1 and 10 days (*42–44*). Paris et al. (*42*) found that phenols substituted in the para position, with either electron-withdrawing or electron-donating groups, were biodegraded more slowly than phenol itself. We therefore assume that the *lower*

bound for biodegradation half-lives of substituted phenols in most natural waters ranges between 0.1 and 10 days. This may be compared with DOM-sensitized photooxidation half-lives in Table I.

Regardless of the identity of the DOM-derived transient oxidant, the functional dependence of $[OX]_{ss}$ values on [DOM] is affected by the controlling termination step (reactions 1–4). For waters with low [DOM], where unimolecular decay (reaction 4) controls the lifetime of OX, surface $[OX]_{ss}$ is proportional to [DOM], but depth-averaged (for $\alpha_\lambda L > 1$, see eq 7) $[OX]_{ss}$ is independent of [DOM] and inversely proportional to depth. However, for waters where scavenging reactions of the DOM (reaction 2, with $S_i \equiv$ DOM) control the lifetime of OX, surface $[OX]_{ss}$ is independent of [DOM], but depth-averaged (for $\alpha_\lambda L > 1$) $[OX]_{ss}$ is inversely proportional to [DOM] and depth.

The formation rate of the transient oxidant reported on here (proposed ROO•) could not be estimated because (1) rate constants for its decomposition processes (reactions 2 and 4) are unknown and (2) complete scavenging of the transient oxidant by TMP (using [TMP] $\gg$ 20 μM) was not attained because TMP reacted with precursors of the transient oxidant.

Compilations of absolute rate constants for reactions of ROO• in the liquid phase are available (*41*, *45*), but only a few of the reactions were studied in water. The reactivity of compounds with ROO• in hydrogen abstraction reactions is lower in H_2O than in many other solvents, due to hydrogen bonding between ROO• and H_2O (*41*). Consequently, absolute rate constants for ROO• reactions determined in nonaqueous solvents are not recommended for use in environmental fate modeling of chemicals. However, relative reactivities of different compounds toward the same ROO• in the same solvent should be useful for planning ROO• kinetic experiments in aqueous systems.

Conclusions

A photogenerated DOM-derived transient oxidant, which is probably an organic peroxy radical (ROO•), exhibits high reactivity toward various phenols. This oxidant largely controls photooxidations of alkylphenols in sunlit natural waters (half-lives ranging from 1 day to months); singlet oxygen and hydroxyl radical play only minor roles in these photooxidations.

Reactivity of alkylphenols toward the transient oxidant increases with increasing ring substitution by methyl groups but decreases with increasing size of the alkyl group for 4-alkylphenols.

For the above reasons, 2,4,6-trimethylphenol is recommended as a probe molecule for calibrating the peroxy radical activity of sunlit natural waters.

For well-mixed waters with lower DOM concentrations, the steady-state concentration of the transient oxidant is proportional to [DOM] in the surface layer but independent of [DOM] when averaged over depths for which most of the photoactive light is absorbed. Depth-averaged $[OX]_{ss}$ values are inversely proportional to depth for depths where most of the photoactive light is absorbed.

Absolute reaction rate constants for DOM-derived ROO• cannot be given, because DOM-derived ROO• (like DOM) are a mixture with unknown and source water dependent speciation.

Acknowledgments

We thank F. E. Scully and M. Ahel for preliminary observations that led to this study and R. Zepp for discussions. We also thank R. Schwarzenbach, L. Nowell, and B. Sulzberger for reviewing the manuscript and H. Ambühl and R. Ribi for the light photometry data.

Registry No. O_2, 7782-44-7; phenol, 108-95-2; 4-nonylphenol, 104-40-5; 4-isopropylphenol, 99-89-8; 2-methylphenol, 95-48-7; 4-methylphenol, 106-44-5; 4-ethylphenol, 123-07-9; 4-methoxyphenol, 150-76-5; 2,6-dimethylphenol, 576-26-1; 2,4,6-trimethylphenol, 527-60-6; 4-dimethoxybenzene, 150-78-7; *o*-hydroxybenzoic acid, 69-72-7; *m*-hydroxybenzoic acid, 99-06-9; *p*-hydroxybenzoic acid, 99-96-7; 9,10-dihydro-9-anthracenyldioxy, 20387-25-1; 1,2,3,4-tetrahydro-1-naphthalenyldioxy, 20387-23-9.

Literature Cited

(1) Haag, W. R.; Hoigné, J. *Environ. Sci. Technol.* **1986**, *20*, 341–348.
(2) Zepp, R. G.; Wolfe, N. L.; Baughman, G. L.; Hollis, R. C. *Nature (London)* **1977**, *267*, 421–423.
(3) Zepp, R. G.; Hoigné, J.; Bader, H. *Environ. Sci. Technol.* **1987**, *21*, 443–450.
(4) Haag, W. R.; Hoigné, J. *Chemosphere* **1985**, *14*, 1659–1671.
(5) Russi, H.; Kotzias, D.; Korte, F. *Chemosphere* **1982**, *11*, 1041–1048.
(6) Zafiriou, O. C. *J. Geophys. Res.* **1974**, *79*, 4491–4497.
(7) Mill, T.; Hendry, D. G.; Richardson, H. *Science (Washington, D.C.)* **1980**, *207*, 886–887.
(8) Mill, T.; Richardson, H.; Hendry, D. G. In *Aquatic Pollutants: Transformations and Biological Effects*; Hutzinger, O., Van Lelyveld, I. H., Zoeteman, B. C. J., Eds.; Pergamon: New York, 1978; Vol. 1, pp 223–236.
(9) Hoigné, J.; Bader, H. *Ozone: Sci. Eng.* **1979**, *1*, 357–372.
(10) Julkunen-Tiitto, R. *J. Agric. Food Chem.* **1985**, *33*, 213–217.
(11) Leuenberger, C.; Ligocki, M. P.; Pankow, J. F. *Environ. Sci. Technol.* **1985**, *19*, 1053–1058.
(12) Goerlitz, D. F.; Troutman, D. E.; Godsy, E. M.; Franks, B. J. *Environ. Sci. Technol.* **1985**, *19*, 955–961.
(13) Leenheer, J. A.; Noyes, T. I.; Stuber, H. A. *Environ. Sci. Technol.* **1982**, *16*, 714–723.
(14) Throop, W. W. *J. Hazard. Mater.* **1975**, *1*, 319–329.
(15) Ahel, M.; Giger, W. *Anal. Chem.* **1985**, *57*, 1577–1583.
(16) Baker, E. L.; Landrigan, P. J.; Field, P. H.; Basteyns, B. J.; Bertozzi, P. E.; Skinner, H. G. *Arch. Environ. Health* **1978**, *33*, 89–94.
(17) McLeese, D. W.; Zitko, V.; Sergeant, D. B.; Burridge, L.; Metcalfe, C. D. *Chemosphere* **1981**, *10*, 723–730.
(18) Farhataziz; Ross, A. B. *Natl. Stand. Ref. Data Ser. (U.S., Natl. Bur. Stand.)* **1977**, *No. 59*.
(19) Wilkinson, F.; Brummer, J. G. *J. Phys. Chem. Ref. Data* **1981**, *10*, 809–999.
(20) Scully, F. E.; Hoigné, J. *Chemosphere* **1987**, *16*, 681–694.
(21) Smith, J. H.; Mabey, W. R.; Bohonos, N.; Holt, B. R.; Lee, S. S.; Chou, T.-W.; Bomberger, D. C.; Mill, T. *Environmental Pathways of Selected Chemicals in Freshwater Systems: Part II. Laboratory Studies*; U.S. Government Printing Office: Washington, DC, 1978; EPA Report EPA-600/7-78-074.
(22) Mill, T. *Structure Reactivity Correlations for Environmental Reactions*; U.S. Government Printing Office: Washington, DC, 1979; EPA Report EPA-560/11-79-012.
(23) Pohlman, A.; Mill, T. *J. Org. Chem.* **1983**, *48*, 2133–2138.
(24) Pohlman, A. A.; Mill, T. *Soil Sci. Soc. Am. J.* **1983**, *47*, 922–927.
(25) Underdown, A. W.; Langford, C. H.; Gamble, D. S. *Environ. Sci. Technol.* **1985**, *19*, 132–136.
(26) Omaye, S. T.; Turnbull, J. D.; Sauberlich, H. E. *Methods Enzymol.* **1979**, *62*, Part D, 6–7.
(27) Zepp, R. G. In *The Handbook of Environmental Chemistry*; Hutzinger, O., Ed.; Springer-Verlag: Berlin, 1982; Vol. 2, Part B, pp 19–41.
(28) Zepp, R. G.; Schlotzhauer, P. F. *Chemosphere* **1981**, *10*, 479–486.
(29) Martell, A. M.; Smith, R. M. *Critical Stability Constants*; Plenum: New York, 1977; Vol. 3.
(30) Zepp, R. G.; Baughman, G. L.; Schlotzhauer, P. F. *Chemosphere* **1981**, *10*, 119–126.
(31) Zechner, J.; Köhler, G.; Grabner, G.; Getoff, N. *Chem. Phys. Lett.* **1976**, *37*(2), 297–300.

(32) Wagner, P. J. *J. Chem. Phys.* **1966**, *45*, 2335–2336.
(33) Merkel, P. B.; Kearns, D. R. *J. Am. Chem. Soc.* **1972**, *94*, 1029–1030.
(34) Rodgers, M. A. J.; Snowden, P. T. *J. Am. Chem. Soc.* **1982**, *104*, 5541–5543.
(35) Haag, W. R.; Mill, T. *Photochem. Photobiol.* **1987**, *45*, 317–321.
(36) Haag, W. R.; Hoigné, J.; Gassmann, E.; Braun, A. M. *Chemosphere* **1984**, *13*, 631–640.
(37) Das, P. K.; Encinas, M. V.; Steenken, S.; Scaiano, J. C. *J. Am. Chem. Soc.* **1981**, *103*, 4162–4166.
(38) Das, P. K.; Encinas, M. V.; Scaiano, J. C. *J. Am. Chem. Soc.* **1981**, *103*, 4154–4162.
(39) Zepp, R. G.; Schlotzhauer, P. F.; Sink, R. M. *Environ. Sci. Technol.* **1985**, *19*, 74–81.
(40) Burton, G. W.; Doba, T.; Gabe, E. J.; Hughes, L.; Lee, F. L.; Prasad, L.; Ingold, K. U. *J. Am. Chem. Soc.* **1985**, *107*, 7053–7065.
(41) Howard, J. A.; Scaiano, J. C. *Landolt Börnstein New Series, Kinetic Rate Constants of Radical Reactions in Solution: Part d, Oxyl-, Peroxyl-, and Related Radicals*; Springer-Verlag: Berlin-Heidelberg, 1984; Series II/13d.
(42) Paris, D. F.; Wolfe, N. L.; Steen, W. C.; Baughman, G. L. *Appl. Environ. Microbiol.* **1983**, *45*(3), 1153–1155.
(43) Rubin, H. E.; Alexander, M. *Environ. Sci. Technol.* **1983**, *17*, 104–107.
(44) Subba-Rao, R. V.; Rubin, H. E.; Alexander, M. *Appl. Environ. Microbiol.* **1982**, *43*(5), 1139–1150.
(45) Hendry, D. G.; Mill, T.; Piszkiewicz, L.; Howard, J. A.; Eigenmann, H. K. *J. Phys. Chem. Ref. Data* **1974**, *3*, 937–978.

Received for review September 23, 1986. Accepted May 29, 1987. This work was supported by the Presidential Foundation of the Swiss Federal Institute of Technology under the project title "Abiotische photochemische Oxidationsprozesse in Gewässern".

Polychlorinated Dibenzofurans and Dibenzo-*p*-dioxins and Other Chlorinated Contaminants in Cow Milk from Various Locations in Switzerland

Christoffer Rappe,* Martin Nygren, and Gunilla Lindström

Department of Organic Chemistry, University of Umeå, S-901 87 Umeå, Sweden

Hans Rudolf Buser

Swiss Federal Research Station, CH-8820 Wädenswil, Switzerland

Otto Blaser and Claude Wüthrich

Swiss Federal Office of Public Health, CH-3000 Bern, Switzerland

■ Six samples of cow milk from various locations in Switzerland were analyzed for polychlorinated dibenzofurans (PCDFs), polychlorinated dibenzo-*p*-dioxins (PCDDs), and other chlorinated contaminants. Sub parts per trillion levels of 2,3,7,8-substituted PCDFs and PCDDs were found in all samples. The levels were higher in samples collected in the vicinity of incinerators. Non-2,3,7,8-substituted PCDDs and PCDFs were not found in the milk samples.

Introduction

The polychlorinated dibenzo-*p*-dioxins (PCDDs) and the polychlorinated dibenzofurans (PCDFs) are two groups of compounds that exhibit similar chemical and physical properties; the chemical structures are given in Figure 1. The number of chlorine atoms in these compounds can vary between one and eight ($x + y = 1$–8, see Figure 1) to produce 75 PCDD and 135 PCDF positional isomers. Twelve of these isomers have strong toxic effects (*1*), specifically 2,3,7,8-tetra-CDD but also other 2,3,7,8-substituted PCDDs and PCDFs with four, five, and six chlorine atoms. They are listed in Table I.

In 1977, Olie et al. (*2*) reported on the occurrence of PCDDs and PCDFs in fly ash from municipal incinerators in The Netherlands. Although their results indicated the presence of up to 17 PCDD peaks, quantification or isomer identification was not possible because of the lack of synthetic standards. In a series of papers, Buser et al. (*3–5*) investigated fly ash from a municipal solid waste (MSW) incinerator and an industrial heating facility, both in Switzerland. A series of PCDDs and PCDFs were identified, and the levels in fly ash were in the range of 0.1–10 μg/g total PCDDs and PCDFs. Since then, many reports from Europe, USA, Canada, and Asia have confirmed these original findings. However, for many years the interest was focused on the analysis of fly ash samples and not on the analysis of actual emissions, probably due to sampling difficulties.

Table I. Most Toxic PCDD and PCDF Isomers

PCDDs	PCDFs
2,3,7,8-tetra-CDD	2,3,7,8-tetra-CDF
1,2,3,7,8-penta-CDD	1,2,3,7,8-penta-CDF
1,2,3,6,7,8-hexa-CDD	2,3,4,7,8-penta-CDF
1,2,3,7,8,9-hexa-CDD	1,2,3,6,7,8-hexa-CDF
1,2,3,4,7,8-hexa-CDD	1,2,3,7,8,9-hexa-CDF
	1,2,3,4,7,8-hexa-CDF
	2,3,4,6,7,8-hexa-CDF

Most of the analyses of emissions from incinerators have been done with nonvalidated and non-isomer-specific sampling and analytical methods. Recent studies show the presence of a multitude of PCDD and PCDF congeners, in the emission samples (*6*). Moreover, a striking similarity in the isomeric pattern of PCDDs and PCDFs was found between samples from different incinerators (*6, 7*).

Various models have been used to convert a multitude of levels of more or less toxic PCDDs and PCDFs into a more simple expression like "TCDD equivalents" or "toxic equivalents" (*8*). In Sweden and in this paper, the approach discussed by Eadon et al. (*9*) has been used.

Emissions from MSW incinerators operating under good condition are in the range of 1–100 ng of TCDD equiv/normalized m^3 (9, 10), resulting in total annual emissions of 1–100 g of TCDD equiv from a normal size MSW incinerator (50–200 000 tons of waste/year). The major chlorine source in the MSW is plastic material such as

 0013-936X/87/0921-0964$01.50/0

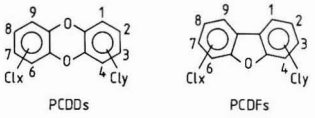

Figure 1. Structures of PCDDs and PCDFs.

Table II. Analytical Data on Milk Samples

sample no.[a]	amount of milk, g	extracted fat, g	amount of fat for analysis, g	amount of fat for analysis, %
1	601.09	23.90	21.40	89.54
2	600.08	26.20	23.66	90.31
3	600.25	25.70	23.23	90.39
4	600.82	26.88	24.27	90.29
5	603.13	19.12	16.69	87.29
6	601.49	20.99	18.34	87.37
blank				92.0

[a] For origin of the sample, see text.

PVC and bleached and unbleached paper. New technologies are now available to reduce these emissions.

In April 1984, Rappe et al. (*10*) reported on a series of the toxic 2,3,7,8-substituted PCDDs and PCDFs in samples of human adipose tissue from Northern Sweden. A series of reports presented at the dioxin conferences in Ottawa, Canada, in October 1984, Miami, FL, in April 1985, and in Bayreuth, West Germany, in September 1985 confirmed these observations, and it is clearly shown that there is a background of PCDDs and PCDFs in the general human population in the industrialized part of the world.

In April 1984, Rappe et al. also reported on the analysis of five samples of breast milk from West Germany (*10*). Later data from Sweden, Denmark, The Netherlands, Yugoslavia, and Vietnam have also been published (*11*) indicating the same background in the general population.

It is generally accepted that the major route of exposure to these compound is via food. The same 2,3,7,8-substituted PCDDs and PCDFs have been identified in ppt levels in fish from the Baltic Sea and The Great Lakes (*12, 13*). In this paper we report on ppt levels or below of these congeners in samples of cow milk from Switzerland.

Experimental Section

Milk Samples. The following six milk samples (about 1 L each) were collected by the provincial authorities:

(1) Consumer's milk, pasteurized from Bern, Switzerland. This was a pooled control sample.

(2) Milk from a single cow in Bowil, BE, Switzerland. Bowil is situated 9 km from the community of Langnau and 16 km from a small MSW incinerator (Krauchtal) and 20 km from a larger MSW incinerator, Bern.

(3) Milk from the local dairy in Bowil, BE (13 producers). This was a pooled control sample.

(4) Milk from a single cow in Hunzenschwil, AG, Switzerland. The farmland is situated 200–1000 m SE from a typical middle-sized MSW incinerator (40 000 ton/year), Buchs, AG.

(5) Milk from a single cow in Suhr, Switzerland. The farmland is situated 300–1000 m SW from the same incinerator as in sample four.

(6) Milk from a single cow in Rheinfelden, AG, Switzerland. The farmland is situated 1000 m SE from Rheinfelden, FRG, a production site for various chlorinated products.

(7) Blank sample treated as a cow milk sample.

The amount of milk analyzed is given in Table II.

Table III. Ions Used for Detection and Quantification of PCDDs and PCDFs in GC/MS Analyses

compound	mode	ions monitored[a]
tetra-CDFs	NICI	304 (M^-), *306*
penta-CDFs	NICI	338 (M^-), *340*
hexa-CDFs	NICI	372 (M^-), *374*
hepta-CDFs	NICI	406 (M^-), *408*
octa-CDF	NICI	442 ($M^- + 2$), *444*
penta-CDDs	NICI	354 (M^-), *356*
hexa-CDDs	NICI	353 ($M^- - Cl$), *355*
hepta-CDDs	NICI	387 ($M^- - Cl$), *389*
octa-CDD	NICI	423 ($M^- + 2 - Cl$), *425*
[$^{13}C_{12}$]-2,3,7,8-tetra-CDF	NICI	*318* ($M^- + 2$)
[$^{13}C_{12}$]octa-CDD	NICI	*435* ($M^- + 2 - Cl$)
tetra-CDDs	EI	*320* (M^+)
[$^{13}C_{12}$]-2,3,7,8-tetra-CDD	EI	*332* (M^+)

[a] Ion used for quantification is italicized.

Extraction Procedure. The milk samples were extracted in two portions of about 300 mL each. Each milk portion was fortified with 500 pg of [^{13}C]-2,3,7,8-tetra-CDD. Thereafter, 3 g of sodium oxalate dissolved in 50 mL of boiling water, 300 mL of ethanol, and 125 mL of diethyl ether were added. After vigorous shaking, 175 mL of *n*-hexane was added, and the mixture was then shaken again. After separation of the two phases, the aqueous layer was reextracted twice with 100-mL portions of *n*-hexane. The combined extracts were washed twice with 200 mL of water each and dried by passage through a column of sodium sulfate. The solvent was evaporated until a constant weight was obtained, and the amount of fat was recorded (Table II). A portion of about 10% of the dried material was removed for pesticide analyses. The remaining portion (18–24 g of milk fat, Table II) was used for the analyses of PCDDs and PCDFs.

Determination of PCDDs and PCDFs. For the analyses of milk fat we have used the cleanup method discussed in detail by Smith et al. (*14*). This procedure involves passing the sample through five chromatographic columns in sequence, and the key step in this procedure is a column of carbon dispersed on glass fibers. This column adsorbs most planar polynuclear polychlorinated aromatics and allows the major portion of biological coextractants to pass through. Along with similar chemicals, the PCDDs and PCDFs are then removed from the carbon column by reverse elution with toluene. Due to differences in column material and solvent quality between Europe and the U.S., some slight modifications of the Stalling–Smith sample workup methods have been introduced in our laboratory (to be published). The modified method has recently been verified by analyzing blanks and fish samples fortified at two different levels (*15*) and also by analyzing samples of cow milk and human milk fortified at three different levels (to be published). Before cleanup the milk fat extracts (18–24 g) were fortified with 500 pg each of [$^{13}C_{12}$]-2,3,7,8-tetra-CDF and [$^{13}C_{12}$]octa-CDD.

After cleanup the extracts were analyzed by gas chromatography–mass spectrometry using high-resolution fused silica or glass capillary columns specific for 2,3,7,8-substituted PCDDs (*16*) and PCDFs (*1*). The instruments, columns, and conditions were as follows:

A Finnigan 4023 instrument with a 4500 ion source operating in the negative ion chemical ionization mode (NICI) was used for tetra- to octachlorinated dibenzofurans and penta- to octachlorinated dioxins. For the chromatographic separation, we used a 60-m SP 2330 fused silica column. The temperature program for the GC oven was 100 °C isothermal for 2 min, then 100–180 °C (20 deg/min), followed by 180–260 °C (3 deg/min). The temper-

Table IV. PCDF and PCDD Content of Swiss Cow Milk from Various Locations[a]

compound	blank	Bern	Bowil	Bowil	Hunzen-schwil	Suhr	Rhein-felden
recovery of [^{13}C]-2,3,7,8-tetra-CDF, %	65	64	57	57	63	57	51
recovery of [^{13}C]-2,3,7,8-tetra-CDD, %	80	90	100	105	90	78	88
recovery of [^{13}C]octa-CDD, %	86	59	55	77	72	72	48
2,3,7,8-tetra-CDF	ND (<0.01)	≤0.028	≤0.035	≤0.021	≤0.022	≤0.032	≤0.028
1,2,3,7,8-penta-CDF	ND (<0.01)	≤0.020	≤0.022	≤0.021	≤0.020	≤0.036	≤0.032
2,3,4,7,8-penta-CDF	ND (<0.01)	0.084	0.066	0.069	0.43	0.22	0.23
1,2,3,4,7,8-hexa-CDF	ND (<0.01)	≤0.020	≤0.026	≤0.017	0.13	0.06	0.084
1,2,3,6,7,8-hexa-CDF	ND (<0.01)	0.028	≤0.018	≤0.021	0.19	0.095	0.059
2,3,4,6,7,8-hexa-CDF	ND (<0.01)	≤0.020	≤0.018	ND (<0.02)	0.28	0.12	0.049
1,2,3,4,6,7,8-hepta-CDF	ND (<0.1)	≤0.12	ND (<0.13)	ND (<0.08)	0.49	0.28	≤0.18
octa-CDF	ND (<0.1)	≤0.20	ND (<0.13)	ND (<0.09)	ND (<0.16)	ND (<0.21)	≤0.52
2,3,7,8-tetra-CDD	ND (<0.01)	ND (<0.012)	ND (<0.013)	ND (<0.013)	0.049	0.038	0.021
1,2,3,7,8-penta-CDD	ND (<0.06)	ND (<0.04)	ND (<0.08)	ND (<0.06)	0.25	≤0.086	ND (<0.1)
1,2,3,4,7,8-hexa-CDD	ND (<0.06)	≤0.068	ND (<0.1)	ND (<0.06)	0.23	0.14	≤0.14
1,2,3,6,7,8-hexa-CDD	ND (<0.06)	≤0.068	ND (<0.1)	ND (<0.06)	0.29	0.16	≤0.21
1,2,3,7,8,9-hexa-CDD	ND (<0.06)	≤0.068	ND (<0.1)	ND (<0.06)	0.17	≤0.080	≤0.11
1,2,3,4,6,7,8-hepta-CDD	ND (<0.05)	≤0.064	≤0.066	≤0.064	0.26	≤0.095	0.42
octa-CDD	≤0.1	≤0.16	≤0.26	≤0.12	0.28	≤0.16	0.59

[a] Results in ng/kg (ppt), whole milk basis. Note: detection limit values are given in parentheses.

ature was then kept at 260 °C for 30 min. The total time of an analysis is 62 min. The ions used for detection are listed in Table III. Methane was used as reagent gas (0.78 Torr/6 × 10^{-5} Torr, 130 eV). An INCOS data system was used.

A Finnigan 4000 instrument operating in the electron-impact mode (EI) was used for tetra-CDDs with a 53-m Silar 10 c glass capillary column (similar to SP 2330). The temperature program for these analyses was 100–180 °C (20 deg/min) and then 180–260 °C (5 deg/min); in addition, some samples were analyzed at 2 deg/min. The ions used for detection of the native and the [^{13}C]-2,3,7,8-tetra-CDD are also listed in Table III. These EI analyses had to be carried out because tetra-CDDs have low sensitivity in the NICI mode. An analog system (PROMIM) was used for quantification.

The samples were dissolved in 30 μL of toluene, and an aliquot of 3 μL ($^1/_{10}$) was injected. Quantification is based on authentic, native compounds injected prior, during, and after a series of samples (typically 10 pg for NICI and 25 pg for EI analyses). Detection limits ranged from about 0.5 to 2 pg per compound injected in both the NICI and EI modes. Recovery data for the [^{13}C]PCDD and [^{13}C]P-CDF analogues were calculated from the signals observed at the proper m/z values in comparison to reference samples with the same amounts of internal standards but not carried through the cleanup procedure.

The recoveries (Table IV) of the [^{13}C]-2,3,7,8-tetra-CDF in the six milk samples and in the blank sample ranged from 51 to 64%; that of [^{13}C]octa-CDD in the same samples ranged from 48 to 77%. The recoveries of [^{13}C]-2,3,7,8-tetra-CDD ranged from 78 to 105% and are high due to some concentration of the sample because of solvent evaporation of the sample prior to EI analysis. All results are corrected for these recovery values (recovery values for the penta-, hexa-, and heptachloro compounds are interpolated from those of tetra- and octachlorinated congeners).

Identifications of PCDDs and PCDFs were based on the fact that signals were observed at the characteristic m/z values (Table IV) at the proper retention times on the high-resolution gas chromatographic columns used and on the proper ratio of these responses at the two m/z values. The identifications are further supported by the fact that these compounds are found in the proper fractions after an extensive cleanup highly specific for planar chlorinated aromatic compounds such as PCDDs and PCDFs.

Determination of Chlorinated Pesticides and Other Contaminants. A sample of 1.3–1.5 g of milk fat was used to determine and quantify the chlorinated pesticides and other contaminants. These substances were separated from fat and other coextractives by gel-permeation chromatography on a polystyrene gel (Bio-Beads SX-3) as described by Specht and Tillkes (*17*), followed by a cleanup step with a small silica gel column. To separate the PCBs, HCB, *p,p'*-DDE, and octachlorostyrene from other pesticides, these substances were eluted from the silica gel column in a first elution step with *n*-hexane. All the further eluting steps were carried out as described in ref 17. The eluates were then analyzed by gas chromatography, using EC and FP detectors. For recovery studies, milk fat was spiked with a mixture of chlorinated pesticides, PCBs, and octachlorostyrene in the range of 5–100 ppb. The mean recovery obtained was 82 ± 10% (exception, β-HCH = 69%).

Determination of Pentachlorophenol (PCP). The milk sample was hydrolyzed with HCl and extracted with diethyl ether. PCP was then separated from the main part of the other coextractants by shaking it with a solution of 0.2 M KOH. After acidification with HCl (pH <1), the PCP was extracted into petroleum ether. The solution containing PCP was then methylated with diazomethane and the sample solution filled up to a fixed volume with *n*-hexane. A portion of this solution was pressed through a Sep-Pak-Florisil cartridge (Waters Assoc., Milford, MA). The methylated PCP was then eluted from the cartridge with petroleum ether–diethyl ether (96:4 v/v). The eluate was analyzed by gas chromatography, using an EC detector. For recovery, milk was spiked with 2.5 ppb PCP. The recovery obtained was 115%.

Results and Discussion

The results obtained for PCDDs and PCDFs found in the cow milk samples are reported in Table IV. They are classified into 3 categories as follows:

ND, not detected (limits of detection given in parentheses)

likely presence of a compound at or below a set significance level; in these cases a signal was observed at a signal to noise ratio S/N ≤ 3

presence of a compound at the level indicated; in these cases the signals observed had a S/N ratio ≥ 3

Table V. Levels of Pesticides and Other Contaminants in Milk Samples (μg/g on Fat Basis)

compound	Bern	Bowil	Bowil	Hunzenschwil	Suhr	Rheinfelden
p,p'-DDE[a]	<15	<9.3	<9.2	<42	<8	<17
p,p'-DDD						<2
p,p'-DDT						2.1
dieldrin	12	6.6	5.5	15	9.5	33
endosulfan sulfate	1.9	2.4	3.5	2.4	1.3	4.8
heptachlorepoxide	2.1	2.0	2.1	3.5	1.5	1.9
HCB	12	7.0	9.6	18	8.8	138
α-HCH	18	27	22	18	14	9.5
β-HCH	1.7	4.0	1.7	2.2	1.0	1.0
lindane	3.1	3.3	3.6	3.0	4.3	5.1
octachlorostyrene	<0.2	<0.2	<0.2	0.4	0.2	4.5
pentachlorophenol	0.6	1	0.4	1.3	0.6	1.4
PCB	41	34	43	144	64	142

[a] With interfering PCBs.

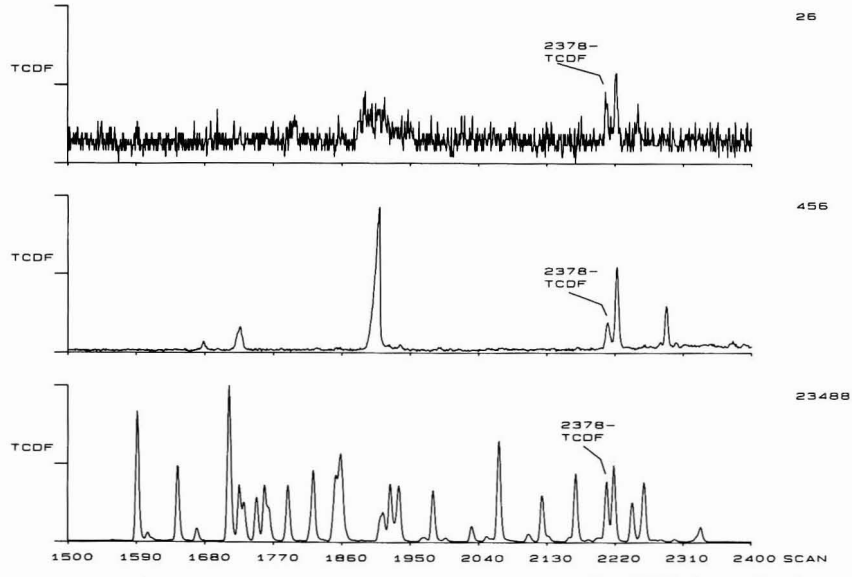

Figure 2. Ion curves of tetra-CDFs of cow milk (upper), human milk (middle), and emission from MSW incinerator (lower), see text.

The results for the other chlorinated pesticides or contaminants are collected in Table V.

All milk samples analyzed showed the presence of some PCDDs or PCDFs, tetra through octa. A blank sample analyzed in the same way however showed no detectable amounts of these compounds, except a trace of octa-CDD (S/N < 3). The PCDD and PCDF isomers detected in these milk samples exclusively are 2,3,7,8-substituted (compare Tables I and IV), including 2,3,7,8-tetra-CDD in some of the samples.

Among the PCDDs detected, two samples (Hunzenschwil and Rheinfelden) showed significant levels of hepta- and octa-CDD; some other samples likely contain some traces but not at a significant level. Two of the samples also contain significant levels of penta- and hexa-CDDs. In the samples from Rheinfelden and Bern the penta- and hexa-CDDs are detectable but not at a significant level. Three of the milk samples contain 2,3,7,8-tetra-CDD (Hunzenschwil, Suhr, and Rheinfelden). Among the PCDF isomers, 2,3,4,7,8-penta-CDF is a major component found in all the milk samples analyzed (range 0.066–0.43 ppt). Additionally, 2,3,7,8-tetra- and 1,2,3,7,8-penta-CDF are likely to be present but not at a significant level (S/N ratio < 3). The milk samples with the highest levels of 2,3,4,7,8-penta-CDF, those from Hunzenschwil, Suhr, and Rheinfelden, also showed the presence of significant levels of hexa- and/or hepta-CDFs, mainly 2,3,4,6,7,8-hexa-CDF and 1,2,3,4,6,7,8-hepta-CDF. Octa-CDF was normally at or below detection limit.

On the basis of these results, the six milk samples can be grouped into two categories. The first category is milk samples that contain low and just-detectable quantities of these compounds. These are the two milk samples from Bowil and that from Bern. 2,3,4,7,8-Penta-CDF is present in these samples at 0.066–0.084 ppt. The second group of milk samples contains somewhat higher levels of these contaminants. The milk samples in these group are from Hunzenschwil, Suhr, and Rheinfelden. They contain several PCDF isomers and also PCDDs. 2,3,7,8-Tetra-CDD is detectable in these samples; 2,3,4,7,8-penta-CDF is among the main contaminants and present at 0.22–0.43 ppt. The combined level of all the 2,3,7,8-substituted tetra-, penta-, and hexachloro isomers in these samples is in the range of 1–2 ppt.

In Figures 2–6 (upper curves) we show the ion curves of tetra-, penta-, and hexa-CDFs and penta- and hexa-CDDs in the milk sample from Hunzenschwil.

Recent studies have demonstrated a background of 2,3,7,8-substituted PCDDs and PCDFs, including human milk and adipose tissue (*10–12*). The levels found in the

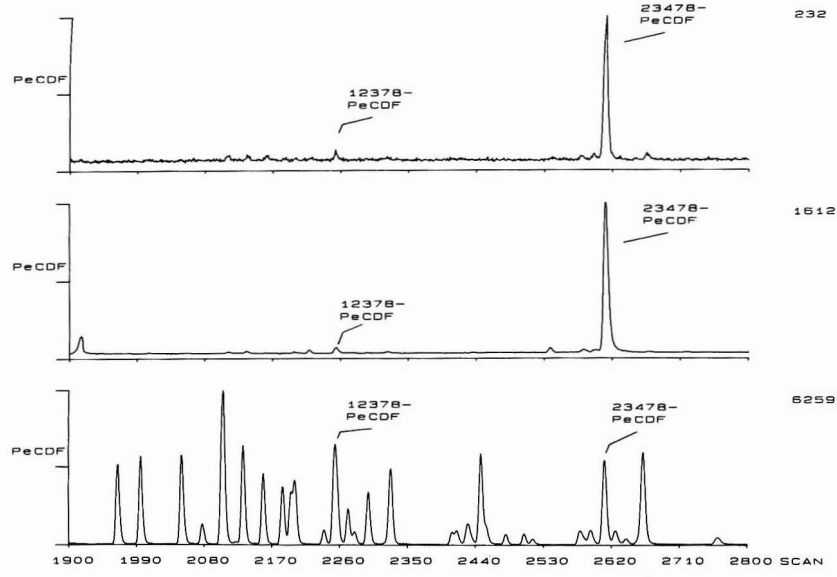

Figure 3. Ion curves of penta-CDFs of cow milk (upper), human milk (middle), and emission from MSW incinerator (lower), see text.

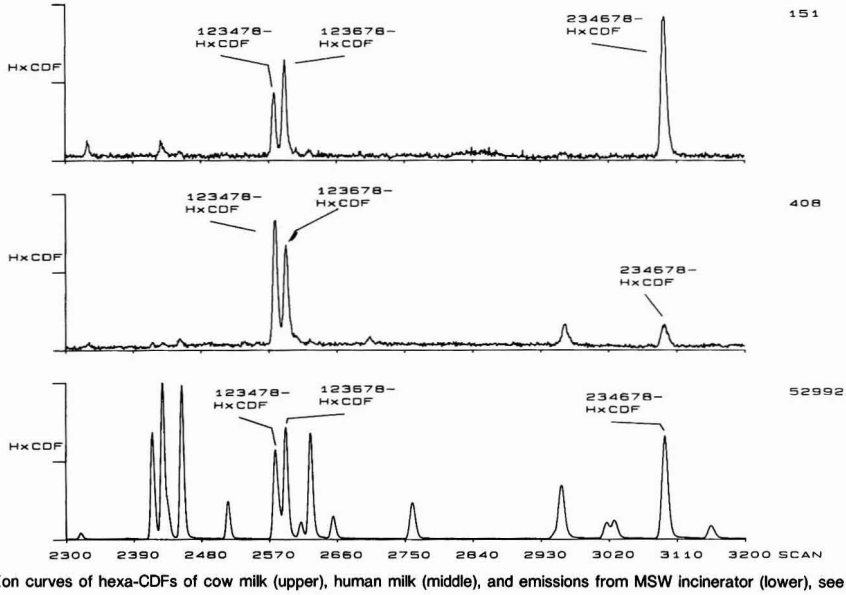

Figure 4. Ion curves of hexa-CDFs of cow milk (upper), human milk (middle), and emissions from MSW incinerator (lower), see text.

human milk samples from Sweden and Germany are higher then those reported here. Typical ion curves are shown in Figures 2–6 (middle curves). It is interesting to note the great similarity in the isomeric pattern between cow milk and human milk.

Emissions from incinerators are known to contain a series of PCDDs and PCDFs, including 2,3,7,8-substituted congeners. A very likely source for the presence of these compounds in the case of the more contaminated milk samples from Hunzenschwil, Suhr, and Rheinfelden is municipal incineration or other combustion sources. 1,2,3,7,8-Penta-CDD, present in two of the samples, has been implicated with emissions from combustion sources, and more recently, this particular isomer has also been identified in the exhausts from cars running on leaded gasoline (*18*) and in used motor oil (*19*). In the case of the milk from Rheinfelden, additionally the production of pentachlorophenol (PCP) may be implicated for at least some of the contaminants. This milk sample showed the highest levels of hepta- and octa-CDD, both major contaminants of PCP. Furthermore, the highest level of hexachlorobenzene (HCB) was detected in this sample (Table V).

Typical ion curves of penta- and hexa-CDDs as well as tetra-, penta-, and hexa-CDFs from emissions of MSW incinerators are given in Figures 2–6 (lower curves). A

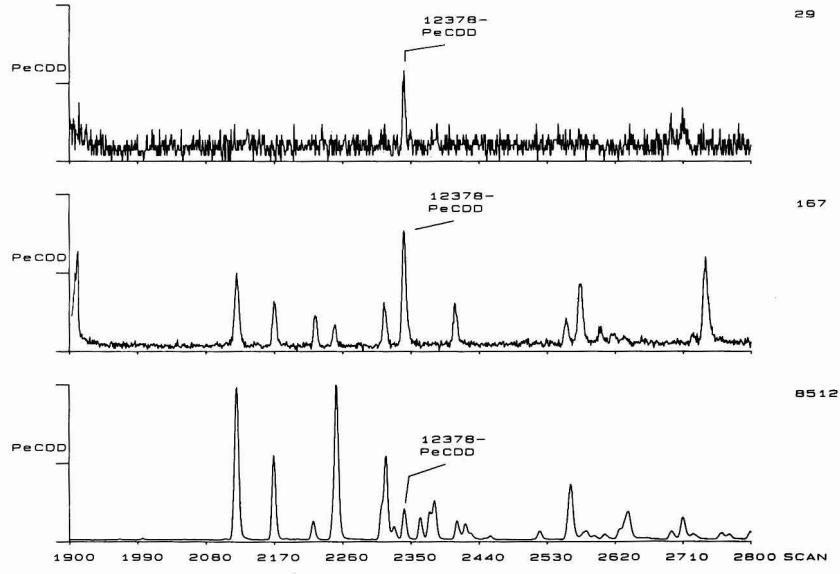

Figure 5. Ion curves of penta-CDDs of cow milk (upper), human milk (middle), and emissions from MSW incinerator (lower), see text.

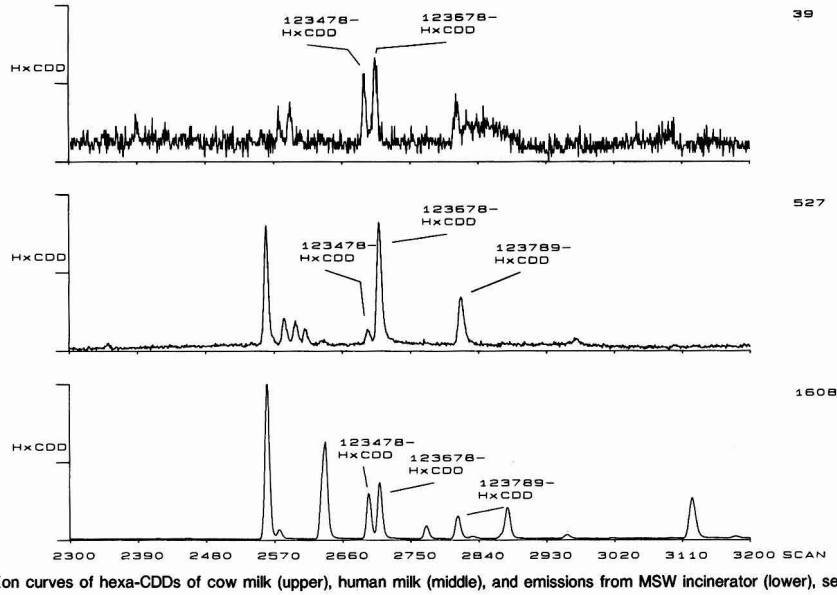

Figure 6. Ion curves of hexa-CDDs of cow milk (upper), human milk (middle), and emissions from MSW incinerator (lower), see text.

direct comparison between these curves and the curves from the milk sample demonstrate a dramatic decrease in the number of congeners present in the emissions and in the milk of the cows grazing near such installations. Only the toxic 2,3,7,8-substituted congeners are found in the milk. This observation can be explained by differences in bioaccumulation and/or biodegradation.

Rappe et al. (*20*) compared the structure of the PCDF congeners present in the Yusho oil and in liver samples from people exposed to this oil. Again, this comparison demonstrates structural relationships between the isomers retained by the patients and between the isomers apparently excreted. None of the isomers retained had two *vicinal* unchlorinated C atoms in any of the two C rings of the dibenzofuran system. Most of these isomers had all lateral (2, 3, 7, and 8) positions chlorinated. In contradiction, all the PCDF isomers apparently excreted had two *vicinal* unchlorinated C atoms in at least one of the two rings. A similar relationship for the metabolism of the closely related dibenzo-*p*-dioxins has been reported by Tulp and Hutzinger (*21*).

Registry No. 2,3,7,8-Tetra-CDF, 51207-31-9; 1,2,3,7,8-penta-CDF, 57117-41-6; 2,3,4,7,8-penta-CDF, 57117-31-4; 1,2,3,4,7,8-hexa-CDF, 70648-26-9; 1,2,3,6,7,8-hexa-CDF, 57117-44-9; 2,3,4,6,7,8-hexa-CDF, 60851-34-5; 1,2,3,4,6,7,8-hepta-CDF, 67562-39-4; octa-CDF, 39001-02-0; 2,3,7,8-tetra-CDD, 1746-01-6; 1,2,3,7,8-penta-CDD, 40321-76-4; 1,2,3,4,7,8-hexa-CDD, 39227-28-6; 1,2,3,6,7,8-hexa-CDD, 57653-85-7; 1,2,3,7,8,9-hexa-CDD, 19408-

74-3; 1,2,3,4,6,7,8-hepta-CDD, 35822-46-9; octa-CDD, 3268-87-9; *p,p'*-DDE, 72-55-9; *p,p'*-DDD, 72-54-8; *p,p'*-DDT, 50-29-3; HCB, 118-74-1; α-HCH, 319-84-6; β-HCH, 319-85-7; dieldrin, 60-57-1; endosulfan sulfate, 1031-07-8; heptachlorepoxide, 1024-57-3; lindane, 58-89-9; octachlorostyrene, 29082-74-4; pentachlorophenol, 87-86-5.

Literature Cited

(1) Rappe, C. *Environ. Sci. Technol.* **1983**, *18*, 78A–90A.
(2) Olie, K.; Vermeulen, P. L.; Hutzinger, O. *Chemosphere* **1977**, *6*, 455–459.
(3) Buser, H. R.; Bosshardt, H.-P. *Mitt. Geb. Lebensmittelunters. Hyg.* **1978**, *69*, 191–199.
(4) Buser, H. R.; Bosshardt, H.-P.; Rappe, C. *Chemosphere* **1978**, *7*, 165–172.
(5) Buser, H.-R.; Bosshardt, H.-P.; Rappe, C.; Lindahl, R. *Chemosphere* **1978**, *7*, 419–429.
(6) Rappe, C.; Marklund, S.; Kjeller, L.-O.; Bergqvist, P.-A.; Hansson, M. in *Chlorinated Dioxins and Dibenzofurans in the Total Environment*; Keith, L. H., Rappe, C., Choudhary, G., Eds.; Butterworth: Boston, 1985; Vol. II, pp 401–424.
(7) Tysklind, M.; Marklund, S.; Rappe, C. *Chemosphere*, in press.
(8) Bellin, J. S.; Barnes, D. G. *Toxicol. Ind. Health* ***1985***, *1*, 235–248.
(9) Eadon, G.; Aldous, K.; Frenkel, G.; Gierthy, J.; Hilker, D.; Kaminsky, L.; O'Keefe, P.; Silkworth, J.; Smith, R. *Comparison of Chemical and Biological Data on Soot Samples from the Binghamton State Office Building*; Report NYSDH; 1982.
(10) Rappe, C.; Bergqvist, P.-A.; Hansson, M.; Kjeller, L.-O.; Lindström, G.; Marklund, S.; Nygren, M. Banbury Report 18; Cold Spring Harbor Laboratory: Cold Spring Harbor, NY, 1985; pp 17–25.
(11) Rappe, C. In *Solving Hazardous Waste Problems: Dioxins*; Exner, J. H. Ed.; ACS Symposium Series; American Chemical Society: Washington, DC; in press.
(12) Nygren, M.; Rappe, C.; Lindström, G.; Hansson, M.; Bergqvist, P.-A.; Marklund, S.; Domellöf, L.; Hardell, L.; Olsson, M. In *Chlorinated Dioxins and Dibenzofurans in Perspective*; Rappe, C., Choudhary, G., Keith, L., Eds.; Lewis: Chelsea, MI, 1986; pp 17–34.
(13) Stalling, D. L.; Smith, L. M.; Petty, J. D.; Hogan, J. W.; Johnson, J. L.; Rappe, C.; Buser, H. R. In *Human and Environmental Risks of Chlorinated Dioxins and Related Compounds*; Tucker, R. E., Young, A. L.; Gray, A. P., Eds.; Plenum: New York, 1983; pp 221–240.
(14) Smith, L. M.; Stalling, D. L.; Johnson, J. L. *Anal. Chem.* **1984**, *56*, 1830–1842.
(15) Rappe, C.; Bergqvist, P.-A.; Marklund, S. In *Chlorinated Dioxins and Dibenzofurans in the Total Environment*; Keith, L. H., Rappe, C., Choudhary, G., Eds.; Butterworth: Boston, 1985; Vol. II, pp 125–138.
(16) Buser, H. R.; Rappe, C. *Anal. Chem.* **1984**, *56*, 442–448.
(17) Specht, W.; Tillkes, M. *Fresenius' Z. Anal. Chem.* **1980**, *301*, 300–307.
(18) Marklund, S.; Rappe, C.; Tysklind, M. *Chemosphere*, **1987**, *16*, 29–36.
(19) Ballschmiter, K.; Buchert, H.; Niemczyk, R.; Munder, A.; Swerv, M. *Chemosphere* **1986**, *15*, 901–915.
(20) Rappe, C.; Buser, H. R.; Kuroki, H.; Masuda, Y. *Chemosphere* **1979**, *8*, 259–266.
(21) Tulp, M.; Hutzinger, O. *Chemosphere* **1978**, *7*, 761–768.

Received for review September 17, 1986. Accepted May 26, 1987.

Environ. Sci. Technol. 1987, 21, 971–979

Isomer-Specific Determination of Polychlorinated Dibenzo-*p*-dioxins and Dibenzofurans in Incinerator-Related Environmental Samples

Akio Yasuhara,* Hiroyasu Ito, and Masatoshi Morita

Chemistry and Physics Division, National Institute for Environmental Studies, Onogawa, Yatabe, Tsukuba, Ibaraki 305, Japan

■ Polychlorinated dibenzo-*p*-dioxins (PCDDs) and dibenzofurans (PCDFs) ranging from tetra- to octachloro congeners in ash and fly ash from incinerators, river water, effluent water from incinerators, groundwater, soil, and sediment were determined isomer specifically by high-resolution gas chromatography–mass spectrometry in order to manifest an environmental situation polluted with those compounds in Japan. The most toxic 2,3,7,8-tetrachlorodibenzo-*p*-dioxin was detected only in fly ash. In many samples, octachlorodibenzo-*p*-dioxin had the highest abundance in PCDDs, and heptachlorodibenzofurans had the highest abundance in PCDFs. Gas chromatographic patterns of PCDDs and PCDFs in all samples were compared with each other by use of the pattern similarity method in order to classify the pollution pattern with PCDDs and PCDFs. Gas chromatographic patterns of PCDDs and PCDFs in fly ash, effluent water, and sediment were different from each other.

Introduction

Polychlorinated dibenzo-*p*-dioxins (PCDDs) and polychlorinated dibenzofurans (PCDFs) are a group of toxic and hazardous compounds in the environment. There are a total of 75 PCDD congeners and a total of 135 PCDF congeners substituted with one to eight chlorine atoms. The toxicity of PCDDs and PCDFs has not been entirely clarified (*1*). PCDD and PCDF congeners ranging from tetra- to hexachloro compounds having chlorine atoms at the 2-, 3-, 7-, and 8-positions are strongly toxic according to the reviews (*2*, *3*). Since PCDDs and PCDFs are resistant against chemical and microbial degradation, these compounds are easily accumulated in the environment. Therefore, it is very important and necessary to investigate the situation and trends of pollution with PCDDs and PCDFs in Japan.

Isomer-specific determination of PCDDs and PCDFs in various kinds of environmental samples and investigation of the behavior and fate of PCDDs and PCDFs in the environment are important and emergent problems. Formation and emission of PCDDs and PCDFs from incineration sources are well-known (*4–8*). Other sources of PCDDs and PCDFs are contaminants in herbicides and polychlorinated biphenyls (PCBs) (*9–12*). Lots of data concerning the concentration of PCDDs and PCDFs in fly ash, soil, and biological materials have been reported by many research workers in the U.S., Canada, European countries, etc. In Japan, an accident occurred in 1968 that is well-known as the Kanemi-Yusho (*13*). It was a mass food poisoning by a contamination of rice oil with PCBs and PCDFs. In recent years, attention has been paid to environmental pollution with PCDDs and PCDFs from incinerators and herbicide contamination (*14–16*). However, information on the environmental situation polluted with PCDDs and PCDFs in Japan is very poor.

Many analytical methods have already been developed for PCDDs and PCDFs. Most of them involve high-resolution gas chromatography–mass spectrometry (*17–27*). Isomer-specific determination of PCDDs and PCDFs is very important and necessary for the assessment of biological effects because of the large differences of toxicity between congeners, although the complete separation of all congeners is impossible at the present time even if capillary columns are used.

This reseach has two objectives. One is to manifest the present situation of pollution with PCDDs and PCDFs in Japan, and the other is to estimate the origin of pollution by PCDDs and PCDFs. For the sake of these purposes, PCDDs and PCDFs ranging from tetra- to octachloro compounds in water, soil, sediment, incinerator's ash, and fly ash were isomer specifically determined by high-resolution gas chromatography–low-resolution mass spectrometry according to the method reported in ref 26. Gas chromatographic peak patterns of PCDDs and PCDFs congeners in each sample were compared with each other by means of the pattern similarity method in order to investigate the relation between the gas chromatographic pattern of PCDD and PCDF congeners and the property of samples.

Experimental Section

Synthesis of PCDDs. All syntheses were carried out according to the literature (*27–31*). Several compounds described below were isolated in pure form. 1,2,3,4-Tetrachlorodibenzo-*p*-dioxin (1,2,3,4-TCDD) was prepared from catechol and pentachloronitrobenzene and recrystallized with acetone; colorless needles, mp 191–192 °C. 1,3,7,8-TCDD was prepared from 4,5-dichlorocatechol and 1,2,3,5-tetrachlorobenzene and recrystallized with benzene; colorless fine needles, mp 191–192 °C. 1,3,6,8-TCDD was prepared by heating potassium 2,4,6-trichlorophenolate and was isolated by recrystallization with benzene/methanol from the reaction mixture; colorless crystals, mp 219–220 °C. Purification of 1,3,7,9-TCDD, which formed a byproduct in the reaction, was unsuccessful. 1,2,8,9-TCDD was prepared by heating potassium 2,3,4-trichlorophenolate and recrystallized with benzene; colorless crystals, mp 227–230 °C. Purification of 1,2,6,7-TCDD, which formed as a byproduct of the Smiles rearrangement in the reaction, was unsuccessful.

Reference Samples. 2,3,7,8-TCDD solution, $^{13}C_{12}$-labeled 2,3,7,8-TCDD solution, and dioxin mixture solution, including 1,2,3,4-TCDD, 1,2,3,4,7-P_5CDD, 1,2,3,4,6,7-H_6CDD, and 1,2,3,4,6,7,8-H_7CDD, were purchased from Cambridge Isotope Laboratories, Inc. Octachlorodibenzofuran (OCDF) and octachlorodibenzodioxin (OCDD) were purchased from Gasukuro Kogyo Inc. (Tokyo). 2,3,6,8-TCDF, 2,4,6,8-TCDF, 2,3,4,7,8-P_5CDF, and 1,2,3,6,7,8-H_6CDF were provided by Dr. A. S. Kende.

Additional Reference Mixture of PCDDs and PCDFs. A mixture solution of PCDDs and PCDFs for confirmation of peak positions in the gas chromatography–mass spectrometry analyses was obtained from a large amount of fly ash (ca. 100 g). The fly ash was treated in the same manner as described under Extraction and Cleanup. It was confirmed by gas chromatography–mass spectrometry that this mixture solution contained all congeners ranging from tetrachloro- to octachlorodibenzo-*p*-dioxins and from tetrachloro- to octachlorodi-

0013-936X/87/0921-0971$01.50/0

Table I. Contents of Samples

no.	contents	sample amount	internal standard, ng
1	ash before afterburner in institute's incinerator A	16 g	3.0
2	ash after afterburner in institute's incinerator A	10.4	3.0
3	ash in municipal incinerator B	10 g	10.0
4	fly ash in municipal incinerator C	10 g	10.0
5	fly ash in municipal incinerator D	10 g	10.0
6	fly ash in municipal incinerator E	20 g	20.0
7	fly ash from municipal incinerator F	20 g	20.0
8	soil near incinerator F	10 g	3.0
9	effluent water from incinerator F	3.5 L	3.8
10	river water mixed with effluent water from incinerator F	3.5 L	3.8
11	groundwater near incinerator F	3.5 L	3.8
12	sediment in river that receives effluent water from incinerator F	10 g	3.0
13	river water mixed with effluent water from municipal incinerator G	3.5 L	3.8
14	sediment in river that recieves effluent water from incinerator G	20 g	3.0
15	effluent water from industrial incinerator H	3.5 L	3.8
16	river water mixed with effluent water from incinerator H	3.5 L	3.8
17	sediment in river that receives effluent water from incinerator H	15 g	3.0
18	sediment in reservoir of effluent water from incinerator H	3 g	3.8
19	leached water from reclaimed land with residue from incinerator H	3.5 L	3.8
20	soil near incinerator H	3 g	3.8
21	river water down incinerator H	3.5 L	3.8
22	river water mixed with effluent water from industrial incinerator J	3.5 L	3.8
23	soil near incinerator J	10 g	3.0
24	river water mixed with effluent water from municipal incinerator K	3.5 L	3.8
25	water in lower part of river that receives effluent water from incinerator K	3.5 L	3.8
26	sediment in river that receives effluent water from incinerator K	10 g	3.0
27	soil near incinerator K	10 g	3.0
28	sediment in lake[a]	10 g	3.0

[a] This sample is not concerned with any incinerator.

benzofurans. Peak positions of all congeners on the gas chromatogram were then determined by comparison with the literature (*26*, *32*).

Samples. Ashes, fly ashes, soils, river water, and groundwater were collected in relation to different types of incinerators. Samples were transferred to our laboratory either under cooled or frozen conditions and stored at −20 °C. The details are shown in Table I.

Extraction and Cleanup. [^{13}C]-2,3,7,8-TCDD was spiked in all samples as an internal standard. Approximately 3–30 g of fly ash and other solid samples, which were spiked in advance with an ethanol solution of [^{13}C]-2,3,7,8-TCDD (0.1 ng/μL) at the level of 0.5–20 ng, was put into a Soxhlet filter cup and was extracted with toluene (100 mL) for 16 h. The extracted solutions were concentrated to a few milliliters by a rotary evaporator and dissolved with hexane. Water samples were extracted with dichloromethane after being spiked with [^{13}C]-2,3,7,8-TCDD. The extracts were concentrated to a few milliliters by a rotary evaporator and dissolved with hexane. The hexane solution was partitioned twice with the same volume of concentrated sulfuric acid. The hexane layer was subjected to column chromatography with neutral alumina (3 g). After 50 mL of hexane was passed through the column, the dioxin and furan fraction was collected by eluting with 50 mL of dichloromethane/hexane (50:50). The fraction was concentrated to 100 μL by a rotary evaporator and nitrogen gas flashing and subjected to high-performance liquid chromatography (HPLC), where an ODS silica column (4.6 mm i.d. × 150 mm) was used. The dioxin and furan fraction (2.5–7 min), eluted with methanol at the flow rate of 1 mL/min, was collected. The solution was evaporated together with benzene to remove methanol by a rotary evaporator and finally was concentrated to a small volume (around 0.1–0.5 mL) by nitrogen gas flashing. For samples of soil and sediment, column chromatography with Florisil was put before the alumina column chromatography. Florisil (10 g) was used without any activation. After 100 mL of hexane was passed through the column, the dioxin and furan fraction was collected by eluting with 200 mL of dichloromethane/hexane (80:20).

Table II. Setting Mass Number for Selected Ion Monitoring

no. of chlorine atoms	dibenzo-*p*-dioxin	dibenzofuran
4	319.9, 321.9	303.9, 305.9
5	353.9, 355.9	337.9, 339.9
6	387.9, 389.9	371.9, 373.9
7	423.9, 425.9	407.9, 409.9
8	457.9, 459.9	441.9, 443.9
4[a]	331.9, 333.9	

[a] This compound is [$^{13}C_{12}$]-2,3,7,8-TCDD.

Table III. List of Object Compounds and Reference Compounds for Quantification

object compounds	reference compounds
1,3,6,8-TCDD	1,3,6,8-TCDD
1,3,7,8-TCDD	1,3,7,8-TCDD
1,2,8,9-TCDD	1,2,8,9-TCDD
1,2,3,4-, 1,2,3,7-, 1,2,3,8-, 1,2,4,6-, and 1,2,4,7-TCDDs	1,2,3,4-TCDD
other TCDDs	2,3,7,8-TCDD
all P_5CDDs	1,2,3,7,8-P_5CDD
all H_6CDDS	1,2,3,6,7,8-H_6CDD
all H_7CDDs	1,2,3,4,6,7,8-H_7CDD
OCDD	OCDD
2,3,6,8-TCDF	2,3,6,8-TCDF
other TCDFs	2,4,6,8-TCDF
all P_5CDFs	2,3,4,7,8-P_5CDF
all H_6CDFs	1,2,3,6,7,8-H_6CDF
all H_7CDFs	1,2,3,4,6,7,8-H_7CDD
OCDF	OCDF

Gas Chromatography–Mass Spectrometry. A JEOL Model JMS-DX300 double-focusing mass spectrometer

Table IV. Concentration of TCDDs[a]

sample[b]	1,3,6,8	1,3,7,9	1,3,7,8	1,2,4,7, 1,2,4,8, 1,3,6,9	1,2,6,8	1,4,7,8	2,3,7,8	1,2,3,4, 1,2,3,7, 1,2,3,8, 1,2,4,6, 1,2,4,9	1,2,3,6, 1,2,7,9	1,2,7,8, 1,4,6,9	1,2,3,9	1,2,6,9	1,2,6,7	1,2,8,9	total	unit
1 (ash)	0.08	0.09	0.04	0.03	–[c]	–	–	0.03	0.04	0.02	–	–	–	–	0.33	ng/g
2 (ash)	0.04	0.05	–	–	–	–	–	–	–	–	–	–	–	0.29	0.38	ng/g
3 (ash)	0.21	0.22	0.10	0.09	–	–	0.08	0.16	0.09	–	–	–	–	–	0.95	ng/g
4 (FAsh)	8.26	6.39	1.52	2.20	0.92	0.15	0.23	2.52	1.35	0.52	0.38	0.39	0.15	0.19	25.2	ng/g
5 (FAsh)	21.2	16.7	2.65	4.12	1.59	0.23	0.40	6.19	2.41	0.60	0.59	0.62	2.24	2.14	61.7	ng/g
6 (FAsh)	0.41	0.31	0.23	0.18	0.10	0.06	0.07	0.19	0.12	0.08	0.06	–	–	–	1.81	ng/g
7 (FAsh)	0.45	0.52	0.10	0.08	0.08	–	0.05	0.07	0.07	–	0.07	–	0.10	0.11	1.70	ng/g
8 (soil)	0.69	0.37	0.37	0.23	–	–	–	0.20	–	–	–	–	–	–	1.86	ng/g
9 (EWat)	0.57	0.33	0.17	–	–	–	–	0.15	–	–	–	–	–	–	1.22	ng/L
12 (sed)	–	0.29	–	–	–	–	–	–	–	–	–	–	–	–	0.29	ng/g
13 (RWat)	3.72	2.31	0.16	–	–	–	–	0.98	–	–	–	–	–	–	7.17	ng/L
14 (sed)	0.67	0.27	–	–	–	–	–	–	–	–	–	–	–	–	0.94	ng/g
15 (EWat)	3.13	1.40	0.56	–	–	0.65	–	0.56	–	–	–	–	–	–	6.30	ng/L
16 (RWat)	9.14	3.04	0.30	–	–	–	–	0.39	–	–	–	–	–	0.65	13.5	ng/L
17 (sed)	35.7	12.1	–	0.10	–	–	–	0.09	0.04	0.04	0.19	–	–	0.55	48.8	ng/g
18 (sed)	0.59	0.35	–	–	–	–	–	–	–	–	–	–	–	–	0.94	ng/g
19 (LWat)	0.20	0.12	0.06	–	–	–	–	–	–	–	–	–	–	–	0.38	ng/L
20 (soil)	0.42	0.19	–	–	–	–	–	–	–	–	–	–	–	–	0.61	ng/g
22 (RWat)	1.03	0.78	0.41	–	–	0.82	–	1.04	–	–	–	–	–	–	4.08	ng/L
23 (soil)	–	0.06	–	–	–	–	–	–	–	–	–	–	–	–	0.06	ng/g
25 (RWat)	0.05	–	–	–	–	–	–	–	–	–	–	–	–	–	0.05	ng/L
26 (sed)	0.29	0.21	–	–	–	–	–	0.15	–	–	–	–	–	–	0.65	ng/g
27 (soil)	0.48	0.29	–	–	–	–	–	0.28	–	–	–	–	–	–	1.05	ng/g
28 (sed)	0.94	0.43	–	–	–	–	–	0.20	–	–	–	–	–	–	1.57	ng/g

[a] Samples without data did not contain any TCDD. [b] Sample notation: ash, ash in the incinerator; FAsh, fly ash in the incinerator; soil, soil; sed, sediment; EWat, effluent water from the incinerator plant; RWat, river water; LWat, leached water from reclaimed land with the ash from the incinerator. [c] –, ND.

Table V. Concentration of P_5CDDs[a]

sample[b]	1,2,4,6,8, 1,2,4,7,8	1,2,3,6,8	1,2,4,7,8	1,2,3,7,9	1,2,3,4,7, 1,2,4,6,9	1,2,3,7,8	1,2,3,6,9	1,2,4,8,9	1,2,4,6,7	1,2,3,4,6	1,2,3,6,7	1,2,3,8,9	total	unit
3 (Ash)	0.03	0.02	–[c]	–	0.01	0.01	–	–	–	–	–	–	0.07	ng/g
4 (FAsh)	0.74	0.60	0.08	0.43	0.13	0.08	0.05	0.03	0.04	0.05	–	0.05	2.28	ng/g
5 (FAsh)	1.52	1.15	0.15	0.84	0.32	0.16	0.09	0.08	0.10	0.13	–	0.09	4.63	ng/g
7 (FAsh)	3.34	2.59	0.43	2.44	0.54	0.56	–	–	–	–	–	0.35	10.3	ng/g
8 (soil)	0.44	0.27	0.11	0.19	0.09	0.14	0.04	0.05	0.06	0.05	–	0.09	1.53	ng/g
17 (sed)	0.27	0.80	–	–	–	–	–	–	–	–	–	–	1.07	ng/g

[a] Samples without data did not contain any P_5CDD. [b] Sample notation: ash, ash in the incinerator; FAsh, fly ash in the incinerator; soil, soil; sed, sediment. [c] –, ND.

Table VI. Concentration of TCDFs[a]

sample[b]	1,3,6,8	1,3,7,8, 1,3,7,9	1,3,4,7	1,4,6,8	1,2,4,7, 1,3,6,7	1,3,4,8	1,2,4,8, 1,3,4,6	1,2,3,7, 1,2,4,6, 1,2,6,8, 1,3,6,9, 1,4,7,8	1,2,3,4, 2,3,4,9	1,2,3,6, 1,2,3,8, 1,4,6,7, 2,4,6,8	1,3,4,9	1,2,7,8
1 (ash)	0.03	0.05	0.02	0.02	0.05	0.02	0.03	0.14	0.05	0.09	–[c]	0.06
3 (ash)	0.04	0.57	0.01	0.02	0.46	0.10	0.27	1.29	0.90	1.13	0.08	0.35
4 (FAsh)	0.89	4.36	0.53	0.34	4.08	1.46	3.20	11.2	6.10	9.17	0.58	4.89
5 (FAsh)	0.83	4.33	0.22	0.19	5.43	1.93	4.89	15.4	16.8	14.1	0.95	6.17
6 (FAsh)	0.27	0.39	0.17	0.15	0.33	0.14	0.25	0.93	0.35	0.36	0.06	0.29
7 (FAsh)	0.24	0.23	0.12	0.08	0.26	0.21	0.34	1.06	2.43	0.61	0.16	0.17
8 (soil)	0.20	0.23	0.10	0.11	0.24	0.13	0.26	0.80	0.33	0.41	0.07	0.21
12 (sed)	0.09	–	–	0.11	–	–	–	–	–	–	–	–
17 (sed)	0.03	–	–	0.03	–	0.05	–	–	0.03	–	–	–
22 (RWat)	–	0.32	–	0.33	0.32	0.25	0.60	–	–	0.86	–	–
26 (sed)	–	0.04	–	–	–	–	–	–	–	–	–	–

[a] Samples without data did not contain any TCDF. [b] Sample notation: ash, ash in the incinerator; FAsh, fly ash in the incinerator; soil,

Table VII. Concentration of P_5CDFs[a]

sample[b]	1,3,4,6,8	1,2,4,6,8	2,3,4,7,9	1,3,4,7,9	1,2,3,6,8, 1,3,4,7,8	1,2,4,7,8	1,2,4,7,9, 1,3,4,6,7	1,2,4,6,7	1,2,3,4,7, 2,3,4,6,9	1,3,4,6,9	1,2,3,4,8, 1,2,3,7,8	1,2,3,4,6
3 (ash)	0.12	0.09	0.02	0.04	0.21	0.14	0.21	0.15	0.19	0.06	0.22	0.16
4 (FAsh)	0.67	0.71	0.79	0.23	1.81	1.08	1.22	1.08	1.76	0.29	1.87	0.86
5 (FAsh)	1.72	1.84	1.58	0.35	3.91	2.20	2.96	2.72	4.65	0.58	4.60	2.61
6 (FAsh)	0.19	0.18	0.14	0.04	0.33	0.22	0.22	0.17	0.20	0.04	0.21	0.09
7 (FAsh)	0.78	0.83	0.54	0.29	1.79	0.62	2.30	0.97	1.28	0.53	1.09	1.22
8 (soil)	0.09	0.10	0.07	0.03	0.16	0.12	0.13	0.10	0.12	0.04	0.11	0.06
17 (sed)	–	0.07	–	–	–	0.04	–	–	–	–	0.02	–

[a] Samples without data did not contain any P_5CDFs. [b] Sample notation: ash, ash in the incinerator; FAsh, fly ash in the incinerator; soil,

was used in combination with a Hewlett-Packard 5710A gas chromatograph and a JEOL JMA3500 mass data analysis system. Gas chromatographic conditions for PCDDs and PCDFs with four to six chlorine atoms were as follows: column, SP2330 cross-linked fused silica capillary column (30 m × 0.2 mm i.d. × 0.25 μm) purchased from Supelco Inc.; column temperatures, 90 °C for 2 min isothermal, 8 deg/min (for TCDDs and TCDFs) or 16 deg/min (for others) to 230 °C; injection port temperature, 250 °C. Gas chromatographic conditions for H_7CDDs, OCDD, H_7CDFs, and OCDF were as follows: column OV-1 chemically bonded fused silica capillary column (10 m × 0.35 mm i.d. × 0.25 μm) purchased from Gasukuro Kogyo Inc.; column temperatures, 90 °C for 2 min isothermal, 16 deg/min to 260 °C; injection port temperature, 300 °C. Sample aliquots of 1–2 μL in benzene or toluene were injected with a splitless mode. The end of the fused silica capillary column was inserted directly into the ion source of the mass spectrometer and was always heated at 250 °C. Mass spectrometric conditions were as follows: ionization mode, electron impact (EI); ion source temperature, 250 °C; ion source pressure, (2–4) × 10^{-5} Torr; resolution, ca. 500; ionizing energy, 70 eV; ionizing current, 300 μA; initial (highest) accelerating voltage, 3 kV; switching rate for multi-ion detection, 0.1 s. Multiple ions were monitored by decreasing the accelerating voltage. All operations were controlled by the computer system. All compounds were measured by monitoring two isotopes of the molecular ions. The values of setting mass for detection of PCDDs and PCDFs are shown in Table II. Although it is desirable to use a considerable number of ions in selected ion monitoring in order to separate overlapped congeners, only two ions were used in this study because of two reasons. One is time and labor saving. The other is the high level of background at ions except for molecular ions. The internal standard method with [^{13}C]-2,3,7,8-TCDD was used for quantification of all congeners. Peak area was calculated by the computer. Concentrations were calculated on every peak detected. Therefore, two concentrations were obtained for each congener. If there was not a discrepancy of more than around 30% between the two concentrations, they were averaged. Otherwise, the concentrations were tentatively set at below the minimum detection limit on the presumption that the peaks were interfered with by other substances. Polychlorinated diphenyl ethers are considered as interference materials in the determination of PCDFs. But the interference with these compounds was not investigated because all congeners of polychlorinated diphenyl ethers were not obtainable. Reference compounds used for quantification are listed in Table III.

Results and Discussion

Peak positions of all congeners were confirmed with reference samples and the reference mixture on the basis of gas chromatographic patterns reported by Rappe (*26*) and of relative retention times summarized by Bell and Gåra (*32*). Relative retention times with 2,3,7,8-TCDD as a reference were measured and used for peak assignment of all congeners in this research. The SP-2330 fused silica capillary column was used for the gas chromatographic separation of many of the congeners, since Rappe (*26*) and Bell and Gåra (*32*) have reported on the superiority of this column. But the column was not effective for the analysis of hepta- and octachloro congeners because the column cannot be used as temperatures of more than 230 °C, which is necessary to elute these congeners. Then the OV-1 fused silica capillary column was used for these isomers. Fortunately, the congeners were separated satisfactorily with this column.

Calibration curves of reference PCDDs and PCDFs almost intersected the origin. Linearity of calibration curves was confirmed from 2 to 200 pg. Instrumental detection limits defined as S/N = 2 were as follows: 1,3,6,8-TCDD,

1,2,6,7, 1,2,7,9	1,4,6,9	1,2,4,9, 2,3,6,8	2,4,6,7	1,2,3,9, 2,3,4,7	1,2,6,9	2,3,7,8	2,3,4,8	2,3,4,6, 2,3,6,7	3,4,6,7	1,2,8,9	total	unit
0.06	–	0.05	0.07	0.04	0.01	0.09	0.07	0.13	0.16	–	1.24	ng/g
0.62	0.06	0.24	0.47	0.45	0.08	0.21	0.70	0.49	0.78	0.06	9.38	ng/g
4.36	0.64	2.11	4.35	5.99	0.96	2.13	4.71	3.26	5.30	0.52	81.1	ng/g
5.71	1.29	3.26	7.40	8.75	1.17	4.73	7.79	4.55	11.3	1.20	128	ng/g
0.19	0.06	–	0.15	0.22	–	–	0.15	–	0.11	0.12	4.69	ng/g
0.27	0.40	0.57	0.38	0.79	0.11	0.05	0.38	0.09	0.36	0.15	9.46	ng/g
0.19	0.08	0.10	0.20	0.25	–	0.04	0.23	0.05	0.17	0.07	4.47	ng/g
–	0.08	–	–	–	–	–	–	–	–	–	0.28	ng/g
–	–	–	–	–	–	–	–	–	–	–	0.14	ng/g
–	–	0.40	–	–	–	0.94	–	–	–	–	4.02	ng/L
–	–	–	–	–	–	–	–	–	–	–	0.04	ng/g

soil; sed, sediment; RWat, river water. [c] –, ND.

1,2,3,7,9	1,2,3,6,7	1,2,4,6,9, 2,3,4,8,9	1,3,4,8,9	1,2,4,8,9	1,2,3,6,9	2,3,4,6,8	1,2,3,4,9	2,3,4,7,8	1,2,3,8,9	2,3,4,6,7	total	unit
0.02	0.16	0.20	0.03	–[c]	0.15	0.05	0.04	0.24	0.06	0.44	3.00	ng/g
0.24	0.93	1.41	0.32	0.19	1.50	0.25	0.28	2.36	0.20	2.10	22.2	ng/g
0.41	2.16	3.62	0.67	0.81	6.23	0.76	0.64	2.66	0.42	4.99	53.1	ng/g
0.02	0.11	0.20	0.04	0.02	0.34	0.04	0.05	0.23	0.04	0.59	3.71	ng/g
0.44	0.82	2.08	1.01	0.36	5.32	1.50	1.50	1.42	0.66	12.3	39.7	ng/g
0.02	0.07	0.15	0.03	0.03	0.22	0.04	0.03	0.17	0.02	0.38	2.29	ng/g
–	–	–	–	–	–	–	–	–	–	–	0.13	ng/g

soil; sed, sediment. [c] –, ND.

Table VIII. Concentration of H_6CDDs[a]

sample[b]	1,2,3,4,6,8, 1,2,4,6,7,9, 1,2,4,6,8,9	1,2,3,6,7,9, 1,2,3,6,8,9	1,2,3,4,7,8	1,2,3,6,7,8	1,2,3,4,6,9	1,2,3,7,8,9	1,2,3,4,6,7	total	unit
3 (ash)	0.04	0.02	–[c]	0.01	–	–	–	0.07	ng/g
4 (FAsh)	1.35	0.53	0.05	0.15	0.05	0.11	0.08	2.32	ng/g
5 (FAsh)	2.21	1.06	0.11	0.27	0.10	0.24	0.19	4.18	ng/g
6 (FAsh)	2.01	1.71	0.29	0.48	0.06	0.45	0.23	5.23	ng/g
7 (FAsh)	18.0	11.3	0.82	3.80	0.36	2.29	0.94	37.5	ng/g
8 (soil)	1.07	0.85	0.15	0.26	0.03	0.19	0.11	2.66	ng/g
17 (sed)	0.10	0.06	–	–	–	–	–	0.16	ng/g

[a] Samples without data did not contain any H_6CDD. [b] Sample notation: ash, ash in the incinerator; FAsh, fly ash in the incinerator; soil, soil; sed, sediment. [c] –, ND.

0.29, pg; 1,3,7,8-TCDD, 0.21 pg; 2,3,7,8-TCDD, 1.00 pg; 1,2,3,4-TCDD, 0.24 pg; 1,2,8,9-TCDD, 0.46 pg; 1,2,3,7,8-P_5CDD, 6.01 pg; 1,2,3,6,7,8-H_6CDD, 4.00 pg; 1,2,3,4,6,7,8-H_7CDD, 2.00 pg; OCDD, 4.00 pg; 2,4,6,8-TCDF, 0.33 pg; 2,3,6,8-TCDF, 0.30 pg; 2,3,4,7,8-P_5CDF, 1.67 pg; OCDF, 2.67 pg. But quantification limits in real samples are around several picograms because of the high noise level. Therefore, the minimum concentration for quantification of TCDDs and TCDFs is around 0.01 ng/g for the solid sample and 0.05 ng/L for the water sample. Relative standard deviations on four replicate measurements of 1,3,6,8-, 1,3,7,8-, 2,3,7,8-, 1,2,3,4-, and 1,2,8,9-TCDDs were as follows: 100-pg injection, ca. 4%; 50-pg injection, ca. 6%; 20-pg injection, ca. 14%; 10-pg injection, ca. 16%. Recovery was calculated on the amount of [^{13}C]-2,3,7,8-TCDD recovered from various kinds of samples spiked with [^{13}C]-2,3,7,8-TCDD. Recovery coefficients were 44–95% for river water and groundwater, 22–92% for effluent water from an industrial or municipal incineration plant, 22–32% for sediment, 14–44% for soil, and 10–47% for incinerator's ash and fly ash. It seems likely that recovery coefficients depend upon the sample matrix. Namely, recovery was not good for solid samples and highly polluted water samples that have a complex matrix. Loss of PCDDs and PCDFs seemed to occur during the extraction process and not during the cleanup process. Therefore, the extraction method should be improved further.

Determination of trace amounts of P_5CDD, P_5CDF, H_6CDD, and H_6CDF was very difficult because of the presence of interfering substances. Although these peaks seemed to be similar to PCDD and PCDF isomers, the relative retention times were not consistent with reference values at all. These interferences were not removed by the procedure of cleanup described here.

Determination of TCDFs, P_5CDFs, H_6CDFs, H_7CDFs, and OCDFs might be interfered with by hexa-, hepta-, octa-, nona-, and decachlorinated diphenyl ethers, respectively. Gas chromatographic separation between all PCDFs and all congeners of these polychlorinated diphenyl ethers was not checked because of the absence of authentic compounds.

Table IX. Concentration of H_6CDFs[a]

sample[b]	1,2,3,4,6,8	1,3,4,6,7,8, 1,3,4,6,7,9	1,2,4,6,7,8	1,2,4,6,7,9	1,2,3,4,7,8, 1,2,3,4,7,9	1,2,3,6,7,8	1,2,4,6,8,9	1,2,3,4,6,7	1,2,3,6,7,9	1,2,3,4,6,9, 1,2,3,4,8,9	1,2,3,7,8,9	1,2,3,4,8,9	2,3,4,6,7,8	total	unit
3 (ash)	0.03	0.07	0.05	0.01	0.05	0.05	–[c]	0.08	0.01	0.02	0.01	0.01	0.06	0.45	ng/g
4 (FAsh)	0.33	0.52	0.48	0.11	0.42	0.39	0.04	0.46	0.07	0.15	0.06	0.08	0.41	3.52	ng/g
5 (FAsh)	1.04	1.36	2.06	0.23	0.98	0.90	0.10	1.33	0.14	0.40	0.14	0.26	1.21	10.2	ng/g
6 (FAsh)	0.79	1.81	1.47	0.54	0.88	1.04	0.27	1.01	0.27	0.45	0.10	0.18	1.56	10.4	ng/g
7 (FAsh)	8.89	19.0	12.4	8.54	7.92	10.2	5.20	16.5	4.72	8.46	0.82	4.20	41.7	149	ng/g
8 (soil)	0.39	1.06	0.89	0.28	0.46	0.51	0.14	0.64	0.12	0.13	0.04	0.04	1.06	5.76	ng/g
17 (sed)	0.03	–	0.17	–	–	–	0.43	–	–	–	–	–	–	0.63	ng/g

[a] Samples without data did not contain any H_6CDF. [b] Sample notation: ash, ash in the incinerator; FAsh, fly ash in the incinerator; soil, soil; sed, sediment. [c] –, ND.

Table X. Concentration of H_7CDDs and OCDD[a]

sample[b]	1,2,3,4,6,7,9	1,2,3,4,6,7,8	total	1,2,3,4,6,7,8,9	unit
1 (ash)	–[c]	–	–	0.07	ng/g
2 (ash)	0.03	0.04	0.07	0.33	ng/g
3 (ash)	1.32	1.48	2.80	7.33	ng/g
4 (FAsh)	38.7	42.7	81.4	84.1	ng/g
5 (FAsh)	498	512	1010	1700	ng/g
6 (FAsh)	52.6	60.9	114	278	ng/g
7 (FAsh)	364	413	777	1140	ng/g
8 (soil)	7.95	9.86	17.8	55.9	ng/g
10 (RWat)	–	–	–	0.49	ng/L
11 (GWat)	–	–	–	0.09	ng/L
12 (sed)	–	–	–	0.69	ng/g
14 (sed)	0.26	0.33	0.59	10.1	ng/g
15 (EWat)	–	–	–	0.73	ng/L
16 (RWat)	0.87	4.72	5.59	19.0	ng/L
17 (sed)	0.85	0.90	1.75	30.3	ng/g
18 (sed)	–	–	–	19.9	ng/g
19 (LWat)	0.44	0.39	0.83	2.84	ng/L
20 (soil)	–	–	–	2.57	ng/g
21 (RWat)	–	–	–	0.83	ng/L
22 (RWat)	0.55	0.68	1.23	149	ng/L
23 (soil)	0.02	0.02	0.04	1.17	ng/g
24 (RWat)	–	–	–	0.33	ng/L
25 (RWat)	–	–	–	0.08	ng/L
26 (sed)	–	–	–	0.60	ng/g
27 (soil)	–	–	–	1.11	ng/g
28 (sed)	1.60	1.72	3.32	11.5	ng/g

[a] Samples without data did not contain any H_7CDD and OCDD. [b] Sample notation: ash, ash in the incinerator; FAsh, fly ash in the incinerator; soil, soil; sed, sediment; EWat, effluent water from the incinerator plant; RWat, river water; GWat, groundwater; LWt, leached water from reclaimed land with the ash from the incinerator. [c] –, ND.

Concentrations of PCDD and PCDF isomers are shown in Tables IV–XI. It is noteworthy that there may be considerable deviation in these concentrations because of the poor recovery and only a single internal standard. Quantification of penta- to hexachloro congeners was less accurate, and it was not sure that samples marked with ND did not contain any isomer at all, since there were considerable interferences on the analysis and the background level on selected ion monitoring was fairly high. The most toxic 2,3,7,8-TCDD was detected only in the incinerator's fly ash and ash. The extraordinarily high concentrations of PCDDs and PCDFs in fly ash are impressive. It has been proved that the soil near incinerators has been polluted heavily with PCDDs and PCDFs. This is a special case of soil that has been contaminated with PCDDs and PCDFs from an incinerator. Since incinerator A is controlled very well and the burning temperature is over 1000 °C, the concentration of PCDDs and PCDFs in the ash from incinerator A (samples 1 and 2) has been significantly low when compared with those of other ash or fly ash. Amounts of PCDDs and PCDFs produced from incinerators were diverse according to the incinerator's type or operating conditions. High concentrations of 1,3,6,8- and 1,3,7,9-TCDDs in sample 17 were due to contaminants from the manufacturing of several herbicides in the factory. Most of TCDFs, P_5CDDs, P_5CDFs, H_6CDDs, and H_6CDFs were detected in fly ashes. Effluents from industrial plants contained considerable amounts of PCDDs. OCDD is the most abundant of the PCDDs and is present in higher concentrations than OCDF, and the total of H_7CDFs is the most abundant among PCDFs in most of the samples. These observations are consistent with the report by Czuczwa and Hites (*8*, *33*). High concentrations of OCDD in most environmental samples are very prominent. A large amount of OCDD has been contained even in the lake sediment (sample 28). Since there are no incineration plants near the lake, the source of OCDD might be contaminants of pentachlorophenol, which had been used

Table XI. Concentration of H_7CDFs and OCDF[a]

sample[b]	1,2,3,4,6,7,8	1,2,3,4,6,7,9	1,2,3,4,6,8,9	1,2,3,4,7,8,9	total	1,2,3,4,6,7,8,9	unit
1 (ash)	0.19	–[c]	–	–	0.19	0.05	ng/g
2 (ash)	0.06	0.04	0.03	–	0.13	0.04	ng/g
3 (ash)	9.07	1.40	1.40	0.65	12.5	0.46	ng/g
4 (FAsh)	70.3	5.00	10.1	2.62	88.0	–	ng/g
5 (FAsh)	464	63.8	81.5	35.3	645	115	ng/g
6 (FAsh)	33.9	13.5	11.3	5.13	63.8	25.4	ng/g
7 (FAsh)	328	220	214	125	887	398	ng/g
8 (soil)	18.9	6.16	5.03	2.38	32.5	0.31	ng/g
12 (sed)	0.09	0.05	–	–	0.14	–	ng/g
14 (sed)	0.22	0.08	0.28	0.04	0.62	0.24	ng/g
17 (sed)	1.30	0.48	3.88	0.29	5.95	0.76	ng/g
18 (sed)	0.38	–	0.95	–	1.33	1.04	ng/g
19 (LWat)	1.39	–	–	–	1.39	–	ng/L
22 (RWat)	1.55	0.30	0.15	0.06	2.06	–	ng/L
28 (sed)	1.06	0.68	0.71	0.42	2.87	1.96	ng/g

[a] Samples without data did not contain any H_7CDF and OCDF. [b] Sample notation: ash, ash in the incinerator; FAsh, fly ash in the incinerator; soil, soil; sed, sediment; RWat, river water; LWat, leached water from reclaimed land with the ash from the incinerator. [c] –, ND.

Table XII. Pattern Similarity of TCDDs in Environmental Samples[a]

	sample[b]												
sample[b]	3 (ash)	6 (FAsh)	7 (FAsh)	8 (soil)	12 (sed)	14 (sed)	15 (EWat)	16 (RWat)	17 (sed)	19 (LWat)	20 (soil)	23 (soil)	28 (sed)
1 (ash)	0.95	0.95	0.91	0.90	0.61	0.77	0.83	0.76	0.75	0.86	0.79	0.61	0.81
3 (ash)		0.95	0.88	0.89	0.86	0.92	0.80	0.72	0.70	0.80	0.73	0.56	0.80
6 (FAsh)			0.88	0.94	0.47	0.76	0.85	0.77	0.75	0.85	0.77	0.47	0.81
7 (FAsh)				0.86	0.71	0.84	0.86	0.83	0.82	0.90	0.86	0.71	0.86
8 (soil)					0.41	0.85	0.91	0.86	0.84	0.93	0.85	0.41	0.88
12 (sed)						0.37	0.39	0.32	0.32	0.49	0.42	1.00	0.41
14 (sed)							0.96	1.00	1.00	0.95	1.00	0.37	0.98
15 (EWat)								0.96	0.95	0.96	0.96	0.39	0.97
16 (RWat)									1.00	0.95	0.99	0.32	0.98
17 (sed)										0.94	1.00	0.32	0.98
19 (LWat)											0.96	0.49	0.94
20 (soil)												0.42	0.98
23 (soil)													0.41

[a] The number of components (factors) was 14. [b] Sample notation: ash, ash in the incinerator; FAsh, fly ash in the incinerator; soil, soil; sed, sediment; EWat, effluent water from the incinerator plant; RWat, river water; LWat, leached water from reclaimed land with the ash from the incinerator.

Table XIII. Pattern Similarity of TCDFs in Environmental Samples[a]

	sample[b]									
sample[b]	3 (ash)	4 (FAsh)	5 (FAsh)	6 (FAsh)	7 (FAsh)	8 (soil)	12 (sed)	17 (sed)	22 (RWat)	26 (sed)
1 (ash)	0.89	0.89	0.86	0.70	0.57	0.78	0.07	0.15	0.46	0.15
3 (ash)		0.98	0.97	0.85	0.77	0.92	0.27	0.20	0.43	0.22
4 (FAsh)			0.97	0.89	0.76	0.95	0.05	0.20	0.46	0.20
5 (FAsh)				0.82	0.86	0.90	0.03	0.27	0.44	0.12
6 (FAsh)					0.70	0.98	0.21	0.32	0.36	0.29
7 (FAsh)						0.76	0.12	0.46	0.25	0.08
8 (soil)							0.19	0.30	0.42	0.19
12 (sed)								0.49	0.14	0.00
17 (sed)									0.19	0.00
22 (RWat)										0.20

[a] The number of components (factors) was 23. [b] Sample notation: ash, ash in the incinerator; FAsh, fly ash in the incinerator; soil, soil; sed, sediment; RWat, river water.

formerly as a herbicide and is still used as a fungicide.

Mass spectra in the full-scan mode were measured for samples 5, 7, and 17, which contained a large amount of PCDDs and PCDFs, in order to confirm the presence of PCDDs and PCDFs clearly. These mass spectra were consistent with ones of the corresponding congener. Any spectra of polychlorinated diphenyl ethers or polychlorinated methoxybiphenyls were not observed. The mass spectrum that is identical with that of OCDD was contaminated with the mass spectrum of OCDF. Peaks of OCDD and OCDF overlap because the relative retentions of both compounds are the same.

In order to compare gas chromatographic patterns with each other, pattern similarity $S(A,B)$ was calculated according to

$$S(A,B) = \sum_i (A_i B_i) \Big/ \sqrt{\sum_i (A_i)^2} \sqrt{\sum_i (B_i)^2}$$

where A_i and B_i are the concentrations of congener i in samples A and B, respectively. This pattern similarity means the product of two vectors A and B in general. All

Table XIV. Pattern Similarity of PCDDs and PCDFs Including Tetra- through Octachloro Congeners in Environmental Samples[a]

	sample[b]												
sample[b]	6 (FAsh)	7 (FAsh)	8 (soil)	9 (EWat)	12 (sed)	13 (RWat)	14 (sed)	15 (EWat)	19 (LWat)	23 (soil)	26 (sed)	27 (soil)	28 (sed)
3 (ash)	0.71	0.77	0.84	0.03	0.63	0.03	0.62	0.14	0.87	0.60	0.52	0.53	0.69
6 (FAsh)		0.94	0.97	0.00	0.86	0.00	0.96	0.19	0.94	0.95	0.80	0.83	0.99
7 (FAsh)			0.93	0.00	0.76	0.00	0.84	0.16	0.88	0.82	0.68	0.71	0.94
8 (soil)				0.01	0.86	0.01	0.93	0.20	0.98	0.92	0.78	0.81	0.96
9 (EWat)					0.18	0.98	0.07	0.95	0.07	0.02	0.51	0.46	0.08
12 (sed)						0.19	0.90	0.32	0.85	0.91	0.86	0.86	0.88
13 (RWat)							0.07	0.95	0.07	0.03	0.53	0.48	0.09
14 (sed)								0.27	0.90	1.00	0.87	0.90	0.97
15 (EWat)									0.25	0.22	0.66	0.62	0.28
19 (LWat)										0.89	0.78	0.80	0.92
23 (soil)											0.85	0.88	0.96
26 (sed)												1.00	0.85
27 (soil)													0.87

[a] The number of components (factors) was 100. [b] Sample notation: ash, ash in the incinerator; FAsh, fly ash in the incinerator; soil, soil; sed, sediment; EWat, effluent water from the incinerator plant; RWat, river water; LWat, leached water from reclaimed land with the ash from the incinerator.

components in each vector are supposed to be perpendicular to each other. The components refer here to the peaks in the gas chromatography–mass spectrometry analysis. The most important thing is not the magnitude of the vectors, but the angle between the two vectors. The pattern similarity gives herein the degree of similarity between two gas chromtographic patterns irrespective of concentration. S(A,B) becomes 1.0 when two gas chromatographic patterns are completely equal. If gas chromatograms of samples A and B do not possess any common peak, S(A,B) is zero. Pattern similarity is very effective for investigation of the origin for PCDDs and PCDFs. Also, it is very useful to estimate the change of the gas chromatographic pattern with congener-selective decomposition, distribution, or transportation. Tables XII and XIII show pattern similarity of several samples of TCDDs and TCDFs, respectively. Regarding the TCDDs, samples were divided into two groups from a point of view of pattern similarity. One group (no. 1, 3, 6–8, 14–17, 19, 20, and 28) had the pattern typical to fly ash. The pattern of the other group (no. 12 and 23), which showed high similarity each other, was not similar to that of fly ash. Regarding the TCDFs, samples 1, 3–6, and 8 showed a similar pattern with each other. It is very reasonalbe that patterns of TCDFs in ash or fly ash are very similar with each other. Patterns of TCDFs in sediments and river water are dissimilar to those in ash and fly ash. But the pattern of TCDFs in soil (no. 8) is very similar to that in ash or fly ash. Pattern similarity for several samples for all congeners of PCDDs and PCDFs ranging from tetra- to octachloro congeners is shown in Table XIV. The pattern of PCDDs and PCDFs in ash was a little different from that in fly ash, although patterns of TCDDs and TCDFs in ash and fly ash were very similar to each other. It is very interesting that the leached water from reclaimed land with ash from the incinerator (no. 19) had a similar pattern to that of fly ash or ash. Therefore, reclamation with ash or fly ash from incinerators could pollute water with PCDDs and PCDFs. Samples listed in Table XIV are roughly divided into three groups according to the pattern similarity of total isomers. The first group, which is composed of samples 3, 6–8, and 19, has a pattern characteristic of fly ash. The second group, which is constituted with the samples 9, 13, and 15, shows a typical pattern of effluent water. The third group, which is made up of the samples 12, 14, 23, and 26–28 represents the pattern from soil. Gas chromatographic patterns of these three groups were not similar to each other. It is not clear now whether these differences of patterns in PCDDs and PCDFs come from congener-selective degradation, distribution, or transportation. Patterns between fly ash (for example, sample 7) and sample 28 were very similar because H_7CDDs, OCDD, H_7CDFs, and OCDF had high abundances in both samples. But the source of PCDDs and PCDFs in the sediment sample (no. 28) is not fly ash from the incinerator, since no TCDFs have been detected in the sample.

Acknowledgments

We thank A. S. Kende for providing the reference samples.

Literature Cited

(1) Safe, S. *Chemosphere* **1983**, *12*, 447–451.
(2) Huff, J. E.; Moore, J. A.; Saracci, R.; Tomatis, L. *EHP, Environ. Health Perspect.* **1980**, *36*, 221–240.
(3) Associate Committee on Scientific Criteria for Environmental Quality *Polychlorinated Dibenzo-p-dioxins; Limitations to the Current Analytical Techniques*; National Research Council of Canada: Ottawa, Canada, 1981; pp 172.
(4) Lustenhouwer, J. W. A.; Olie, K.; Hutzinger, O. *Chemosphere* **1980**, *9*, 501–522.
(5) Gizzi, F.; Reginato, R.; Benfenati, E.; Fanelli, R. *Chemosphere* **1982**, *11*, 577–583.
(6) Chiu, C.; Thomas, R. S.; Lockwood, J.; Li, K.; Halman, R.; Lao, R. C. C. *Chemosphere* **1983**, *12*, 607–616.
(7) Shaub, W. M.; Tsang, W. *Environ. Sci. Technol.* **1983**, *17*, 721–730.
(8) Czuczwa, J. M.; Hites, R. A. *Environ. Sci. Technol.* **1984**, *18*, 444–450.
(9) Buser, H. R. *J. Chromatogr.* **1975**, *107*, 295–310.
(10) Firestone, D.; Clower M., Jr.; Borsetti, A. P.; Teske, R. H.; Long, P. E. *J. Agric. Food Chem.* **1979**, *27*, 1171–1177.
(11) Nash, R. G.; Beall, M. L., Jr. *J. Agric. Food Chem.* **1980**, *28*, 614–623.
(12) Young, A. L.; Kang, H. K.; Shepard, B. M. *Environ. Sci. Technol.* **1983**, *17*, 530A–540A.
(13) Hori, S.; Obana, H.; Kashimoto, T.; Otake, T.; Nishimura, H.; Ikegami, N.; Kunita, N.; Uda, H. *Toxicology* **1982**, *24*, 123–139.
(14) Yamagishi, T.; Miyazaki, T.; Akiyama, K.; Morita, M.; Nakagawa, J.; Horii, S.; Kaneko, S. *Chemosphere* **1981**, *10*, 1137–1144.
(15) Kashimoto, T.; Miyata, H. *Kankyo Gijutsu* **1983**, *12*, 779–788 (in Japanese).
(16) Wakimoto, T.; Takasuga, T.; Ohira, S.; Tatsukawa, R. *Kogai to Taisaku* **1984**, *20*, 155–163 (in Japanese).

(17) Buser, H. R. *Anal. Chem.* **1977**, *49*, 918–922.
(18) Langhorst, M. L.; Shadoff, L. A. *Anal. Chem.* **1980**, *52*, 2037–2044.
(19) Lamparski, L. L.; Nestrick, T. J. *Anal. Chem.* **1980**, *52*, 2045–2054.
(20) Brumley, W. C.; Roach, J. A. G.; Sphon, J. A.; Dreifuss, P. A.; Andrzejewski, D.; Niemann, R. A.; Firestone, D. *J. Agric. Food Chem.* **1981**, *29*, 1040–1046.
(21) Raisanen, S.; Hiltunen, R.; Arstila, A. U.; Sipilainen, T. *J. Chromatogr.* **1981**, *208*, 323–330.
(22) Mazer, T.; Hileman, F. D.; Noble, R. W.; Brooks, J. J. *Anal. Chem.* **1983**, *55*, 104–110.
(23) Buser, H. R.; Rappe, C. *Anal. Chem.* **1984**, *56*, 442–448.
(24) Smith, L. M.; Stalling, D. L.; Johnson, J. L. *Anal. Chem.* **1984**, *56*, 1830–1842.
(25) Tong, H. Y.; Shore, D. L.; Karasek, F. W. *Anal. Chem.* **1984**, *56*, 2442–2447.
(26) Rappe, C. *Environ. Sci. Technol.* **1984**, *18*, 78A–90A.
(27) Ligon, W. V., Jr.; May, R. J. *Anal. Chem.* **1986**, *58*, 558–561.
(28) Pohland, A. E.; Yang, G. C. *J. Agric. Food Chem.* **1972**, *20*, 1093–1099.
(29) Kende, A. S.; Wade, J. J.; Ridge, D.; Poland, A. *J. Org. Chem.* **1974**, *39*, 931–937.
(30) Buser, H. R. *J. Chromatogr.* **1975**, *114*, 95–108.
(31) Gray, A. P.; Cepa, S. P.; Solomon, I. J.; Aniline, O. *J. Org. Chem.* **1976**, *41*, 2435–2437.
(32) Bell, R. A.; Gåra, A. *Chlorinated Dioxins and Dibenzofurans in the Total Environment*; Keith, L. H., Rappe, C., Choudhary, G., Eds.; Butterworth: Stoneham, MA, 1985; Vol. 2, pp 3–16.
(33) Czuczwa, J. M.; Hites, R. A. *Environ. Sci. Technol.* **1986**, *20*, 195–200.

Received for review June 16, 1986. Revised manuscript received December 9, 1986. Accepted June 29, 1987. This work was supported financially in part by grants from the Japan Environment Agency and the Japan Ministry of Education.

Reductive Dissolution of Manganese(III/IV) Oxides by Substituted Phenols

Alan T. Stone

Department of Geography and Environmental Engineering, The Johns Hopkins University, Baltimore, Maryland 21218

■ Kinetics of the reaction of manganese(III/IV) oxides with 11 substituted phenols were examined in order to assess the importance of manganese oxides in the abiotic degradation of phenolic pollutants. At pH 4.4, 10^{-4} M solutions of substituted phenols reduced and dissolved synthetic manganese oxide particles in the following order: *p*-methylphenol > *p*-ethylphenol > *m*-methylphenol > *p*-chlorophenol > phenol > *m*-chlorophenol > *p*-hydroxybenzoate > *o*-hydroxybenzoate > 4′-hydroxyacetophenone > *p*-nitrophenol. Rates of reductive dissolution generally decrease as the Hammett constants of ring substituents become more positive, reflecting trends in the basicity, nucleophilicity, and half-wave potential of substituted phenols. Evidence indicates that the fraction of oxide surface sites occupied by substituted phenols is quite low. The apparent reaction order with respect to $[H^+]$ is not a constant but varies between 0.45 and 1.30 as the pH range, phenol concentration, and phenol structure are varied. A mechanism for the surface chemical reaction has been postulated to account for these effects.

Introduction

Iron(III) and manganese(III/IV) oxides, widely distributed as suspended particles in surface waters and as cements and coatings in soils and sediments, are potential oxidizing agents of natural and xenobiotic organic compounds (*1*, *2*):

$$Fe^{III}OOH(s) + 3H^+ + e^- \rightleftarrows Fe^{2+}(aq) + 2H_2O \quad (1)$$
$$E^\circ = +0.67\ V$$

$$Mn^{III}OOH(s) + 3H^+ + e^- \rightleftarrows Mn^{2+}(aq) + 2H_2O \quad (2)$$
$$E^\circ = +1.50\ V$$

$$^1/_2Mn^{IV}O_2(s) + 2H^+ + e^- \rightleftarrows {}^1/_2Mn^{2+}(aq) + H_2O \quad (3)$$
$$E^\circ = +1.23\ V$$

Although the crustal abundance of manganese is only a tenth that of iron (*3*), the oxidant strength and reactivity of manganese oxides make them important participants in environmental oxidation–reduction reactions. In combination with iron oxides and molecular oxygen, they make up the oxidant poising capacity of soils, sediments, and other oxide-rich environments.

Many classes of natural and xenobiotic organic compounds are facile reductants, capable of reducing manganese oxides (*4*, *5*). Phenols are naturally present in surface waters and groundwaters as degradation products of lignin and other plant materials. In addition, anthropogenic inputs of phenolic pesticides and industrial wastes are important. Methylphenols, ethylphenols, chlorophenols, and phenol, for example, have been found in landfill leachate plumes (*6*). These and other substituted phenols pose a direct threat to human health. Chronic toxicity arising from long-term exposure to trace levels of pentachlorophenol, phenol-containing pesticides, and phenolic wastes is a subject of growing concern.

The objectives of this study are (1) to determine rates of reaction between manganese oxides and substituted phenols, (2) to explore structure–reactivity relationships in the oxidative degradation of phenols, and (3) to assess the importance of manganese oxides in degrading substituted phenols in aquatic environments.

Oxidation of Substituted Phenols. The oxidation of substituted phenols by metal ion oxidants is a complex process; reaction rates and product distribution depend not only upon the nature of the oxidant but also upon reactant concentrations and medium composition as well (*7*). Reactions of substituted phenols pertinent to this discussion are shown in Figure 1. In a number of instances, reaction begins with a 1-equiv oxidation of the phenolate anion (ArO^-) yielding phenoxy radicals ($ArO^\bullet$) (*7*, *8*). The protonated form (ArOH) is considerably less reactive. The outer-sphere oxidant hexachloroiridate(IV) anion, for example, oxidizes ArO^- more than 6 orders of magnitude more quickly than ArOH (*9*).

Several competing, irreversible reactions consume phenoxy radicals. Encounters between phenoxy radicals result in radical coupling and dimer formation. Many phenolic dimers are more susceptible toward oxidation than corresponding monomers, and therefore oxidative coupling continues, forming a complex mixture of polymeric oxidation products (*10*). Low radical concentrations limit the frequency of radical–radical encounters and favor competitive pathways. A 1-equiv oxidation of phenoxy radicals to phenoxenium ions (ArO^+) is a possible competitive pathway. Phenoxenium ions are, in turn, con-

0013-936X/87/0921-0979$01.50/0

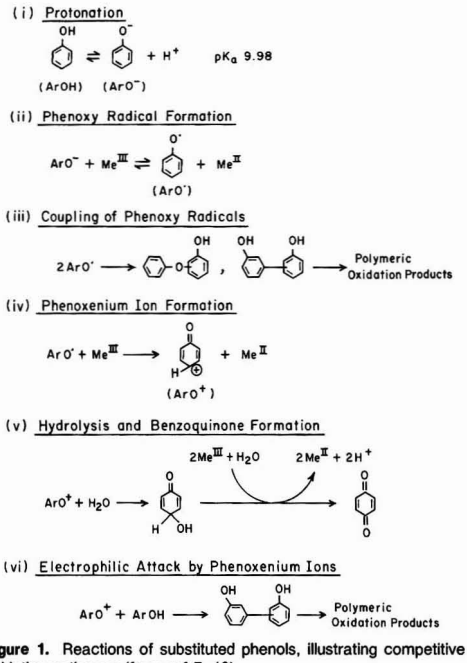

Figure 1. Reactions of substituted phenols, illustrating competitive oxidative pathways (from ref 7–10).

sumed by electrophilic attack on phenol or by hydrolysis and benzoquinone formation (*7*). Low pH favors phenoxenium ion formation and production of quinones over radical coupling (*7*). Ring cleavage of coupled products and benzoquinones to carboxylic acids and other aliphatic products occurs with some oxidants (*11*). Molecular oxygen has a particularly strong impact on the distribution of oxidation products. Addition of molecular oxygen to phenoxy radicals generates organoperoxides and organoperoxy radicals (*12–14*).

Reaction Scheme. Reactions involving manganese(III/IV) oxides differ in several important respects from analogous reactions of metal ion complexes in homogeneous solution. Manganese(III) and manganese(IV) centers are incorporated within an oxide surface when reduction occurs; the flux of Mn(III) and Mn(IV) from the surface into overlying solution is negligible, given the exceedingly low solubility of oxides formed from these oxidation states (*15*). Specific interaction between reductant molecules and oxide surface sites is believed to be necessary for reaction, since adsorbed calcium and phosphate ions strongly inhibit reaction (*15*). Small changes in reductant structure cause large differences in reaction rates, another indication of specific interaction (*5*). Thus, reductive dissolution of manganese(III/IV) oxides is surface chemical reaction controlled and requires close association of reductant molecules with surface sites before electron transfer and metal ion release can occur.

The following reaction scheme is presented to serve as a focus for discussion.

Precursor complex formation:

$$>Mn^{III} + ArOH \underset{k_{-1}}{\overset{k_1}{\rightleftharpoons}} (>Mn^{III},ArOH) \quad (4)$$

Electron transfer:

$$(>Mn^{III},ArOH) \underset{k_{-2}}{\overset{k_2}{\rightleftharpoons}} (>Mn^{II},ArO^{\bullet}) + H^+ \quad (5)$$

Release of phenoxy radical:

$$(>Mn^{II},ArO^{\bullet}) \underset{k_{-3}}{\overset{k_3}{\rightleftharpoons}} >Mn^{II} + ArO^{\bullet} \quad (6)$$

Release of reduced Mn(II):

$$>Mn^{II} \underset{k_{-4}}{\overset{k_4}{\rightleftharpoons}} Mn^{2+} (+ >Mn^{III}) \quad (7)$$

Coupling and further oxidation:

$$ArO^{\bullet} + ArO^{\bullet} \rightarrow \text{quinones, dimers, and polymeric oxidation products} \quad (8)$$

Surface metal centers are denoted by their oxidation state ($>Mn^{III}$ and $>Mn^{II}$). Manganese(IV) is also present on the oxide surface and will take part in reactions similar to the reactions outlined above. For the moment, protonation equilibria of unoccupied surface groups ($>Mn^{III}OH_2^+$, $>Mn^{III}OH$, and $>Mn^{III}O^-$), reductant molecules (ArOH and ArO^-), and reaction intermediates are ignored. Precursor complex formation may be an inner-sphere reaction, when the incoming phenols bind directly to surface metal centers, or an outer-sphere reaction, when a layer of coordinated OH^- or H_2O molecules separates phenols from surface metal centers (*16*). Release of Mn^{2+} uncovers underlying oxide sites; the relationship between moles of Mn^{2+} released and moles of new surface sites generated is unknown. It is difficult to determine whether phenol reactant molecules, phenoxy radical intermediates, or oxidation products participate in the release of Mn(II) from the oxide lattice into solution. Reactions of radical and coupled organic intermediates with manganese oxide surface groups are not written explicitly but may contribute to the overall dissolution rate.

Much recent effort has been directed toward developing a conceptual understanding of surface chemical reactions responsible for reductive dissolution (*16–23*). Of particular interest is the use of reaction schemes, such as the one outlined above, in interpreting results from experiments and predicting reaction rates under unexplored conditions (*21*).

Experimental Section

Unless otherwise stated, all solutions were prepared from reagent-grade chemicals and 18 μΩ resistivity water (DDW, Millipore) and filtered with 0.2 μm pore diameter membrane filters (Nucleopore Corp.) before use. All glassware was soaked in 5 N HNO_3 and thoroughly rinsed with DDW prior to use.

Preparation of Oxide Particles. Four different types of manganese oxide particles were synthesized and characterized for the dissolution experiments. Total manganese in particle suspensions was measured by atomic absorption spectrophotometry (AAS) and oxidizing titer measured by back-titration of excess oxalate with permanganate (*24*). Particles were examined by high-resolution transmission electron microscopy (HRTEM) and crystallographic *d* spacings measured by electron diffraction. Brunauer–Emmett–Teller (BET) analysis was performed on freeze-dried particles. Particle characteristics are summarized in Table I, and HRTEM micrographs are shown in Figure 2.

Type A particles were prepared by adding a stoichiometric amount of stock $MnSO_4$ solution to 2.0×10^{-3} M $NaMnO_4$ in a pH 6.6, 5×10^{-2} M phosphate buffer at 25 °C under air. Settled particles were removed and resuspended in water, sonicated, and then removed again by centrifugation. Particles were rinsed 8 times in this manner before final resuspension in 1×10^{-4} M NaOH. HRTEM shows that type A oxides are aggregates of ex-

Table I. Characteristics of Manganese(III/IV) Oxide Particles

characteristics	type A	type A′	type B	type C
av oxidn state	+3.81	+3.82	+3.70	+3.62
stoichiometry	$MnO_{1.91}$	$MnO_{1.91}$	$MnO_{1.85}$	$MnO_{1.81}$
surface area, m^2/g		25	160	67
crystallographic *d* spacings, Å	4.53	3.55	4.94	2.59
	3.52	1.78	3.10	1.67
	2.26	1.56	2.51	1.27
	1.71		2.07	
	1.52		1.54	
	1.30			
	1.26			

tremely small, spheroidal particles. Type A′ particles were prepared in a similar manner.

Type B particles were prepared by equilibrating a 1.0×10^{-3} M Na_2SO_4–5.0×10^{-3} M NaOH solution with 0.20 atm of oxygen gas (balance nitrogen), chilling to 5 °C in an ice bath, and then adding enough $MnCl_2$ stock solution under rapid stirring to give a 3.0×10^{-4} M manganese solution. Particles were rinsed 4 times as described above before final resuspension in 1×10^{-4} M NaOH. HRTEM photographs indicate that type B particles are extremely thin, crumpled sheets, with high surface area.

Preparation of type C particles began by equilibrating 5.0×10^{-3} M $MnSO_4$ and 1.2×10^{-2} M H_2O_2 at neutral pH in a 5 °C ice bath. Raising the solution pH to 10.4 by addition of 6×10^{-4} M NH_4OH initiated the oxidation reaction and particle production. Particles were rinsed 4 times as described above before final resuspension in 1×10^{-4} M NaOH. HRTEM photographs show type C particles to be extremely thin, crumpled sheets with high surface area.

Surface proton balances were calculated from titrations of type A particle suspensions and particle-free solutions containing 1.0×10^{-1} M and 1.0×10^{-2} M NaCl with 0.1 N NaOH and 0.1 N HCl (see ref 25). Classic behavior was not observed; the apparent pH_{zpc} (zero point of charge) was lower in 1.0×10^{-1} M NaCl than in 1.0×10^{-2} M NaCl, and plots of proton balance as a function of pH parallel each other. One possible explanation is that type A oxide particles undergo an ion-exchange reaction, exchanging lattice-bound H^+ for Na^+ as the concentration of NaCl is increased.

Dissolution Experiments. Substituted phenols listed in Table II were purchased from Aldrich Chemical Co.

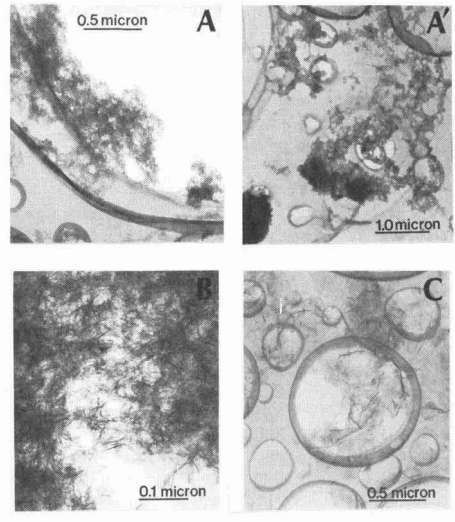

Figure 2. High-resolution transmission electron micrographs of type A, A′, B, and C particles collected on holey carbon grids.

(greater than 99% purity) and used without further purification. Stock 1.0×10^{-2} M substituted phenol solutions contained 25% ethanol and were used within 24 h. Within this time, no changes in UV absorbance of the stock phenol solutions were observed. Preliminary experiments showed that small amounts of ethanol did not influence rates of reductive dissolution. The ionic strength was maintained at 5.0×10^{-2} M with NaCl. Temperature was held constant at 25 °C with jacketed beakers and a circulating constant-temperature bath. Manganese oxide suspensions were equilibrated in the reaction solution under nitrogen purging for over 1 h to keep dissolved oxygen to a minimum.

Constant pH was maintained with either acetate or constant-P_{CO_2} buffers. Acetate had a negligible effect on reaction rate, since varying the concentration of acetate (from 10^{-3} to 10^{-2} M) or maintaining the pH by HCl and NaOH addition in acetate-free solution did not affect the dissolution rate. Constant-P_{CO_2} buffer was employed for reactions at pH above 6.0, alkalinity was set by addition of $NaHCO_3$, and suspensions were purged with 1% CO_2 (balance nitrogen) for at least 2 h before the addition of

Table II. Properties of Substituted Phenols and Rates of Reductive Dissolution

	Hammett constant[a]	pK_a[b]	log K_{Fe}[c]	$E_{1/2}$,[d] V	dissolution rate,[e] mol L^{-1} min^{-1} type A oxide	dissolution rate,[e] mol L^{-1} min^{-1} type B oxide
			Meta- and Para-Substituted Phenols			
p-methylphenol	−0.16	10.26	9.26	0.543	2.06×10^{-6}	7.67×10^{-7}
p-ethylphenol	−0.15	10.21		0.567	1.97×10^{-6}	
m-methylphenol	−0.07	10.01	8.51	0.607	4.48×10^{-7}	
phenol	+0.00	9.98	8.20	0.633	2.22×10^{-7}	1.25×10^{-7}
p-chlorophenol	+0.22	9.42	7.92	0.653	3.89×10^{-7}	2.50×10^{-7}
m-chlorophenol	+0.37	9.13	7.89	0.734	3.84×10^{-8}	
p-hydroxybenzoic acid	+0.45	9.46 (4.58)		0.716	1.93×10^{-8}	1.48×10^{-8}
p-hydroxyacetophenone	+0.50	8.05		0.791	1.42×10^{-9}	8×10^{-10}
p-nitrophenol	+0.78	7.15	5.74	0.924	$<10^{-9}$	
			Ortho-Substituted Phenols			
o-chlorophenol		8.29	7.32	0.625	2.48×10^{-7}	
o-hydroxybenzoate		13.74 (2.97)		0.845	1.15×10^{-8}	3.0×10^{-9}

[a] From ref 30. [b] From ref 31–33. [c] From ref 31. [d] From ref 37. [e] Dissolution rates were measured in pH 4.4 (1×10^{-3} M acetate buffer) solutions containing 5.0×10^{-2} M NaCl and 1×10^{-4} M substituted phenol. Total manganese added (as oxide particles) was 4.8×10^{-5} and 3.5×10^{-5} M for experiments with type A and type B oxide particles, respectively.

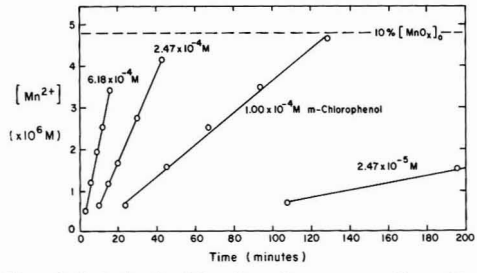

Figure 3. Reductive dissolution of type A manganese oxide particles with increasing amounts of *m*-chlorophenol. Reaction conditions: 4.8 × 10^{-5} M total manganese (added as oxide particles), pH 4.4 (1 × 10^{-3} M acetate buffer), 5.0 × 10^{-2} M NaCl.

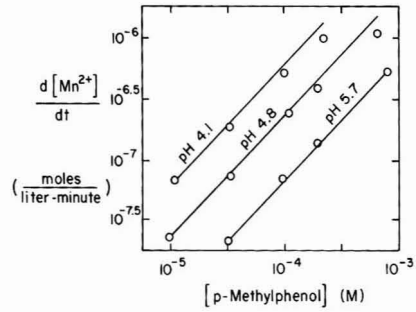

Figure 4. Reductive dissolution of type C oxide particles (6.35 × 10^{-5} M total manganese) by increasing amounts of *p*-methylphenol in 1.0 × 10^{-3} M acetate buffer. A solid line having a 1:1 slope is drawn through the lowest value for each set of points; data fall on this line when the dissolution rate is directly proportional to *p*-methylphenol concentration.

substituted phenols. Negligible differences were observed between reactions performed with acetate buffer and reactions at the same pH performed with constant-P_{CO_2} buffer.

Dissolved and particulate manganese were distinguished by filtering aliquots of the reaction solution with 0.2 μm pore diameter × 25 mm membrane filters (Nucleopore Corp.), as described previously (*15*). Particles retained by 0.2-μm membrane filters are actually aggregates of much smaller, high surface area particles. Concentrations of dissolved manganese were determined by AAS. In the absence of reductant, dissolution of manganese oxide particles was below the detection limit.

Surface coverage by phenol and *p*-chlorophenol during reductive dissolution of type B oxide was measured by the following procedure: (1) removal of oxide particles by membrane filtration, (2) fast reduction of oxide particles by addition of ascorbate in phosphate buffer, releasing phenols, (3) extraction of phenols into 60:40 hexane/ether, and (4) analysis of phenols using a Hewlett-Packard 5890A capillary gas chromatograph. The amount of adsorbed phenols detected by this technique was quite small (on the order of 1 × 10^{-7} mol/L in 10^{-4} M phenol suspensions), near the detection limit of this technique. It is estimated that between 1 × 10^{-6} and 1 × 10^{-5} mol of manganese oxide surface site/L is available for adsorption, on the basis of BET surface area measurements and assuming between 4 and 10 surface sites per square nanometer (*26*). Thus, phenol and *p*-chlorophenol apparently occupy less than 10% of the available oxide surface sites.

Results and Discussion

Results of a typical reductive dissolution experiment are shown in Figure 3, in which type A particles are reduced and dissolved by increasing amounts of *m*-chlorophenol. Loading of manganese oxide particles provides an equivalent of 4.8 × 10^{-5} M manganese. Rates of [Mn^{2+}] release gradually decrease as the reaction progresses, causing curvature in plots of [Mn^{2+}] as a function of time. Up to the point where 10% of the oxide has been dissolved, this curvature is small, and the increase in [Mn^{2+}] with time is nearly linear. Initial rates of reductive dissolution are calculated by linear regression within this time interval. A decision was made to investigate initial rates, since substantial changes in oxide surface characteristics and coating of the oxide surface with oxidized organic products may complicate the kinetic behavior once a significant amount of reaction has taken place. The fitted regression lines calculated during the first 10% of the reaction are shown in Figure 3.

Effect of Substituted Phenol Concentration. Rates of type C manganese oxide particle dissolution as a function of *p*-methylphenol concentration are shown in Figure 4, with a log–log plot. Experiments were performed at three different pH values with 1.0 × 10^{-3} M acetate buffers. A solid line having a 1:1 slope is drawn through the lowest value for each set of points; data fall on this line when the dissolution rate is directly proportional to *p*-methylphenol concentration. At constant *p*-methylphenol concentration, the reductive dissolution rate increases as the pH is decreased. At pH 5.7, the dissolution rate is directly proportional to *p*-methylphenol concentration over the concentration range studied. At pH 4.8 and pH 4.1, points fall slightly below the 1:1 proportionality line as the *p*-methylphenol concentration is increased.

Reductive dissolution rates as a function of substituted phenol concentration were also measured for reaction of *m*-chlorophenol and *o*-hydroxybenzoate with type B oxide particles. At pH 4.4, the reaction order with respect to reductant concentration is close to 1.0 in both cases.

The reaction scheme outlined in eq 4–8 can be used to explore the effect of substituted phenol concentration on overall rates of reductive dissolution. A mass balance equation for oxide surface sites is (*21*)

$$S_T = [>Mn^{III}] + [>Mn^{III},ArOH] + [>Mn^{II},ArO^{\bullet}] + [>Mn^{II}] \quad (9)$$

Consider the special case where precursor complex formation and electron transfer are rate-limiting steps (reactions 6–8 are fast) and back electron transfer is negligible ($k_2 \gg k_{-2}$). Under these conditions, surface concentrations of reduced surface sites (>Mn^{II},$ArO^{\bullet}$) and >Mn^{II} are low and can be left out of the mass balance equation. The dissolution rate is given by

$$\frac{d[Mn^{2+}]}{dt} = k_2[>Mn^{III},ArOH] \quad (10)$$

Assuming steady-state phenol surface coverage, eq 10 can be written in terms of S_T and the phenol concentration:

$$v = \frac{d[Mn^{2+}]}{dt} = \frac{k_1 k_2 S_T[ArOH]}{k_1[ArOH] + k_{-1} + k_2} \quad (11)$$

This result resembles classic Michaelis–Menten kinetics (*27*), and the relationship between substituted phenol concentration and dissolution rate resembles an absorption isotherm. Rates of reductive dissolution initially increase in direct proportion to phenol concentration [in the concentration range where ($k_{-1} + k_2$) > k_1[ArOH]]. Reaction

rate eventually levels out as the surface becomes saturated with phenol, and electron transfer becomes rate-limiting [when $k_1[\mathrm{ArOH}] \gg (k_{-1} + k_2)$].

Taking the reciprocal of eq 11 shows that $1/v$ is proportional to $1/[\mathrm{ArOH}]$, similar to the Lineweaver–Burk equation (*27*):

$$\frac{1}{v} = \frac{k_{-1} + k_2}{k_1 k_2 S_T[\mathrm{ArOH}]} + \frac{1}{k_2 S_T} \qquad (12)$$

The maximum rate of reductive dissolution is given by $v_m = k_2 S_T$ and occurs when the surface is saturated with adsorbed phenol. The quantity $(k_{-1} + k_2)/k_1$, analogous to a Michaelis–Menten constant, is a measure of the binding constant of phenol to oxide surface sites.

Lineweaver–Burk plots were constructed from the data shown in Figure 4. In every case, the calculated value of the Michaelis–Menten constant (phenol concentration at which the surface coverage is one-half of S_T) is considerably higher than the concentration range of the reductive dissolution experiments. In all three cases, *p*-methylphenol concentrations are significantly below concentrations necessary for saturation of the oxide surface to occur. These results indicate that the fraction of surface sites occupied by substituted phenols during reductive dissolution is, in fact, low under the conditions of study. Results from determinations of adsorbed phenols by gas chromatography are consistent with this finding.

In one study using a sensitive radiotracer technique, the adsorption of phenol onto iron oxide particles was found to be below the detection limit (1–2% of the phenol activity in solution) (*28*). Since manganese oxides have surface characteristics similar to iron oxides, this work supports the conclusion that phenol surface coverage on manganese oxides is low.

Substituent Effects. Reductive dissolution experiments were performed with type A and type B manganese oxide particles and 11 substituted phenols. Rates of reductive dissolution, along with pertinent chemical properties of substituted phenols, are listed in Table II. Initial rates of reductive dissolution were all measured under the same set of chemical conditions: 1.0×10^{-4} M phenol, 1.0×10^{-3} M acetate buffer (pH 4.4), and 5.0×10^{-2} M NaCl. Manganese oxide particle loadings were 4.8×10^{-5} and 3.5×10^{-5} M manganese in experiments with type A and type B particles, respectively.

Ring substituents influence the reactivity of phenolic compounds through steric, resonance, and field effects (*29*). Meta- and para-substituted phenols are listed in order of increasing Hammett constants [σ_m and σ_p (*30*)] in Table II. Carboxy, aceto, nitro, chloro, and other σ electron-withdrawing substituents (with positive Hammett constants) decrease the basicity (lower the pK_a) of phenol (*31–33*). Alkyl, alkoxy, and other σ electron-donating substituents (with negative Hammett constants) increase the basicity of phenol. Steric effects are negligible for meta- and para-substituted phenols on this list.

Effects of ring substituents on rates of precursor complex formation will now be considered. Rates of outer-sphere complex formation in homogeneous solution are near diffusion controlled (*34*) and relatively insensitive to changes in ligand nucleophilicity. Inner-sphere complexes are formed when H_2O and OH^- ligands in the inner coordination spheres of surface metal centers are exchanged for entering ArOH and ArO^- ligands. Inner-sphere ligand substitution by a purely dissociative mechanism is insensitive to the nature of the incoming ligand, while substitution by associative mechanisms may depend upon the nucleophilicity of the incoming ligand (*35*). Inner-sphere complex formation between Fe^{3+} and substituted phenols has been shown to take place via a dissociative interchange mechanism; the rate-limiting step is the release of coordinated water, and rates are insensitive to changes in ring substituents (*36*). If electron transfer between manganese oxide surface groups and substituted phenols occurs via inner-sphere precursor complexes, similar behavior may be observed. Release of phenoxy radicals is also a ligand substitution reaction, and rates may be sensitive to substituent effects.

If rates of adsorption and desorption are fast, relative to the subsequent electron transfer, then precursor complex formation can be treated as a preequilibrium step. Equilibrium constants for manganese oxide surface complex formation ($K_1 = k_1/k_{-1}$) are analogous to complex formation reactions of metal ions in homogeneous solution. In either case, electron-withdrawing substituents reduce the electron density on the hydroxy group, lowering the stability of complexes with metal centers. Equilibrium constants are available for the complexation of Fe^{3+} with phenolate anions (*31*):

$$Fe^{3+} + ArO^- \rightleftarrows Fe^{III}(ArO)^{2+} \qquad \log K_{Fe} \qquad (13)$$

As shown in Table II, $\log K_{Fe}$ values decrease as the Hammett constant is increased. Inner-sphere complex formation with manganese oxide surface sites can be expected to follow the same trend.

Electron-transfer reactions also experience substituent effects. When the solution pH is significantly below the pK_a of the parent phenol, concentrations of phenolate anion and phenoxy radical are both low, and reaction ii in Figure 1 is fast, relative to subsequent irreversible reactions (*7*). Under these conditions, phenoxy radical formation can be treated as a reversible reaction. Half-wave potentials ($E_{1/2}$, in volts) given in Table II were measured by Suatoni et al (*37*) in 1.0 M acetate buffer at pH 5.6 and reported with reference to the saturated calomel electrode. Half-wave potentials are experimentally derived reduction potentials that depend upon the chemical speciation and diffusion coefficients of oxidant and reductant as well as the thermodynamic driving force for reaction (*38*). Half-wave potentials decrease as the Hammett constant of meta and para substituents increase, indicating that phenols with electron-withdrawing substituents are more resistant to oxidation than phenols with electron-donating substituents. Electron-transfer rates between substituted phenols and iron(III) cyanide (*39*), 1,10-phenanthroline (*40*, *41*), and 2,2′-bipyridine (*42*, *43*) complexes in homogeneous solution correlate well with the electron-donating or electron-withdrawing nature of ring substituents, as represented by their Hammett constants. In an analogous manner, rates of electron transfer with manganese oxide surface sites can be expected to decrease going down the list of substituted phenols in Table II, as ring substituents become more electron withdrawing.

Trends in pK_a, $\log K_{Fe}$, and $E_{1/2}$ all predict decreases in the rates of reductive dissolution as the Hammett constant becomes more positive; decreases in basicity (and nucleophilicity) inhibit precursor complex formation, while increased resistance to phenoxy radical formation inhibits electron transfer. Results from the reductive dissolution experiments support these expectations. The substituent effects are quite pronounced, causing more than 3 orders of magnitude variation in rates of reductive dissolution. Rates generally decrease when electron-donating substituents are replaced by electron-withdrawing substituents.

Logarithms of the initial rates of reductive dissolution are plotted against half-wave potentials in Figures 5 and 6. For both type A and type B particles, dissolution rate

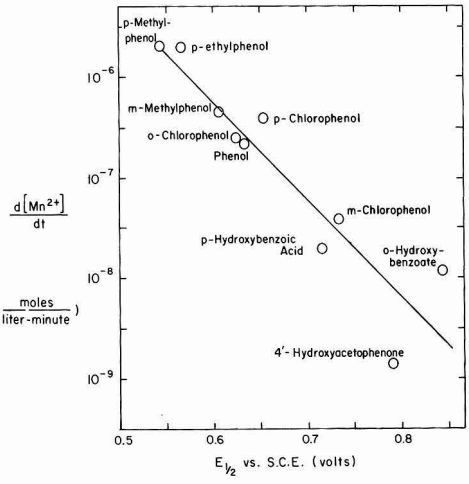

Figure 5. Rates of reductive dissolution of type A particles decrease as the half-wave potentials of the substituted phenols (as reported in ref 37) increase (4.8×10^{-5} M total manganese, pH 4.4).

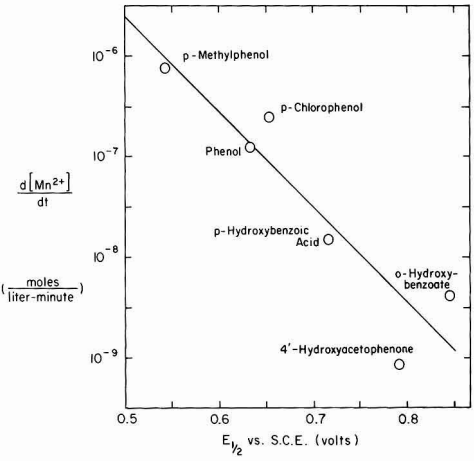

Figure 6. Rates of reductive dissolution of type B particles decrease as the half-wave potentials of the substituted phenols (as reported in ref 37) increase (3.5×10^{-5} M total manganese, pH 4.4).

generally decreases with increasing half-wave potential. *p*-Methylphenol, for example, has the lowest half-wave potential and reacts most quickly with manganese oxide particles, while *p*-nitrophenol, with the highest half-wave potential, is the least reactive. Linear regression of dissolution rate against half-wave potentials highlights the overall trend and points out unusually reactive and unreactive substituted phenols. *p*-Chlorophenol and *o*-hydroxybenzoate react more quickly than trends in $E_{1/2}$ would indicate, while *p*-hydroxybenzoate and *p*-hydroxyacetophenone react less quickly.

Hammett constants often underestimate the effect of resonance interactions. The higher than expected reactivity of *p*-chlorophenol may arise from π resonance interaction that provides an electron-donating conjugative effect, which partially counteracts the σ electron-withdrawing effect (*29*).

In the case of ortho-substituted phenols, steric and other neighboring group interactions complicate the interpretation of substituent effects. Rates of reductive dissolution by *o*-chlorophenol agree well with trends in $E_{1/2}$ but not with trends in pK_a and log K_{Fe}. *o*-Hydroxybenzoate occupies a special position in this list, because it is the only phenol possessing two ligand donor groups, making it capable of chelating metals. The fact that it reacts more quickly than trends in basicity or $E_{1/2}$ would predict is not surprising; chelation makes surface complex formation more favorable, promoting reaction.

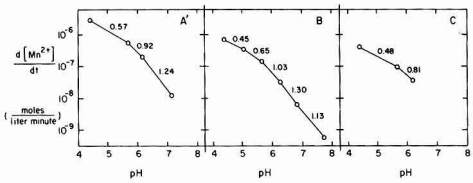

Figure 7. Reductive dissolution of type A', B, and C oxide particles by 1.0×10^{-4} M *p*-methylphenol as a function of pH. Reactions were performed in 5.0×10^{-2} M NaCl with either 1×10^{-3} M acetate or constant-P_{CO_2} buffers. Total added manganese was 5.16×10^{-5}, 3.53×10^{-5}, and 6.35×10^{-5} M for experiments with type A', B, and C particles, respectively. Values of n, the apparent order with respect to $[H^+]$, are given for each successive pair of points.

Thus, substituent effects and their effect on chemical properties provide a basis for explaining relative rates of manganese oxide dissolution by a homologous series of substituted phenols. Meta- and para-substituted phenols exhibit the best correlation with known chemical properties. In the case of ortho-substituted phenols, steric and other neighboring group interactions complicate predictions of reactivity.

Effect of pH. The apparent reaction order with respect to $[H^+]$ is an experimentally derived quantity given by the slope of the log of the reaction rates plotted as a function of pH:

$$\frac{d[Mn^{2+}]}{dt} = k[\text{phenol}]^m[H^+]^n \qquad (14)$$

$$\log (d[Mn^{2+}]/dt) = \log k + m \log [\text{phenol}] + n \log [H^+] \qquad (15)$$

There are no a priori reasons for assuming that the apparent order n is constant or an integer number.

p-Methylphenol is the most reactive of the substituted phenols included in this study and is the focus of most of this discussion. Figure 7 shows that dissolution rate increases as the pH is decreased for reaction of 1.0×10^{-4} M *p*-methylphenol with type A', B, and C particles. Rates of manganese oxide dissolution in the absence of reductants are negligible within the pH range of study. The apparent order of the reductive dissolution reaction with respect to $[H^+]$ (n) is calculated from successive pairs of points. In all three cases, the pH dependence defines a curve, rather than a straight line, with reaction rates leveling out at low pH. Values of n are generally above 1.0 at pH values above 6.0 but decrease to below 0.5 as pH 4.0 is approached.

Experiments described in an earlier section examined rates of reductive dissolution of type C particles measured as a function of *p*-methylphenol concentration at three different pH values (Figure 4). Values of n are apparently functions of reductant concentration. At low *p*-methylphenol concentrations, dissolution rates are proportional to reductant concentration, regardless of pH. As the *p*-methylphenol concentration is increased, however, dissolution rates at pH 4.1 fall below 1:1 proportionality before similar behavior is observed at pH 4.8. Dissolution rates

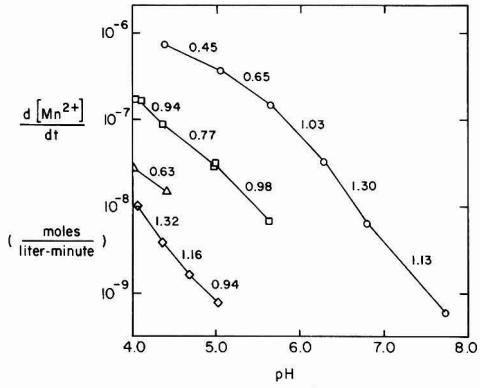

Figure 8. Reductive dissolution of 3.5×10^{-5} M type B oxide particles by four substituted phenols: 1.0×10^{-4} M (○) *p*-methylphenol, (□) phenol, (△) *p*-hydroxybenzoic acid, and (◇) *o*-hydroxybenzoate (5.0×10^{-2} M NaCl, acetate, and constant-P_{CO_2} buffers). Values of *n*, the apparent order with respect to $[H^+]$, are given for each successive pair of points.

at pH 5.7 continue obeying 1:1 proportionality throughout the range of concentrations considered. As a consequence, the apparent order *n* is higher in 1.0×10^{-5} M *p*-methylphenol, for example, than in 1.0×10^{-3} M *p*-methylphenol.

Rates of reductive dissolution of type B oxide particles by 10^{-4} M *p*-methylphenol, phenol, *p*-hydroxybenzoic acid, and *o*-hydroxybenzoate are shown as a function of pH in Figure 8. Considerable differences exist in values of *n*. At pH 4.5, for example, *n* has a range between 0.45 for reaction with *p*-methylphenol and 1.16 for reaction with *o*-hydroxybenzoate. Values of *n* decrease as the pH is decreased in the presence of *p*-methylphenol but show little variation with pH in the presence of phenol. In the presence of 10^{-4} M *o*-hydroxybenzoate, *n* increases substantially as the pH is decreased. A series of experiments were also performed in the presence of 10^{-3} M *o*-hydroxybenzoate, and a similar increase in *n* with decreasing pH was obtained. Note that pK_a values of carboxylic acid groups are 2.80 for *o*-hydroxybenzoic acid and 4.58 for *p*-hydroxybenzoic acid. As a consequence, anionic *o*-hydroxybenzoate is the predominant species within the pH range of study, while *p*-hydroxybenzoic acid shifts from a neutral to an anionic species at pH 4.58.

Several factors contribute to the observed pH dependence of the reductive dissolution reaction. Rates of precursor complex formation depend upon the degree of reactant protonation. A three-site model (*44*) is used to formulate the protonation reactions of unoccupied sites:

$$>Mn^{III}OH_2^+ \rightleftarrows >Mn^{III}OH + H^+ \quad pK^s_{a1} \quad (16)$$

$$>Mn^{III}OH \rightleftarrows >Mn^{III}O^- + H^+ \quad pK^s_{a2} \quad (17)$$

Rates of ligand exchange at $>Mn^{III}OH_2^+$, $>Mn^{III}OH$, and $>Mn^{III}O^-$ surface groups may differ substantially because of changes in the characteristics of the leaving group. In addition, when protonated sites ($>Mn^{III}OH_2^+$) outnumber deprotonated ($>Mn^{III}O^-$) sites, oxide surfaces carry a net positive charge. When the reverse is true, the oxide surface is negative. Isoelectric points of manganese oxides reported in the literature range from 1.40 to 2.8 for δ-MnO_2 (*45*) to as high as 7.2 for other manganese oxides (*1*). Electrostatic interactions arising from surface charge may affect rates of precursor complex formation and other surface chemical reactions.

ArOH and ArO^- may react with oxide surface groups at different rates. It should be noted, however, that pK_a values of phenolic –OH groups of the four substituted phenols included in the pH study are above 9. At pH 6.0, the concentration of phenolate anions is more than 3 orders of magnitude lower than the concentration of neutral phenol and drops an additional order of magnitude for every additional unit decrease in pH. In order for phenolate anions to be important in the reductive dissolution reaction, their reactivity must be more than 3 orders of magnitude greater than that of neutral phenols.

Surface coverage by substituted phenols is a function of pH, since substituted phenols must compete with protons and hydroxide ions for surface sites and protonation of substituted phenols lowers their affinity for surface groups. In order to examine the effect of pH on surface coverage, precursor complex formation will be treated as a preequilibrium step taking place before rate-limiting electron transfer. The pH dependence is determined by the protonation stoichiometry of the precursor complex. Consider, for example, the following two inner-sphere complex formation reactions:

$$>Mn^{III}\text{—}OH + ArOH \overset{K_1(A)}{\rightleftharpoons} >Mn^{III}\text{—}O\text{—}Ar + H_2O \quad (18)$$

I

$$>Mn^{III}\text{—}OH_2^+ + ArOH \overset{K_1(B)}{\rightleftharpoons} >Mn^{III}\text{—}\overset{+}{O}(H)\text{—}Ar + H_2O \quad (19)$$

II

Studies of the adsorption of organic compounds onto metal oxide surfaces (*46*, *47*) have shown that the pH dependence can be predicted by considering the protonation stoichiometry of surface complexes. On the basis of reaction 18, an adsorption maximum for surface complex I is expected to occur in the pH region where the product concentration $[ArOH][>Mn^{III}OH]$ is highest. Since [ArOH] is approximately constant at pH values 2 or more units below the pK_a of the substituted phenol, the maximum will occur near the isoelectric point of the manganese oxide (somewhere below pH 7.5), where $[>Mn^{III}OH]$ is highest. Surface complex II has a somewhat different proton stoichiometry. In this case, the surface complex increases in abundance as the pH is decreased, in direct proportion to increases in $[>Mn^{III}OH_2^+]$. Of these two possible stoichiometries for inner-sphere surface complexes, complex I is likely to be the most abundant on the oxide surface. Although less abundant, the pH dependence shown by complex II could influence dissolution kinetics if its structure is more favorable for electron transfer than that of complex I. Thus, overall rates of reaction as a function of pH depend both upon the total amount of adsorbed phenol and upon rates of electron transfer within the predominant protonation level species (*21*).

Outer-sphere complexes with stoichiometries of ($>Mn^{III}$–OH,ArOH) or ($>Mn^{III}OH_2^+$,ArO^-) yield a pH dependence similar to complex I. The outer-sphere complex ($>Mn^{III}$–OH_2^+,ArOH), in contrast, yields a pH dependence similar to complex II. Regardless of the stoichiometries envisioned, the net surface coverage by substituted phenols is quite low, as discussed in an earlier section.

In a study of the reductive dissolution of magnetite (Fe_3O_4) by thioglycolic acid ($HSCH_2COOH$), a similar treatment of surface complex protonation stoichiometry was successful in explaining the pH dependence (*48*). In this case, the effect of pH is quite dramatic; the dissolution rate attains a maximum value at pH 4.5 and drops off sharply at higher and lower pH values. It is thought that protonated surface sites and deprotonated thioglycolate anion are joined together in the precursor complex. The

concentration of thioglycolate anion increases with increasing pH (pK_a of 3.5) while the concentration of protonated Fe(III) surface groups ($>Fe^{III}OH_2^+$) decreases with increasing pH. The product $[HSCH_2COO^-][>Fe^{III}OH_2^+]$ reaches a maximum value at pH 4.5, explaining the observed pH dependence (*48*).

Once reduced manganese oxide surface sites have been produced, protonation reactions are involved in the release of the reduced metal ion into overlying solution (*49*). When release of reduced metal ion is rate-limiting, overall rates of reductive dissolution are relatively insensitive to changes in reductant structure. It is known, however, that hydroquinone and other dihydroxybenzenes reduce and dissolve manganese oxides approximately 3 orders of magnitude faster than substituted phenols (*5*). Thus, it is unlikely that release of the reduced metal ion is rate-limiting in this case.

One interesting finding of this study is that the reaction rate with *p*-methylphenol begins to level out as the pH is decreased below pH 5.0, while the reaction rate with *o*-hydroxybenzoate increases substantially in the same pH region. Reactions of the two substituted phenols are likely to occur via precursor complexes with different protonation stoichiometries. *p*-Methylphenol apparently reaches a maximum in surface coverage or electron-transfer rate 2 or 3 pH units higher than *o*-hydroxybenzoate. Adsorption of *o*-hydroxybenzoate onto both aluminum oxide (*46*) and iron oxide (*47*) has been studied and found to increase as the pH is decreased. This dependence most likely arises from the involvement of the carboxyl substituent (pK_a of 2.97) in the formation of a chelate surface complex.

Low surface coverage arises when the sum of first-order rate constants for electron transfer and desorption ($k_2 + k_{-1}$) are larger than the pseudo-first-order rate constant for precursor complex formation (k_1[ArOH]) (*21*). Unfortunately, without simultaneous measurement of surface coverage by substituted phenols and rates of reductive dissolution, rate-limiting precursor complex formation and electron transfer cannot be distinguished.

The observed pH dependence arises, therefore, from one or a combination of the following two effects: (1) protonation reactions that promote the formation of precursor complexes or (2) increases in the protonation level of surface precursor complexes that increase rates of electron transfer.

Effect of Manganese Oxide Composition and Structure. Significant differences exist in the chemical composition, surface area, mineralogy, and morphology of oxide particles used in the dissolution experiments (Table I). None of these preparations are single phases, and therefore only differences in composite properties can be examined. Oxidizing equivalents per mole of manganese differ by 12%, and BET surface areas differ by a factor of 6. The relative proportions of Mn(II), Mn(III), and Mn(IV) are not known. *d* spacings reported for these synthetic oxides do not match published values for known mineral phases, such as those determined by Bricker (*2*).

Since rates of reductive dissolution are proportional to oxide surface area (*15*), reaction rates should be corrected for differences in oxide surface loadings. BET surface area measurements are probably lower than actual particle surface areas in aqueous suspensions, because of aggregation and cementation during drying. For this reason, these BET surface areas are not a satisfactory basis for comparing differences in dissolution rates.

It is interesting to note, however, that experiments with different oxide preparations all exhibit the same trends when reductant structure or pH are changed. Ring substituents have essentially the same effect on reactions of type A and type B oxide particles (Figures 5 and 6). Apparent reaction orders with respect to $[H^+]$ are surprisingly similar for type A′, B, and C particles (Figure 7).

These results can be interpreted in two different ways. It is possible that all particle preparations are mixtures that share a particularly reactive phase. Dissolution rates during the first 10% of reaction may be dominated by this most reactive mineral fraction. If, on the other hand, the preparations have no component minerals in common, the results would indicate that oxide structure has relatively little impact on observed dissolution behavior. Experiments performed with very pure oxide phases are necessary to distinguish between these two possibilities.

How similar are these synthetic oxides to naturally occurring particles? Addition of Mn(II) to artificial lake water has been shown to form hausmannite (oxidation state of +2.67) that converts to manganite (oxidation state of +3.0) after several months of aging (*50*, *51*). Tipping et al. (*52*) added Mn(II) to actual lake waters, which formed crumpled thin sheets of vernadite-like manganese oxide with oxidation state values between +3.1 and +3.9. The oxidation state, morphology, and crystallographic *d* spacings of type B and C synthetic particles bear strong resemblance to this material. Thus, the synthetic oxide particles are similar to some types of natural oxides but do not represent the full range of possibilities.

Significance. The increase in reaction rate between manganese(III/IV) oxides and substituted phenols with decreasing pH appears to be a general phenomenon, with important ramifications. Low pH values measured in rainwater and fogwater (*53*) are very favorable toward reaction. Methyl-, methoxy-, chloro-, and nitro-substituted phenols have been identified in rainwater in the microgram per liter range (*54*). Total manganese concentrations as high as 1.5×10^{-5} M have been found in urban fogwater and rainwater droplets (*55*). Manganese oxides derived from dust and ash may bring about the oxidative degradation of phenols in time scales less than a few hours. Even resistant phenols, such as nitro-substituted phenols, are degraded at appreciable rates in low-pH environments.

On the other hand, rates of reaction drop off substantially as the pH is increased; apparent orders with respect to $[H^+]$ are greater than 1.0 at pH values above 6.0. Phenols with electron-withdrawing substituents, such as *p*-nitrophenol, react quite slowly with manganese oxides in neutral or alkaline pH.

When oxygen is present and the pH is above 8, rates of Mn^{2+} oxidation and regeneration of manganese(III/IV) oxides become significant. Under these conditions, manganese may act as a catalyst for the oxidation of phenols by oxygen. In a cyclic process, manganese is reduced by phenols and then reoxidized by oxygen. Similar cyclic processes have been postulated to explain the persistence of Fe^{2+} in oxygenated solutions containing dissolved organic matter (*56*).

The importance of manganese oxides in the oxidative degradation of substituted phenols depends, in part, on the rates of competitive degradation pathways. Bacterial degradation of substituted phenols, for example, has been demonstrated under aerobic, anaerobic, and methanogenic conditions (*57*).

Conclusions

Phenols with alkyl, alkoxy, or other electron-donating substituents are very susceptible to oxidative degradation by manganese(III/IV) oxides, while phenols with carboxyl, aceto, nitro, chloro, or other electron-withdrawing substituents are degraded more slowly. Even *p*-nitrophenol,

the most resistant phenol included in this study, reacted at a slow rate with manganese(III/IV) oxides. Clearly, abiotic oxidation by manganese oxides is a potentially important degradative pathway for a variety of substituted phenols, especially when the rates of competitive degradative pathways, such as biodegradation, are relatively slow.

Substituent effects and the effects of pH and reductant concentration on the rates of reductive dissolution are all consistent with the postulated mechanism for the surface chemical reaction (reactions 4–8). Rates of reductive dissolution generally decrease as the Hammett constants of ring substituents become more positive, reflecting trends in the basicity, nucleophilicity, and half-wave potential of substituted phenols. The experimental evidence indicates that the fraction of oxide surface sites occupied by substituted phenols is quite low and that surface protonation reactions promote reductive dissolution. The apparent reaction order with respect to $[H^+]$ is not a constant but varies between 0.45 and 1.30 as the pH range, phenol concentration, and phenol structure are varied. The observed pH dependence arises from one or a combination of the following two effects: (1) protonation reactions that promote the formation of surface precursor complexes or (2) increases in the protonation level of surface precursor complexes that increase rates of electron transfer.

Acknowledgments

Assistance with HRTEM and electron diffraction analysis by David Veblen, Ken Livi, and Judy LaKind is gratefully acknowledged. Useful comments by Judy LaKind are gratefully acknowledged. BET surface area measurements were provided by Chemetals Corp. of Baltimore, MD, and by C. P. Huang of the University of Delaware.

Registry No. 4-MeC_6H_4OH, 106-44-5; 4-$MeCH_2C_6H_4OH$, 123-07-9; 3-MeC_6H_4OH, 108-39-4; C_6H_5OH, 108-95-2; 4-ClC_6H_4OH, 106-48-9; 3-ClC_6H_4OH, 108-43-0; 4-$HOC_6H_4CO_2H$, 99-96-7; 4-HOC_6H_4COMe, 99-93-4; 4-$O_2NC_6H_4OH$, 100-02-7; 2-ClC_6H_4OH, 95-57-8; 2-$HOC_6H_4CO_2H$ (anion), 63-36-5; manganese oxide, 11129-60-5.

Literature Cited

(1) Stumm, W.; Morgan, J. J. *Aquatic Chemistry*, 2nd ed.; Wiley-Interscience: New York, 1981.
(2) Bricker, O. *Am. Mineral.* **1965**, *50*, 1296.
(3) Krauskopf, K. B. *Introduction to Geochemistry*; McGraw-Hill: New York, 1967.
(4) Larson, R. A.; Hufnal, J. M. *Limnol. Oceanogr.* **1980**, *25*, 505.
(5) Stone, A. T.; Morgan, J. J. *Environ. Sci. Technol.* **1984**, *18*, 617.
(6) Reinhard, M.; Goodman, N. L.; Barker, J. F. *Environ. Sci. Technol.* **1984**, *18*, 953.
(7) Waters, W. A. *J. Chem. Soc. B* **1971**, 2026.
(8) Bailey, S. I.; Ritchie, I. M.; Hewgill, F. R. *J. Chem. Soc., Perkin Trans. 2* **1983**, 645.
(9) Cecil, R.; Littler, J. S. *J. Chem. Soc. B* **1968**, 1420.
(10) Musso, H. In *Oxidative Coupling of Phenols*; Taylor, W. I., Battersby, A. R., Ed.; Dekker: New York, 1967.
(11) Nilsson, A.; Ronlan, A.; Parker, V. D. *J. Chem. Soc., Perkin Trans. 1* **1973**, 2337.
(12) Shibaeva, L. V.; Metelitsa, D. I.; Denisov, E. T. *Kinet. Catal. (Engl. Transl.)* **1969**, *10*, 832.
(13) Shibaeva, I. V.; Metalitsa, D. I.; Denisov, E. T. *Kinet. Catal. (Engl. Transl.)* **1969**, *10*, 1022.
(14) Pohlman, A.; Mill, T. *J. Org. Chem.* **1983**, *48*, 2133.
(15) Stone, A. T.; Morgan, J. J. *Environ. Sci. Technol.* **1984**, *18*, 450.
(16) Stone, A. T. In *Geochemical Proceses at Mineral Surfaces*; Davis, J. A., Hayes, K. F., Eds.; ACS Symposium Series 323; American Chemical Society: Washington, DC, 1986; Chapter 21.
(17) Valverde, N.; Wagner, C. *Ber. Bunsen-Ges. Phys. Chem.* **1976**, *80*, 330.
(18) Segal, M. G.; Sellers, R. M. *J. Chem. Soc., Chem. Commun.* **1980**, 991.
(19) Gorichev, I. G.; Kipriyanov, N. A. *Usp. Khim.* **1984**, *53*, 1039.
(20) Bruyere, V. I.; Blesa, M. A. *J. Electroanal. Chem. Interfacial Electrochem.* **1985**, *182*, 141.
(21) Stone, A. T.; Morgan, J. J. In *Aquatic Surface Chemistry*; Stumm, W., Ed.; Wiley: New York, 1986; Chapter 9.
(22) Waite, T. D. In *Geochemical Processes at Mineral Surfaces*; Davis, J. A., Hayes, K. F., Eds.; ACS Symposium Series 323; American Chemical Society: Washington, DC, 1986; Chapter 20.
(23) Zinder, B.; Furrer, G.; Stumm, W. *Geochim. Cosmochim. Acta* **1986**, *50*, 1861.
(24) Skoog, D. A.; West, D. M. *Fundamentals of Analytical Chemistry*; Holt, Rinehart and Winston: New York, 1976.
(25) Davis, J. A.; James, R. O.; Leckie, J. O. *J. Colloid Interface Sci.* **1978**, *63*, 480.
(26) Sigg, L.; Stumm, W. *Colloids Surf.* **1980**, *2*, 101.
(27) Moore, J. W.; Pearson, R. G. *Kinetics and Mechanism*, 3rd ed.; Wiley: New York, 1981.
(28) Yost, E. C.; Anderson, M. A. *Environ. Sci. Technol.* **1984**, *18*, 101.
(29) March, J. *Advanced Organic Chemistry*, 2nd ed.; McGraw-Hill: New York, 1985.
(30) Exner, O. In *Advances in Linear Free Energy Relationships*; Shorter, J., Chapman, N. B., Eds.; Plenum: New York, 1972; pp 29–30.
(31) Martell, A. E.; Smith, R. M. *Critical Stability Constants*; Plenum: New York, 1977; Vol. 3.
(32) Martell, A. E.; Smith, R. M. *Critical Stability Constants*; Plenum: New York, 1982; Vol. 5.
(33) Serjeant, E. P.; Dempsey, B. *Ionization Constants of Organic Acids in Aqueous Solution*; Pergamon: Oxford, 1979.
(34) Wilkins, R. G. *The Study of Kinetics and Mechanism of Reactions of Transition Metal Complexes*; Allyn and Bacon: Boston, 1974.
(35) Purcell, K. F.; Kotz, J. C. *Inorganic Chemistry*; Saunders: Philadelphia, 1977.
(36) Cavasino, F. P.; DiDio, E. *J. Chem. Soc. A* **1970**, 1151.
(37) Suatoni, J. C.; Snyder, R. E.; Clark, R. O. *Anal. Chem.* **1961**, *33*, 1894.
(38) Bard, A. J.; Faulkner, L. R. *Electrochemical Methods*; Wiley: New York, 1980.
(39) Murty, P. S. R.; Panda, R. K. *Indian J. Chem.* **1973**, *11*, 1003.
(40) Rao, P. V. S.; Murty, B. A. N.; Murty, R. V. S.; Murty, K. S. *J. Indian Chem. Soc.* **1978**, *55*, 207.
(41) Kimura, M.; Kaneko, Y. *J. Chem. Soc., Dalton Trans.* **1984**, 341.
(42) Mentasti, E.; Pelizzetti, E. *Transition Metal Chem. (Weinheim, Ger.)* **1976**, *1*, 281.
(43) Rao, P. V. S.; Subbaiah, K. V.; Murty, P. S. N.; Murty, R. V. S. *Indian J. Chem., Sect. A* **1980**, *19A*, 257.
(44) Westall, J. C. In *Aquatic Surface Chemistry*; Stumm, W., Ed.; Wiley: New York, 1986; Chapter 1.
(45) Balistrieri, L. S.; Murray, J. W. *Geochim. Cosmochim. Acta* **1982**, *46*, 1041.
(46) Kummert, R.; Stumm, W. *J. Colloid Interface Sci.* **1980**, *75*, 373.
(47) Balistrieri, L. S.; Murray, J. W. *Geochim. Cosmochim. Acta* **1987**, *51*, 1151.
(48) Baumgartner, E.; Blesa, M. A.; Maroto, A. J. G. *J. Chem. Soc., Dalton Trans.* **1982**, 1649–1654.
(49) Stumm, W.; Furrer, G.; Wieland, E.; Zinder, B. In *The Chemistry of Weathering*; Drever, Ed.; NATO ASI Series C.; Reidel: Dordrecht, 1986; Vol. 149.
(50) Stumm, W.; Giovanoli, R. *Chimia* **1976**, *30*, 423.
(51) Murray, J. W.; Dillard, J. G.; Giovanoli, R.; Moers, H.; Stumm, W. *Geochim. Cosmochim. Acta* **1985**, *49*, 463.
(52) Tipping, E.; Thompson, D. W.; Davison, W. *Chem. Geol.* **1984**, *44*, 359.

(53) Waldman, J. M.; Munger, J. W.; Jacob, D. J.; Flagan, R. C.; Morgan, J. J.; Hoffmann, M. R. *Science (Washington, D.C.)* **1982**, *218*, 677.
(54) Leuenberger, C.; Ligocki, M. P.; Pankow, J. F. *Environ. Sci. Technol.* **1985**, *19*, 1053-1058.
(55) Munger, J. W.; Jacob, D. J.; Waldman, J. M.; Hoffmann, M. R. *J. Geophys. Res., C: Oceans Atmos.* **1983**, *88*, 5109.
(56) Theis, T. L.; Singer, P. C. *Environ. Sci. Technol.* **1974**, *8*, 569.
(57) Chapman, P. J. In *Degradation of Synthetic Organic Molecules in the Biosphere*; National Academy of Sciences: Washington, DC, 1971; pp 17-55.

Received for review August 25, 1986. Accepted June 15, 1987. This work was supported by the Environmental Engineering Program of the National Science Foundation under Grant CEE-04076.

Comparison of Terrestrial and Hypolimnetic Sediment Generation of Acid Neutralizing Capacity for an Acidic Adirondack Lake†

Gary C. Schafran* and Charles T. Driscoll

Department of Civil Engineering, Syracuse University, Syracuse, New York 13244

■ The importance of in-lake generation of acid neutralizing capacity (ANC) to the neutralization of acidic deposition has been determined for an acidic Adirondack (NY) lake relative to its surrounding watershed. Microbial processes within the sediments of Dart's Lake significantly altered the aqueous chemistry of the hypolimnion. Reduction of NO_3^- and SO_4^{2-} and the production of NH_4^+ contributed 45, 14, and 32%, respectively, to the production of hypolimnetic ANC. The reduction of NO_3^- was a more significant source of ANC generation than has been reported in other lake districts. On an areal basis, in-lake ANC generation (2990 equiv ha^{-1} yr^{-1}) was greater than terrestrial ANC production (1204 equiv ha^{-1} yr^{-1}). However on a watershed basis, in-lake ANC generation was minor (<5%) due to the short hydraulic retention time of Dart's Lake. Neutralization of acidic precipitation in the Adirondack region predominately occurs in the terrestrial system since the hydraulic retention time of Adirondack lakes is short.

Introduction

Acidification of surface waters in the northeastern U.S. (*1*, *2*), Canada (*3*, *4*), and Europe (*5*) has been linked to the atmospheric deposition of strong acids. Proton budget calculations have shown that substantial neutralization of acidic deposition occurs through a variety of biogeochemical processes within the terrestrial environment (*6*). Geochemical weathering, ion exchange, adsorption, and biological assimilation may all contribute to the immobilization (or mobilization) of H^+. Due to these processes, water leaving terrestrial systems is generally enriched in acid neutralizing capacity (ANC) relative to atmospheric deposition.

Although it has long been recognized that terrestrial processes mediate surface water acidity, it has recently been shown that in-lake processes can generate ANC (*7-12*). In aqueous systems, ANC production has been observed through assimilative NO_3^- reduction (*13*, *14*) or through dissimilatory NO_3^- and SO_4^{2-} reduction (*7-12*). Biologically mediated oxidation-reduction (redox) reactions, which utilize either NO_3^- or SO_4^{2-} as terminal electron acceptors or nutrients, are prevalent within lake systems (*7-12*, *15-17*). Although the hypolimnetic region has been thought to be the most important location for anaerobic respiration reactions, recent evidence reveals that microbial activity in anoxic, epilimnetic sediments may be significant and contribute more to in-lake ANC (than hypolimnetic sediments) on a whole lake basis (*18*, *19*). Thus, the role of lake processes in producing ANC may be more significant than previously realized.

Table I. Example Reactions of Acid Neutralizing Capacity Generation

$$5CH_2O + 4NO_3^- + 4H^+ = 2N_2 + 5CO_2 + 7H_2O$$
$$2CH_2O + SO_4^{2-} + 2H^+ = H_2S + 2CO_2 + 2H_2O$$
$$CH_2O + 2MnO_2 + 4H^+ = 2Mn^{2+} + CO_2 + 3H_2O$$
$$CH_2O + 4FeOOH + 8H^+ = 4Fe^{2+} + CO_2 + 7H_2O$$
$$CH_2ONH_3 + O_2 + H^+ = NH_4^+ + CO_2 + H_2O$$

In a whole lake acidification study, Schindler et al. (*8*) detailed the loss of SO_4^{2-} and resulting ANC generation in Lake 223. Sulfate reduction increased with increasing SO_4^{2-} concentration and neutralized 36-45% of the added acidity. Kelly et al. (*7*) studied the hypolimnetic regions of three lakes in the Experimental Lakes Area (ELA) in Ontario, Canada, to determine the importance of bacterial processes in the production of ANC. They observed that SO_4^{2-} reduction resulted in the largest contribution to hypolimnetic ANC generation. Additional studies in Ontario, Canada, have likewise shown that reactions within lake sediments are capable of generating significant alkalinity (*9*, *10*, *12*). Within-lake SO_4^{2-} reduction and NO_3^- immobilization have also been credited as the major alkalinity source in an acidic Florida lake (*11*). Base cation exchange with H^+, NH_4^+ release, and SO_4^{2-}, NO_3^-, Fe(III), and Mn(IV) reduction have been reported to be the major ANC-generating processes in lakes (Table I). The contribution of each process to the total in-lake generation of ANC varies among lakes.

Nitrate reduction is energetically more favorable than SO_4^{2-} reduction (*20*). In ELA lakes, low production of ANC due to NO_3^- retention (*7*, *8*) was due to low surface water concentrations of NO_3^-. In the northeastern U.S. substantial watershed export of NO_3^- is evident (*21*), resulting in elevated surface water concentrations (*22*). In lakes of this region, biologically mediated NO_3^- retention might be expected to produce significant quantities of ANC (*19*).

Because in-lake processes potentially influence the acid-base chemistry of surface waters, the magnitude of these transformations is important for regional assessments of acidification effects. For example, the chemistry of

† Contribution No. 71 of the Upstate Freshwater Institute.

* Address correspondence to this author at his present address: Department of Civil Engineering, Old Dominion University, Norfolk, VA 23509.

0013-936X/87/0921-0988$01.50/0

Table II. Physical and Chemical Characteristics of Dart's Lake[a]

surface area, ha	58
maximum depth, m	15
mean depth, m	7
elevation, m	576
hydraulic retention, yr	0.06
catchment area, ha	10700
lake volume below 12 m, %	6
pH	5.18
NO_3^-, μequiv L^{-1}	24.4
SO_4^{2-}, μequiv L^{-1}	137.6
organic anion, μequiv L^{-1}	12.2

[a] Mean concentrations for the whole lake (25 October 1981 to 21 November 1982).

Adirondack lakes is considerably different than that of the ELA. Adirondack lakes generally are more acidic with higher concentrations of NO_3 and Al (*22*). These variations may be due to differences in deposition of strong acids, hydrology, geology, and biological processes that influence the acid–base chemistry of surface waters. To assess in-lake production of ANC, we analyzed water chemistry data from a site in the Adirondack region of New York. This analysis included a quantitative evaluation of processes and rates of acid–base transformations within the hypolimnion of an acidic lake. Moreover, through mass balance calculations of bulk precipitation input, lake inflow, and lake outflow, we compared in-lake ANC production with terrestrial ANC production.

Methods

Study Site. Dart's Lake (74° 52′ W, 43° 48′ N) is located in the drainage basin of the North Branch of the Moose River in the Adirondack Mountain region of New York state. Bedrock geology is granitic gneiss (*23*) while vegetation is predominately secondary growth hardwoods. Soil depth within the Dart's Lake watershed is predominately shallow (<3 m). The Dart's Lake watershed area is 107 km^2 with 97% of the basin draining into the major inlet. Water entering through the major inlet is comprised largely of outflow from Big Moose Lake (74° 51′ W, 43° 49′ N). Groundwater inputs directly to Dart's Lake likely represent a small portion of the hydrologic budget. This trend is to be expected from the large area draining into the inlet. Groundwater inputs to the lake have been monitored in the years subsequent to this study and verify this assumption. Water draining from Dart's Lake exits through a single outlet. Due to the large drainage basin, the hydraulic retention time of the lake is short, 0.06 yr. Lake characteristics are presented in Table II.

Sample Collection and Analysis. Samples were collected every 2–3 weeks from 25 October 1981 to 21 November 1982 (*24*). Samples (1 L) were collected at the major inlet and outlet and at 2–3-m intervals from the surface to 14-m depth at the deepest section of the lake by using a submersible pump. After removal of an aliquot (25 mL) for Al extraction, samples were quickly sealed and transported to the laboratory. Analysis for dissolved inorganic carbon (DIC) and pH occurred within 12 h of collection. Dissolved oxygen was determined on a separate sample that was fixed immediately following collection and analyzed by the Winkler method (*25*).

Fractionation and analysis of Al was similar to the method described by Driscoll (*26*). pH was measured potentiometrically with a glass electrode. Dissolved inorganic carbon was measured by a gas partitioner following syringe stripping of CO_2 (*27*). Dissolved organic carbon (DOC) analysis was by persulfate oxidation (*28*) followed by syringe stripping and CO_2 analysis (*27*). Sulfate (methylthymol blue method, *29*), NO_3 (hydrazine reduction, *30*), and NH_4 (alkaline phenol, *31*) were analyzed on an autoanalyzer. Within 24 h of collection, samples for Fe and Mn determination were centrifuged for 30 min at 5720*g* followed by collection of the supernatant (*32*). The supernatant was acidified to pH 1 with Ultrex nitric acid and analyzed by atomic absorption spectroscopy (AAS) with a graphite furnace. Base cation (Ca, Mg, Na, and K) analyses were conducted by flame AAS.

Sulfate analysis with the methylthymol blue method is prone to color interferences by DOC and Fe. We analyzed SO_4^{2-} by ion chromatography for a number of Dart's Lake samples (n = 17) and found no statistically significant difference between the two methods.

Precipitation chemistry and quantity monitored at a Utilities Acid Precipitation Studies Program (UAPSP) station at Big Moose, NY (43° 49′ N, 74° 55′ W), for the period 25 October 1981 to 21 November 1982 were used to calculate inputs to the Dart's Lake watershed. The station was located 3 km from Dart's Lake. The precipitation monitoring station and the Dart's Lake watershed are situated in a geographical region where precipitation quantity is relatively uniform (*33*) so that errors associated with variations in precipitation quantity over the watershed should be minimal.

Calculations. A chemical equilibrium model (*34*) was used to calculate HCO_3^-; this calculation is most sensitive to DIC and pH values. Organic anion ($RCOO^-$) concentrations were estimated with a proton dissociation constant and a relationship between DOC and proton dissociation sites (*35*). These relationships were determined previously for waters in the Dart's Lake watershed (*22*). The base neutralizing capacity (BNC) of Al (Al-BNC) was calculated from the Al speciation predicted by the model (eq 1).

$$\text{Al-BNC} = 3[Al^{3+}] + 2[AlOH^{2+}] + [Al(OH)_2^+] + 3[AlF_x^{3-x}] + 3[Al(SO_4)_x^{3-2x}] - [Al(OH)_4^-] \quad (1)$$

Ionic strength and temperature corrections were included in all calculations. Details of these calculations are summarized elsewhere (*26*).

Samples collected from the 12- and 14-m depth were used to compute changes in the total mass of solutes below 12 m. Five sampling dates during the summer stratification period, 29 June to 1 October 1982, were considered for the calculation of hypolimnetic transformation rates. During this period the thermocline was located above the 9-m depth. Exchange of dissolved substances between the upper (above 12 m) and lower hypolimnion (below 12 m) occurred during this period due to developing concentration gradients and eddy diffusion. To account for the loss or accumulation of solutes due to transport across the 12-m plane, changes in mass below 12 m were corrected for diffusion (eq 2), where J is the flux of the constituent of

$$J = D(dc/dz) \quad (2)$$

interest (mass area^{-1} time^{-1}), D is the eddy diffusion coefficient (area time^{-1}), and dc/dz is the change in concentration as a function of depth at the 12-m depth (mass volume^{-1} length^{-1}). Eddy diffusion coefficients were calculated by the flux gradient method (*36*); the coefficient at 12 m was determined by dividing the heat flux across the 12-m depth by the temperature gradient at this depth. Coefficients ranged from 1.2×10^{-3} to 2.3×10^{-3} cm^2 s^{-1} for all periods. Concentration gradients were determined from the slope of the depth as a function of concentration plots for samples at 9-, 12-, and 14-m depth. Transformation rates were determined by regression of the changes in the total mass (±mass diffusing across the 12-m plane)

Table III. Rates of Acid Neutralizing Capacity Generation and Contributing Processes in the Lower Waters (below 12 m) of Dart's Lake[a]

reactions	rate, equiv ha^{-1} day^{-1}	r^2	no. of observations
ANC			
HCO_3^-	+6.7	0.95	5
H^+	−1.0	0.91	5
$RCOO^-$	+0.5	0.97	5
total	+8.2		
processes			
SO_4^{2-} reduction	−1.8	0.75	5
NO_3^- reduction	−5.7	0.96	5
NH_4^+ release	+4.1	0.99	5
Al hydrolysis	−4.6	0.89	5
Ca^{2+} retention	−1.2	0.57	5
Mn reduction	+0.3	0.99	4
Fe reduction	+0.8	0.99	3
total	+6.9		

[a] Positive values indicate component generation; negative values indicate component consumption. Correlation coefficients are for regression of constituent (mass) vs. time.

with time. The calculated diffusive loss or gain of any solute across the 12-m plane was less than 25% of the total mass of the solute below 12 m. This approach has been used previously to calculate hypolimnetic transformation rates (*7*, *10*, *37*).

A hydrologic budget for Dart's Lake was developed with inlet and outlet rating curves and empirical relationships between the Dart's Lake outlet and two continuously recording stations. Uncertainties exist within the mass balance for the lake. The error associated with the hydrologic budget is ±3%. A number of ephemeral streams that drain directly into Dart's Lake (generally at snowmelt and during the fall) were not monitored during the study. Since 97% of the watershed drains through the lake inlet, these streams do not contribute substantially to the hydrologic budget. However, these streams are generally more acidic and lower in base cation concentrations than the inlet. Groundwater inputs to the lake were not monitored during this study but have been quantified in subsequent years. These inputs (no seepage out of the lake has been detected) have been estimated as less than 1% of the hydrologic budget of the lake and are insignificant in the water chemistry budget.

Due to the biweekly sampling that occurred during spring, we may have missed peak inputs of acidity from snowmelt. However, the position of Big Moose Lake in the Dart's Lake watershed tends to attenuate changes in the chemistry of the Dart's Lake inlet during periods of high runoff (*38*) due to mixing within Big Moose Lake. Thus, peak concentrations of solutes at this time of year (e.g., H^+) are reduced, and the period of the event is lengthened relative to values observed in headwater streams. Therefore, uncertainties associated with the sampling frequency should result in reduced uncertainties in budget calculations.

Results

A number of solutes within the lower waters exhibited significant changes in concentration during the summer stratification period (Table III). The change in the total mass (±mass diffusing across the 12-m plane) for these hypolimnetic components was generally linear and suggests that transformation rates were zero order.

Throughout the study period, hypolimnetic concentrations of O_2 decreased but never reached complete depletion. Although anoxia within the water column failed to develop, decreases in NO_3^- and SO_4^{2-} concentrations were evident, indicating that alternative electron accepters were used in respiration reactions. Reduction within the sediment and at the sediment/water interface, where anoxia was probable, likely controlled hypolimnetic concentrations.

Table IV. Rate of Hypolimnetic Electron Transfer in Dart's Lake

reactions	rate, equiv ha^{-1} day^{-1}	r^2
oxidation		
C[a]	188	0.96
reduction		
O_2	152	0.95
NO_3^-[b]	28	0.96
Mn[c]	0.3	0.99
Fe[d]	0.4	0.99
SO_4^{2-}[e]	7.2	0.75
total	188	

[a] Carbon oxidation to C(IV) is assumed with 4 mol of e^- transferred per mole of DIC released. [b] NO_3^- is assumed reduced to N_2 with 5 mol of e^- accepted per mole of NO_3^- reduced. NH_4^+ release is assumed to be derived from the mineralization of organic material and therefore does not involve hypolimnetic electron transfer. [c] Hypolimnetic Mn is assumed to be Mn(II), which is derived from Mn(IV). [d] Hypolimnetic Fe is assumed to be Fe(II), which is derived from Fe(III). [e] SO_4^{2-} depletion is assumed to result from conversion to S(II).

We use an electron mass balance (Table IV) to help verify the accuracy of the calculated transformation rates (Table III). It is assumed that hypolimnetic reduction reactions were entirely the result of mineralization of plant material ($C_{106}H_{263}O_{110}N_{16}P$, which released 4 mol of e^-/mol of organic C when oxidized to inorganic C, *20*). Our calculations suggest that the hypolimnetic oxidation of organic C was balanced by a combination of O_2, NO_3^-, Mn, Fe, and SO_4^{2-} reduction totaling 188 equiv e^- ha^{-1} day^{-1}. Note that we also assumed that NO_3^- was entirely converted to N_2 (denitrification). It is possible that NO_3^- could be converted to other N forms (e.g., N_2O, NH_4^+, and organic N). However, the contribution of denitrification to the total NO_3^- immobilization in anaerobic lake sediments is variable but has often been reported to be the predominate process (*15*, *16*, *39*, *40*). We have not accounted for reduced Fe(II) that may have remained in the sediment due to FeS formation but resulted from the oxidation of organic carbon. An upper limit for this value would be equivalent to the SO_4^{2-} reduction rate [assuming all the Fe(II) was retained as FeS]. Inclusion of this rate would not significantly (<4%) alter our electron balance. Oxidation of organic C was largely accomplished by reduction of molecular O_2 (81%); however, NO_3^- reduction was also significant (15%). Elevated concentrations of water column NO_3^- apparently facilitated the use of this electron acceptor and limited Mn(IV), Fe(III), and SO_4^{2-} reduction.

Transfer rates as determined from hypolimnetic observations enabled us to quantify the relative contribution of individual processes in the generation of hypolimnetic ANC. Through electroneutrality constraints, the production of ANC for the lower waters is approximately equivalent to

$$[HCO_3^-] + [RCOO^-] - [H^+] = [NH_4^+] + n[Al^{n+}] + 2[Fe^{2+}] + 2[Mn^{2+}] + 2[Ca^{2+}] - 2[SO_4^{2-}] - [NO_3^-] \quad (3)$$

where $n[\,]$ is the change in the equivalent concentration of each solute over the summer stratification period (mequiv m^{-2} day^{-1}) and $RCOO^-$ is the equivalence of organic anion [see Driscoll and Schafran (*22*) for calculation of

Table V. Solute Flux for Dart's Lake Watershed for the Period of Study[a]

constituent	pptn input to watershed	drainage input to Dart's Lake	drainage output from Dart's Lake	retained in watershed	retained in Dart's Lake
SO_4^{2-}	518	874	865	−356	9[d]
NO_3^-	298	193	182	105	11
Cl^-	34	88	84	−54	4[d]
Ca^{2+}	50.2	614	612	−564	2[d]
Mg^{2+}	16.3	180	178	−164	2[d]
Na^+	17.6	174	172	−156	2[d]
K^+	11.8	82	82	−70	0
NH_4^+	175	29	36	146	−7
H^+	666	72	58	594	14
Al^{n+}	*b*	118	106	−118[c]	12
$RCOO^-$	*b*	38	39	−38[c]	−1[d]
ANC[e]	−583	42	55	621	13

[a] All values in equiv ha^{-1} yr^{-1}; rates are normalized to the watershed area. [b] Not measured. [c] Assumes negligible input from precipitation. [d] Not significantly different than zero. [e] $ANC = Ca^{2+} + Mg^{2+} + Na^+ + K^+ + NH_4^+ + Al^{n+} - SO_4^{2-} - NO_3^- - Cl^-$.

$RCOO^-$ concentration]. Only solutes that contributed to observed changes in ANC were included in this equation (eq 3).

For the period under consideration, the production of ANC was 8.2 equiv ha^{-1} day^{-1} (Table II). Acid neutralizing capacity generation was primarily the result of NO_3^- reduction (45%) and NH_4^+ release (32%). Sulfate reduction as well as Fe(III) and Mn(IV) reduction contributed lesser amounts to ANC. Reactions that produce acidity also occurred concurrently and served to partially mitigate in-lake generation of ANC. Hydrolysis of aluminum resulted in the largest consumption of ANC (83%) with Ca^{2+} retention contributing significantly less. Aluminum hydrolysis occurred continuously as pH values of the lower hypolimnion (14 m) increased (5.1–5.4) throughout the period.

Similar rates of NO_3^- (5.6 equiv ha^{-1} day^{-1}) and SO_4^{2-} (1.3 equiv ha^{-1} day^{-1}) loss have been reported for epilimnetic sediment cores from Dart's Lake (*19*), supporting the rates we have determined. It would be speculative to conclude that epilimnetic and hypolimnetic sediments in Dart's Lake produce ANC at similar rates. However, similar rates of ANC production between epilimnetic and hypolimnetic sediments have been reported (*10*).

Discussion

The large contribution of NO_3^- retention to the generation of ANC results from elevated concentrations in the lake water. The high NO_3^- concentrations in Adirondack region lakes relative to other lake districts (*22*) suggest that NO_3^- retention is a more significant ANC generating process in these lake sediments than in lake sediments of other regions. This trend is evident when the contribution of NO_3^- reduction relative to SO_4^{2-} reduction toward in-lake generation of ANC for three ELA lakes (*7*) is compared with that of Dart's Lake. Values for the NO_3/SO_4 reduction ratio (on an equivalence basis) for the ELA lakes were 0.002–0.19 while that for Dart's Lake was 3.2. Since denitrification is an irreversible process, in-lake generation of ANC in Adirondack sediments may be more effective in producing permanent ANC than lake systems where other ANC-producing processes (e.g., SO_4^{2-} reduction) predominate. The importance of NO_3^- immobilization to ANC generation (and the reduction of H^+ and Al-BNC) in the hypolimnion is consistent with whole lake observations that short-term variations of H^+ and Al-BNC were most significantly correlated with NO_3^- (*22*).

Ammonia release from sediments also provided a significant source of ANC to the lower waters of Dart's Lake. The source of ammonia was presumably the decomposition of organic matter at the sediment/water interface and in the sediments, with subsequent release to the water column. The ANC produced by ammonification can be temporary if the NH_4^+ released to the water column is assimilated or nitrified in oxic waters. We did not readily observe ANC consumption due to assimilation and/or nitrification of NH_4^+ produced in the hypolimnion. If this NH_4^+ were eventually assimilated, the net ANC produced would be 50% (4.1 equiv ha^{-1} day^{-1}) of the value we calculated.

The most significant consumption of ANC occurred through aluminum hydrolysis. Aluminum mobilization to surface waters is believed to be enhanced by acidic deposition. Dissolution/exchange of Al in the terrestrial system results initially in aqueous ANC generation (*2*). However, it eventually consumes ANC as pH values in lakes and streams increase. Thus, when considering both watershed and lake ecosystems, Al mobilization from soil can be viewed as a temporary source of ANC with its role in surface waters ultimately being ANC consumption with no net affect on ANC.

As biological activity has been shown to generate ANC within Dart's Lake, it is of interest to compare the contribution of in-lake processes with neutralization reactions occurring within the surrounding watershed. Input–output mass balance calculations for the major ions involved in acid–base reactions were conducted for the upstream watershed and for Dart's Lake from 25 October 1981 to 21 November 1982 (Table V). The fluxes of individual solutes from the watershed through Dart's Lake were used to assess the relative contribution of terrestrial and in-lake processes to the generation of ANC in the watershed/lake system. Surface water fluxes to and from the lake were computed from the hydrologic budget and solute concentrations observed in the inlet and outlet streams. For budget purposes, solute concentrations on each sampling date were assumed to be representative of concentrations existing for half the period between previous and subsequent sampling dates.

Bulk precipitation (wet) loading was assumed to represent inputs to the watershed while the inputs for Dart's Lake were considered to be the sum of the surface water influx plus precipitation directly to the lake. Solute efflux from the lake occurred through the lake outlet. Acid neutralizing capacity generated by in-lake processes was determined by calculating the net (drainage input minus drainage output) retention or production of the individual solutes over the study period. Differences in fluxes between bulk precipitation and drainage input to Dart's Lake are largely attributed to terrestrial processes. However,

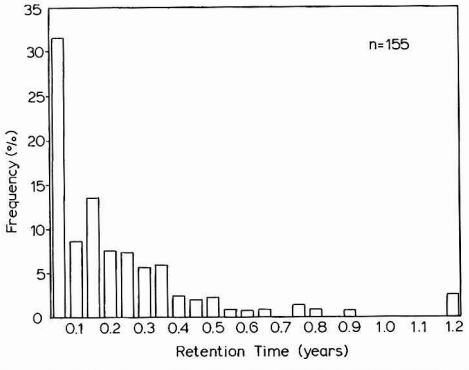

Figure 1. Hydraulic retention time of Adirondack region lakes (n = 155). Data represent a random selection of lakes (source: U.S. EPA National Surface Water Survey).

this assumption is complicated by the upstream position of Big Moose Lake, which may affect drainage water chemistry (discussed below).

Acid–base chemistry transformations occurred as precipitation passed through the terrestrial system. Increases in base cations (C_B = Ca + Mg + Na + K) were apparent and likely resulted from mineral weathering and ion-exchange reactions in the terrestrial system. The increase in C_B represented the largest contribution to ANC generation within the watershed (954 equiv ha^{-1} yr^{-1}). Watershed assimilation of NO_3^- (39% retention) resulted in ANC generation (105 equiv ha^{-1} yr^{-1}), but assimilation of NH_4^+ (83% retention) resulted in ANC consumption (146 equiv ha^{-1} yr^{-1}). Although precipitation inputs of NH_4^+ were 41% lower than those of NO_3^-, the greater NH_4^+ retention in the watershed resulted in a net loss of ANC. It has been suggested that the biological uptake of NH_4^+ in lakes may be a significant process in lake acidification (*41*). However in the North Branch of the Moose River and other systems (*21*, *42–44*), NH_4^+ is efficiently retained in the terrestrial environment, and aqueous NO_3^- concentrations are generally higher than NH_4^+ in surface waters. In these lake systems net NO_3^- uptake generally exceeds NH_4^+ uptake, and net ANC generation is often observed during biologically active periods (*43*, *45*).

The increase in SO_4^{2-} flux between bulk precipitation and drainage inputs to Dart's Lake would suggest unaccounted atmospheric loadings or the presence of a watershed source. No significant sulfur-containing minerals have been observed in the watershed (*23*), suggesting that the unaccounted SO_4^{2-} was largely due to dry deposition. While we have not directly included dry deposition of SO_4^{2-} in the budget because measurements were not available, it is represented indirectly as the difference (–356 equiv ha^{-1} yr^{-1}) between bulk precipitation and drainage input to Dart's Lake. This value may be an underestimation since processes within the watershed and Big Moose Lake may retain SO_4^{2-}. It is unlikely that this underestimation is substantial since vegetative uptake of SO_4^{2-} is believed to be low (*44*) and input–output budgets (*46*) have suggested that Adirondack soils do not significantly retain SO_4^{2-} (on an annual basis). Thus, retention within the terrestrial system, relative to inputs, is believed to be minor. However, this cannot be explicitly determined without an accurate accounting for dry deposition. Little variation in SO_4^{2-} concentrations in the chain of lakes within the Dart's Lake watershed also suggests that little retention, relative to fluxes, occurs (*47*). Thus, in-lake generation of ANC due to SO_4^{2-} retention (e.g., dissimilatory SO_4^{2-} reduction) is likely to be small.

It is useful to compare watershed and in-lake generation of ANC to assess the processes that mitigate H^+ inputs associated with atmospheric deposition. If it is assumed that the annual ANC production from Dart's Lake is similar to that observed during the summer stratification period, the ANC generation rate would be equivalent to 2990 equiv (ha of lake surface)$^{-1}$ yr^{-1}; as a comparison, the ANC production value for the lake determined by the input–output budget, 2400 equiv (ha of lake surface)$^{-1}$ yr^{-1} [=13 equiv (ha of watershed)$^{-1}$ yr^{-1}], is relatively similar given the uncertainties of the lake budget. Thus, the areal production of ANC within Dart's Lake is considerably greater than the areal watershed value of 1210 equiv ha^{-1} yr^{-1}. The relatively high areal rate of in-lake ANC generation makes little contribution to overall watershed ANC generation because of the large ratio of watershed area to lake surface area (180) and the extremely short hydraulic retention time (0.06 yr) of Dart's Lake. Kelly et al. (*48*) reported that the extent of SO_4^{2-} and NO_3^- retention within lakes increased with hydraulic retention time. Thus, a lake with a longer retention time and rates of ANC generation similar to Dart's Lake could be a significant source of ANC generation. However, the majority of lakes present in the Adirondack region have extremely short hydraulic residence times (Figure 1), suggesting that in-lake generation of ANC is unlikely to be an important process for the region.

As indicated previously, the position of Big Moose Lake may influence drainage chemistry and contribute to the component assumed to be terrestrial-generated ANC. However, the increase in ANC (1204 equiv ha^{-1} yr^{-1}) in the upstream watershed relative to bulk precipitation inputs can largely be attributed to the release of metal cationic solutes (Ca, Mg, Na, K, and Al; 1072 equiv ha^{-1} yr^{-1}). Release of base cations from the sediments of Big Moose Lake and Dart's Lake is minimal (*47*); thus, the major source is the terrestrial environment. Therefore, it is reasonable to suggest that terrestrial rather than in-lake processes are largely responsible for the enrichment of ANC relative to precipitation inputs to these lakes.

While in-lake processes represent a minor ANC flux on a watershed basis, they result in significant increases in the concentration of ANC particularly within the hypolimnetic environment. In Dart's Lake, biological processes are the most important source of in-lake generation of ANC. For lakes that are modestly acidic, small increases in ANC could result in significant increases in pH and an improvement in hypolimnetic water quality. However for chronically acidic lakes, such as Dart's Lake, which contain elevated concentrations of Al, increases in pH will induce Al hydrolysis, which may be deleterious to biota and influence element cycling (*49*).

Acknowledgments

We thank L. G. Barnum, N. E. Peters, F. J. Unangst, and J. R. White for their assistance in this study. We also thank the Utilities Acid Precipitation Studies Program (UAPSP) for use of their precipitation data. The hydraulic retention distribution for Adirondack lakes was obtained from the U.S. EPA National Surface Water Survey.

Registry No. NH_4, 14798-03-9; Al, 7429-90-5; Na, 7440-23-5; Fe, 7439-89-6; K, 7440-09-7; hydrogen ion, 12408-02-5.

Literature Cited

(1) Driscoll, C. T.; Newton, R. M. *Environ. Sci. Technol.* **1985**, *19*, 1018.

(2) Johnson, N. M.; Driscoll, C. T.; Eaton, J. S.; Likens, G. E.; McDowell, W. H. *Geochim. Cosmochim. Acta* **1981**, *45*, 1421.
(3) Beamish, R. J.; Harvey, H. H. *J. Fish. Res. Board Can.* **1972**, *29*, 1131.
(4) Dillon, P. J.; Jeffries, D. S.; Snyder, W.; Reid, R.; Yan, N. D.; Evans, D.; Moss, J.; Scheider, W. A. *Can. J. Fish. Aquat. Sci.* **1978**, *35*, 809.
(5) Henriksen, A. In *Ecological Impact of Acid Precipitation*; Drablos, D., Tollan, A., Eds.; Proceedings of the International Conference; SNSF Project: Oslo, 1980.
(6) Driscoll, C. T.; Likens, G. E. *Tellus* **1983**, *34*, 283.
(7) Kelly, C. A.; Rudd, J. W. M.; Cook, R. B.; Schindler, D. W. *Limnol. Oceanogr.* **1982**, *27*, 868.
(8) Schindler, D. W.; Wagemann, R.; Cook, R. B.; Ruszczynski, T.; Prokopowich, J. *Can. J. Fish. Aquat. Sci.* **1980**, *37*, 342.
(9) Carignan, R. *Nature (London)* **1985**, *317*, 158.
(10) Cook, R. B.; Kelly, C. A.; Schindler, D. W.; Turner, M. A. *Limnol. Oceanogr.* **1986**, *31*, 134.
(11) Baker, L.; Brezonik, P. L.; Edgerton, E. S. *Water Resour. Res.* **1986**, *22*, 715.
(12) Schindler, D. W.; Turner, M. A.; Stainton, M. P.; Linsey, G. A. *Science (Washington, D.C.)* **1986**, *232*, 844.
(13) Brewer, P. G.; Goldman, J. C. *Limnol. Oceanogr.* **1976**, *21*, 108.
(14) Goldman, J. C.; Brewer, P. G. *Limnol. Oceanogr.* **1980**, *25*, 352.
(15) Brezonik, P. L.; Lee, G. F. *Environ. Sci. Technol.* **1968**, *2*, 120.
(16) Chan, Y. K.; Campbell, N. E. R. *Can. J. Fish. Aquat. Sci.* **1980**, *37*, 506.
(17) Winfrey, M. R.; Zeikus, J. G. *Appl. Environ. Microbiol.* **1977**, *33*, 275.
(18) Kelly, C. A.; Rudd, J. W. M. *Biogeochemistry* **1984**, *1*, 63.
(19) Rudd, J. W. M.; Kelly, C. A.; St. Louis, V.; Hesslein, R. H.; Furutani, A.; Holoka, M. *Limnol. Oceanogr.* **1986**, *31*, 1267.
(20) Stumm, W.; Morgan, J. J. *Aquatic Chemistry*; Wiley-Interscience: New York, 1981.
(21) Likens, G. E.; Bormann, F. H.; Pierce, R. S.; Eaton, J. S.; Johnson, N. M. *Biogeochemistry of a Forested Ecosystem*; Springer-Verlag: New York, 1977.
(22) Driscoll, C. T.; Schafran, G. C. *Nature (London)* **1984**, *310*, 308.
(23) Newton, R. M.; Weintraub, J.; April, R. *Biogeochemistry* **1987**, *3*, 21.
(24) Schafran, G. C.; Driscoll, C. T. *Biogeochemistry* **1987**, *3*, 105.
(25) *Standard Methods for the Examination of Water and Wastewater*, 16th ed.; American Public Health Association: New York, 1985.
(26) Driscoll, C. T. *Int. J. Environ. Anal. Chem.* **1984**, *16*, 267.
(27) Stainton, M. P. *J. Fish. Res. Board Can.* **1973**, *30*, 1441.
(28) Menzel, D. W.; Vaccaro, R. F. *Limnol. Oceanogr.* **1964**, *9*, 138.
(29) Lazrus, A. L.; Lorange, E.; Lodge, J. P. In *Trace Inorganics in Water*; Baker, R. A., Ed.; Advances in Chemistry 73; American Chemical Society: Washington, DC, 1968; pp 164–171.
(30) Kamphake, L. J.; Hannah, S. A.; Cohen, J. M. *Water Res.* **1967**, *1*, 206.
(31) U.S. EPA *Methods for Chemical Analysis of Water and Wastes*; Environmental Monitoring and Support Laboratory: Cincinnati, OH, 1983; 3501.1-1–350.1-6; EPA-600/4-79-020.
(32) White, J. R. Ph.D. Thesis, Syracuse University, Syracuse, NY, 1984.
(33) Johannes, A. H., personal communication.
(34) Westall, J. C.; Zachary, J. L.; Morel, F. M. *MINEQL a Computer Program for the Calculation of Chemical Equilibrium of Aqueous Systems*; Massachusetts Institute of Technology: Cambridge, MA, 1976; Technical Note 18.
(35) Driscoll, C. T.; Bisogni, J. J. In *Modeling of Total Acid Precipitation Impacts*; Schnoor, J. L., Ed.; Ann Arbor: Ann Arbor, MI, 1984; pp 53–72.
(36) Powell, T.; Jasby, A. *Water Resour. Res.* **1974**, *10*, 191.
(37) Ingvorsen, K.; Brock, T. D. *Limnol. Oceanogr.* **1982**, *27*, 559.
(38) Peters, N. E.; Driscoll, C. T. *Biogeochemistry* **1987**, *3*, 163.
(39) Goering, J. J.; Dugdale, V. A. *Limnol. Oceanogr.* **1966**, *11*, 113.
(40) Keeney, D. R.; Chen, R. L.; Graetz, D. A. *Nature (London)* **1971**, *233*, 66.
(41) Schindler, D. W.; Turner, M. A.; Hesslein, R. H. *Biogeochemistry* **1985**, *1*, 117.
(42) Dillon, P. J.; Jeffries, D. S.; Scheider, W. A. *Water, Air, Soil Pollut.* **1982**, *18*, 241.
(43) Dillon, P. J.; Scheider, W. A. *Sulfur in the Environment, Part II*; Nriagu, J. O., Ed.; Wiley: New York, 1978.
(44) David, M. B. Ph.D. Thesis, State University of New York, Syracuse, NY, 1983.
(45) Schafran, G. C., unpublished data.
(46) Galloway, J. N.; Schofield, C. L.; Peters, N. E.; Hendrey, G. R.; Altwicker, E. R. *Can. J. Fish. Aquat. Sci.* **1983**, *40*, 799.
(47) Driscoll, C. T.; Yatsko, C. P.; Unangst, F. J. *Biogeochemistry* **1987**, *3*, 37.
(48) Kelly, C. A.; Rudd, J. W. M.; Hesslein, R. H.; Schindler, D. W.; Dillon, P. J.; Driscoll, C. T.; Gherini, S. A.; Hecky, R. E. *Biogeochemistry* **1987**, *3*, 129.
(49) Driscoll, C. T. *EHP, Environ. Health Perspect.* **1985**, *63*, 93.

Received for review March 17, 1986. Revised manuscript received November 25, 1986. Accepted June 9, 1987. This study was supported in part by the USEPA/NCSU Acid Deposition Program (APP 0094-1981). This paper does not necessarily reflect the views of the EPA, and no official endorsement should be inferred.

Environ. Sci. Technol. 1987, 21, 994–999

Estimation of Effect of Environmental Tobacco Smoke on Air Quality within Passenger Cabins of Commercial Aircraft

Guy B. Oldaker III* and Fred C. Conrad, Jr.

Research and Development Department, Bowman Gray Technical Center, R. J. Reynolds Tobacco Company, Winston-Salem, North Carolina 27102

■ Nicotine was measured in passenger cabins of Boeing B727-200, B737-200, and B737-300 aircraft in order to estimate the levels of environmental tobacco smoke (ETS) and to assess the effectiveness of smoker segregation as a means of reducing nonsmokers' exposure to ETS. Integrated sampling was performed at seats in smoking and no-smoking sections on flights averaging 55 min. Nicotine was collected on XAD-4 resin and analyzed by gas chromatography with nitrogen–phosphorus detection. Results indicate that significant nicotine concentration gradients exist in cabins and that concentrations increase in magnitude from no-smoking sections to smoking sections. The mean nicotine concentration for samples acquired in no-smoking sections was 5.5 $\mu g/m^3$; in smoking sections of aircraft the mean nicotine concentration was 9.2 $\mu g/m^3$. These concentrations correspond to estimated mean exposures of 0.0041 and 0.0082 cigarette equivalent per flight, respectively.

Introduction

In the U.S., commercial airlines are required during flights to segregate smokers in order to reduce the exposure of nonsmokers to environmental tobacco smoke (ETS), defined as the mixture of diluted and aged sidestream smoke and exhaled mainstream smoke. Since the implementation of this requirement (*1*), its consequences for cabin air quality have not been systematically studied. Although data relative to the levels of ETS in aircraft are contained in a report (*2*) issued jointly by the U.S. Department of Health, Education and Welfare (DHEW) and the U.S. Department of Transportation (DOT), they were obtained before segregation was required.

The literature contains only one report dealing with the quantitation of ETS levels in passenger cabins. Muramatsu et al. (*3*) reported the results of seven samples of vapor-phase nicotine collected during Japanese domestic flights. These researchers, however, provided no information on sampling locations. The choice of nicotine as an indicator of ETS reflects the fact that this compound is uniquely specific for tobacco smoke. At the time these results were reported, the relation between vapor-phase nicotine and ETS had not been characterized. Eudy et al. (*4*) have since then shown that at least 95% of the nicotine associated with ETS exists in the vapor phase.

For the study reported here, vapor-phase nicotine was sampled in passenger cabins of U.S. domestic aircraft in order to gain additional information regarding ETS levels therein and to assess the effectiveness of smoker segregation as a means of reducing the exposure to ETS by persons seated in no-smoking sections. Samples were collected unobtrusively with systems contained in ordinary briefcases in order not to disturb the behavior of passengers or to disrupt airline operations.

Experimental Section

Sampling System. Samples were acquired with sampling systems contained in briefcases that were carefully designed to be inconspicuous (Figure 1). Brass sample inlet and exhaust ports and the on–off switch were located on the front of each briefcase and were positioned symmetrically about the handle. Sample ports were fashioned from 0.25-in. o.d. Swagelok port connectors. Tubing extensions of port connectors were removed, and the resulting flat surfaces were polished. In addition, one of the port connectors was drilled out to a diameter of 0.25 in. to accommodate 6-mm o.d. XAD-4 sorbent tubes.

Major components of the system for sampling nicotine included an XAD-4 sorbent tube and a constant-flow sampling pump (both obtained from SKC, Inc., Eighty Four, PA). Each XAD-4 sorbent tube was positioned through the fitting on the briefcase's front so that approximately 3 mm of the tube's tip projected. Sorbent tube outlets were connected to sampling pumps with short lengths of rubber tubing. Sampling pumps were calibrated with a film flow meter, and flow rates were set at 1 L/min. Calibrations were confirmed with a mercury film flow meter. Flow rates were computed at standard conditions: 298 K (25 °C) and 760 Torr. Temperature and pressure data for adjusting calibration results to standard conditions were obtained from a mercury-in-glass thermometer and a mercury-in-glass barometer, respectively. According to protocol, calibrations were checked at weekly intervals throughout the study. Results from sampling were judged acceptable if the calibrations remained with ±5%.

Sampling Procedure. A written sampling protocol was prepared in conjunction with the study. Persons conducting the sampling were provided with this protocol and also were orally briefed at the start of the study. In addition, persons conducting the sampling had security clearances that permitted them to pass through security stations without revealing the briefcases' contents. All but 14 of the samples were acquired by airline employees, who agreed to participate in the study gratis. The protocol directed that none of the persons conducting the sampling was to smoke during the times when samples were acquired. All sampling operations were performed during scheduled commercial flights that involved business unrelated to the study. Persons conducting the sampling selected flights strictly on the basis of availability and made no effort to select among aircraft types. None of the aircraft that figured in the study had first-class compartments; each aircraft had one smoking section and one no-smoking section.

Sampling was performed during the times when carry-on items such as briefcases could be unobtrusively removed from beneath seats. These times correspond to the times when smoking is permitted in the passenger cabins. Owing to the airline company's seating policy, most samples were obtained at boundary regions between smoking and no-smoking sections. Boundary regions included the last two rows in no-smoking sections adjacent to smoking sections.

Positioning of briefcases during the sampling depended on whether unoccupied seats were available. According to protocol, if an empty seat existed next to the person conducting the sampling, the briefcase was placed in the empty seat and oriented vertically; otherwise, the briefcase was placed in a horizontal position on the sampler's lap

 0013-936X/87/0921-0994$01.50/0

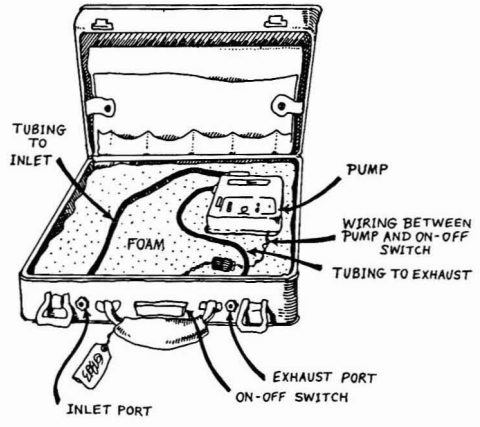

Figure 1. Briefcase sampling system.

with the sampling ports directed away from the body. When briefcases were oriented vertically, samples were acquired within approximately 15 cm of an adult passenger's breathing zone; when briefcases were oriented horizontally, this distance was approximately 45 cm. Airflow to sampling ports was unobstructed. In addition, the protocol specified that the air vents (gaspers) located in the passenger service unit above seats occupied by the briefcase samplers were to be closed during the sample acquisition. The protocol specified that samples be placed in a freezer within 24 h of acquisition.

Barometric pressure was measured on four flights. For the first of these, a hand-held altimeter calibrated against a mercury-in-glass barometer was employed. Response was approximated with a linear least-squares numerical method ($R^2 = 0.999$). Use of the altimeter was determined to be overly conspicuous and burdensome, and consequently its use was discontinued. Additional pressure data were provided by a pressure transducer (Omega Engineering, Inc., Stamford, CT) installed in the briefcase. The transducer was calibrated with a mercury-in-glass barometer and interfaced with a 21X Micrologger (Campbell Scientific, Inc., Logan, UT).

Analytical Procedure. Two methods were used to analyze nicotine, both representing enhancements of the method (*5*) developed by the National Institute of Occupational Safety and Health (NIOSH). From the beginning of the study to 14 January 1986 (corresponding to sample number 36), samples were analyzed with a Model 5880A gas chromatograph equipped with a nitrogen–phosphorus detector (NPD) and a Model 7672A automatic sampler (Hewlett-Packard, Avondale, PA). The column used was a 30-m DB-WAX fused silica capillary with a 0.32-mm i.d. Injections were performed in splitless mode. Column temperature was programmed from 60 to 210 °C at 12 deg/min. Temperatures for the injector and detector were 250 and 300 °C, respectively. Quantitation was accomplished with the use of quinoline as an internal standard.

The method employed for the remainder of the study entailed the use of a 30-m DB5 megabore column with an internal diameter of 0.53 mm and a film thickness of 1.5 μm. Temperatures for the injector and detector were 250 and 300 °C, respectively. Column temperature was programmed from 150 to 175 °C at 5 deg/min. In addition, the ethyl acetate solvent was modified to contain 0.01% (v/v) triethylamine.

Chromatographic systems were calibrated at a minimum of five concentration levels for each set of analyses. Reagent-grade nicotine for these standards was obtained from Eastman Kodak and was used as received. This reagent was stored in a freezer. Field samples were analyzed once; calibration standards were analyzed in duplicate before and after field samples. Results for calibration standards were used in conjunction with a linear least-squares program to compute nicotine levels of field samples and blanks. At least two sample blanks were analyzed with each set of field samples. Nicotine desorption efficiency from XAD-4 resin was determined according to the NIOSH procedure to be 0.92.

Exposures were estimated by computing "cigarette equivalents" from nicotine concentration results and associated sampling times. A breathing rate of 20 L/min (*6*), corresponding to light activity, was assumed for these calculations. Also assumed was a 1983 sales-weighted average cigarette delivering 0.93 mg of nicotine (*7*) as measured by the Federal Trade Commission (FTC) method (*8*, *9*).

Results and Discussion

Results of measurements performed in no-smoking and smoking sections of B727-200, B737-200, and B737-300 aircraft are shown in Tables I and II, respectively. These Boeing aircraft types differ among themselves in terms of seating capacity, location of boundary between smoking and no-smoking sections, and operation and design of heating, ventilating, and air conditioning (HVAC) systems. Ventilation systems of B727-200 and B737-200 aircraft are "once-through" systems; i.e., they are incapable of recirculating air within the cabins. Ventilation systems of B737-300 aircraft, on the other hand, recirculate approximately 40% of the air in the passenger cabins (*10*). Recirculated air is passed through a prefilter and then through a hospital-grade filter (95% efficient for 0.3-μm particles) to remove particulate matter. The population of aircraft studied may be considered representative inasmuch as modern commercial aircraft utilize both ventilation conditions and the three Boeing aircraft types constitute approximately 50% of the U.S. domestic, commercial aircraft fleet (*11*).

Seat entries in the tables identify sampling locations. Numbers indicate seating rows, which are numbered from front to back of the aircraft. Accompanying letters designate positions in rows, which for all rows sampled contained six seats, three seats on each side of the aisle. For the aircraft studied, the location of the smoking boundary is variable, depending for each flight on aircraft type, flight demographics, and number of passengers requesting to sit in either of the sections.

The tabulated number of passengers seated in the smoking sections provides an upper estimate of the number of smokers on a particular flight and allows estimation of an upper limit for the number of cigarettes smoked. The number of cigarettes smoked during a flight was estimated by assuming a smoking rate of two cigarettes per hour per passenger seated in the smoking section. This rate is one of two contained in the joint DHEW/DOT report (*2*); the other measured rate is 0.9 cigarette per smoking passenger per hour. Halfpenny and Starrett (*12*), providing the only other estimate, report 1.34 cigarettes per smoking passenger per hour.

The number of passengers seated in the smoking section was quantified for only a portion of the study. This aspect of the data acquisition process reflected the fact that the study was implemented in phases in order to ensure the quality of results; thus, each successive phase of the study was implemented when data-reliability objectives were met

Table I. Results from Samples Collected in No-Smoking Sections of B727-200, B737-200, and B737-300 Aircraft

sample	aircraft type	seat	no. in smoking section	no. of cig smoked (estd)	sampling time, min	nicotine		cig equiv
						μg	μg/m³	
85	737-200	1F[a]	15	20	41	ND (0.02)	ND (0.5)	NA
1	727-200	3D[a]	20	49	73	ND (0.02)	ND (0.03)[b]	NA
40	737-200	16C	20	30	45	ND (0.02)	ND (0.04)	NA
64	737-300	16E	5	8	50	ND (0.02)	ND (0.4)	NA
66	737-200	19B	35	76	65	ND (0.02)	ND (0.03)	NA
50	727-200	19B	12	26	65	0.04	0.6	0.0009
83	737-300	2B[a]	12	17	42	0.09	0.8	0.0007
41	737-200	12C	30	45	45	0.04	0.8	0.0008
26	737-300	15D	NA	NA	50	0.10	1.5	0.0016
82	737-200	11E	NA	NA	66	0.24	1.6	0.0022
69	737-200	9A[a]	25	63	76	0.17	1.7	0.0027
46	737-200	15C	1	1	41	0.08	1.8	0.0016
3	727-200	19F	20	49	73	0.14	1.9[b]	0.0029
9	737-300	4F[a]	NA	NA	39	0.10	2.1	0.0018
2	727-200	19E	20	49	73	0.17	2.3[b]	0.0037
72	737-200	NA	25	44	53	0.15	2.3	0.0027
32	727-200	19C	NA	NA	40	0.11	2.4	0.0021
75	737-300	6B[a]	NA	NA	32	0.11	2.7	0.0018
7	727-200	22C	NA	NA	132	0.44	2.7	0.0077
21	737-200	14D	NA	NA	51	0.27	3.3	0.0036
44	727-200	20C	14	16	34	0.13	3.4	0.0025
39	737-300	19C	7	13	57	0.28	4.3	0.0052
77	737-200	12B[a]	6	7	36	0.21	4.4	0.0034
31	737-200	15E	NA	NA	30	0.20	6.4	0.0041
33	737-200	15D	NA	NA	45	0.33	6.4	0.0062
17	737-200	15D	NA	NA	42	0.39	6.8	0.0062
20	737-200	15C	NA	NA	75	0.88	7.2	0.0117
10	737-300	11D[a]	NA	NA	39	0.40	8.1	0.0068
29	737-200	15D	20	30	45	0.47	10.0	0.0097
13	737-200	11C[a]	NA	NA	20	0.27	10.1	0.0044
19	737-200	15D	NA	NA	20	0.27	10.1	0.0044
38	737-200	15C	7	12	50	0.64	11.2	0.0120
81	737-300	15E	20	11	17	0.45	11.7	0.0043
80	737-200	15A	15	56	111	3.76	12.8	0.0306
71	737-200	15B	6	8	41	0.71	14.3	0.0126
70	727-200	20E	40	88	66	1.36	14.6	0.0207
30	737-200	15B	25	29	35	0.53	14.6	0.0110
54	737-200	16B	8	15	55	0.89	15.4	0.0182
73	737-200	15C	30	48	48	0.95	16.6	0.0172
58	737-300	16E	10	15	45	0.80	16.7	0.0162
16	737-300	15A	NA	NA	37	1.03	17.2	0.0137
53	737-200	15C	5	8	45	0.95	17.9	0.0173
42	737-200	15C	16	30	56	1.26	19.5	0.0235
22	737-200	14D	NA	NA	50	1.74	21.5	0.0231
57	737-200	15C	14	18	39	1.08	23.3	0.0196
61	727-200	20C	54	128	71	1.26	24.2	0.0369
15	737-200	15D	NA	NA	55	2.18	24.4	0.0288
74	737-200	15C	15	24	47	1.83	32.7	0.0330
18	737-200	15D	NA	NA	13	0.85	40.2	0.0112

[a] Samples collected outside of boundary rows. [b] Concentration at actual conditions.

and maintained. The number of active smokers on a particular flight, and thus the number of cigarettes smoked, was not quantified because this would have disrupted airline operations.

Nicotine results in each table are reported in the manner recommended by the American Chemical Society (*13*). For results below the limit of detection, ND signifies none detected, and the detection limit is shown in parentheses. For results below the limit of quantitation, the measured quantity is given, and the limit of quantitation is presented in parentheses.

Included in Tables I and II are the results of one experiment performed to assess the spatial variability of nicotine concentrations on a single flight. Four concurrent measurements were performed during a 73-min flight. One sample (sample 1) was acquired at seat 3D in the forward portion of the no-smoking section, two samples (samples 2 and 3) were acquired at adjacent seats 19E and 19F in the no-smoking section on the boundary with the smoking section, and one sample (sample 4) was obtained at seat 24F in the smoking section. The observed nicotine concentrations (at actual conditions) were <0.03, 2.3, 1.9, and 42.2 μg/m³, respectively. Twenty persons occupied the smoking section.

The results from this experiment show nicotine levels decreasing substantially from the smoking section to the no-smoking section. The smoker nearest seats 19E and 19F was seated one row distant on the opposite side of the aisle. The results suggest that nicotine (and therefore, ETS) concentration gradients may typically exist at boundary rows.

Bartlett's test for homogeneity of variances was used to test the nicotine concentration data. Test results supported a log-normal distribution. The concentration data were transformed to their logarithms in order to obtain homogeneity of variances and a normal distribution. The transformed data were then analyzed with a 3×2 factorial model ANOVA. Results indicate that the effect of aircraft type is not significant ($P = 0.1802$). On the other hand, the results show the effect of seating section (either

Table II. Results from Samples Collected in Smoking Sections of B727-200, B737-200, and B737-300 Aircraft

sample	aircraft type	seat	no. in smoking section	no. of cig smoked (estd)	sampling time, min	nicotine		cig equiv
						μg	μg/m³	
35	737-200	16E	NA	NA	50	ND (0.004)	ND (0.08)	NA
68	737-200	15C	13	26	60	ND (0.02)	ND (0.03)	NA
67	737-200	17C	20	37	55	0.04 (0.08)	0.6 (1)	NA
65	737-300	19E	22	37	50	0.04 (0.08)	0.7 (2)	NA
45	727-200	20E	25	88	105	0.04	0.4	0.0009
59	727-200	20B	21	50	72	0.05	0.7	0.0010
27	737-200	16D	NA	NA	55	0.15	2.1	0.0024
60	737-200	15B	NA	NA	45	0.11	2.3	0.0022
49	737-200	14C	10	17	52	0.19	3.1	0.0035
6	727-200	22F	NA	NA	179	0.98	4.5	0.0172
63	737-200	20C	24	20	25	0.23	8.6	0.0046
34	737-300	17B	10	17	50	0.46	8.8	0.0095
48	727-200	19B	10	23	70	0.75	10.2	0.0154
28	727-200	21B	17	32	57	0.62	10.5	0.0129
14	727-200	19D	NA	NA	60	1.07	11.0	0.0142
5	727-200	22B	NA	NA	91	1.66	14.9	0.0291
47	737-300	16C	35	123	105	2.05	18.7	0.0423
56	737-200	15C	11	6	16	0.42	22.1	0.0076
51	737-200	18E	7	11	45	1.44	30.2	0.0293
76	737-300	20E	15	19	37	2.01	39.5	0.0314
4	727-200	24F	20	48	72	3.07	42.2[a]	0.0653
78	737-300	23F	22	30	41	4.82	45.0	0.0397
62	737-200	17D	20	17	25	1.51	57.1	0.0307
79	737-300	22D	22	84	114	16.79	59.8	0.1466
52	737-300	16B	23	38	50	4.06	76.7	0.0825
43	737-200	18C	23	31	40	5.18	112.4	0.0967

[a] Concentration at actual conditions.

smoking or no smoking) to be significant ($P = 0.0477$) as well as the effect of interaction, namely, aircraft × seating section ($P = 0.0766$). The model analyzed interaction with a type III sum of squares, which compensates for an unbalanced number of data and any interaction effect on the main effect terms.

The data strongly suggest that the significance of the difference in the nicotine concentrations between smoking and no-smoking sections would have been greater if samples had been collected more evenly in no-smoking sections. Only 9 of the 48 samples associated with no-smoking sections were collected outside of the boundary region; these nine samples tend to be associated with lower nicotine concentrations. The significance of the aircraft–seating section interaction is expected in view of the fact that the areas of smoking and no-smoking sections and ventilation characteristics differ among the three aircraft types.

The number of persons seated in the smoking section and the sampling time, when employed as covariates for the 3 × 2 factorial ANOVA model, were shown to be insignificant: $P > 0.5437$ and $P > 0.3221$, respectively. The absence of significance for the former is exemplified by the 0.4 μg/m³ result of sample 45 acquired in the smoking section of a B727-200 when occupied by 25 persons.

Table III summarizes the concentration results by aircraft type and seating section. Included in the table are data ranges and geometric means.

Mean nicotine levels in the aircraft investigated are substantially lower than mean levels observed in environments where the density of smokers is similar. For example, Muramatsu et al. (*3*) reported mean levels of 26.42, 38.73, and 47.71 μg/m³ in student cafeterias, conference rooms, and automobiles, respectively. The design of the aircrafts' HVAC systems accounts for both the observed relatively low nicotine concentration levels and the absence of significant correlation with number of smokers.

Figure 2 shows the patterns of air circulation along the cross-section of a B727-200 aircraft. (Diagrams for the

Table III. Summary of Results from Sampling Nicotine in Aircraft

aircraft type	seating section	*N*	nicotine concn, μg/m³	
			range	mean
727-200	NS	10	ND (0.03)–24.2	2.6
	S	8	0.4–42.2	6.8
737-200	NS	29	ND (0.04)–40.2	7.7
	S	11	ND (0.08)–112.4	6.5
737-300	NS	10	ND (0.4)–17.2	4.2
	S	7	0.7 (2)–76.7	21.5
total	NS	49	ND (0.03)–40.2	5.5
	S	26	ND (0.08)–112.4	9.2

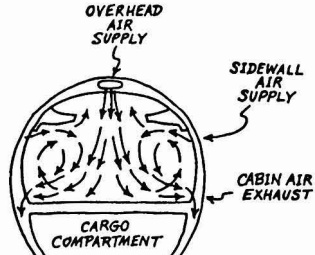

Figure 2. Schematic of airflow patterns for cross-section of B727-200 aircraft (*17*).

B737-200 and B737-300 aircraft are essentially the same.) Air supplies and exhausts are located in a manner that causes air to execute circular movements along a row of seats. Air enters the cabin from overhead vents and exits from vents located at foot level along cabin walls. Mirror-image circulation patterns distinguish port and starboard seats of each row. Air movement within a row also depends on the operation of overhead vents by passengers. Important aspects of the ventilation patterns shown in the

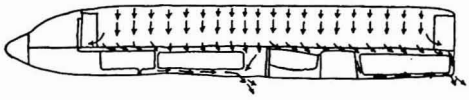

Figure 3. Schematic of airflow patterns along the length of B727-200 aircraft (*17*).

figures are that longitudinal movement of air in the cabins is suppressed, as is movement across the aisles. This longitudinal suppression of air movement is illustrated by Figure 3, showing ventilation patterns along the length of a B727-200's fuselage. (Diagrams for the B737-200 and B737-300 aircraft are essentially the same.) The high ventilation rates of the aircraft studied [for example, 26.5 air changes per hour for B727-200's, 22.7 air changes per hour for B737-200's, and 26.3 air changes per hour for B737-300's (*10*)] minimize the residence time of ETS in passenger cabins. Additionally, ETS will tend to remain within a single port or starboard row of seats owing to the effect of air movement patterns.

The effects of ventilation and air movement patterns and the relative isolation these effects impose on a port or starboard row of seats may account for those results where nicotine concentrations in smoking sections are below the limit of quantitation even though the sections are occupied by substantial numbers of passengers who presumably smoke. Similarly, the nicotine concentration results of this study, when viewed in light of the aircrafts' ventilation characteristics, suggest that the port–starboard segregation approach utilized, for example, by European airlines, may be effective in reducing the exposure of persons seated in the no-smoking section to ETS.

The results of this study show that, to be adequate, models for air quality within aircraft cabins must account for the unique ventilation characteristics of aircraft. Models assuming the complete mixing of ETS in passenger cabins (*14*) are inappropriate for B727-200, B737-200, B737-300, and similar aircraft.

Most of the nicotine concentrations reported here have a high bias component due to the lack of barometric pressure data with which to adjust volumetric data from standard conditions to actual conditions. [Human respiration is not affected by the barometric pressures maintained in passenger cabins (*15*).] Barometric pressure data monitored on four sample runs indicate that concentration biases of up to 15% are possible.

The nicotine concentrations observed for this study are similar in magnitude to those reported by Muramatsu et al. (*3*). These workers, using a portable system attached to persons conducting the sampling, reported nicotine concentrations on Japanese domestic aircraft that ranged from 6.28 to 28.78 $\mu g/m^3$. The mean concentration of the seven samples was 15.18 $\mu g/m^3$. The authors concluded from these results that the exposure of persons to sidestream tobacco smoke, i.e., ETS, is very small. The authors, however, did not provide information regarding the types of aircraft, the sampling locations relative to the smoking sections, or the number of smokers; therefore, comparison with the results from the study reported here are limited.

Some researchers (*3*, *14*, *16*) have used the "cigarette equivalent" computational device to quantify exposure to ETS and thus to place such exposure in a convenient framework for discussion. Such computations assume an average daily breathing rate and an "equivalent cigarette" on the basis of the delivery of nicotine or "tar" in mainstream smoke. However, the term cigarette equivalent is inaccurate inasmuch as it suggests that persons thus exposed are smoking, when in fact they are not. In addition, inhalation during smoking is deeper and more prolonged than during ordinary breathing, and breathing rates are variable rather than constant. Finally, the cigarette equivalent concept is highly manipulatable, because nicotine or tar deliveries vary over a wide range of values for different cigarette brands and because no single definition is currently recognized.

In spite of these shortcomings, the exposures represented by the nicotine levels observed for this study may perhaps be placed in perspective through use of the cigarette equivalent device. Accordingly, concentrations in no-smoking sections represent exposures ranging from 0.00004 to 0.037 cigarette equivalent per sampling period, with a geometric mean of 0.0041 cigarette equivalent per sampling period. Concentrations in smoking sections represent exposures ranging from 0.00008 to 0.15 cigarette equivalent per sampling period, with a geometric mean of 0.0082 cigarette equivalent per sampling period. These estimates in general indicate very low exposure relative to active smoking.

Conclusions

The results of this study show that (a) segregation significantly reduces the exposure of persons seated in no-smoking sections to ETS and (b) aircrafts' HVAC systems are primarily responsible for effecting this reduction. In addition, the results indicate that average exposures to ETS are orders of magnitude less than exposures represented by smoking a single cigarette.

Additional research is needed in order to define more precisely and completely the effect ETS has on air quality in passenger cabins of commercial aircraft. Future studies should be expanded to include measurements of other ETS constituents and to involve wide-bodied aircraft on longer flights.

Acknowledgments

We thank B. C. McConnell and R. F. Walsh for their efforts in fabricating the briefcase sampling systems and M. W. Ogden, D. L. Heavner, L. W. Eudy, R. W. Hawley, B. J. Ingebrethsen, and C. R. Green for their technical assistance.

Registry No. Nicotine, 54-11-5.

Literature Cited

(1) *Fed. Regist.* **1973**, *38*, 19146.
(2) U.S. Department of Health, Education, and Welfare and U.S. Department of Transportation *Health Aspects of Smoking in Transport Aircraft*; U.S. Government Printing Office: Washington, DC, 1971.
(3) Muramatsu, M.; Umemura, S.; Okada, T.; Tomita, H. *Environ. Res.* **1984**, *35*, 218.
(4) Eudy, L. W.; Thome, F. A.; Heavner, D. L.; Green, C. R.; Ingebrethsen, B. J. Presented at the 39th Annual Tobacco Chemists' Research Conference, Montreal, Quebec, Canada, Oct 1985.
(5) *Manual of Analytical Methods*; National Institute for Occupational Safety and Health: Cincinnati, OH, 1977; Part II, Vol. 3, Method No. S293.
(6) International Commission on Radiological Protection *Report of the Task Group on Reference Man*; Pergamon: Oxford, 1974; p 346.
(7) Anon. *Tob. Int.* **1983**, *185*(7), 68.
(8) Pillsbury, H. C.; Bright, C. C.; O'Conner, K. J.; Irish, F. W. *J. Off. Anal. Chem.* **1969**, *52*, 458.
(9) Wagner, J. R.; Thaggard, N. A. *J. Off. Anal. Chem.* **1979**, *62*, 229.
(10) Yorozu, A. S., Boeing Commercial Airplane Co., Seattle, WA, personal communication, 1986.

(11) "Air Transport 1985. The Annual Report of the U.S. Scheduled Airline Industry"; Air Transport Association of America: Washington, DC, June 1985.
(12) Halfpenny, P. F.; Starrett, P. S. *ASHRAE J.* **1961**, *3*, 39.
(13) ACS Committee on Environmental Improvement and Subcommittee on Environmental Analytical Chemistry *Anal. Chem.* **1980**, *52*, 2242.
(14) Repace, J. L.; Lowrey, A. H. *Science (Washington, D.C.)* **1980**, *208*, 464.
(15) McFarland, R. A. *Human Factors in Air Transportation*; McGraw-Hill: New York, 1953; p 158.
(16) Hinds, W. C.; First, M. W. *N. Engl. J. Med.* **1975**, *282*, 844.
(17) "727-200 Maintenance Manual"; Boeing Commercial Airplane Co.: Seattle, WA; Boeing Document No. D6-45267.

Received for review June 23, 1986. Revised manuscript received March 18, 1987. Accepted June 20, 1987.

Oligomerization of 4-Chloroaniline by Oxidoreductases

Kathleen E. Simmons, Robert D. Minard, and Jean-Marc Bollag*

Department of Agronomy and Department of Chemistry, The Pennsylvania State University, University Park, Pennsylvania 16802

■ Oxidation of aromatic amines by oxidoreductases can result in the formation of polyaromatic products. We incubated 4-chloroaniline with horseradish peroxidase and with a laccase from the fungus *Trametes versicolor*. Qualitative and quantitative analyses were performed on the oligomeric products. Both enzymes generated eight oligomers, which were isolated and identified. On the basis of their structures and rates of formation, a reaction scheme for the oxidative oligomerization of 4-chloroaniline was proposed. The scheme shows that, once the substrate was enzymatically oxidized, free-radical coupling followed, and three dimeric intermediates were produced. Each of the dimers initiated a nonenzymatic reaction pathway, and the combined pathways accounted for the formation of the first eight stable 4-chloroaniline-derived oligomers.

Introduction

Aniline-based herbicides readily decompose in the soil, but the resultant degradation products may be transformed into persistent xenobiotic species. Hydrolytic cleavage of the aliphatic portion of the herbicides produces substituted anilines, which often undergo oxidative polymerization and binding to soil organic matter. A study on the fate of substituted anilines in the soil found that at high concentrations (500 ppm) 40% of the applied material was recovered as polyaromatic products and 50% was bound to soil organic matter (*1*). At low concentrations (1.25 ppm), 90% of an aniline soil residue was bound to soil constituents with only trace amounts recovered as extractable oligomers (*2*). It is likely that the processes leading to polymerization are also responsible for incorporation of the anilines into humic substances.

Models of oxidative reactions are essential for understanding the transformation of substituted anilines in soil. Numerous studies have been conducted on the one-electron oxidation of anilines using oxidoreductases, such as horseradish peroxidase and the laccases of *Trametes versicolor* and *Rhizoctonia praticola* (*3–7*). Some of the aniline-derived oligomers were structurally determined, but neither comprehensive product identifications nor quantitative analyses were reported.

In a previous work, we identified the structures of all products formed in the oxidoreductase-initiated polymerization of 4-chloroaniline and developed a method for substrate and product quantitation (*8*). In this investigation, we apply the quantitative method to follow 4-chloroaniline disappearance and product formations as a function of enzyme incubation times. We compare the product profiles resulting from the reactions catalyzed by horseradish peroxidase and the laccase of *T. versicolor*. On the basis of product structures and their relative amounts, we postulate reaction pathways for the oxidative polymerization of substituted anilines in general and for 4-chloroaniline in particular.

Materials and Methods

Chemicals. 4-Chloroaniline was purchased from Aldrich Chemical Co. (Milwaukee, WI) and was 98+% pure as confirmed by thin-layer chromatography (TLC) and high-performance liquid chromatography (HPLC).

Enzyme Assays. Horseradish peroxidase with an RZ (Reinheitszahl) of 0.43 and an activity of 45 purpurogallin units/mg of solid was purchased from Sigma Chemical Co. (St. Louis, MO). A purpurogallin unit is defined as the amount of enzyme that forms 1.0 mg of purpurogallin from pyrogallol in 20 s at pH 6.0 and 20 °C. The absorbance change is measured at 420 nm.

The extracellular laccase of *T. versicolor* was isolated from growth media and purified as previously described (*7*). Laccase activity is given in DMP (2,6-dimethoxyphenol) units. A DMP unit is defined as the amount of enzyme causing a change in absorbance at 468 nm of 1.0 unit min^{-1} at pH 4.2 of a 3.5-mL sample containing 3.24 μmol of 2,6-dimethoxyphenol. Absorbance was measured with a Model 2000 spectrophotometer (Bausch and Lomb, Inc., Rochester, NY).

Unless otherwise specified, enzyme assays were conducted in citrate–phosphate buffers (pH 4.2) with 1 μmol/mL 4-chloroaniline at 25 °C. Horseradish peroxidase assays contained 2.5 μmol/mL hydrogen peroxide and 0.012 purpurogallin unit/mL enzyme; 20 DMP units/mL was used in the laccase assays. Boiled enzymes served as controls.

High-Performance Liquid Chromatography. At the specified times (0–120 min), enzyme activity was halted by the addition of an equal volume of acetonitrile to a 2.5-mL aliquot of the assay solution. The 5.0-mL sample was then passed through a 0.2-μm pore Nylon 66 filter (Schleicher & Schuell, Keene, NH), and 175 μL was immediately analyzed by HPLC. All quantitative data points represent the average value of triplicate sample injections.

Analysis was performed on a Waters Associates (Milford, MA) high-performance liquid chromatograph. The system consisted of a U6K injector, M45 and 6000 pumps run by a Model 720 System Controller, a Lambda Max 450 LC spectrophotometer set at 280 nm (0.05 AUFS), and a Model 730 Data Module.

Reverse-phase separation was performed on a 15 cm × 4.6 mm Supelcosil LC18 (octadecylsilica) column of 5-μm particle size (Supelco, Inc., Bellefonte, PA). The mobile phase at a flow rate of 1.5 mL/min consisted of an aqueous

0013-936X/87/0921-0999$01.50/0

Table I. 4-Chloroaniline and Amount of Products Formed by a Peroxidase and a Laccase at pH 4.2 after 15-min Incubation[a]

	nmol/mL								
assay	A (4-chloroaniline)	B (dimer)	C (dimer)	D (dimer)	E (dimer)	F (trimer)	G (trimer)	H (tetramer)	I (tetramer)
horseradish peroxidase	825.2	2.8	8.4	8.1	5.5	1.5	22.9	1.3	3.1
laccase of *T. versicolor*	750.0	0.5	18.9	12.0	7.4	1.4	26.3	0.8	2.1

[a] The initial substrate concentration was 1.0 μmol/mL.

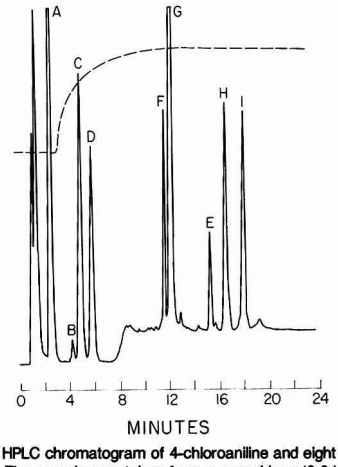

Figure 1. HPLC chromatogram of 4-chloroaniline and eight oligomeric products. The sample was taken from a peroxidase (0.012 purpurogallin unit/mL) reaction solution after 60-min incubation. The dashed line indicates the gradient curve. (A) 4-Chloroaniline; (B) *N*-(4-chlorophenyl)-*p*-phenylenediamine; (C) *N*-(4-chlorophenyl)-*p*-benzoquinone diimine; (D) *N*-(4-chlorophenyl)-*p*-benzoquinone monoimine; (E) 4,4′-dichloroazobenzene; (F) 2-(4-chloroanilino)-*N*-(4-chlorophenyl)benzoquinone monoimine; (G) 2-amino-5-chlorobenzoquinone bis(4-chloroanil); (H) 2-(4-chloroanilino)-5-hydroxybenzoquinone bis(4-chloroanil); (I) 2-amino-5-(4-chloroanilino)benzoquinone bis(4-chloroanil).

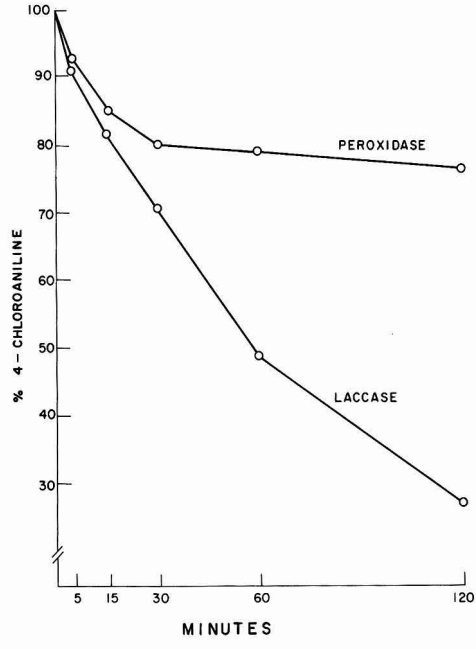

Figure 2. Disappearance of 4-chloroaniline from assay solutions containing a peroxidase (0.012 purpurogallin unit/mL) and a laccase (20 DMP units/mL) at pH 4.2. Figures 3 and 4 show corresponding product formations.

component A (0.01 M KH_2PO_4, 0.05% triethylamine, pH 6.3) and an organic component B (methanol, 0.1% triethylamine). The composition was maintained at 40/60 (volume percent) A/B for the first 3 min and was then brought to 10/90 A/B (see gradient curve in Figure 1) within 15 min. The final composition was maintained for 5 min. The column was equilibrated for 10 min at initial conditions before each injection. Quantitation of 4-chloroaniline and products was performed as previously described (*8*).

Results

The oxidation of 4-chloroaniline by horseradish peroxidase or a laccase of *T. versicolor* resulted in the formation of eight oligomeric products. These products were isolated and identified in a previous study (*8*).

Enzyme assays were conducted in buffered aqueous solutions, and the disappearance of 4-chloroaniline as well as the formation of products was quantitatively monitored with reverse-phase HPLC. The separation of 4-chloroaniline (peak A) and the eight oligomeric products (peaks B–I) is shown in the chromatogram in Figure 1. The HPLC quantitation method has been described previously (*8*).

Analysis of the peroxidase assay solutions showed that 20% of the 4-chloroaniline was transformed within the first 30 min of the reaction. Longer incubation times did not effect further substrate transformation by the peroxidase. During the first 15 min of the reaction, the peroxidase and the laccase caused the disappearance of the substrate at comparable rates. However, the laccase continued to catalyze 4-chloroaniline oxidation, so that after 120 min of incubation less than 30% of the unreacted substrate remained. Substrate disappearance curves for the peroxidase and laccase reactions at pH 4.2 are shown in Figure 2.

Quantitative analysis of the oligomeric products was performed concurrently with the substrate disappearance determinations. The product quantitation studies showed that both the peroxidase and the laccase catalyzed the formation of four dimers (compounds B–E) and a trimer (compound G) within the first 5 min of incubation. Another trimer (compound F) and two tetramers (compounds H and I) were detected after longer reaction times. The amounts of the respective products formed in the peroxidase and laccase assays were approximately equal during the first 15 min of incubation (Table I). Longer reaction times resulted in quantitatively different product mixtures with the two enzymes. Figures 3 and 4 show the product formation curves for peroxidase and laccase, respectively, and correspond to the substrate disappearance curves in Figure 2.

Discussion

Although the active site mechanisms for peroxidase (*9*) and laccase (*10*) are quite different, both enzymes catalyzed

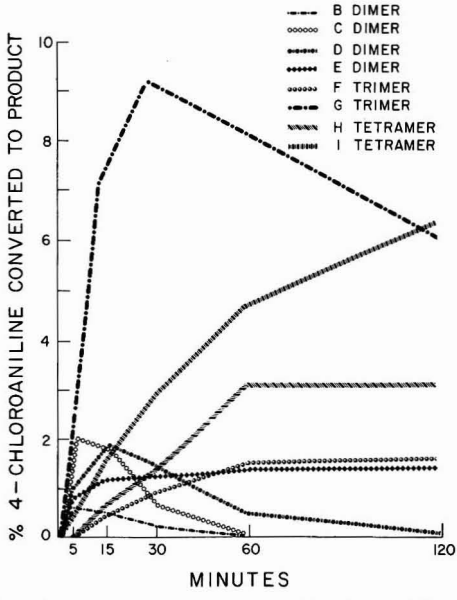

Figure 3. Products formed from 4-chloroaniline after incubation with horseradish peroxidase (0.012 purpurogallin unit/mL).

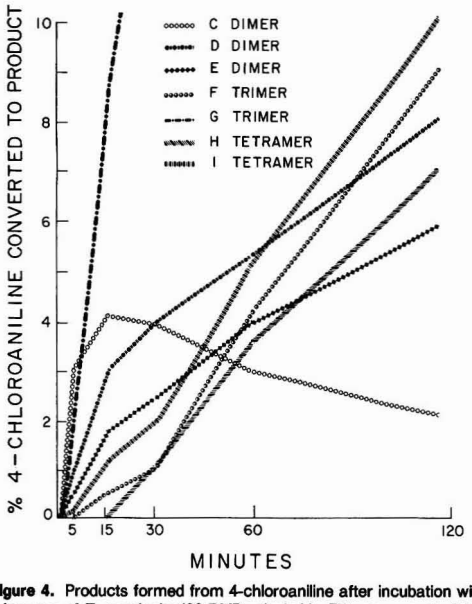

Figure 4. Products formed from 4-chloroaniline after incubation with a laccase of *T. versicolor* (20 DMP units/mL). Fifteen percent of the substrate was converted to compound G after 30-min, 24% after 60-min, and 32% after 120-min incubation.

one-electron oxidation of 4-chloroaniline. The resultant oligomeric product mixtures were qualitatively equivalent.

It is known that one-electron oxidation of substituted anilines by an oxidoreductase can produce azobenzenes, benzoquinone diimines, and benzoquinone monoimines (*4, 5, 11, 12*). However, the reaction mechanisms involved in the formation of these oligomers have not been clarified. Hughes and Saunders (*11*) and Briggs and Ogilvie (*12*) proposed that symmetrical and unsymmetrical pairing of substituted aniline free radicals leads to the formation of azo and diimine compounds. Bordeleau et al. (*4*) suggested that the azobenzene dimers are formed from phenylhydroxylamine intermediates. Iwan et al. (*5*) combined the proposed free-radical pairing and phenylhydroxylamine intermediate mechanisms to explain the generation of dimers and trimers from the one-electron oxidation of 4-chloro-*o*-toluidine. None of these reports included comprehensive product identifications, nor were quantitative studies conducted. We have identified all products generated by the one-electron oxidation of 4-chloroaniline (*8*). Product structure identifications, and the rates of substrate disappearance and product formation, were used in this study to develop a reaction pathway scheme for the oxidative oligomerization of a substituted aniline.

The peroxidase appeared to lose activity after 15-min incubation while the laccase continued to effect 4-chloroaniline transformation (Figure 2). Comparison of the product formation curves obtained from the two assay solutions (Figures 3 and 4) allows for a discrimination between products that increased in amount, products that decreased in amount, and products that remained at a constant concentration in the absence of enzyme activity. The concentrations of compounds B, C, D, and G decreased with the apparent decline in peroxidase activity, while those of compounds F, H, and I increased (Figure 3). Previous experiments have shown that compound C reacts nonenzymatically through the reversible addition of two hydrogen atoms to form compound B, through condensation with 4-chloroaniline to form compound I, or through hydrolysis to form compound D (*8*). Compound D also condenses with 4-chloroaniline to generate compounds F and H. The respective product formation curves in Figure 3 established the nature of these nonenzymatic transformations. The formation rate of compound E was directly proportional to the substrate disappearance rate in both enzyme assay solutions. Therefore, it appeared that compounds C, E, and G were formed first and that compounds B, D, F, H, and I were all formed by nonenzymatic transformations of compound C.

The disappearance of compound G with the decline in peroxidase activity could not be explained. When compound G was isolated and incubated for 120 min with either the peroxidase or 4-chloroaniline, its concentration did not change. In the laccase solutions the amount of compound G increased with incubation time until enzyme activity was stopped by the addition of acetonitrile. After the addition of acetonitrile, the concentration of compound G remained constant for up to 24 h. Compound G did not condense with 4-chloroaniline to form higher oligomers, nor was it a substrate for peroxidase-catalyzed oxidation.

Figure 5 depicts reaction pathways for the oxidative oligomerization of 4-chloroaniline, which explain the observed course of product formations. All alphabetically labeled compounds were isolated and identified, and the proposed reaction intermediates are in brackets. In the initial step, enzymatic oxidation of 4-chloroaniline produces an anilino free radical, which is resonance stabilized by delocalization at the N, para, and ortho positions. Three dimeric intermediates are formed by N–N, N–para, and N–ortho radical couplings, and they initiate three reaction pathways that can account for the formation of the eight 4-chloroaniline-derived oligomers. The predominance of any one pathway depends on the amount of the initial dimeric intermediate formed.

The extent of N–N, N–para, and N–ortho radical coupling is dictated by the degree of lone electron localization in the N, para, and ortho positions. The highest lone electron density is expected at the N and para radical

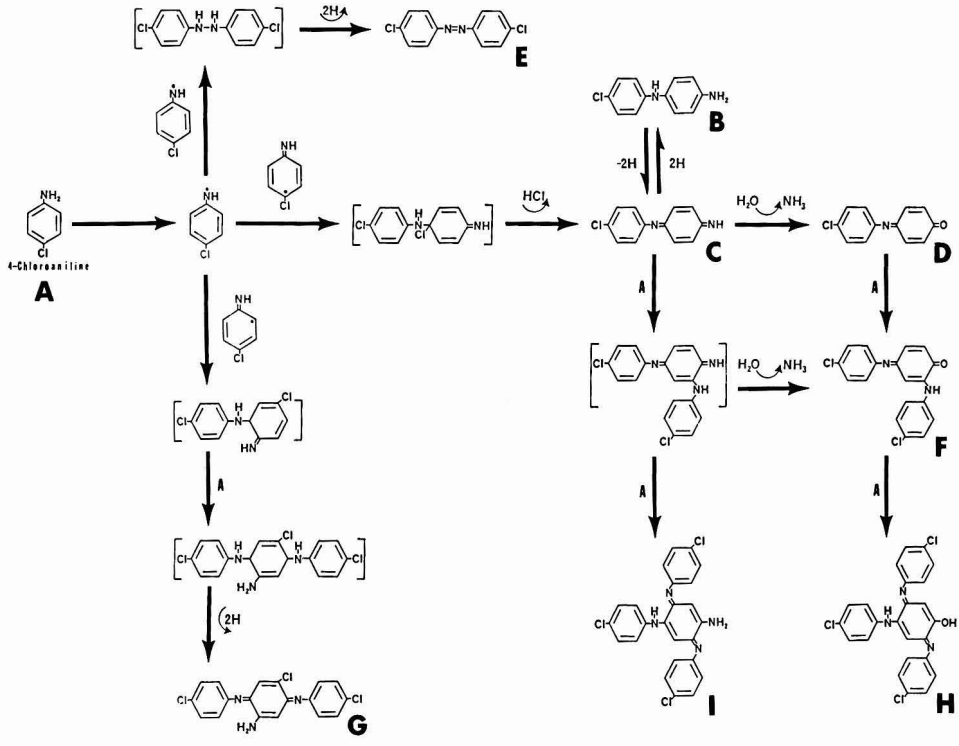

Figure 5. Proposed reaction pathway for the one-electron oxidation of 4-chloroaniline.

positions, but since the para position is substituted, steric hindrance limits the amount of para coupling (*13*). In fact, the ratio of N:para:ortho positional radicals was 2.6:1:1 for the oxidoreductase reactions as determined from the amount of each oligomer found in the product mixtures. The quantity of free-radical molecules that coupled to initiate a particular oligomer-forming pathway was deduced by summation of the amounts of oligomers produced by that pathway. For example, if the product mixture solution contained 5 nmol/mL compound I, then 5 nmol/mL N radical and 5 nmol/mL para radical must have coupled to give the observed amount of compound I. In this manner, the ratios of N:para:ortho radicals were obtained for assay solutions of 4-chloroaniline containing the laccase at pH 4.2 (20 DMP units/mL) and the peroxidase at pH 4.2 (0.012 unit/mL), pH 3.6 (0.023 unit/mL), and pH 4.8 (0.023 unit/mL). The ratio was always 2.6:1:1 and did not change with incubation time. This ratio represents the relative reactivity at the N, para, and ortho positions, as determined by localization of the lone electron and steric factors. Variations in solution pH, enzyme concentration, and enzyme type should not affect this relative reactivity if initial product formation involves the free-radical coupling mechanisms (*14*) as shown in Figure 5. Therefore, the observed constant ratio substantiates the free-radical coupling mechanism.

Although the N:para:ortho ratio did not change with the pH of the reaction solution, the relative amounts of compounds B–I did vary. At low pH, compound C is more readily transformed to compound D, since the hydrolysis of an imine to a carbonyl moiety has an acid-catalyzed rate-determining step (*15*). Compounds H and I are tetramers formed from compounds D and C, respectively, and according to the scheme of Figure 5, a more acidic assay solution would be expected to give a greater amount of compound H relative to compound I. This expectation was met as experiments conducted at various pH values demonstrated (data not shown). At pH 3.6, the tetramer (H) derived from compound D was preferentially formed, and at pH 4.8, the tetramer (I) derived from compound C was formed at a faster rate than the rate at which compound C was hydrolyzed to compound D.

Conclusions

This paper presents reaction pathways for the oxidative oligomerization of a substituted aniline. The reaction scheme was developed with data from qualitative and quantitative analyses of the products obtained from oxidoreductase-catalyzed polymerization of 4-chloroaniline. The scheme shows that free-radical coupling initiates pathways that lead to the formation of a variety of aniline-derived oligomers. The same type of coupling could presumably occur between oxidized substituted anilines and soil organic matter and results in the incorporation of the aniline into humus polymers. At typical herbicide application levels, the bulk of substituted anilines reaching the soil are converted into soil-bound residues. The tenacity of binding indicates covalent bonds with humic substances (*1*, *16*), but the complexity of humus structures precludes the direct characterization of bound residues. Investigations into the oxidative oligomerization of substituted anilines and of phenolic humus constituents are necessary to gain an understanding of the incorporation of xenobiotics into humic structures. This study offers significant insight into the nature of this environmentally important process.

Literature Cited

(1) Bartha, R. *J. Agric. Food Chem.* **1971**, *19*, 385–387.
(2) Freitag, D.; Scheunert, I.; Klein, W.; Korte, F. J. *J. Agric. Food Chem.* **1984**, *32*, 203–207.
(3) Daniels, D. G. H.; Saunders, B. C. *J. Chem. Soc.* **1953**, 822–826.
(4) Bordeleau, L. M.; Rosen, J. D.; Bartha, R. *J. Agric. Food Chem.* **1972**, *20*, 573–578.
(5) Iwan, J.; Hoyer, G.-A.; Rosenberg, D.; Goller, D. *Pestic. Sci.* **1976**, *7*, 621–631.
(6) Sjoblad, R. D.; Bollag, J.-M. *Appl. Environ. Microbiol.* **1977**, *34*, 906–910.
(7) Hoff, T.; Liu, S.-Y.; Bollag, J.-M. *Appl. Environ. Microbiol.* **1985**, *49*, 1040–1045.
(8) Simmons, K. E.; Minard, R. D.; Freyer, A. J.; Bollag, J.-M. *Int. J. Environ. Anal. Chem.* **1986**, *26*, 209–227.
(9) Chance, B. *Arch. Biochem. Biophys.* **1952**, *41*, 416–424.
(10) Malmström, B. G. *Annu. Rev. Biochem.* **1982**, *51*, 21–59.
(11) Hughes, G. M. K.; Saunders, B. C. *J. Chem. Soc.* **1954**, 4630–4634.
(12) Briggs, G. G.; Ogilvie, S. Y. *Pestic. Sci.* **1971**, *2*, 165–168.
(13) Musso, H. In *Oxidative Coupling of Phenols*; Taylor, W. I., Battersby, A. R., Eds.; Dekker: New York, 1967; pp 1–94.
(14) March, J. *Advanced Organic Chemistry, Reactions, Mechanisms, and Structures*, 2nd ed.; McGraw-Hill: New York, 1977; pp 619–671.
(15) Layer, R. W. *Chem. Rev.* **1963**, *63*, 489–510.
(16) Bollag, J.-M.; Blattmann, P.; Laanio, T. *J. Agric. Food Chem.* **1978**, *26*, 1302–1306.

Received for review November 11, 1986. Accepted June 18, 1987. Primary funding for this research project was provided by the Office of Research and Development, Environmental Protection Agency (EPA Grant R-811518). The EPA does not necessarily endorse any commercial products used in the study, and the conclusions represent the views of the authors and do not necessarily represent the opinions, policies, or recommendations of the EPA. Additional funding was provided by the Pennsylvania Agricultural Experiment Station (Journal Series No. 7499).

Mixed-Substrate Utilization by Acclimated Activated Sludge in Batch and Continuous-Flow Stirred Tank Reactors

Sarvottam D. Deshpande, Tapan Chakrabarti,* and P. V. R. Subrahmanyam

National Environmental Engineering Research Institute, Nagpur, India

■ A number of biodegradability studies using acclimated activated sludge and batch and continuous-flow reactors were conducted. *m*-Nitrobenzenesulfonate, sodium salt (*m*-NBS), acclimated activated sludge demonstrated different substrate utilization capacity when compared to resorcinol-acclimated activated sludge exposed to the same set of substrates. Out of the four mixed feeds treated in batch reactors, utilization of *m*-NBS from the *m*-NBS–catechol system was found to be aided by exogenous cyclic adenosine cyclic monophosphate (cAMP). In a continuous-flow reactor, the substrate utilization pattern with *m*-NBS–catechol, resorcinol–*m*-aminophenol (*m*-AP), and catechol–resorcinol mixed feeds was simultaneous at a dilution rate of 0.042/h. In the resorcinol–*m*-NBS mixed-feed system, resorcinol was the preferred substrate, and an increase in resorcinol concentration in the mixed feed resulted in the progressive reduction in *m*-NBS utilization. However, with the *m*-AP–resorcinol mixed feed at a dilution rate of 0.323/h, the simultaneous utilization pattern changed into the preferential utilization pattern.

Introduction

In waste process biotechnology, multiple-substrate utilization in a biological waste water treatment system is a common phenomenon. Waste waters containing multisubstrates are common in organic chemical manufacturing industrial complexes where a variety of products are manufactured. In biological treatment plants, the substrate removal pattern in a multisubstrate system may include simultaneous, preferential, or sequential utilization. The diauxic growth observed by Monod (*1*) in *Escherichia coli* suggests that the very presence of a particular substrate in a waste water stream might prevent an organism from acclimatizing to another substrate until the first one has been completely metabolized. The blockage of metabolism of one compound by another may lead to preferential or sequential substrate removal from a multisubstrate environment. Chian and Dewalle (*2*) have presented evidence for the sequential removal of waste components during biological treatment of a leachate from a sanitary landfill. Degradation of *p*-nitrobenzoate by acclimated sludge was found to be inhibited by benzoate (*3*). Deshpande and Chakrabarti (*4*), in a batch reactor, demonstrated preferential removal of *m*-nitrobenzenesulfonate, sodium salt (*m*-NBS), from a mixture of *m*-NBS and resorcinol, compounds that are known to be present in *m*-aminophenol (*m*-AP) manufacturing waste waters. However, resorcinol was found to be the preferred substrate when the same substrate mixture was fed to a continuous unit with *m*-NBS-acclimated activated sludge (*5*). Mateles et al. (*6*) have collected steady-state data from the continuous culture of *Pseudomonas fluorescens* and *E. coli* b_6 on a mixed-substrate feed capable of producing a diauxic phenomenon in batch cultures. The data for the growth of *E. coli* b_6 on glucose and lactose show simultaneous utilization of both sugars over a wide range of dilution rates. At higher dilution rates, however, a sudden change to preferential utilization of glucose was observed, suggesting that dilution rates have a profound influence on the substrate utilization pattern when a mixed-substrate feed is subjected to biological treatment processes.

Mechanisms of repression and induction involved in the regulatory processes when an organism is exposed to a multisubstrate environment would be explained by the operon theory of Jacob and Monod (*7*). The induction of operon requires the participation of adenosine cyclic monophosphate (cAMP) and cAMP receptor protein (CRP), and exogenous cAMP has been reported to trigger cAMP-mediated responses in a wide variety of microorganisms (*8–10*). Knowledge of the cAMP requirement in mixed-substrate utilization could help in understanding whether an operon type of mechanism is responsible for sequential removal of substrates by the acclimated activated sludge.

The purpose of this investigation is to study the utilization of substituted benzenes of industrial relevance from

0013-936X/87/0921-1003$01.50/0

a multisubstrate environment and to determine the involvement, if any, of cAMP in the utilization process.

Materials and Methods

Acclimation. Activated sludge from an oxidation ditch treating domestic waste water was divided into 10 parts and separately exposed to catechol, resorcinol, *m*-NBS, *m*-AP, benzenesulfonic acid (BSA), metanilic acid (*m*-AA), and mixed feed containing (i) *m*-NBS and catechol, (ii) *m*-NBS and resorcinol, (iii) resorcinol and *m*-AP, and (iv) catechol and resorcinol for acclimation. The organic loading in each case was maintained at 0.11 g of total organic carbon (TOC)/g of mixed liquor volatile suspended solids (MLVSS). Diammonium orthophosphate (200 mg/L) provided the required nitrogen and phosphorus. The fill and draw technique (*4*, *5*) was employed, and acclimation was determined from the rate of TOC utilization by the respective sludges.

Substrate Utilization Studies. *m*-NBS-acclimated activated sludge was divided into six parts and separately exposed to catechol, *m*-NBS, resorcinol, pyrogallol, hydroquinone, and phloroglucinol at an organic loading of 0.11 g of TOC/g of MLVSS in batch reactors of 1-L capacity each and equipped with sintered glass diffusers. Biodegradation experiments were also carried out with resorcinol-acclimated activated sludge using the same substrates under similar experimental conditions. The experiments were conducted for a period of 6 h, and the TOC of 0- and 6-h samples in each case was monitored with a Beckman TOC analyzer (Model 915 A) as per ref 11.

HPLC Analyses. The organic components present in samples were quantified with the help of high-performance liquid chromatogrpahy (HPLC) (Model 204, Water Associates Inc., Milford, MA) in a system equipped with M-6000 and M-45 pumps, a u6K septumless injector, a Model 440 UV absorption detector with a 254-nm primary filter, and an HPLC recorder (Houston Instrument Series B-5000 dual pen, Austin, TX). Solvents used were double-distilled spectroscopic-grade dioxane and water in the ratio of 1:24 in the case of catechol–resorcinol system and only water in the case of all other systems investigated. The column used for HPLC analyses was μBondapac C-18. Samples filtered through Millipore membrane filter were analyzed by reverse-phase chromatography. Operating conditions were (i) chart speed, 25 cm/h; (ii) flow rate, 2 mL/min; and (iii) column temperature, ambient. Analytical-grade standards were run with each experiment.

cAMP Addition Experiments. Adenosine cyclic 3′,5′-monophosphate (cAMP), anhydrous crystalline variety, was obtained from Sigma Chemical Co., St. Louis, MO. Four aerobic batch reactors were employed to study the effect of cAMP addition (1 mM) on the utilization of substrates from a mixed-substrate environment. The four reactors were fed with mixed feed consisting of (i) *m*-NBS (1000 mg/L) and catechol (200 mg/L), (ii) *m*-NBS (1000 mg/L) and resorcinol (500 mg/L), (iii) resorcinol (180 mg/L) and *m*-AP (160 mg/L), and (iv) catechol (425 mg/L) and resorcinol (475 mg/L), respectively. The experiment was conducted for 90 h in the case of the first reactor and for 24 h in the cases of the second, third, and fourth reactors. Influent and effluent samples from these reactors were subjected to HPLC analyses.

Continuous-Flow Experiments. An activated sludge unit (*12*) having a 2.725-L aeration cell and a built-in 0.725-L settling compartment was used for continuous-flow experiments. The unit with the acclimated activated sludge was operated at room temperature (25 ± 2 °C) by feeding continuously the mixed feeds (one feed at a time) and maintaining a 24-h hydraulic detention time. The mixed feeds in the case (i) of *m*-NBS and catechol consisted of 300 mg/L and *m*-NBS and 450 mg/L or catechol, (ii) of resorcinol and *m*-AP consisted of 500 mg/L of resorcinol and 250 mg/L of *m*-AP, and (iii) of resorcinol and catechol consisted of 475 mg/L of resorcinol and 425 mg/L of catechol. The mixed feed containing *m*-NBS and resorcinol had a constant amount of *m*-NBS (1000 mg/L) and varying amounts of resorcinol (210–690 mg/L). Diammonium orthophosphate (200 mg/L) added to the mixed feeds provided the required nitrogen and phosphorus. A requisite volume of mixed liquor was wasted from time to time to maintain constant MLVSS in the aeration cell. After a stable condition was attained as indicated by constant TOC in the affluent, the influent and effluent samples from all sets of experiments carried out were subjected to HPLC analyses. The dilution rate maintained was around 0.042/h for the above experiments.

In another experiment, the continuous-flow activated sludge unit was operated at different dilution rates with resorcinol (500 mg/L) and *m*-AP (250 mg/L) as the mixed feed, and the effluent was monitored by HPLC for the presence of substrates. The dilution rates tried ranged from 0.042/h to 0.323/h. Suspended solids in the effluent were estimated as per ref 11. The filtered effluent was subjected to HPLC analyses.

The sludge from the continuous unit was then divided equally, transferred to three batch reactors, and aerated with resorcinol, *m*-AP, and the mixed feed. Samples were collected at hourly intervals and analyzed by HPLC for resorcinol and *m*-AP.

Table I. Biodegradation of Substituted Benzenes by Acclimated Activated Sludge[a]

substrate	mg of TOC utilized (g of MLVSS)$^{-1}$ h^{-1}
(i) catechol	26.4 ± 0.7
(ii) resorcinol	21.0 ± 1.9
(iii) BSA	10.7 ± 0.6
(iv) *m*-NBS	6.8 ± 0.6
(v) *m*-AP	1.4 ± 0.1
(vi) *m*-AA	not utilized

[a] Loading: 0.11 g of TOC/g of MLVSS. Results are the average of six experiments ± standard deviation.

Table II. Utilization of Substituted Benzenes[a]

substrate	mg of TOC removed (g of MLVSS)$^{-1}$ h^{-1}	
	m-NBS-acclimated activated sludge	resorcinol-acclimated activated sludge
(i) catechol	22.1	8.9
(ii) *m*-NBS	16.9	not utilized
(iii) resorcinol	8.7	22.0
(iv) pyrogallol	7.7	3.2
(v) phloroglucinol	not utilized	not utilized
(vi) hydroquinone	not utilized	5.7

[a] Loading: 0.11 g of TOC/g of MLVSS. Results are the average of three experiments.

Results and Discussion

Results of biodegradation studies by acclimated activated sludge are summarized in Tables I and II showing the degrading ability of an activated sludge from an oxidation ditch treating domestic waste water acclimated to a variety of substituted benzenes. It can be seen from Table I that the activated sludge possesses the necessary catabolic enzyme systems required to degrade catechol, resorcinol, *m*-NBS, BSA, and *m*-AP. The sludge, however,

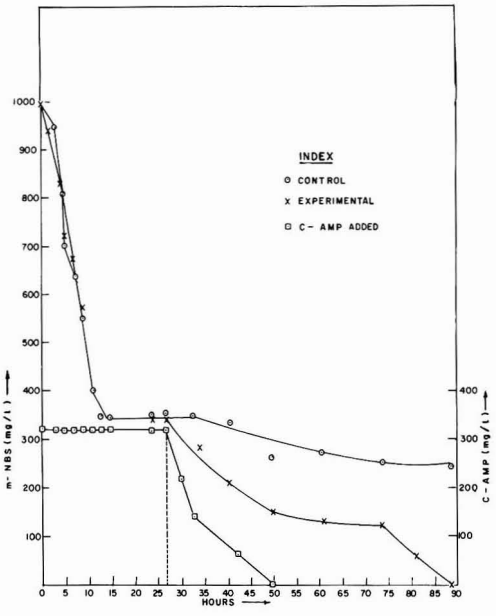

Figure 1. Effect of cAMP addition on the utilization of *m*-NBS from a mixed feed containing *m*-NBS and catechol after catechol removal by acclimated activated sludge.

could not be acclimated to *m*-AA under similar experimental conditions. Table II shows catechol, *m*-NBS, resorcinol, and pyrogallol utilization at a loading of 0.11 g of TOC/g of MLVSS, the order of removal rate being catechol > *m*-NBS > resorcinol > pyrogallol when sludge acclimated to *m*-NBS was employed. However, the sludge could not degrade hydrquinone and phloroglucinol. On the other hand, resorcinol-acclimated activated sludge could degrade resorcinol, catechol, hydroquinone, and pyrogallol at a loading of 0.11 g of TOC/g of MLVSS, the order of removal rate being resorcinol > catechol > hydroquinone > pyrogallol. Resorcinol-acclimated activated sludge could not, however, degrade *m*-NBS and phloroglucinol. It could be seen from these results that an activated sludge obtained from the same source and acclimated separately to *m*-NBS and resorcinol assumes different biochemical characteristics as is evident from the substrate utilization rates when exposed to the same set of substrates. However, neither *m*-NBS- nor resorcinol-acclimated activated sludge could degrade phloroglucinol, although this compound has been reported to be biodegradable by acclimated activated sludge (*13*). These results also suggest that *m*-NBS-acclimated activated sludge loses the capacity to degrade hydroquinone whereas resorcinol-acclimated activated sludge loses the capability to degrade *m*-NBS.

Figure 1 shows the effect of cAMP addition on the utilization of *m*-NBS from a mixed feed containing *m*-NBS and catechol by activated sludge acclimated to the mixed feed. It could be seen from Figure 1 that *m*-NBS utilization was only partial (74%) in the control system without cAMP addition, whereas with the addition of cAMP complete utilization of *m*-NBS occurred in the experimental system, both systems being run for 90 h. The utilization of *m*-NBS began only after catechol was fully utilized and continued for 13 h in both the systems. This was followed by a 14-h lag period. At the 28th hour, removal of both *m*-NBS and cAMP started taking place in the experimental system. cAMP removal was complete in 50 h (Figure 2) whereas that of *m*-NBS was complete in 90 h. On the other hand, *m*-NBS degradation between 27 and 90 h in the control system was only around 31%. It is, therefore, evident from Figure 1 that exogenous cAMP facilitates biodegradation of *m*-NBS by the acclimated microbial consortium present in the activated sludge. This presumption is strengthened by the simultaneous disappearance of *m*-NBS and cAMP in the experimental system at the 27th hour of the experiment. The observed sequential catechol and *m*-NBS utilization and cAMP requirement for complete utilization of *m*-NBS indicate the existence of an operon-like mechanism for *m*-NBS utilization by acclimated organisms from a mixed-substrate environment containing *m*-NBS and catechol.

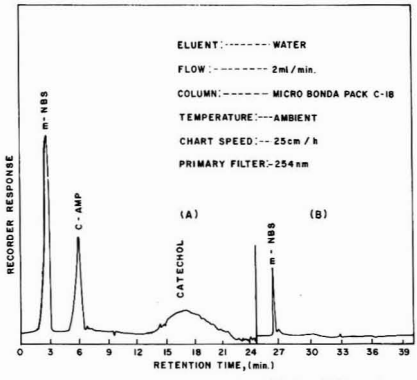

Figure 2. HPLC scan for separation of *m*-NBS, cAMP and catechol. Influent (A) and effluent (B) after 50 h.

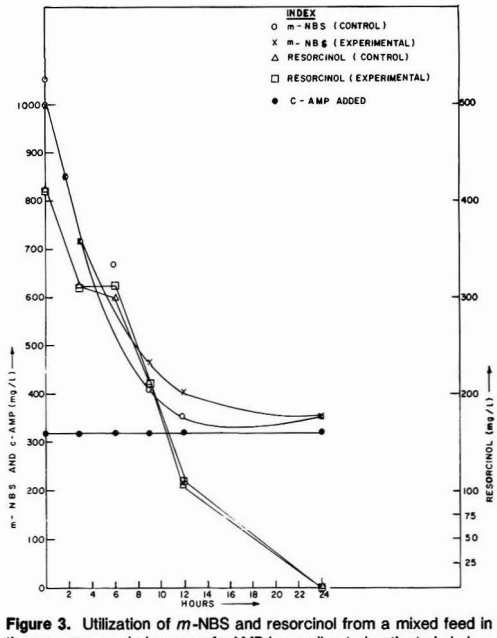

Figure 3. Utilization of *m*-NBS and resorcinol from a mixed feed in the presence and absence of cAMP by acclimated activated sludge.

Figures 3–5 show the effect of cAMP addition on the utilization of *m*-NBS and resorcinol, *m*-AP and resorcinol, and catechol and resorcinol from mixed-substrate systems using acclimated activated sludges. Resorcinol was found

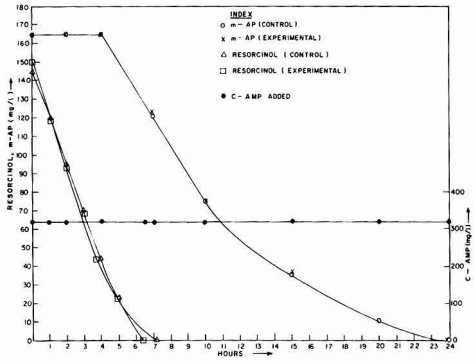

Figure 4. Effect of cAMP addition on the utilization of resorcinol and *m*-aminophenol (*m*-AP) by acclimated activated sludge.

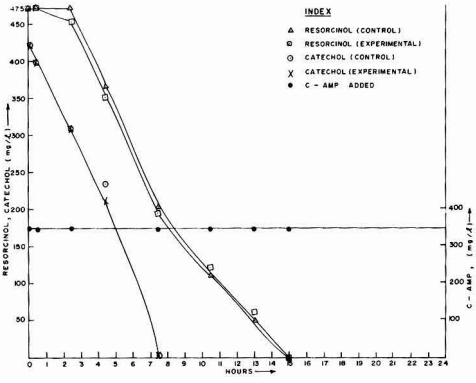

Figure 5. Effect of cAMP addition on the utilization of resorcinol and catechol by acclimated activated sludge.

to be preferentially utilized over *m*-NBS and *m*-AP from the respective mixed feeds, and the utilization rates were unaffected by cAMP addition. Similarly, preferential utilization of catechol folllowed by resorcinol was observed, and the utilization was unaffected by cAMP addition. Also, the level of cAMP exogenously added to these three systems remained unaltered throughout the experimental period. It has been reported that cAMP is not the only compound that plays a role in mediation of catabolic repression (*14*). Factors other than cAMP such as indoleacetic acid and imidazoleacetic acid can replace cAMP for expression of the arabinose operon (*15, 16*). It is interesting as well as significant to conclude from Figures 3–5 that the catabolic repression caused by resorcinol in both systems appears to be distinct from cAMP-mediated effects as observed in the case of the *m*-NBS–catechol system. Further, there is little or no lag between utilization of resorcinol and *m*-NBS or *m*-AP, suggesting that cAMP is not required for the initiation of utilization of either of the second substrates when present with resorcinol. Thus, more than one genetic mechanism is involved in *m*-NBS degradation.

The substrate utilization pattern from the mixed feeds in the continuous-flow activated sludge unit by appropriate acclimated sludge in this investigation was found to vary with the characteristics of the influents as well as with the dilution rate. For example, when the influent contained *m*-NBS and catechol, resorcinol and *m*-AP, or resorcinol and catechol, the substrates were simultaneously utilized at the dilution rate of 0.042/h (Figures 6–8). On the other

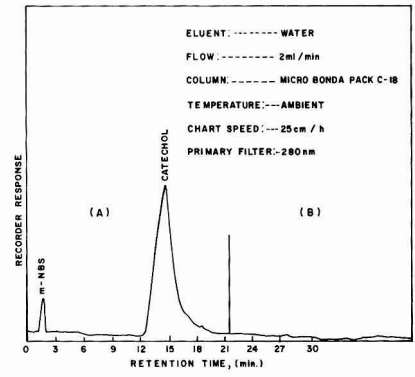

Figure 6. HPLC scan for separation of *m*-NBS and catechol. Influent (A) and effluent (B) from a continuous-flow activated sludge unit.

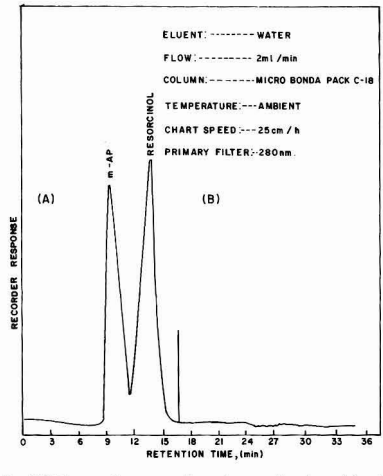

Figure 7. HPLC scan for separation of *m*-aminophenol (*m*-AP) and resorcinol. Influent (A) and effluent (B) from a continuous-flow activated sludge unit.

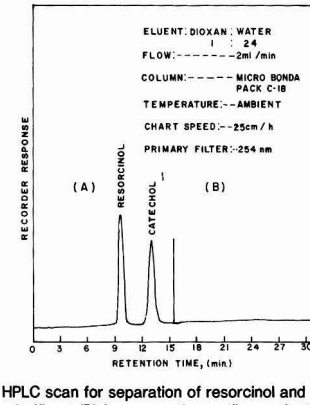

Figure 8. HPLC scan for separation of resorcinol and catechol. Influent (A) and effluent (B) from a continuous-flow activated sludge unit.

hand, when a mixed feed containing *m*-NBS and resorcinol was fed on a continuous basis to an activated sludge acclimated to the mixed feed at the same dilution rate of 0.042/h, resorcinol was found to be utilized completely whereas *m*-NBS was found to be utilized to the extent of

Table III. Effect of Increasing Resorcinol Concentration in a Mixed Feed[a] on the Utilization of Resorcinol and *m*-NBS by an Acclimated Activated Sludge in a Continuous Unit[b]

sr. no.	pH		*m*-NBS			resorcinol		
	influent	effluent	influent, mg/L	effluent, mg/L	reduction, %	influent, mg/L	effluent, mg/L	reduction, %
1	6.3–6.5	4.0–4.6	1051 ± 24.5	638 ± 22.2	39.3	208 ± 4.2	0.0	100
2	6.9–7.2	6.2–6.4	992 ± 66.4	741 ± 19.1	25.2	449 ± 7	0.0	100
3	6.3–6.5	5.2–5.5	1007 ± 42.6	797 ± 49.9	20.8	686 ± 42.2	0.0	100

[a] Resorcinol (ranging from 210 to 690 mg/L), *m*-NBS (1000 mg/L), and MLVSS at 2370–3000 mg/L. [b] Results are the average of six experiments ± standard deviation. pH values are expressed as a range indicating minimum and maximum.

Table IV. Effect of Different Dilution Rates on Resorcinol and *m*-AP Utilization from a Mixed Feed by an Acclimated Activated Sludge in a Continuous Unit[a]

sr. no.	dilution rate, h	influent		effluent		
		m-AP, mg/L	resorcinol, mg/L	*m*-AP, mg/L	resorcinol, mg/L	suspended solids, mg/L
1	0.042			ND	ND	22
2	0.055			ND	ND	55
3	0.081	246 ± 19	510 ± 18	ND	ND	96
4	0.162			ND	ND	130
5	0.322			224 ± 21	ND	260

[a] MLVSS at 2500–3820 mg/L. Results are the average of six experiments ± standard deviation. ND, not detected.

Table V. Utilization of Resorcinol and *m*-AP from Single Feeds and Mixed Feed by Mixed-Feed Acclimated Activated Sludge

time, h	*m*-AP feed		resorcinol feed		mixed feed		
	pH	*m*-AP, mg/L	pH	resorcinol, mg/L	pH	*m*-AP, mg/L	resorcinol, mg/L
0	7.7	250	7.7	475	7.5	255	490
0.5	7.9	150	7.9	290	7.6	255	300
3	8.0	90	8.0	ND[a]	7.8	130	ND
5	8.3	40	8.0	ND	8.6	70	ND
24	8.6	ND	8.0	ND	8.2	ND	ND
MLVSS[b]		2596		2080		2200	

[a] ND, not detected. [b] mg/L.

25% only (Figure 9). Table III shows the effect of increasing resorcinol concentration in a mixed feed containing resorcinol and *m*-NBS on the utilization of resorcinol and *m*-NBS by acclimated sludge when the system was operated on a continuous-flow basis at a dilution rate of 0.042/h. Resorcinol was found to be utilized under all experimental conditions. *m*-NBS utilization was only partial; the extent of *m*-NBS utilization decreased from 39 to 21% as the resorcinol concentration was progressively increased from 210 to 690 mg/L (Table III).

Table IV shows the effect of varying dilution rates on the substrate utilization pattern from a mixed feed containing resorcinol and *m*-AP. These substrates were utilized simultaneously when the dilution rates were maintained at 0.042, 0.055, 0.081, and 0.162 per hour. At a dilution rate of 0.323/h, however, resorcinol was found to be preferentially utilized. Our observations agree well with the observations made by Mateles et al. (*6*), who observed simultaneous utilization of glucose and fructose from a mixed-substrate feed by *P. fluorescens* and *E. coli* b_6 at low dilution rate and sudden change to preferential utilization of glucose at a higher dilution rate. It appears that at low dilution rates both resorcinol and *m*-AP can support the growth of microorganisms utilizing these substrates. At a high dilution rate, however, the microbial consortium utilizes resorcinol, only causing *m*-AP to appear in the effluent. However, when the acclimated sludge from the continuous unit is separately exposed to resorcinol, *m*-AP, and the mixed feed (Table V), the oxidation of resorcinol and *m*-AP, when fed as the sole source of carbon, commences without any lag period, although from mixed feed *m*-AP utilization commences only when resorcinol is completely utilized.

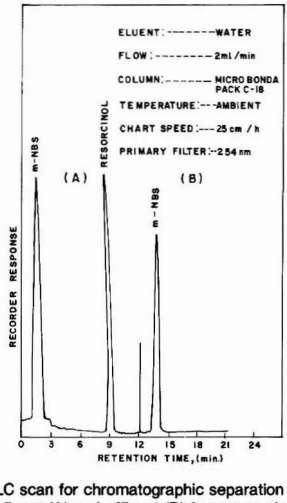

Figure 9. HPLC scan for chromatographic separation of *m*-NBS and resorcinol. Influent (A) and effluent (B) from a continuous-flow activated sludge unit.

It could be seen from the above experiments that the oxidizing properties of activated sludge acclimated to

mixed feed is different from batch and continuous systems. cAMP-dependent diauxic removal of substrates in batch reactors was observed only in the case of the catechol and *m*-NBS mixed feed. In continuous-flow reactors, a simultaneous substrate utilization pattern may become a preferential utilization one at a high dilution rate as was observed in case of resorcinol and *m*-AP systems.

Conclusions

(1) Activated sludge treating domestic waste is versatile in degrading a number of substituted benzenes of industrial origin.

(2) *m*-NBS-acclimated activated sludge had a different substrate utilization capacity when compared to resorcinol-acclimated activated sludge.

(3) Substrate utilization in four mixed feeds, namely, *m*-NBS and catechol, *m*-NBS and resorcinol, resorcinol and *m*-AP, and catechol and resorcinol, was studied in batch and continuous reactors. In batch reactors, sequential utilization of catechol followed by *m*-NBS was observed. Resorcinol was found to be preferentially utilized over *m*-NBS and *m*-AP from the respective mixed feeds in batch reactors. Similarly, preferential utilization of catechol followed by resorcinol was observed in batch reactors. Utilization of *m*-NBS from the *m*-NBS–catechol system was found to be aided by cAMP addition. Utilization of substrates from other mixed feeds was unaffected by cAMP addition.

Acknowledgments

We thank the Director, NEERI, for facilities and constant encouragement and Hindustan Organic Chemicals Limited, Rasayani, for providing the chemicals required for the investigation.

Registry No. *m*-NBS, 127-68-4; *m*-AP, 591-27-5; BSA, 98-11-3; *m*-AA, 121-47-1; cAMP, 60-92-4; catechol, 120-80-9; resorcinol, 108-46-3; pyrogallol, 87-66-1; phloroglucinol, 108-73-6; hydroquinone, 123-31-9.

Literature Cited

(1) Monod, J. *Recherche suila croisceance des Cultures Bacteriennos*; Hermann: Paris, 1942.
(2) Chian, E. S. K.; Dewalle, F. B. *Prog. Water Technol.* **1975**, *7*, 235.
(3) Halter, H. D.; Finn, R. K. *Appl. Environ. Microbiol.* **1978**, *35*, 890.
(4) Deshpande, S. D.; Chakrabarti, T. *Proceedings of the National Symposium on Biotechnology*; Jain, S. C., Ed.; Punjab University: Chandigarh, India, 1982; pp 83–99.
(5) Deshpande, S. D.; Chakrabarti, T.; Subrahmanyam, P. V. R.; Sundaresan, B. B. *Water Res.* **1985**, *19*, 293.
(6) Mateles, R. I.; Chian, E. S. K.; Silver, R. in *Microbial Physiology and Continuous Cultures*; Powell, E. D., Evans, C. G. T., Strange, R. E., Tempest, D. W., Eds.; Academic: New York, 1967; p 232.
(7) Jacob, F.; Monod, J. *J. Mol. Biol.* **1961**, *3*, 318.
(8) Bhattacharya, A.; Datta, A. *Biochem. Biophys. Res. Commun.* **1977**, *77*, 1438–1444.
(9) Mahler, H. R.; Lin, C. C. *Biochem. Biophys. Res. Commun.* **1978**, *83*, 1039–1047.
(10) Martin, L. P. *Microbiol. Rev.* **1981**, *45*, 462.
(11) *Standard Methods for the Examination of Water and Wastewater*, 14th ed.; APHA, AWWA, WPCF: New York, 1976.
(12) Ludjack, F. J. *J.—Water Pollut. Control Fed.* **1960**, *32*, 605–609.
(13) Pitter, P. *Water Res.* **1976**, *10*, 231.
(14) Wanner, B. L.; Kodaira, R.; Naidhardt, F. C. *J. Bacteriol.* **1978**, *136*, 947–954.
(15) Kline, E. L.; Bankaitis, V. A.; Brown, C. S.; Montefiori, D. C. *J. Bacteriol.* **1980**, *141*, 770–778.
(16) Kline, E. L.; Brown, C. S.; Bankaitis, V. A.; Montefiori, D. C.; Craig, K. *Proc. Natl. Acad. Sci. U.S.A.* **1980**, *77*, 1768–1772.

Received for review August 22, 1986. Revised manuscript received March 9, 1987. Accepted June 26, 1987.

Environ. Sci. Technol. 1987, 21, 1009–1013

Prediction of Algal Bioaccumulation and Uptake Rate of Nine Organic Compounds by Ten Physicochemical Properties†

Hélène Mailhot

Biology Department, McGill University, Montréal, Québec, Canada H3A 1B1

■ Many quantitative structure–activity relationships describe steady-state levels of accumulation of organic contaminants in aquatic organisms, but few treat the dynamics by which these levels are achieved. This paper extends this approach by developing relations to describe the time course of uptake for different organic compounds. The instantaneous rates of uptake and the bioconcentration factors (BCF) of nine organic compounds were determined by following the bioaccumulation of radioactively labeled compounds in the green alga *Selenastrum capricornutum*. When all nine compounds are used in regression, capacity ratio and the octanol/water partition coefficient predict BCF equally well. However, if the hydrocarbons alone are considered, the capacity ratio predicts BCF most effectively. The uptake rate, which could only be measured effectively for five compounds, is best predicted by the connectivity index. These two regressions were effective in reconstructing the original experiment; they may also be effective at predicting the time course of contaminant bioaccumulation.

Introduction

Because new chemicals are produced at a rate exceeding our capacity to test their environmental impact, we need models to predict their biological activity (*1*). This need has led to the development of quantitative structure–activity relationships (QSARs), which relate one or more physicochemical properties of a group of compounds to their biological activity. In ecotoxicology, QSAR studies have been applied to predict toxicity, absorption, distribution, transformation, excretion, and persistence of organic compounds in contaminated aquatic ecosystems, and QSARs are among the most promising tools for the assessment of environmental hazard (*2–5*).

Most applications of QSAR have predicted the bioconcentration factor at equilibrium (*6–11*) and the acute toxicity (*12–14*). Although these are essentially static properties, bioconcentration factor is often calculated as the ratio of the uptake rate and the clearance rate (*6, 15–17*). Therefore, there is good reason to believe that rates of contaminant flux may also be predictable from physicochemical properties. Recent studies have demonstrated this by developing QSARs to treat the time course of uptake of organic compounds by fish (*18*) and invertebrates (*19*) but not by algae.

Both initial rate of uptake and final concentration are of great importance because these two parameters are sufficient to predict the time course of biological uptake. This paper examines biological uptake of nine organic contaminants by the green alga *Selenastrum capricornutum* to develop relationships that describe these parameters as functions of quantitative indices of chemical structure. An alga was chosen because phytoplankton are important entry points through which entire food webs may be contaminated. This alga was selected because it is an easily grown, widely available, laboratory species. The compounds studied—atrazine, benzoic acid, anthracene, chloroform, 1,1-bis(4-chlorophenyl)-2,2,2-trichloroethane (DDT), benzene hexachloride, hexachlorobenzene, 2,4,5,2′,4′,5′-hexachlorobiphenyl, and 1,2,4,5-tetrachlorobenzene—were selected because they could be purchased in a ^{14}C-labeled form and because they differ greatly in many physicochemical properties that could be used as independent variables in quantitative relationships to predict bioconcentration and rate of uptake. Such relations should allow us to predict the immediate biological fate of organic contaminants in aquatic systems (*20*) and may form an important subcomponent in larger models that describe the transfers and effects of such contamination over the longer term.

Materials and Methods

Physicochemical Properties. The sources, the specific activities, and the physicochemical properties of the nine organic compounds used are listed in Table I. These organic compounds represent three chemical families including one triazine (atrazine), one acid (benzoic acid), and seven hydrocarbons: one polycyclic aromatic (anthracene), one cyclic halogenated (benzene hexachloride), one aliphatic halogenated (chloroform), and four aromatic halogenated (DDT, hexachlorobiphenyl, hexachlorobenzene, and tetrachlorobenzene).

Values for solubility, 1-octanol/water partition coefficient, molecular weight, boiling point, melting point, and density were found in the literature. The molar volume is the volume occupied by 1 mol, and it is numerically equal to the molecular weight divided by the density. The connectivity index was calculated following Kier et al. (*21*), who derived this index from the numerical extent of branching in the molecular skeleton. The parachor is a molecular size parameter that can be thought of as a molar volume corrected for surface tension. The parachor is an additive-constitutive property (*22*), because it can be approximated by summing the atomic parachors of individual atoms constituting the molecule; thus, the atomic and structural constants of Vogel (*23*) were used to calculate the parachor value for the nine organic chemicals used in this study.

The capacity ratio for a chromatographic column is computed as $(T_r - T_m)/T_m$, where T_r and T_m are the retention times of the sample solute and the mobile phase (KNO_3), respectively. Many investigators (*24–27*) have correlated partition coefficients to the retention times of chemicals in a reversed-phase HPLC column system. Therefore capacity ratio could be used instead of log P_{ow} in structure–activity relationships. Capacity ratios were determined experimentally with a reverse-phase high-pressure liquid chromatograph, equipped with a Varian UV detector. The separations were performed on a 25 cm long ALL TECH RP-18 column in which particles 5 μm in diameter provided solid support. The column was conditioned at 60 °C, and the effluent flow rate (2 mL/min) was monitored continuously. The compounds were

†A contribution to the Limnology Research Center, McGill University. The LRC is funded by NSERC, FCAR, and the Donner Canada Foundation.

0013-936X/87/0921-1009$01.50/0

Table I. Specific Activity, Chemical Supplier, and Value of the Ten Physicochemical Properties for the Organic Compounds Used in This Study

compound	sp act., Ci/mol	log P	log k'	log S, M	connectivity index	parachor	molar volume, cm^3	molecular weight	melting point, °C	density, g/cm^3	boiling point, °C
benzoic acid[a]	29.4	1.87	−0.24	−1.65	3.01	175	92.4	122	122	1.32	249
anthracene[b]	15.1	4.49	1.01	−6.45	4.81	410	143	178	216	1.25	340
atrazine[b]	25.0	2.69	0.16	−3.84	5.71	456		216	174		
DDT[b]	40.0	5.70	1.58	−7.68	7.01	663	228	353	109	1.55	
benzene hexachloride[b]	62.0	4.06	0.62	−4.70	5.46	479	156	291	112	1.87	323
chloroform[c]	13.9	1.94	−0.10	−1.15	1.73	190	80	119	−64	1.49	62
hexachlorobenzene[c]	13.5	5.64	1.66	−7.36	4.50	443	182	285	229	1.57	324
hexachlorobiphenyl[c]	12.5	7.08	1.98	−7.98	6.56	618	232	361	103	1.56	
tetrachlorobenzene[c]	7.2	4.60	1.06	−5.08	3.65	364	116	216	139	1.86	245

[a] New England Nuclear, Lachine, Québec. [b] Amersham Canada Limited, Oakville, Ontario. [c] Pathfinder Laboratories Inc., St. Louis, MO.

eluted in a mixture of methanol–water (65:35) containing 0.01% H_3PO_4. Compounds not readily soluble in the eluent were initially dissolved in pure methanol. Retention time is unaffected by this addition (*26*). All estimates of capacity factor were made at least in triplicate. The coefficient of variation of the solute retention time (T_m) measurements varies between 0.25% and 7% depending on the compound (mean = 1.75%).

Algal Culture and Uptake Experiment. Stock cultures of the test organism *Selenastrum capricornutum* were maintained in the synthetic medium recommended in the *S. capricornutum* Printz algal assay: bottle test (*28*). Flasks were maintained at a constant temperature (24 ± 1 °C), shaken at 100 rpm, and constantly illuminated from above at 4.3 klx by cool white fluorescent light (approximately 1.4 W m^{-2}, *29*). Stock cultures were transferred to fresh medium every 7–10 days. Bacterial and fungal contamination was monitored by plating 1-mL aliquots of stock on nutrient agar and incubating the plates along with the cultures. Contaminated cultures were discarded. The algal cells were used when in exponential growth, since such cultures are less variable (*30*). Cell densities were determined from haemocytometer counts made at the start of each experiment.

For uptake experiments, the cultures were diluted with sterile stock solution to yield 300 mL at approximately 10^5 cells/mL, in 500-mL Erlenmeyer flasks. The radioactive xenobiotic in a solution of ethanol or 0.1% aqueous dimethyl sulfoxide (DMSO) was added to these flasks, and two 1-mL aliquots were withdrawn at intervals. One aliquot was placed in a scintillation minivial for determination of total activity. The other was placed in a microcentrifuge tube and centrifuged at 13000 rpm (11600*g*) for 6 min. A 0.5-mL sample of supernatant was then placed in a scintillation minivial, and the algal pellet and the remaining supernatant were vortexed. The resulting algal suspension was also placed in a scintillation minivial. A similar procedure was followed with a control flask containing isotope but no algae. Pellet radioactivity was corrected for the activity of the supernatant to determine the amount of activity associated with the cells. Each uptake experiment involved 3, 4, or 6 replicates, depending on the amount of chemical available, and each run included 6 analyses of the control, 6 determinations of total activity, and 12 analyses of the radioactivity in algal cells. This method is a modified version of the procedure of Harding and Phillips (*31*), who found that this procedure precludes possible reequilibration during washing of the pellet and is highly reproducible. It also avoids problems with adsorption of the radiolabeled compounds by filters. Samples were placed in 4 mL of scintillation cocktail and counted in an LKB Wallac 1215 RackBeta II liquid scintillation counter.

Benzoic acid, chloroform, atrazine, and benzene hexachloride were the most hydrophilic compounds. Because these compounds were taken up very slowly by the algal cells, the uptake experiments were long, and the amount of radioactive uptake by the algae was near the detection level of the scintillation counter. As a result, the experimental procedure had to be modified. After the algal culture was spiked with a radiolabeled compound, it was returned to the incubator for 28 h (atrazine), 44 h (benzene hexachloride), or 6 days (benzoic acid and chloroform). Appropriate times were selected on the basis of a preliminary uptake experiment. Four replicates plus a control containing the radiotracer, but no algae, were treated. After this exposure, five 10-mL aliquots of each of the four replicates and the control were filtered through a 0.6-μm Nuclepore filter and rinsed with 50 mL of distilled water. The activity in the algae was determined as the average proportion of total activity on the filters from the four replicates less the proportion of total activity on the control filter.

A nonlinear, iterative, statistical method (*32*) was used to fit the data to the empirical model

$$y = ax/(b + x) \tag{1}$$

where y is uptake of radiolabeled compound by the cells expressed as a percentage of total activity and x is time in minutes. This model (a square hyperbola) is easy to fit, has a high coefficient of determination ($r^2 > 0.9$), and is equivalent to the familiar Michaelis–Menten equation. The first derivative of eq 1 at $x = 0$ is the instantaneous rate of uptake and corresponds to a/b. The asymptotic value obtained from the model [a (%)] was transformed to the bioconcentration factor (BCF), the ratio of the activity in 1 mL of algal cells to the activity in 1 mL of water, as

$$\text{BCF} = a/[(100 - a)(\text{cell volume})(\text{cell concentration})] \tag{2}$$

The BCFs and the uptake rates were regressed against each of the physicochemical properties with the method of least squares after the variables were transformed to stabilize the variance and to linearize the data. Taylor's power law (*33*, *34*) was used in some cases to choose the best power transformation of the dependent variable, which stabilizes the variance. In each case, several relationships were developed, and that with the highest r^2, which also appeared to be linear and to have stable variance on visual inspection, was selected as the best regression. An F test ($p = 0.05$) identified regressions that did not differ significantly from the model with the highest r^2. Spiegel's (*35*) test for the significance ($p = 0.05$) of differences in correlation coefficients was used for relationships that had different dependent variables.

Table II. Means and Standard Deviations (SD) of Measured Bioconcentration Factors and Instantaneous Rates of Uptake

compound	BCF mean	BCF SD	uptake rate, %/min mean	uptake rate, %/min SD
benzoic acid	7.6	0.65		
atrazine	20	3.0		
chloroform	690	160		
benzene hexachloride	1500	190		
tetrachlorobenzene	7700	4400	0.03	0.01
anthracene	7800	2700	0.11	0.03
DDT	12000	6000	0.44	0.08
hexachlorobenzene	26000	4700	0.09	0.02
hexachlorobiphenyl	37000	15000	0.29	0.08

Results and Discussion

Mean estimates of uptake rates and bioconcentration factors for the chemicals studied are presented in Table II. Overall, individual values for BCF range from 6.9 to 56 000, and the average coefficient of variation within compounds was 28% (range 8% to 56%). Individual estimates of uptake rate range from 0.02 to 0.48 (%/min). The coefficient of variation over all compounds averaged 27% and ranged from 18% to 41% within compounds.

Bioconcentration Factors. The relationships for BCF were based on only the five most lipophilic compounds, because the BCF of the other four compounds were estimated from only a single sampling, which was assumed to represent equilibrium. BCF was best predicted by capacity factor (k') and 1-octanol/water partition coefficient (P_{ow}). These two relationships are significantly better than all others, and there is no significant difference between them.

$$\log \mathrm{BCF} = 3.1 + 0.74 \log k' \quad (3)$$

$$\log \mathrm{BCF} = 2.6 + 0.28 \log P_{ow} \quad (4)$$

These equations explain 68% and 64% of the variance of log BCF, respectively. When BCF estimates for the four hydrophobic compounds are included in the regression, the data are linearized best by a power transformation of BCF. For all nine compounds, capacity factor and partition coefficient predict BCF with success. These relationships are significantly better than any others and do not differ significantly (Figure 1).

$$\mathrm{BCF}^{0.4} = 6.9 + 28 \log k' \quad (5)$$

$$\mathrm{BCF}^{0.4} = -21 + 12 \log P_{ow} \quad (6)$$

These models are more general because they include compounds from three different families. They suggest that BCF values for both compounds that accumulate rapidly and compounds that accumulate slowly can be described with the same relation. However, when the data are plotted (Figure 2), the two non-hydrocarbons, benzoic acid and atrazine, fall well below the regression line. This can be explained in two ways. Either these two compounds did not reach equilibrium, so the values of BCF are underestimated, or as some investigators suggest (*35–37*), structure–activity relationships are family specific. If so, an equation should be calculated for the hydrocarbons alone. Again capacity factor, partition coefficient, and solubility are the best descriptors of the bioconcentration factor of hydrocarbons, but capacity ratio is significantly better than the others:

$$\log \mathrm{BCF} = 2.9 + 0.86 \log k' \quad (7)$$

The relationship between BCF and partition coefficient was used to compare this study with the work of other

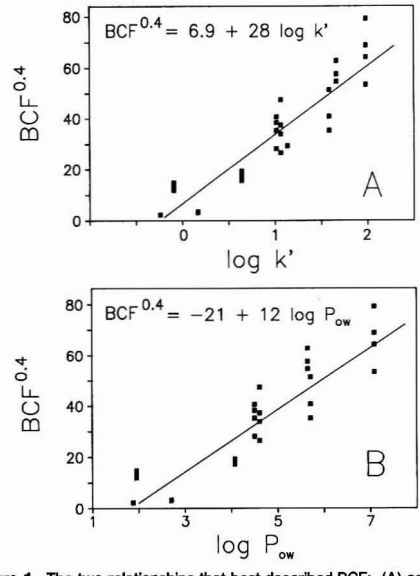

Figure 1. The two relationships that best described BCF: (A) capacity ratio (n = 36, r^2 = 0.88, MSE = 60.9); (B) 1-octanol/water partition coefficient (n = 36, r^2 = 0.85, MSE = 74.4).

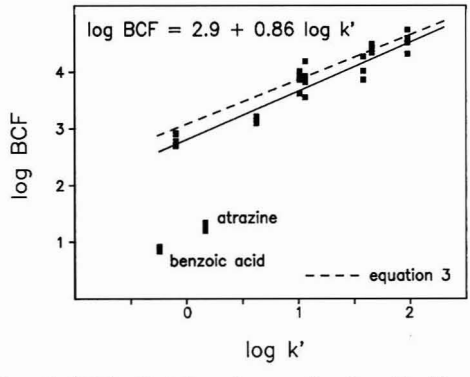

Figure 2. Relationship between log capacity ratio and log bioconcentration factor for the hydrocarbons (n = 28, r^2 = 0.89, MSE = 0.04). The dashed line corresponds to the regression for the five lipophilic compounds (eq 3).

investigators. The literature relationships are quite heterogeneous. One study uses microorganisms (curve A in Figure 3), one uses *S. capricornutum* (curve B), and 11 involve fish in either flowing or static systems (curves C–M). Some are based on original experimental values and others on values from different authors. Finally, most of these relations are based on several families of organic compounds. The relationship for hydrocarbons developed in this study has a much lower slope than any of the others, except that for algae. This suggests that, compared to fish, algal BCFs may be higher for hydrophilic compounds but lower for lipophilic compounds. When all nine compounds are included in the regression, the slope of the regression increases (dashed line in Figure 3). Both relations and the data lie within the range described by previously published relationships, so it appears that BCFs measured in this study are consistent with expectation.

Instantaneous Rate of Uptake. The best relationships between the rate of uptake and various physicochemical

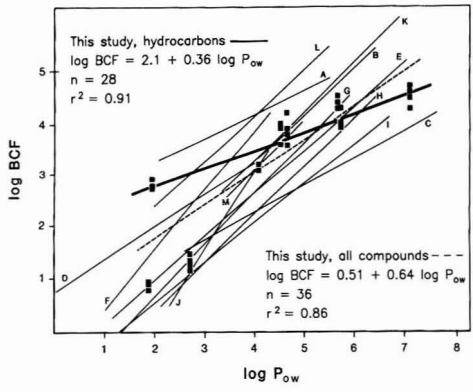

Figure 3. Comparison of literature relationships describing bioconcentration factor (BCF) as a function of partition coefficient (P_{ow}) with those determined in this study (line A corresponds to ref 39; B, ref 40; C, ref 6; D, ref 41; E, ref 16; F, ref 11; G, ref 42; H, ref 2; I, ref 2; J, ref 43; K, ref 45; L, ref 44; M, ref 10).

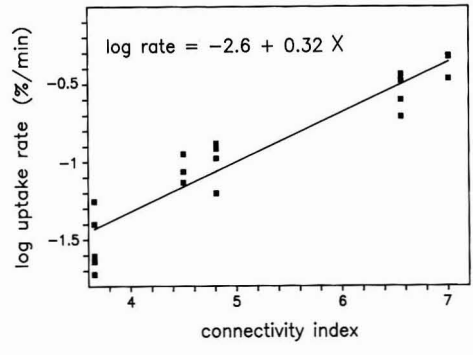

Figure 4. Relationship between the common logarithm of instantaneous uptake rate and connectivity index (n = 20, r^2 = 0.90, MSE = 0.002).

Table III. Relationships between Logarithm of Instantaneous Rates of Uptake and Various Physicochemical Properties

property	slope	intercept	n	r^2	MSE
connectivity index	0.32	−2.6	20	0.90	0.002
parachor	0.003	−2.6	20	0.84	0.035
molar volume	0.008	−2.4	20	0.82	0.038
solubility	0.026	−2.2	20	0.79	0.045
log solubility	−0.34	−3.2	20	0.79	0.045
log partition coefficient	0.31	−2.7	20	0.49	0.11

properties are listed in Table III. Because only 20 data points representing only 5 organic compounds were used to calculate these regressions, the relations can only provide a direction for further work. The highest r^2 was achieved in regression (Figure 4) with connectivity index (X):

$$\log \text{rate} = -2.6 + 0.32X \quad (8)$$

The time course of uptake of organic compounds by the green alga *S. capricornutum* can be estimated for values of BCF and uptake rate. These are predicted by eq 5 and 8 and then used to calculate a and b of eq 1:

$$a_{\text{calcd}} = \text{BCF}_{\text{pred}}(\text{cell biomass})/[1 + \text{BCF}_{\text{pred}}(\text{cell biomass})] \quad (9)$$

$$b_{\text{calcd}} = a_{\text{calcd}}/\text{rate}_{\text{pred}} \quad (10)$$

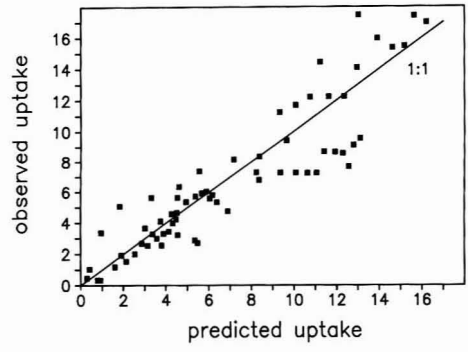

Figure 5. Regression between observed (Y) and predicted uptake (X) of organic compounds by *S. capricornutum*. $Y = 0.12 + 0.94X$ (S_a = 0.44, S_b = 0.06, r^2 = 0.83, and n = 66, where a refers to the intercept and b the regression coefficient).

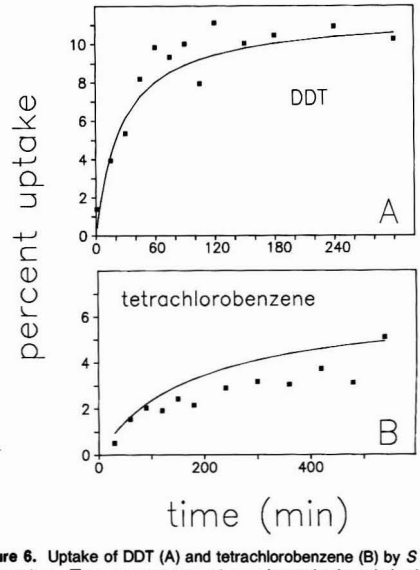

Figure 6. Uptake of DDT (A) and tetrachlorobenzene (B) by *S. capricornutum*. The squares represent experimental values derived from single experiments; the line is the time course predicted with eq 5 and 8. The DDT experiment had one of the best fits of observation to prediction; the tetrachlorobenzene experiment had one of the worst.

where cell biomass is the product of cell volume and cell concentration. Although this calculation used eq 5 (because it is the most general), any of the equations describing BCF would be as effective. These calculated values are then substituted into eq 1 to estimate the percent uptake over time:

$$\text{predicted percent uptake} = a_{\text{calcd}}(\text{time})/[b_{\text{calcd}} + \text{time}] \quad (11)$$

Predicted uptakes were calculated for every sample time in every experiment in order to compare them with the observed data. A regression between the predicted values and the means of the observed uptake values for all replicates of the five compounds shows that this approach is generally successful (Figure 5). The intercept is not different from zero, and the slope is slightly, but not significantly, less than unity. Figure 6 shows that this also holds for representative examples, DDT and tetrachlorobenzene. Although some lack of fit is apparent, the pattern

is reasonably well represented in both panels. These comparisons show that the process of abstracting experimental results through two regression analyses has not led to a fatal loss of information. In other words, the final abstracted equations still describe the original data fairly well. Future studies will have to examine the predictive power of this approach.

Registry No. DDT, 50-29-3; benzoic acid, 65-85-0; anthracene, 120-12-7; atrazine, 1912-24-9; benzene hexachloride, 58-89-9; chloroform, 67-66-3; hexachlorobenzene, 118-74-1; hexachlorobiphenyl, 26601-64-9; tetrachlorobenzene, 12408-10-5.

Literature Cited

(1) Garten, C. T.; Trabalka, J. R. *Environ. Sci. Technol.* **1983**, *17*, 590–595.
(2) Kenaga, E. E.; Goring, C. A. I. In *Aquatic Toxicology*; Eaton, J. G., Parrish, P. R., Eds.; American Society for Testing and Materials: Philadelphia, 1978; ASTM STP 707, pp 78–115.
(3) Verschueren, K. *Handbook of Environmental Data on Organic Chemicals*, 2nd ed.; Van Nostrand-Reinhold: New York, 1983.
(4) Kaiser, K. L. E. *Environ. Int.* **1984**, *10*, 241–250.
(5) Dearden, J. C. *EHP, Environ. Health Perspect.* **1985**, *61*, 203–228.
(6) Neely, W. B.; Branson, D. R.; Blau, G. E. *Environ. Sci. Technol.* **1974**, *8*, 1113–1115.
(7) Chiou, C. T.; Freed, V. H.; Schmedding, D. W.; Kohnert, R. L. *Environ. Sci. Technol.* **1977**, *11*, 475–478.
(8) Tulp, M. Th. M.; Hutzinger, O. *Chemosphere* **1978**, *10*, 849–860.
(9) Veith, G. D.; Austin, N. M.; Morris, R. T. *Water Res.* **1979**, *13*, 43–47.
(10) Oliver, B. G.; Niimi, A. J. *Environ. Sci. Technol.* **1983**, *17*, 287–291.
(11) Metcalf, R. L.; Sanborn, J. R.; Lu, P. Y.; Nye, D. *Arch. Environ. Contam. Toxicol.* **1975**, *3*, 151–165.
(12) Veith, G. D.; Call, D. J.; Brooke, L. T. *Can. J. Fish. Aquat. Sci.* **1983**, *40*, 743–748.
(13) Hodson, P. V.; Dixon, D. G.; Kaiser, K. L. E. In *Workshop on Quantitative Structure Activity Relationships (QSAR) in Environmental Toxicology*; Kaiser, K. L. E., Ed.; McMaster University: Hamilton, Ontario, 1984, pp 179–188.
(14) Zitko, V. In *Structure-Activity Correlations in Studies of Toxicity and Bioconcentration with Aquatic Organisms, Proceedings of a Symposium*, Burlington, Ontario, 1975; Veith, G. D., Konasewich, D. E., Eds.; Great Lakes Regional Office, International Joint Commission: Windsor, Ontario, 1975; pp 7–24.
(15) Branson, D. R.; Neely, W. B.; Blau, G. E. In *Structure-Activity Correlations in Studies of Toxicity and Bioconcentration with Aquatic Organisms, Proceedings of a Symposium*, Burlington, Ontario, 1975; Veith, G. D., Konasewich, D. E., Eds.; Great Lakes Regional Office, International Joint Commission: Windsor, Ontario, 1975; pp 98–118.
(16) Veith, G. D.; DeFoe, D. L.; Bergstedt, B. V. *J. Fish. Res. Board Can.* **1979**, *36*, 1040–1048.
(17) Blanchard, F. A.; Takahashi, I. T.; Alexander, H. C.; Bartlett, E. A. In *Aquatic Toxicology and Hazard Evaluation*; Mayer, F. L., Hamelink, J. L., Eds.; American Society for Testing and Materials: Philadelphia, 1977; ASTM STP 634, pp 162–177.
(18) Spacie, A.; Hamelink, J. L. *Environ. Toxicol. Chem.* **1982**, *1*, 309–320.
(19) Lohner, T. W.; Collins, W. J. *Environ. Toxicol. Chem.* **1987**, *6*, 137–146.
(20) Vězina, A. *J. Plankton Res.* **1986**, *8*, 939–956.
(21) Kier, L. B.; Hall, L. H.; Murray, W. J.; Randic, M. *J. Pharm. Sci.* **1975**, *64*, 1971–1974.
(22) Quayle, O. R. *Chem. Rev.* **1953**, *53*, 439–589.
(23) Vogel, A. I.; Cresswell, W. T.; Jeffery, G. J.; Leicester, J. *Chem. Ind. (London)* **1950**, *1950*, 358.
(24) Hammers, W. E.; Meurs, G. L.; deLigny, C. L. *J. Chromatogr.* **1982**, *247*, 1–13.
(25) Konemann, H.; Zelle, R.; Busser, F.; Hammers, W. E. *J. Chromatogr.* **1979**, *178*, 559–565.
(26) Mirrlees, M. S.; Moulton, S. J.; Murphy, C. T.; Taylor, P. J. *J. Med. Chem.* **1976**, *19*, 615–619.
(27) McCall, J. M. *J. Med. Chem.* **1975**, *18*, 549–552.
(28) Miller, W. E.; Greene, J. C.; Shiroyama, T. *The Selenastrum capricornutum Printz algal assay bottle test: experimental design, application and data interpretation protocol*; U.S. EPA: Corvallis, OR, 1978.
(29) Gaastra, P. *Meded. Landbouwhogesch. Wageningen* **1959**, *59*, 1–68.
(30) Sodergren, A. *Oikos* **1968**, *19*, 126–138.
(31) Harding, L. W., Jr.; Phillips, J. H., Jr. *Mar. Biol. (Berlin)* **1978**, *49*, 103–111.
(32) Mailhot, H. M.Sc. Thesis, McGill University, Montréal, Québec, 1986.
(33) Taylor, L. R. *Nature (London)* **1961**, *189*, 732–735.
(34) Downing, J. A. *J. Fish. Res. Board Can.* **1979**, *36*, 1454–1463.
(35) Spiegel, M. R. *Schaum's Outline of Theory and Problems of Probability and Statistics*; McGraw-Hill: New York, 1975.
(36) Miller, M. M.; Waslk, S. P.; Huang, G. L.; Shiu, W. Y.; Mackay, D. *Environ. Sci. Technol.* **1985**, *19*, 522–529.
(37) Oliver, B. G. In *Workshop on Quantitative Structure Activity Relationships (QSAR) in Environmental Toxicology*; Kaiser, K. L. E., Ed.; McMaster University: Hamilton, Ontario, 1984; pp 301–317.
(38) Leo, A.; Hansch, C.; Church, C. *J. Med. Chem.* **1969**, *12*, 766–771.
(39) Casserley, D. M.; Davies, E. M.; Downs, T. D.; Guthrie, R. K. *Water Res.* **1983**, *17*, 1591–1594.
(40) Baughman, G. L.; Paris, D. F. *CRC Crit. Rev. Microbiol.* **1981**, *8*, 205–228.
(41) Lu, P. Y.; Metcalf, R. L. *EHP, Environ. Health Perspect.* **1975**, *10*, 269–284.
(42) Mackay, D. *Environ. Sci. Technol.* **1982**, *16*, 274–278.
(43) Kanazawa, J. *Rev. Plant Prot. Res.* **1980**, *13*, 27–36.
(44) Chiou, C. T. *Environ. Sci. Technol.* **1985**, *19*, 57–62.
(45) Oliver, B. G.; Niimi, A. J. *Environ. Sci. Technol.* **1985**, *19*, 842–849.

Received for review November 11, 1986. Accepted July 6, 1987.

Environ. Sci. Technol. 1987, 21, 1014–1022

Kinetics and Products of the Gas-Phase Reactions of OH Radicals and N_2O_5 with Naphthalene and Biphenyl

Roger Atkinson,* Janet Arey, Barbara Zielinska, and Sara M. Aschmann

Statewide Air Pollution Research Center, University of California, Riverside, California 92521

■ Naphthalene and biphenyl are two polycyclic aromatic hydrocarbons (PAH) present in ambient air, and their atmospheric chemical removal processes are known to be via gas-phase reactions with the OH radical and with N_2O_5. The kinetics of the gas-phase reactions of N_2O_5 with naphthalene and biphenyl have been investigated, and the products of their reactions with the OH radical in the presence of NO_x and with N_2O_5 have been studied. The rate constant for the reaction of naphthalene with N_2O_5 at 298 ± 2 K was determined to be $(1.4 \pm 0.2) \times 10^{-17}$ cm^3 molecule^{-1} s^{-1}. The 1- and 2-nitronaphthalene products formed in the reactions of naphthalene with N_2O_5 and with the OH radical in the presence of NO_x were determined to have yields of 0.153 ± 0.022 and 0.0032 ± 0.0028 for 1-nitronaphthalene, respectively, and 0.069 ± 0.021 and 0.0027 ± 0.0034 for 2-nitronaphthalene, respectively. The OH radical initiated reaction of naphthalene also produced the 1- and 2-naphthols. Biphenyl was observed to react only with the OH radical, with 2-hydroxybiphenyl (yield 0.204 ± 0.078) and 3-nitrobiphenyl (yield 0.047 ± 0.034) being the major products identified and quantified. The nitroarene products and yields are consistent with ambient air measurements and suggest that many, if not most, of the nitroarenes observed in ambient air are formed from their parent PAH via atmospheric reactions.

Introduction

A wide variety of organic compounds are present in the troposphere, arising from direct emissions from both anthropogenic and biogenic sources as well as from in situ formation as a result of atmospheric transformations. In recent years, much attention has focused on the ambient atmospheric concentrations and the atmospheric chemistry of polycyclic aromatic hydrocarbons (PAH) and related compounds (for example, polychlorobiphenyls) and their derivatives. In particular, numerous measurements of the ambient atmospheric concentrations of PAH and nitroarenes have been reported at a variety of locations (see, for example, ref 1–4). Recent kinetic and product studies show that gas-phase reactions with OH radicals and with N_2O_5 can be atmospherically important loss processes for the PAH (*5–10*). Indeed, it is now apparent that 2-nitrofluoranthene and 2-nitropyrene, two of the most abundant nitroarenes observed in collected ambient particulate matter, can be formed from their parent PAH via gas-phase reactions involving N_2O_5 and/or OH radicals during atmospheric transport from source to receptor (*3*, *4*, *7*, *9–11*).

In a recent study (*4*) we have analyzed gaseous and particulate ambient air samples and have identified a number of aromatic hydrocarbons and their nitro derivatives that are distributed between the gas and particle phases and that are not collected with any significant efficiency by conventional filter sampling techniques. Among the compounds identified were naphthalene, methylnaphthalenes, dimethyl- and/or ethylnaphthalenes, and biphenyl and nitro derivatives including 1- and 2-nitronaphthalenes, 3-nitrobiphenyl, and methylnitronaphthalenes.

Naphthalene and biphenyl react in the gas phase with the OH radical at room temperature with rate constants of 2.17×10^{-11} and 7×10^{-12} cm^3 molecule^{-1} s^{-1}, respectively (*5*), and naphthalene has been shown to react in the gas phase with N_2O_5 with a room temperature rate constant of $\sim(2\text{–}3) \times 10^{-17}$ cm^3 molecule^{-1} s^{-1} (*6*). This reaction of N_2O_5 with naphthalene produces the 1- and 2-nitronaphthalene isomers with yields of ~18% and ~7.5%, respectively (*6*). However, data are not available concerning the products of the reactions of the OH radical with naphthalene or biphenyl, and only a qualitative observation exists that the reaction of biphenyl with N_2O_5 and/or the NO_3 radical is slow (*12*).

In this work, we have conducted a detailed investigation of the kinetics of the gas-phase reactions of N_2O_5 with naphthalene and biphenyl and have carried out product studies of the OH radical initiated reactions of naphthalenes and biphenyl in the presence of NO_x and of the reaction of N_2O_5 with naphthalene. These product studies specifically focused on the nitroarene products due to their possible toxicity (*13*) and their importance in elucidating the transformations of PAH in ambient atmospheres.

Experimental Section

Kinetics of Reactions of N_2O_5 with Naphthalene and Biphenyl. Rate constants for the gas-phase reactions of N_2O_5 with naphthalene and biphenyl were determined at 298 ± 2 K. For naphthalene, the rate constant was determined by monitoring the enhanced decay rate of N_2O_5 in the presence of known concentrations of naphthalene. In the absence of secondary reactions, the reactions removing N_2O_5 are

$$N_2O_5 \xrightarrow{\text{wall}} \text{loss of } N_2O_5 \qquad (1)$$

$$N_2O_5 + \text{naphthalene} \rightarrow \text{products} \qquad (2)$$

Under these conditions, and assuming exponential decays of N_2O_5, then

$$d \ln [N_2O_5]/dt = k_1 + k_2[\text{naphthalene}] \qquad (I)$$

where k_1 and k_2 are the rate constants for reactions 1 and 2, respectively. Hence a plot of the N_2O_5 decay rate against the naphthalene concentration should be a straight line with a slope of k_2.

Experiments were carried out in a 5800-L evacuable, Teflon-coated, environmental chamber equipped with an in situ multiple reflection optical system interfaced to a Fourier transform infrared (FT-IR) absorption spectrometer (*14*). Naphthalene was introduced into the chamber by flowing N_2 (>99.998% stated purity) at a measured flow rate through a Pyrex tube filled with crystalline naphthalene and was monitored by FT-IR absorption spectroscopy at 785 cm^{-1} with a spectral resolution of 1 cm^{-1} and a path length of 62.9 m. The infrared absorption coefficient was determined by addition of incremental amounts of naphthalene to the chamber, with the Pyrex tube containing the naphthalene being weighed before and after each addition of naphthalene.

0013-936X/87/0921-1014$01.50/0

Known pressures of N_2O_5 in calibrated Pyrex bulbs were introduced into the chamber by flushing the contents of the bulbs with a stream of N_2, with simultaneous rapid mixing by a fan rated at 300 L s^{-1}. N_2O_5 was monitored at 1246.3 cm^{-1}, and its concentrations were determined with the absorption coefficient of Graham and Johnston (*15*). N_2O_5 decay rates were obtained in the presence and absence of naphthalene, with synthetic air (80% N_2 + 20% O_2) being used as the diluent gas. The initial reactant concentrations in the experiments where naphthalene was present were naphthalene at (1.1–15) × 10^{13} molecules cm^{-3} and N_2O_5 at (1.4–6.1) × 10^{13} molecules cm^{-3}. NO_2, at concentrations of up to 2.4 × 10^{14} molecules cm^{-3}, was added to the majority of the experiments to minimize the concentrations of NO_3 radicals formed from the thermal decomposition of N_2O_5 and to scavenge any radical species formed in these reactions.

An upper limit to the rate constant for the reaction of N_2O_5 with biphenyl was obtained from a relative rate technique in which the relative decay rates of biphenyl and naphthalene were measured in the presence of N_2O_5. Experiments were carried out in a 6400-L all-Teflon chamber, and naphthalene, biphenyl, and N_2O_5 were introduced as described above and previously (*12*). Dry purified air was used as the diluent gas, and NO_2, at a concentration of 1.2 × 10^{14} molecules cm^{-3}, was also added for the reasons noted above. Biphenyl and naphthalene were monitored by gas chromatography with flame ionization detection (GC-FID) (*12*) prior to and after the addition of N_2O_5 to the chamber. Under these conditions

$$\ln\left(\frac{[\text{biphenyl}]_{t_0}}{[\text{biphenyl}]_t}\right) - D_t = \frac{k_3}{k_2}\left[\ln\left(\frac{[\text{naphthalene}]_{t_0}}{[\text{naphthalene}]_t}\right) - D_t\right] \quad \text{(II)}$$

where $[\text{biphenyl}]_{t_0}$ and $[\text{naphthalene}]_{t_0}$ are the concentrations of biphenyl and naphthalene, respectively, at time t_0, $[\text{biphenyl}]_t$ and $[\text{naphthalene}]_t$ are the corresponding concentrations at time t, D_t is the small amount of dilution (0.0064) at time t caused by the (single) addition of N_2O_5 to the chamber, and k_3 is the rate constant for the reaction

$$N_2O_5 + \text{biphenyl} \rightarrow \text{products} \quad (3)$$

Products of Reaction of N_2O_5 with Naphthalene. The yields of the 1- and 2-nitronaphthalene products formed from the gas-phase reaction of N_2O_5 with naphthalene in the presence of differing concentrations of NO_2 were determined as described previously (*6*). Two experiments were carried out in the dark in a 6400-L all-Teflon chamber. Naphthalene (at initial concentrations of ~1.2 × 10^{13} molecules cm^{-3}) and NO_2 (at initial concentrations of 2 × 10^{13} and 2.2 × 10^{14} molecules cm^{-3} for the two experiments) were introduced into the chamber as described above. Two additions of N_2O_5 (yielding initial concentrations in the chamber of ~6 × 10^{12} molecules cm^{-3} per addition) were then made to the chamber for each experiment. Naphthalene was monitored prior to and during the reactions by GC-FID (*12*). The 1- and 2-nitronaphthalene products were monitored by collecting ~8-L gas samples onto Tenax GC solid adsorbent, with subsequent elution by 2 mL of diethyl ether and quantification by high-performance liquid chromatography (HPLC), on a Vydac 201TP5415 octadecylsilane column (4.6 mm × 15 cm) eluted with acetonitrile/H_2O (50/50) at a flow rate of 1 mL min^{-1}. Phenanthrene was used as an internal standard, and the 1- and 2-nitronaphthalene isomers were quantified on the basis of their UV absorptions at 254 nm.

In preliminary experiments, the Tenax GC adsorbent was doped with naphthalene-d_8 and, after sample collection, analyzed by gas chromatography–mass spectrometry (GC–MS) for the presence of nitronaphthalene-d_7 products. No nitronaphthalene-d_7 products were observed, showing that no significant reactions of adsorbed naphthalene with N_2O_5 and/or NO_2 + HNO_3 to form nitronaphthalenes were occurring during the sample collection.

Product Studies of OH Radical Reactions with Naphthalene and Biphenyl. These experiments were carried out in a collapsible 6400-L all-Teflon chamber equipped with black lamps emitting in the ~300–400-nm region. Naphthalene and biphenyl were introduced into the chamber as described above, and their concentrations were monitored by GC-FID (*12*). Hydroxyl radicals were generated by the photolysis of methyl nitrite in air at wavelengths ≥300 nm (*12*), and NO was added to the reactant mixtures to avoid the formation of O_3 or N_2O_5.

In order to calculate the integrated OH radical concentrations during these irradiations, and hence the fractions of naphthalene and biphenyl reacting with OH radicals, cyclohexane was added to the chamber and monitored by GC-FID (*16*). The initial reactant concentrations were as follows: CH_3ONO, ~2.4 × 10^{14} molecules cm^{-3}; NO, ~(0.4–2.1) × 10^{14} molecules cm^{-3}; NO_2, (0.05–1.2) × 10^{14} molecules cm^{-3}; cyclohexane, ~1 × 10^{13} molecules cm^{-3}; naphthalene, (2.2–33) × 10^{12} molecules cm^{-3}; biphenyl, (3.5–31) × 10^{12} molecules cm^{-3}.

The first set of experiments (ITC-1010 to ITC-1013) consisted of 3.0- or 3.5-min irradiations of the reactant mixtures at maximum light intensity, with gas samples of 4060–4740 L (calculated from the cyclohexane concentrations measured in the chamber after irradiation and after refilling the chamber with pure dry air) being collected on polyurethane foam (PUF) plugs during these irradiation periods. In all subsequent experiments, the reactant mixtures were irradiated for 1.5 min at maximum light intensity, and after the lights were turned off, gas samples of 2620–4050 L were then collected onto PUF plugs. In all experiments, the initial and final NO and initial NO_2 concentrations were measured with an NO–NO_x chemiluminescence analyzer.

The chamber was cleaned prior to each experiment by flushing with dry pure air with the lights on at 100% of the maximum intensity for several hours. In addition to the above irradiations, the following control experiments were carried out: (a) sampling ~5000 L of pure dry air containing 1.2 × 10^{14} molecules cm^{-3} of NO_2 onto a PUF plug doped with 2-hydroxybiphenyl to investigate whether nitrobiphenyls could be formed from adsorbed-phase reactions between NO_2 and 2-hydroxybiphenyl; (b) sampling ~5000 L of an irradiated CH_3ONO–NO–air mixture onto PUF plugs doped with biphenyl-d_{10}, naphthalene-d_8, 2-hydroxybiphenyl, and the 1- and 2-naphthols with the sampling being carried out while the irradiation was in progress; (c) sampling ~5000 L of an irradiated CH_3ONO–NO–air mixture onto PUF plugs doped with biphenyl-d_{10}, naphthalene-d_8, 2-hydroxybiphenyl, and the 1- and 2-naphthols with the sampling being carried out after the irradiation had been terminated. In all cases no nitroarene products were observed, showing that any formation of nitroarenes from adsorbed PAH or hydroxy aromatics during sampling was negligible.

The PUF plug samples were Soxhlet extracted with CH_2Cl_2. Initial product identification was conducted by GC–MS with a Finnigan 3200 GC–MS interfaced to a

Table I. Experimental Conditions Employed and N_2O_5 Decay Rates Observed for the Gas-Phase Reaction of N_2O_5 with Naphthalene

EC run	10^{-13} × concn, molecules cm^{-3} naphthalene (av)	NO_2 (av)	N_2O_5 (initial)	$10^4 \times N_2O_5$ decay rate, s^{-1} [a]
1090		1.44	5.57	1.32 ± 0.03
1091	1.51	20.5	2.47	4.42 ± 0.05
1092	2.62	20.4	2.78	6.05 ± 0.17
1093	4.03	22.3	5.64	7.13 ± 0.20
1094	0.96	20.7	1.51	2.82 ± 0.10
1095	2.78	2.45	3.53	6.28 ± 0.15
1096	4.13	3.14	6.07	10.7 ± 0.3
1097		2.16	8.45	0.83 ± 0.05
1097[b]		24.6	~5.95	0.88 ± 0.03
1098		1.85	5.98	0.88 ± 0.02
1099	4.15	20.8	1.42	6.47 ± 0.20
1100	7.34	21.8	2.90	12.1 ± 0.3
1101	8.69	22.9	4.37	11.9 ± 0.3
1102	11.4	23.6	5.69	12.7 ± 0.3
1103	5.62	3.24	1.46	9.93 ± 0.20
1105	14.3	5.45	4.82	22.8 ± 0.6
1106	9.89	5.33	4.39	18.0 ± 0.4
1107		3.82	5.71	0.78 ± 0.03
1203		4.10	15.6	1.73 ± 0.03
1204	7.08	3.02	5.86	17.6 ± 1.4
1205	7.44	22.4	3.72	12.1 ± 0.2
1206	7.20	1.97	3.86	23.0 ± 0.7
1207	7.90	0.98	1.73	20.3 ± 0.8
1208	7.90	3.46	1.73	15.2 ± 0.9

[a] Indicated error limits are 2 least-squares standard deviations. [b] NO_2 added during background N_2O_5 decay experiment.

Teknivent data system and operated in the electron impact mode. A cool on-column injector and a 30-m DB-5 capillary column eluting directly into the ion source were used. For quantification, the PUF plug extracts were concentrated under reduced pressure to 5 mL and filtered through an Acrodisc (Gelman Sciences, Ann Arbor, MI). After the addition of phenanthrene as an internal standard, the samples were analyzed by HPLC (Beckman Model 334 equipped with a Beckman Model 164 UV detector). Initially, an Altex ultrasphere ODS column (1 cm × 25 cm) was used with isocratic elution by CH_3OH/H_2O (80/20) at a flow rate of 2 mL min^{-1}. Subsequently, a Vydac 201TP5415 octadecylsilane column was used, eluted with CH_3CN/H_2O at a flow rate of 1 mL min^{-1} according to the following program: CH_3CN/H_2O at 40/60 for 5 min; then linearly to 60/40 over a 6-min period. Naphthalene, biphenyl, 1- and 2-naphthol, 1- and 2-nitronaphthalene, 2-hydroxybiphenyl, and 3-nitrobiphenyl were quantified on the basis of their UV absorptions at 254 nm. Calibration curves were constructed for each compound prior to analysis.

Materials. N_2O_5 was prepared according to the method of Schott and Davidson (*17*) and stored at 77 K under vacuum. Methyl nitrite was prepared as described previously (*18*) and also stored at 77 K under vacuum. The following compounds were obtained from the Aldrich Chemical Co. and were used as received: biphenyl, naphthalene, 1-nitronaphthalene, 2-nitronaphthalene, 1-naphthol, 2-naphthol, 2-nitrobiphenyl, 3-nitrobiphenyl, 4-nitrobiphenyl, 2-hydroxybiphenyl, 3-hydroxybiphenyl, 4-hydroxybiphenyl, naphthalene-d_8, and 1-nitronaphthalene-d_7. Biphenyl-d_{10} was obtained from Cambridge Isotopes Inc.

Results

Kinetic Studies of Reactions of N_2O_5. (A) Naphthalene. The experimental conditions employed and the N_2O_5 decay rates determined for the reaction of N_2O_5 with naphthalene are given in Table I. The maximum consumption of naphthalene during these experiments was 28% and was generally ~10%. The average naphthalene concentrations during each experiment are given in Table I. While for several experiments the naphthalene concentration was similar to the initial N_2O_5 concentrations, the N_2O_5 decays were always exponential within the experimental uncertainties. The observed N_2O_5 decay rates are plotted against the average naphthalene concentrations in Figure 1. It can be seen from Table I and Figure 1 that the N_2O_5 decay rates for the experiments in which the $[NO_2]_{av}/[N_2O_5]_{initial}$ ratio was <1 were significantly higher than the decay rates for conditions where this concentration ratio was >1. Consistent with this observation, the addition of excess NO_2 is expected to decrease the importance of any secondary reactions involving NO_3 radicals and/or reactive reaction products, since the presence of NO_2 lowers the NO_3 radical concentrations in N_2O_5–NO_2–air mixtures and NO_2 may scavenge any radical reaction products.

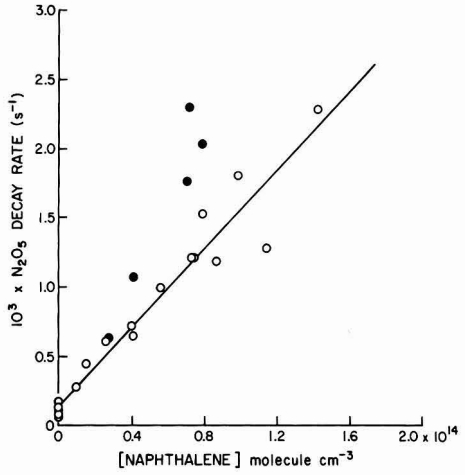

Figure 1. Plot of the N_2O_5 decay rates against the average naphthalene concentrations: (●) $[NO_2]_{av}/[N_2O_5]_{initial} < 1$; (○) $[NO_2]_{av}/[N_2O_5]_{initial} > 1$).

Accordingly, a least-squares analysis of the data obtained under conditions where $[NO_2]_{av}/[N_2O_5]_{initial} > 1$ was carried out to yield the rate constant

$$k_2 = (1.4 \pm 0.2) \times 10^{-17}\ cm^3\ molecule^{-1}\ s^{-1}$$

at 298 ± 2 K, where the indicated error limit is two least-squares standard deviations of the slope of the plot in Figure 1 combined with an estimated 10% maximum uncertainty in the naphthalene concentration calibration.

(B) Biphenyl. The concentrations of naphthalene and biphenyl were monitored prior to and after addition of N_2O_5 to a biphenyl–naphthalene–NO_2–air mixture. Within the analytical uncertainties of ≲5%, no disappearance of biphenyl was observed, while 97% of the naphthalene reacted over the course of the experiment (this consumption of naphthalene is consistent with the rate constant k_2 determined in this work). From these data, an upper limit to the rate constant ratio of $k_3/k_2 < 0.014$ is obtained, leading to

$$k_3 < 2 \times 10^{-19}\ cm^3\ molecule^{-1}\ s^{-1} \text{ at } 298 \pm 2\ K$$

Product Studies. (A) Reaction of N_2O_5 with Naphthalene. As observed in our previous investigation of this reaction (*6*), 1- and 2-nitronaphthalene were formed

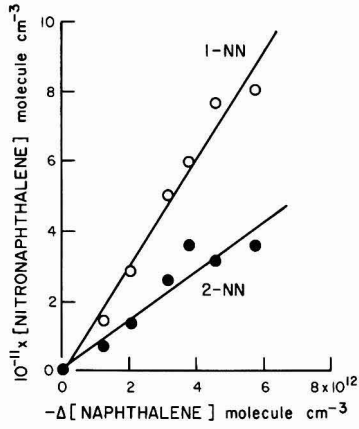

Figure 2. Plot of the 1-nitronaphthalene (1-NN) and 2-nitronaphthalene (2-NN) concentrations against the amount of naphthalene consumed in N_2O_5–NO_2–naphthalene–air reaction mixtures.

in significant yields. Two experiments with differing initial concentrations of NO_2 were carried out for product analyses, and the concentrations of naphthalene and of the 1- and 2-nitronaphthalene products measured during these experiments are given in Table II. A plot of the concentrations of the nitronaphthalenes formed against the amount of naphthalene consumed in these experiments is shown in Figure 2. The data from these two experiments,

Table II. Amounts of Naphthalene Remaining and Nitronaphthalenes Formed in N_2O_5–NO_2–Naphthalene–Air Mixtures

	10^{-12} × concn, molecules cm^{-3}			
			nitronaphthalene (NN)[b]	
ITC run	NO_2 (initial)	naphthalene[a]	1-NN	2-NN
1030	216	11.52		
		10.27	0.143	0.071
		8.38	0.500	0.260
		7.73	0.596	0.360
1033	20	12.00		
		9.94	0.285	0.136
		7.42	0.764	0.314
		6.24	0.800	0.357

[a] By GC–FID. [b] By HPLC.

with NO_2 concentrations differing by a factor of ~11, are indistinguishable within the experimental uncertainties, confirming our previous conclusion (*6*) that N_2O_5, and not the NO_3 radical, is the dominant reactant species under these conditions. The yields of 1- and 2-nitronaphthalene, obtained from the slopes of these plots by least-squares analyses, are 0.153 ± 0.022 and 0.069 ± 0.021, respectively, where the error limits are two least-squares standard deviations of the slopes of the plots shown in Figure 2.

(B) Reactions of OH Radicals with Naphthalene and Biphenyl. The products identified and quantified from the gas-phase reactions of the OH radical with naphthalene and biphenyl in the presence of NO_x were the

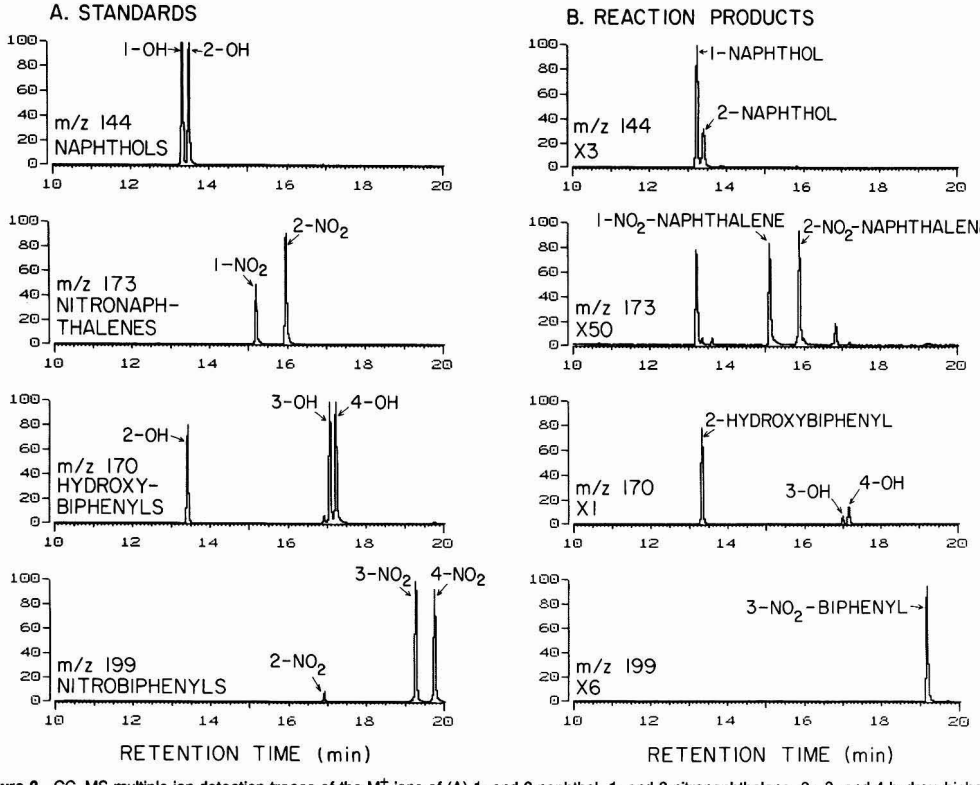

Figure 3. GC–MS multiple ion detection traces of the M^+ ions of (A) 1- and 2-naphthol, 1- and 2-nitronaphthalene, 2-, 3- and 4-hydroxybiphenyls, and 2-, 3- and 4-nitrobiphenyl standards and (B) the corresponding M^+ ions observed from the extract of a PUF plug sample of the gas-phase products of the reaction of OH radicals with naphthalene and biphenyl in the presence of NO_x.

Table III. Initial and Final Concentrations and Volumes Sampled for the CH_3ONO–NO–Naphthalene–Biphenyl–Air Irradiations

	10^{-13} × concn, molecules cm^{-3}							
	initial				final			
ITC run	NO	NO_2	naphthalene	biphenyl	NO	NO_2[a]	ln ([cyclohexane]$_{t_0}$/[cyclohexane]$_t$)	volume sampled, L
1010	20.6	2.4	2.38	2.62	13.9	~19	0.238	4740
1011	10.1	12.2	2.02	2.32	9.1	~22	0.213	4740
1012	14.2	1.0	3.29	2.41	5.0	~18	0.434	4060
1013	5.5	5.8	2.66	2.32	1.0	~18	0.398	4480
1018	9.4	9.8	2.57	3.12	8.2	~16	0.092	3260
1019	10.1	0.6	2.50	2.79	6.0	~10	0.176	3460
1020	5.1	5.3	3.27	2.69	2.3	~13	0.175	3710
1021	20.3	1.1	2.64	2.74	16.4	~10	0.114	3840
1024	16.8	4.1	0.245	0.384	14.6	~11	0.104	2620
1025	8.9	12.5	0.300	0.346	8.8	~18	0.105	3390
1026	9.6	0.5	0.228	0.362	6.1	~9	0.304	3650
1027	3.8	5.6	0.662	0.384	4.6	~10	0.285	4050

[a] Approximate value; calculated assuming that $[NO_2]_{final} = [NO_2]_{initial} + [NO]_{initial} - [NO]_{final} + [CH_3ONO]_{initial} - [CH_3ONO]_{final}$, where the initial CH_3ONO concentration was obtained from the amount added to the chamber and the fraction of the CH_3ONO reacted was determined by GC–FID analyses.

1- and 2-naphthols and 1- and 2-nitronaphthalenes from naphthalene and 2-hydroxybiphenyl and 3-nitrobiphenyl from biphenyl (Figure 3). The reaction of OH radicals with biphenyl also formed the 3- and 4-hydroxybiphenyls in lesser yields than the 2-hydroxybiphenyl isomer (Figure 3), with the relative yields of the hydroxybiphenyl isomers being similar to those of *o*-, *m*-, and *p*-cresol from the reaction of toluene with OH radicals (*19–21*).

In addition to these identified products, it was evident from GC–MS total ion chromatograms that the OH radical reaction with naphthalene produced a number of other, as yet unidentified, products. In particular, two products with apparent molecular ions of m/z 132 were observed from these naphthalene reactions, with estimated yields higher than those of the nitronaphthalenes, together with a less abundant peak tentatively identified as a hydroxynitronaphthalene.

The initial concentrations of NO, NO_2, naphthalene, and biphenyl, the final NO and NO_2 concentrations, the amount of cyclohexane reacted, and the chamber volumes sampled for these reactions are given in Table III. The fractions of the initial naphthalene and biphenyl reacting were calculated from the fraction of cyclohexane reacted by use of eq III, where $k_{aromatic}$ and $k_{cyclohexane}$ are the OH

$$\ln\left(\frac{[\text{aromatic}]_{t_0}}{[\text{aromatic}]_t}\right) = \frac{k_{\text{aromatic}}}{k_{\text{cyclohexane}}} \ln\left(\frac{[\text{cyclohexane}]_{t_0}}{[\text{cyclohexane}]_t}\right) \quad \text{(III)}$$

radical rate constants for biphenyl and naphthalene and for cyclohexane, respectively (*5*). For these irradiations, the volumes sampled from the chamber ranged from ~2600 to ~4700 L, and the average OH radical concentrations were calculated from the measured cyclohexane concentrations before and after irradiation to be (1.5–3) × 10^8 molecules cm^{-3}.

For the first four irradiations, samples were collected during the entire 3.0- or 3.5-min irradiation times. This procedure complicated the derivation of product yields from these data since the amounts of reaction ranged from zero at the start of the irradiations to those at the termination of the irradiations. In addition, the products were also reacting with the OH radical during the sampling periods. Over these short irradiation times, the OH radical concentrations could be considered to be approximately constant, and the amounts of naphthalene and biphenyl in the sampled volumes that had reacted were calculated from the analytical expression given in the Appendix, which is available as supplementary material (see paragraph at end of text regarding supplementary material). Corrections were also made to the observed product yields to take into account their reactions with OH radicals (see Appendix).

For the remaining eight irradiations, the gas samples were collected after the irradiations had been terminated. Thus, the amounts of naphthalene, biphenyl, and cyclohexane reacted were given by the decreases in their concentrations as measured prior to and after the irradiations. The fractional amounts of biphenyl, cyclohexane, and naphthalene reacted were consistent with the relative OH radical reaction rate constants for these compounds (*5*). However, because of the higher precision of the cyclohexane measurements, the cyclohexane data were used to calculate the fractions of biphenyl and naphthalene reacting, and these fractional amounts reacted were then combined with the observed preirradiation biphenyl and naphthalene concentrations to calculate the amounts reacted. Corrections for reactions of the products with OH radicals during these eight irradiations were determined as described previously (*22*).

Rate constants of 3 × 10^{-11} cm^3 $molecule^{-1}$ s^{-1} and ~1 × 10^{-10} cm^3 $molecule^{-1}$ s^{-1} were estimated for the reactions of the OH radical with 2-hydroxybiphenyl and the 1- and 2-naphthols, respectively, on the basis of the available literature data and estimation techniques (*5*). These lead to rate constant ratios of $k_{\text{hydroxy aromatic}}/k_{\text{aromatic}} = 4.5$ for both naphthalene and biphenyl. The resulting correction factors to take into account hydroxy aromatic losses via reaction with the OH radical are given in Table IV, together with the calculated yields of these products. The rate constants for OH radical reaction with the nitroarene products are expected to be lower, by at least a factor of 2, than those for the parent PAH (*5*). The calculated correction factors to take into account reactions of the nitro aromatics with the OH radical are then <1.2 for the 1- and 2-nitronaphthalenes and <1.1 for 3-nitrobiphenyl. These correction factors are sufficiently small so that no corrections were made to the observed nitroarene yields, which are also given in Table IV.

For the first eight irradiations (ITC runs 1010–1013 and 1018–1021), the initial naphthalene and biphenyl concentrations were each ~2.5 × 10^{13} molecules cm^{-3}, and it was observed that the nitroarene products were generally not completely collected on the two or three PUF plugs used for sample collection. Hence, where indicated, the values given in Table IV are lower limits. The last four irradia-

Table IV. Hydroxy Aromatic and Nitroarene Product Yields from the Gas-Phase Reaction of OH Radicals with Naphthalene and Biphenyl[a]

	product yields							
	biphenyl		naphthalene				$10^{-13} \times NO_x$ concn	
ITC run[b]	2-HOB[c]	3-NB	1-HON	2-HON	1-NN	2-NN	NO	NO_2
1010	0.190 (1.39)	>0.045[d]	0.076 (2.41)	0.045 (2.41)	>0.0024[d]	>0.0014[d]	21 → 14	2 → 19
1021	0.208 (1.27)	>0.058[d]	0.082 (2.03)	0.023 (2.03)	0.0029	0.0017	20 → 16	1 → 10
1024	0.273 (1.25)	0.075	e (1.91)	e (1.91)	0.0041	0.0045	17 → 15	4 → 11
1011	0.136 (1.39)	>0.039[d]	0.024 (2.20)	0.047 (2.20)	>0.0035[d]	>0.0027[d]	10 → 9	12 → 22
1018	0.214 (1.21)	>0.049[d]	0.067 (1.79)	0.030 (1.79)	0.0049	0.0045	9 → 8	10 → 16
1025	0.257 (1.25)	0.068	e (1.92)	e (1.92)	0.0058	0.0064	9 → 9	13 → 18
1012	0.216 (1.80)	>0.032[d]	0.078 (3.95)	0.061 (3.95)	>0.0018[d]	>0.0011[d]	14 → 5	1 → 18
1019	0.163 (1.46)	>0.029[d]	0.069 (2.86)	0.034 (2.86)	0.0013	0.00080	10 → 6	1 → 10
1026	0.162 (1.88)	0.035	e (5.29)	e (5.29)	0.0018	0.0017	10 → 6	1 → 9
1013	0.203 (1.67)	>0.032[d]	0.075 (3.59)	0.049 (3.59)	>0.0031[d]	>0.0020[d]	6 → 1	6 → 18
1020	0.226 (1.45)	>0.071[d]	0.10 (2.84)	0.047 (2.84)	>0.0047[d]	>0.0034[d]	5 → 2	5 → 13
1027	0.202 (1.81)	0.030	e (4.84)	e (4.84)	0.0021	0.0018	4 → 5	6 → 10

[a] The observed hydroxy aromatic concentrations were corrected for their reaction with OH radicals by use of the correction factors given in parentheses. Abbreviations: 2-hydroxybiphenyl (2-HOB), 3-nitrobiphenyl (3-NB), 1-naphthol (1-HON), 2-naphthol (2-HON), 1-nitronaphthalene (1-NN), radicals 2-nitronaphthalene (2-NN). [b] Grouped by initial NO and NO_2 concentrations. [c] Approximate value (see text for explanation). [d] Not completely collected on number of PUF plugs used, hence a lower limit. [e] Not available (see text for explanation).

tions (ITC runs 1024–1027) utilized initial naphthalene and biphenyl concentrations a factor of ~10 lower (~3×10^{12} molecules cm^{-3}), resulting in the nitroarene products being collected mainly on the first PUF plug, with markedly lesser amounts being observed on the second and third PUF plugs. However, because of the low amounts of products collected, the 1- and 2-naphthols could not be quantified from these irradiations.

The yields listed in Table IV for 2-hydroxybiphenyl have a likely uncertainty of up to ±30–40%. In the initial HPLC quantification, the 2-, 3-, and 4-isomers were not resolved, resulting in a potential overestimation of the amount of 2-hydroxybiphenyl present. While subsequent HPLC analyses were carried out with a Vydac 201TP5415 octadecylsilane column to resolve these isomers, loss of the more volatile 2-hydroxybiphenyl isomer during the workup procedure led to an underestimation of the amounts of 2-hydroxybiphenyl formed. These lower limits to the 2-hydroxybiphenyl yields are ~45% lower than those obtained from the measured combined 2-, 3-, and 4-isomer yields, which may also have suffered from some losses due to volatilization and/or incomplete sampling. Because of these factors and the relatively low 3- and 4-hydroxybiphenyl/2-hydroxybiphenyl product ratios (see Figure 3), we have used our initial HPLC quantification of the combined isomers as the 2-hydroxybiphenyl yield, with the realization that the uncertainties in these yields are likely to be ca. ±30–40%.

After correction for reaction with OH radicals, the formation yields of the 1- and 2-naphthols, the 1- and 2-nitronaphthalenes, 2-hydroxybiphenyl, and 3-nitrobiphenyl are given in Table IV, together with the correction factors used. The factors used to correct for the OH radical reactions with the 1- and 2-naphthols were high, being in the range ~2–4, and introduced additional uncertainties into the derived formation yields of these products. However, within the relatively large experimental uncertainties there is no dependence of any of the product yields on the average NO and NO_2 concentrations during these irradiations. Figure 4 shows plots of the 3-nitrobiphenyl yield and of the 3-nitrobiphenyl/2-hydroxybiphenyl yield ratio against the mean NO_2 concentration for each irradiation. It can be seen from this figure that there is no correlation of either the 3-nitrobiphenyl yield or the 3-nitrobiphenyl/2-hydroxybiphenyl yield ratio with the NO_2 concentration. Thus, least-squares analyses of these data yield small positive slopes (shown in Figure 4), which are within

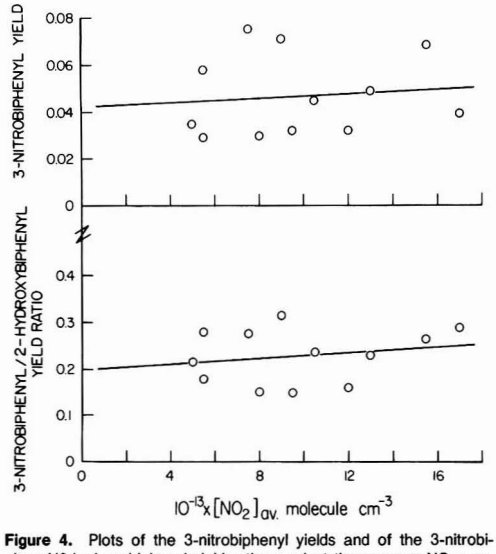

Figure 4. Plots of the 3-nitrobiphenyl yields and of the 3-nitrobiphenyl/2-hydroxybiphenyl yield ratios against the average NO_2 concentrations for the CH_3ONO–NO–NO_2–biphenyl–naphthalene–air irradiations carried out.

Table V. Observed Average Hydroxy Aromatic and Nitroarene Product Yields from the Gas-Phase Reactions of OH Radicals (in the Presence of NO_x) with Naphthalene and Biphenyl

product	formation yield[a]
naphthalene	
1-naphthol	0.071 ± 0.043
2-naphthol	0.042 ± 0.025
1-nitronaphthalene	0.0032 ± 0.0028
2-nitronaphthalene	0.0027 ± 0.0034
biphenyl	
2-hydroxybiphenyl	0.204 ± 0.078
3-nitrobiphenyl	0.047 ± 0.034

[a] Corrected for reaction with OH radicals (see text). Indicated errors are 2 standard deviations.

1 standard deviation of zero, and intercepts which are ≥3 standard deviations from zero. The average yields of the hydroxy aromatic and nitroarene products are given in

Table V, together with the associated two standard deviation error limits.

Discussion

Reactions of N_2O_5 with Naphthalene and Biphenyl. The rate constant measured here for the gas-phase reaction of N_2O_5 with naphthalene of $(1.4 \pm 0.2) \times 10^{-17}$ cm^3 molecule^{-1} s^{-1} supercedes that of $\sim(2\text{–}3) \times 10^{-17}$ cm^3 molecule^{-1} s^{-1} reported previously (*6*) from a computer fit of the time–concentration profiles of N_2O_5 and naphthalene for a single N_2O_5–naphthalene–air reactant mixture without initially added NO_2. The lower rate constant determined in this study is consistent with our previous data (*6*), since it is apparent that secondary reactions occur in the absence of added NO_2 leading to enhanced decays of N_2O_5. The more accurate rate constant k_2 leads to a calculated atmospheric lifetime of naphthalene due to this N_2O_5 reaction of $\sim$80 days, for an estimated ambient N_2O_5 concentration of 2×10^{10} molecules cm^{-3} during 12-h nighttime periods (*23*).

The yields of 1- and 2-nitronaphthalenes determined in this study of 0.153 ± 0.022 for 1-nitronaphthalene and 0.069 ± 0.021 for 2-nitronaphthalene, independent of the NO_2 concentration, are in excellent agreement with our previous values of 0.172 ± 0.034 and 0.075 ± 0.012, respectively, determined in the absence of added NO_2 (the values given in ref 6 are slightly incorrect due to typographical errors). Clearly, other products, possibly including hydroxynitronaphthalenes, are formed in significant yields, and further work is necessary to identify and quantify these products.

The absence of any gas-phase reaction of N_2O_5 with biphenyl (with $k_3 < 2 \times 10^{-19}$ cm^3 molecule^{-1} s^{-1}) is consistent with our previous data concerning the monocyclic aromatic hydrocarbons (*24*), since no reaction of benzene with NO_3 radicals or N_2O_5 has been observed and the reactions of NO_3 radicals with alkyl-substituted monocyclic aromatic hydrocarbons are postulated to occur via H atom abstraction from the alkyl substituent groups (*24*).

Products of the OH Radical Initiated Reactions of Naphthalene and Biphenyl. The products identified and quantified in this study of the gas-phase OH radical initiated reactions of naphthalene and biphenyl are analogous to those observed from the reactions of the OH radical with toluene and other monocyclic aromatic hydrocarbons in the presence of NO_x (*19–21*, *25–27*). Thus, the major aromatic ring containing products observed from toluene are benzaldehyde (which is formed subsequent to H atom abstraction from the $-CH_3$ substituent group), *o*-cresol (together with much smaller yields of *m*- and *p*-cresol), and *m*-nitrotoluene (together with lesser amounts of *o*- and *p*-nitrotoluene). The reported hydroxy aromatic yields from toluene (*21*, *25–27*) are similar to those observed in this work for biphenyl, as is the isomer distribution.

For neither naphthalene nor biphenyl will H atom abstraction from the ring be important (*5*), and hence the OH radical reactions will proceed via OH radical addition to the aromatic ring. For example, for biphenyl OH radical addition will occur mainly at the 2-position:

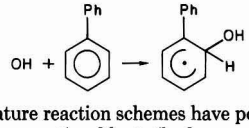

Previous literature reaction schemes have postulated that these hydroxy aromatic adducts (hydroxycyclohexadienyl radicals) then react with O_2 via two routes, (a) an overall H atom abstraction process to yield the hydroxy aromatic and (b) reversible addition of O_2 to the aromatic ring to yield a hydroxy aromatic–O_2 adduct (*5*, *21*, *25–27*):

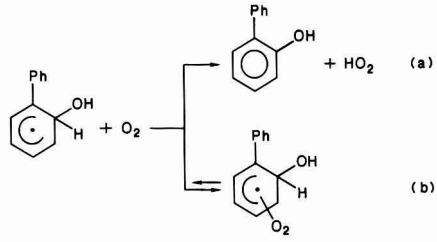

A further postulated reaction of these hydroxycyclohexadienyl radicals involves the initial addition of NO_2, leading to the formation of nitroarenes (*20*, *25*):

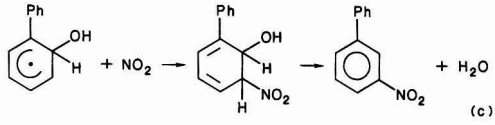

The reaction schemes proposed to date for the reactions of monocyclic aromatic hydrocarbons with OH radicals in the presence of NO_x postulate that the hydroxy aromatic–O_2 adducts formed via reaction b undergo ring-opening reactions leading to a wide variety of ring-opened products (see, for example, ref 21 and 25–31). Indeed, the limited data available, including those obtained in this study, show that the formation of hydroxy aromatics and nitroarenes accounts for a relatively minor fraction of the total products formed from these OH radical initiated reactions.

Reaction pathways a and c are consistent with the hydroxy aromatic and nitroarene isomers observed from biphenyl and naphthalene. Thus, OH radicals are expected to add at approximately comparable rates to the 1- and 2-positions on naphthalene, leading to the formation of the 1- and 2-naphthols and the 2- and 1-nitronaphthalenes, respectively. Similarly, OH radical addition to biphenyl is expected to occur mainly at the 2-position, with addition at the 4- and 3-positions being much less important. Hence, the expected hydroxy- and nitro-substituted products from biphenyl are mainly 2-hydroxybiphenyl and 3-nitrobiphenyl.

The reaction scheme a–c predicts that

$$\frac{Y_{NA}}{Y_{HOA}} = \frac{k_c}{k_a}\frac{[NO_2]}{[O_2]} \qquad \text{(IV)}$$

$$Y_{NA} = \frac{k_c[NO_2]}{(k_a + k_b)[O_2] + k_c[NO_2]} \qquad \text{(V)}$$

and

$$Y_{HOA} = \frac{k_a[O_2]}{(k_a + k_b)[O_2] + k_c[NO_2]} \qquad \text{(VI)}$$

where Y_{HOA} and Y_{NA} are the hydroxy aromatic and nitroarene yields respectively, and k_a, k_b, and k_c are the rate constants for reaction pathways a, b, and c, respectively. From the data obtained in this work, $k_c[NO_2]/\{(k_a + k_b)[O_2]\} \ll 1$, and hence

$$Y_{NA} \sim k_c[NO_2]/\{(k_a + k_b)[O_2]\} \qquad \text{(VII)}$$

and

$$Y_{HOA} \sim k_a/(k_a + k_b) \qquad \text{(VIII)}$$

The data obtained in this work, as shown in Tables IV and V and Figure 4, are not consistent with the presently accepted reaction scheme a–c, since for biphenyl there is

no observed dependence of Y_{NA} or of the ratio Y_{NA}/Y_{HOA} on the average NO_2 concentration (the data for naphthalene are more uncertain because of the lower yields of the naphthols and nitronaphthalenes and the higher factors necessary to account for secondary reactions of the naphthols). This is in agreement with the data of Gery et al. (*21*), who observed no dependence of the *m*-nitrotoluene yield from the reaction of toluene with OH radicals on the initial NO_x (HONO + NO + NO_2) concentration, which was varied by a factor of ~4 from ~(1.1–4.8) × 10^{14} molecules cm^{-3}.

A further reaction yielding hydroxy aromatic products was postulated by Hoshino et al. (*19*) for benzene, toluene, and ethylbenzene, involving the reaction of the hydroxycyclohexadienyl radical with NO_2, for example

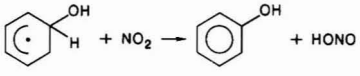

This general reaction pathway, which is significantly more exothermic [by ~28 kcal mol^{-1} (*32*)] than that with O_2 leading to HO_2 production, would lead to an independence of the ratio Y_{NA}/Y_{HOA} on NO_2 concentration and would not necessitate any reaction of the hydroxycyclohexadienyl radical with O_2. Clearly, further kinetic and product studies are needed to elucidate the formation pathways of hydroxy aromatics and nitroarenes from the parent aromatic hydrocarbons and to identify and quantify the products not yet identified.

Atmospheric Implications. The nitroarene products arising from the gas-phase reactions of the OH radical with naphthalene and biphenyl in the presence of NO_x are those isomers that we have recently observed in ambient air (*4*). Specifically, 1- and 2-nitronaphthalenes, at similar concentrations, and 3-nitrobiphenyl (but not the 2- and 4-nitrobiphenyls) were measured in ambient air samples collected at Torrance, CA, during a wintertime 2–3-day, high-NO_x episode (*4*). Additionally, 2-nitrofluoranthene and 2-nitropyrene, nitroarenes that are also formed via OH radical initiated reactions (*9*), were observed in these samples. These data strongly suggest the atmospheric formation of these nitroarenes via OH radical initiated reactions (*4*, *9*).

However, our observations of significant concentrations of these nitroarenes, with the observed daytime concentration ratio of 3-nitrobiphenyl/biphenyl of ~0.1 (*4*), are difficult to rationalize if the nitroarene yields are dependent on the NO_2 concentrations as suggested by previous literature reaction schemes, i.e., a–c above. Thus, the ambient near-ground-level concentrations of NO_2 measured at our Torrance sampling site were $\lesssim 6 \times 10^{12}$ molecules cm^{-3}, a factor of $\gtrsim$20 lower than the average NO_2 concentrations present in this study. Assuming an initial release of biphenyl into the atmosphere with a reaction time of ~10 h and using our measured 3-nitrobiphenyl formation yield of 0.05, an average atmospheric OH radical concentration of ~4×10^6 molecules cm^{-3} is necessary to achieve a 3-nitrobiphenyl/biphenyl concentration ratio of 0.1. While the estimated OH radical concentration is consistent with our present knowledge of ambient OH radical concentrations, unrealistically high ambient OH radical levels would be necessary to account for our ambient measurements if the 3-nitrobiphenyl yield is dependent on the NO_2 concentration and was thus lower by a factor of ~20 (corresponding to the lower ambient NO_2 concentrations) during our sampling period.

Thus, while it is now clear that certain nitroarenes may be formed in the atmosphere via reaction with the OH radical [and in some cases with N_2O_5 (*6–8*, *10*)], there are still important issues to be resolved before we have a complete understanding of the atmospheric chemistry of aromatic hydrocarbons, especially with respect to the formation of nitroarenes.

Of further interest is the observation that hydroxy aromatics are formed in appreciable yields from these OH radical initiated reactions (~20% for 2-hydroxybiphenyl and ~10% for the combined 1- and 2-naphthols). This class of compounds reacts rapidly in the gas phase with OH and NO_3 radicals (*5*, *24*) and is hence expected to be present at only low concentrations in ambient air. The NO_3 radical reactions are postulated to occur with the formation in large yield of less reactive hydroxynitro products (*24*, *27*). Since these hydroxynitro aromatics can also be formed, though in much lower yields, from the OH radical initiated reactions of nitroarenes and of hydroxy aromatics in the presence of NO_x, it is possible that ambient particulate organic matter contains appreciable quantities of hydroxynitro aromatic compounds formed during atmospheric transport. Clearly, studies of the ambient concentrations of these and other aromatic products are needed.

Acknowledgments

Patricia A. McElroy is thanked for very able technical assistance.

Supplementary Material Available

The Appendix detailing the expressions used to correct for secondary reactions occurring during the experiments in which sampling was carried out concurrent with irradiation (2 pages) will appear following these pages in the microfilm edition of this volume of the journal. Photocopies of the supplementary material from this paper or microfiche (105 × 148 mm, 24× reduction, negatives) may be obtained from Microforms Office, American Chemical Society, 1155 16th St., N.W., Washington, DC 20036. Full bibliographic citation (journal, title of article, authors' names, inclusive pagination, volume number, and issue number) and prepayment, check or money order for $10.00 for photocopy ($12.00 foreign) or $10.00 for microfiche ($11.00 foreign), are required.

Literature Cited

(1) Wise, S. A.; Chesler, S. N.; Hilpert, L. R.; May, W. E.; Rebbert, R. E.; Vogt, C. R.; Nishioka, M. G.; Austin, A.; Lewtas, J. *Environ. Int.* **1985**, *11*, 147–160.
(2) Daisey, J. M.; Cheney, J. L.; Lioy, P. J. *J. Air Pollut. Control Assoc.* **1986**, *36*, 17–33.
(3) Ramdahl, T.; Zielinska, B.; Arey, J.; Atkinson, R.; Winer, A. M.; Pitts, J. N., Jr. *Nature (London)* **1986**, *321*, 425–427.
(4) Arey, J.; Zielinska, B.; Atkinson, R.; Winer, A. M. *Atmos. Environ.* **1987**, *21*, 1437–1444.
(5) Atkinson, R. *Chem. Rev.* **1986**, *86*, 69–201.
(6) Pitts, J. N., Jr.; Atkinson, R.; Sweetman, J. A.; Zielinska, B. *Atmos. Environ.* **1985**, *19*, 701–705.
(7) Sweetman, J. A.; Zielinska, B.; Atkinson, R.; Ramdahl, T.; Winer, A. M.; Pitts, J. N., Jr. *Atmos. Environ.* **1986**, *20*, 235–238.
(8) Zielinska, B.; Arey, J.; Atkinson, R.; Ramdahl, T.; Winer, A. M.; Pitts, J. N., Jr. *J. Am. Chem. Soc.* **1986**, *108*, 4126–4132.
(9) Arey, J.; Zielinska, B.; Atkinson, R.; Winer, A. M.; Ramdahl, T.; Pitts, J. N., Jr. *Atmos. Environ.* **1986**, *20*, 2339–2345.
(10) Zielinska, B.; Arey, J.; Atkinson, R.; Winer, A. M.; Pitts, J. N., Jr. Presented at the 192nd National Meeting of the American Chemical Society, Anaheim, CA, Sept 7–12, 1986.
(11) Pitts, J. N., Jr.; Sweetman, J. A.; Zielinska, B.; Winer, A. M.; Atkinson, R. *Atmos. Environ.* **1985**, *19*, 1601–1608.
(12) Atkinson, R.; Aschmann, S. M.; Pitts, J. N., Jr. *Environ. Sci. Technol.* **1984**, *18*, 110–113.
(13) Tokiwa, H.; Ohnishi, Y. *CRC Crit. Rev. Toxicol.* **1986**, *17*, 23–60.

(14) Winer, A. M.; Graham, R. A.; Doyle, G. J.; Bekowies, P. J.; McAfee, J. M.; Pitts, J. N., Jr. *Adv. Environ. Sci. Technol.* **1980**, *10*, 461–511.
(15) Graham, R. A.; Johnston, H. S. *J. Phys. Chem.* **1978**, *82*, 254–268.
(16) Atkinson, R.; Aschmann, S. M. *Environ. Sci. Technol.* **1985**, *19*, 462–464.
(17) Schott, G.; Davidson, N. *J. Am. Chem. Soc.* **1958**, *80*, 1841–1853.
(18) Taylor, W. D.; Allston, T. D.; Moscato, M. J.; Fazekas, G. B.; Kozlowski, R.; Takacs, G. A. *Int. J. Chem. Kinet.* **1980**, *12*, 231–240.
(19) Hoshino, M.; Akimoto, H.; Okuda, M. *Bull. Chem. Soc. Jpn.* **1978**, *51*, 718–724.
(20) Kenley, R. A.; Davenport, J. E.; Hendry, D. G. *J. Phys. Chem.* **1981**, *85*, 2740–2746.
(21) Gery, M. W.; Fox, D. L.; Jeffries, H. E.; Stockburger, L.; Weathers, W. S. *Int. J. Chem. Kinet.* **1985**, *17*, 931–955.
(22) Atkinson, R.; Aschmann, S. M.; Carter, W. P. L.; Winer, A. M.; Pitts, J. N., Jr. *J. Phys. Chem.* **1982**, *86*, 4563–4569.
(23) Atkinson, R.; Winer, A. M.; Pitts, J. N., Jr. *Atmos. Environ.* **1986**, *20*, 331–339.
(24) Atkinson, R.; Carter, W. P. L.; Plum, C. N.; Winer, A. M.; Pitts, J. N., Jr. *Int. J. Chem. Kinet.* **1984**, *16*, 887–898.
(25) Atkinson, R.; Carter, W. P. L.; Darnall, K. R.; Winer, A. M.; Pitts, J. N., Jr. *Int. J. Chem. Kinet.* **1980**, *12*, 779–836.
(26) Leone, J. A.; Flagan, R. C.; Grosjean, D.; Seinfeld, J. H. *Int. J. Chem. Kinet.* **1985**, *17*, 177–216.
(27) Atkinson, R.; Lloyd, A. C. *J. Phys. Chem. Ref. Data* **1984**, *13*, 315–444.
(28) Dumdei, B. E.; O'Brien, R. J. *Nature (London)* **1984**, *311*, 248–250.
(29) Shepson, P. B.; Edney, E. O.; Corse, E. W. *J. Phys. Chem.* **1984**, *88*, 4122–4126.
(30) Bandow, H.; Washida, N.; Akimoto, H. *Bull. Chem. Soc. Jpn.* **1985**, *58*, 2531–2540.
(31) Tuazon, E. C.; Mac Leod, H.; Atkinson, R.; Carter, W. P. L. *Environ. Sci. Technol.* **1986**, *20*, 383–387.
(32) Benson, S. W. *Thermochemical Kinetics*, 2nd ed.; Wiley: New York, 1976.

Received for review February 3, 1987. Revised manuscript received June 8, 1987. Accepted June 29, 1987. The financial support of the U.S. Environmental Protection Agency, Grant R812973-01 (Project Monitor, Louis Swaby), and of the California Air Resources Board, Contract A5-104-32 (Project Monitor, Jack K. Suder) (for the kinetic study of the reaction of N_2O_5 with naphthalene), is gratefully acknowledged. Although the research described in this paper has been funded mainly by the Environmental Protection Agency, it has not been subjected to Agency review and therefore does not necessarily reflect the views of the Agency, and no official endorsement should be inferred.

NOTES

Soil-Gas Measurement for Detection of Groundwater Contamination by Volatile Organic Compounds

Henry B. Kerfoot

Environmental Programs, Lockheed Engineering Management Services Company, Las Vegas, Nevada 89109

■ A soil-gas sampling probe was designed and field tested in soil above a chloroform-contaminated aquifer. The field investigation included correlating the results of soil-gas analyses with groundwater contamination and evaluating overall method precision. Soil-gas analysis results for chloroform were significantly correlated with chloroform concentrations in underlying groundwater samples. Chloroform concentrations in the unsaturated zone increased linearly with depth.

Introduction

Sampling and analysis of soil gases as a technique for locating volatile organic compounds (VOCs) below the ground surface was originally used for oil exploration (*1*). Only recently has this technique been used for locating groundwater contamination by VOCs. Few evaluations of the method have been reported. This paper describes the performance of a grab sampling technique for soil-gas measurement. The study assessed the correlation between soil-gas and groundwater analyses with trichloromethane (chloroform) as a model VOC. The study was conducted under contract to the U.S. Environmental Protection Agency (*2*).

Experimental Section

Apparatus. The sampling probe was a 2.3-m, 19-mm o.d. pipe of high-strength steel with horizontal 3-mm sampling ports in the conical tip. The ports led to a central plenum connected to a 3-mm stainless steel tube inside the pipe. The stainless steel tubing was connected at the top of the probe to a septum-equipped stainless steel sampling manifold constructed from commercially available fittings. Figure 1 shows the sampling probe and the manifold attached to it. Soil gas was drawn from the subsurface into the manifold by use of an MSA Samplair manual air-sampling pump. Subsamples were drawn from the manifold with Hamilton gas-tight syringes. Soil-gas analyses were performed on-site with an Analytical Instruments Development Model 511 gas chromatograph (GC) with a ^{3}H electron capture detector (ECD) and a 183-cm × 3-mm stainless steel column packed with 10% DC-200 on Chromosorb W HP (80/100). The GC was operated at 43 °C (oven), 37 °C (injector), and 37 °C (detector). Chloroform gas standards were prepared by serial dilution of neat chloroform (Alltech Associates) headspace vapors in 45-mL septum-capped vials (Pierce Chemical Co.). A Shimadzu C-R3A integrator and Hewlett-Packard 7155A recorder were used to record the chromatograms. Analytical instruments were operated in a van, which received electrical power from a gasoline-powered generator located approximately 6.4 m (20 ft) downwind. Water samples were taken with a bladder pump, collected in 45-mL septum-capped vials (Pierce Chemical Co.), and analyzed by

 0013-936X/87/0921-1022$01.50/0

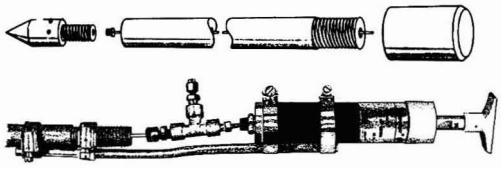

Figure 1. Sampling probe (top) and manifold attached to probe (bottom).

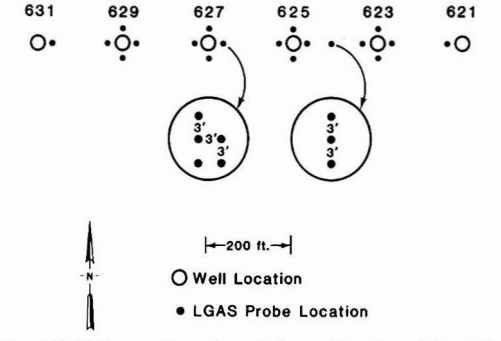

Figure 2. Soil-gas probe and monitoring well locations at the study site.

U.S. Environmental Protection Agency procedures on a Finnegan GC/MS (*4*).

Procedure. Sampling probes were hammered 1.3 m (4 ft) into the ground with a sledge hammer, after which the sampling manifold was attached. Seventy-five cubic centimeters of gas was drawn through the sampling assembly by the air pump. Subsamples were withdrawn from the sampling manifold and transported in an opaque plastic box to the analytical instruments for soil-gas analyses. In an attempt to reduce cross-contamination, blanks of ambient air were drawn through the probes and analyzed before use, and syringes were purged with ultrapure nitrogen between uses. Groundwater analyses were performed at a remote laboratory. The GC/ECD detection limit for chloroform in soil gas was 5 ppbv. The GC/MS detection limit for chloroform in groundwater was 5 μg/L.

Survey Site

A site of known groundwater contamination by chloroform was chosen for the study. A set of groundwater monitoring wells have been installed at distances of 64 m (200 ft) apart in a line perpendicular to the northward direction of groundwater flow. Groundwater is present at 3–5 m below the ground surface.

The hydrogeology of the site is relatively simple. Unconfined groundwater is present at a depth of 3–4 m in calcified unconsolidated alluvium overlying a clay aquitard at 8–13 m below the ground surface. The soil is a gravelly sandy loam with a clay content of 2–8% that decreases with depth (*3*). The soil has a low shrink–swell potential and a permeability that is relatively high [i.e., 5–15 cm/h at a depth of 0–40 cm and 15–50 cm/h at 40–150 cm (*3*)]. The ground surface, water table, and aquiclude all slope down to the north at approximately 1°. Groundwater samples from five wells ranged in chloroform concentration from 11 to approximately 1000 μg/L.

Experimental Design

The study was designed to evaluate soil-gas analyses and assess their correlation with groundwater analyses. Soil-gas

Table I. Chloroform Concentrations in Groundwater (μg/L) and Soil Gas (ppbv)

well	ground-water concn	soil-gas concn[a] mean	6.4 m west	6.4 m north	6.4 m east	6.4 m south
631	ND[b]	5.0			5.0	
629	11	23	10 (2)	25 (2)	27 (5)	31 (1)
627	175	67	28 (5)	72.9 (0.1)	124 (53)	45.6 (0.2)
625	866	370	266 (6)	326 (10)	376 (6)	511 (17)
623	555	40	115 (6)	12 (5)	6 (3)	27 (2)
621	28	10.5	10.5 (0.3)			

[a] Triplicate analyses; standard deviation in parentheses. [b] Not detected; value of 5 used in regression.

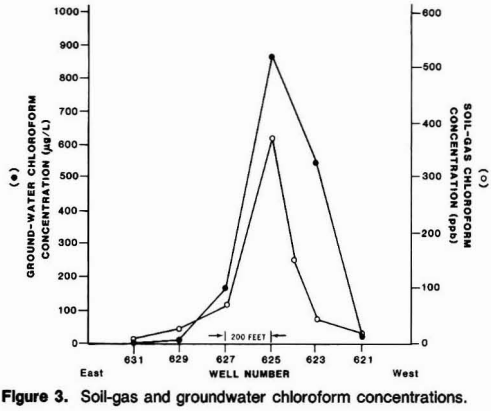

Figure 3. Soil-gas and groundwater chloroform concentrations.

samples were collected from four 1.3 m (4 ft) depth locations symmetrically placed at 6.4 m (20 ft) from each of four groundwater monitoring wells (Figure 2). The mean concentration of these four samples was compared to the groundwater concentration at the corresponding well. One sample was collected at a distance of 6.4 m (20 ft) from wells 621 and 631 in order to delineate the edges of the plume.

Three locations separated by 1 m along a north–south line were also sampled. Samples were taken at five depths between 0.3 (1 ft) and 1.7 (5 ft) m in 0.3-m (1-ft) increments at these locations, and the results were used to determine the vertical distribution of VOCs. Assuming that the soil has a 30% air-filled porosity, the 75-cm^3 purge corresponds to a sampling sphere of influence of approximately 250 cm^3 (radius of 4 cm). These calculations suggest that minimal disruption of soil gases took place as a result of sampling at 0.3-m intervals.

Results and Discussion

Table I lists the mean values of chloroform concentrations in soil gas, which were measured in units of parts per billion by volume (ppbv). Also listed are chloroform concentrations in groundwater (μg/L) from six monitoring wells. A linear correlation coefficient of 0.85 was calculated for chloroform concentrations in soil gas and groundwater; for six data points, this indicates a statistical significance of greater than 95%. Figure 3 shows the spatial distribution of chloroform concentrations in groundwater and in the soil gas.

The precision of the method is limited by variability due to sampling procedures. The analytical precision, as indicated by analyses of external standards over the course of a day, yielded a relative standard deviation (rsd) of 2%. The rsd values for replicate soil-gas subsamples collected

Table II. Chloroform Concentrations from the Three-Probe Depth Study

depth, m	chloroform concn, ppbv[a]	depth, m	chloroform concn, ppbv[a]
0.3	21.6 (2.3)	1.3	145 (11)
0.6	68.0 (9.2)	1.6	185 (19)
1.0	106 (6)	1.8	236 (29)

[a] Mean of three locations along a 2-m line; standard deviation in parentheses.

at the same location and for closely spaced (ca. 1-m) locations were 12–40%. Comparison of these rsd values indicates that the combined sampling and analysis process is less precise than the analytical procedure alone. There is a linear correlation between the rsd of chloroform and carbon tetrachloride measurements in these soil-gas samples, suggesting that precision is affected primarily by factors that affect the whole sample. Such factors would include leakage of sample from syringes between sampling and analysis.

The results of the study of the depth dependence of chloroform concentrations are listed in Table II. A comparison between chloroform concentrations and sampling depth produces a linear correlation coefficient of greater than 0.99. This result can provide useful information for planning sampling networks.

In summary, the soil-gas survey technique produced results that correlated with levels of groundwater contamination. Chloroform concentrations in soil gas at this site increase linearly with depth. Work is under way to develop additional sampling techniques and to evaluate the method at other sites and for other VOCs.

Acknowledgments

The assistance in this study of J. C. Curtis, L. J. Barrows, E. N. Amick, and J. A. Kohout of Lockheed EMSCO and of L. J. Blume (Soils Science) of the U.S. EPA Environmental Monitoring Systems Laboratory in Las Vegas, NV, is appreciated.

Registry No. $CHCl_3$, 67-66-3.

Literature Cited

(1) Horvitz, L. *Science (Washington, D.C.)* **1985**, *229(4716)*, 821–827.
(2) Kerfoot, H. B.; Barrows, L. J. *Soil Gas Measurement for Detection of Subsurface Organic Contamination*; U.S. EPA: Las Vegas, NV, 1986.
(3) Soil Conservation Service *Soil Survey of Las Vegas Valley Area, Nevada*; U.S. Department of Agriculture: Washington, DC, 1985.
(4) *Methods of Organic Chemical Analysis of Municipal and Industrial Wastewater*; Longbottom, J., Lichtenburg, J., Eds.; U.S. EPA: Cincinnati, OH, 1982.

Received for review April 17, 1986. Revised manuscript received March 31, 1987. Accepted July 10, 1987. Although the research described in this paper was funded by the U.S. Environmental Protection Agency under Contract 68-03-3249 to Lockheed Engineering and Management Services Co., Inc., it has not been subjected to Agency review. Therefore, it does not necessarily reflect the views of the Agency, and no official endorsement should be inferred. Mention of trade names or commercial products does not constitute endorsement or recommendation for use.

ONLY CARLO ERBA CAN MAKE IT THIS SIMPLE...

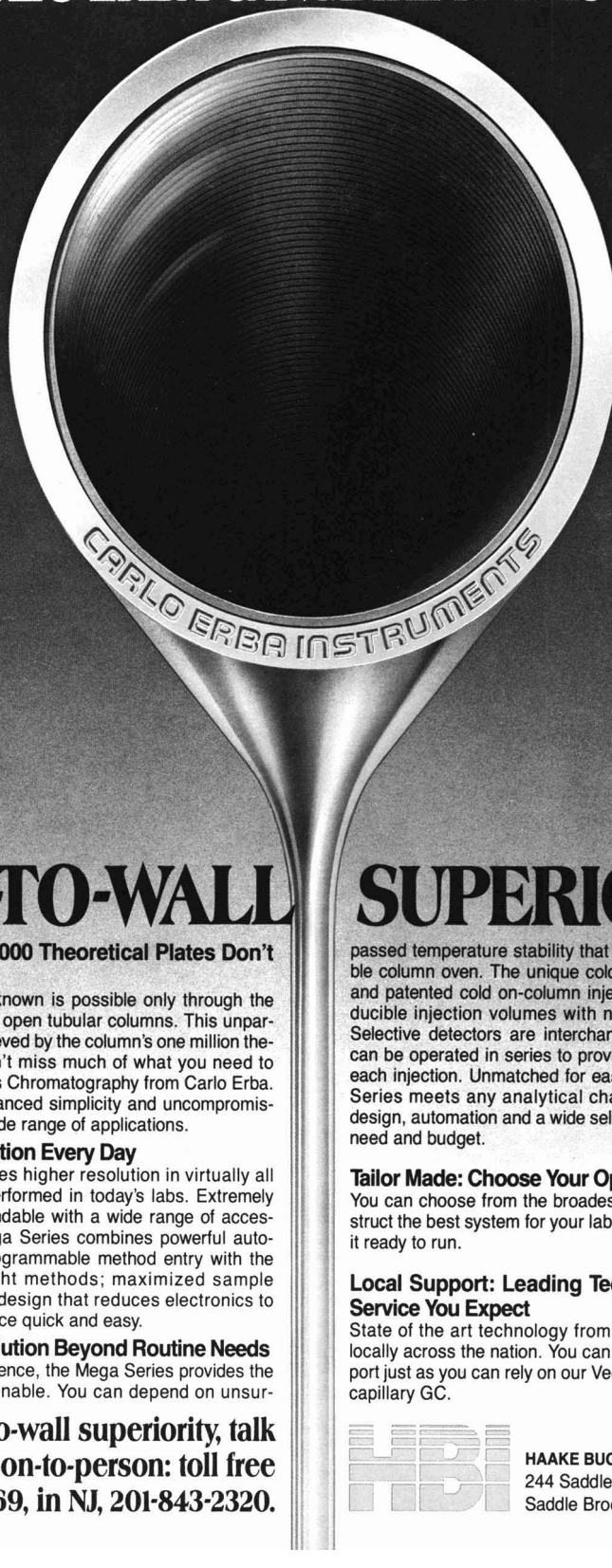

WALL-TO-WALL SUPERIORITY

Capillary GC: 1,000,000 Theoretical Plates Don't Miss Much

The highest resolution known is possible only through the utilization of wall-coated open tubular columns. This unparalleled resolution is achieved by the column's one million theoretical plates. You don't miss much of what you need to detect with capillary Gas Chromatography from Carlo Erba. You are assured of enhanced simplicity and uncompromising performance for a wide range of applications.

Vega: Higher Resolution Every Day

The Vega Series provides higher resolution in virtually all applications routinely performed in today's labs. Extremely compact, yet fully expandable with a wide range of accessories. Easy to use Vega Series combines powerful automation that includes programmable method entry with the capability to store eight methods; maximized sample throughput and unique design that reduces electronics to two boards making service quick and easy.

Mega: Highest Resolution Beyond Routine Needs

For true analytical excellence, the Mega Series provides the highest resolution obtainable. You can depend on unsurpassed temperature stability that results from our ultra stable column oven. The unique cold on-column auto sampler and patented cold on-column injector provide highly reproducible injection volumes with no sample discrimination. Selective detectors are interchangeable in seconds. They can be operated in series to provide more information from each injection. Unmatched for ease of operation, the Mega Series meets any analytical challenge through modular design, automation and a wide selection of options based on need and budget.

Tailor Made: Choose Your Options and Run

You can choose from the broadest range of options to construct the best system for your laboratory. And...you receive it ready to run.

Local Support: Leading Technology Backed by Service You Expect

State of the art technology from Carlo Erba is supported locally across the nation. You can rely on our technical support just as you can rely on our Vega and Mega—the best of capillary GC.

For wall-to-wall superiority, talk to us person-to-person: toll free 1-800-631-1369, in NJ, 201-843-2320.

HBI

HAAKE BUCHLER INSTRUMENTS, INC.
244 Saddle River Road
Saddle Brook, NJ 07662-6001

Get rid of the overtime in your waste treatment facility.

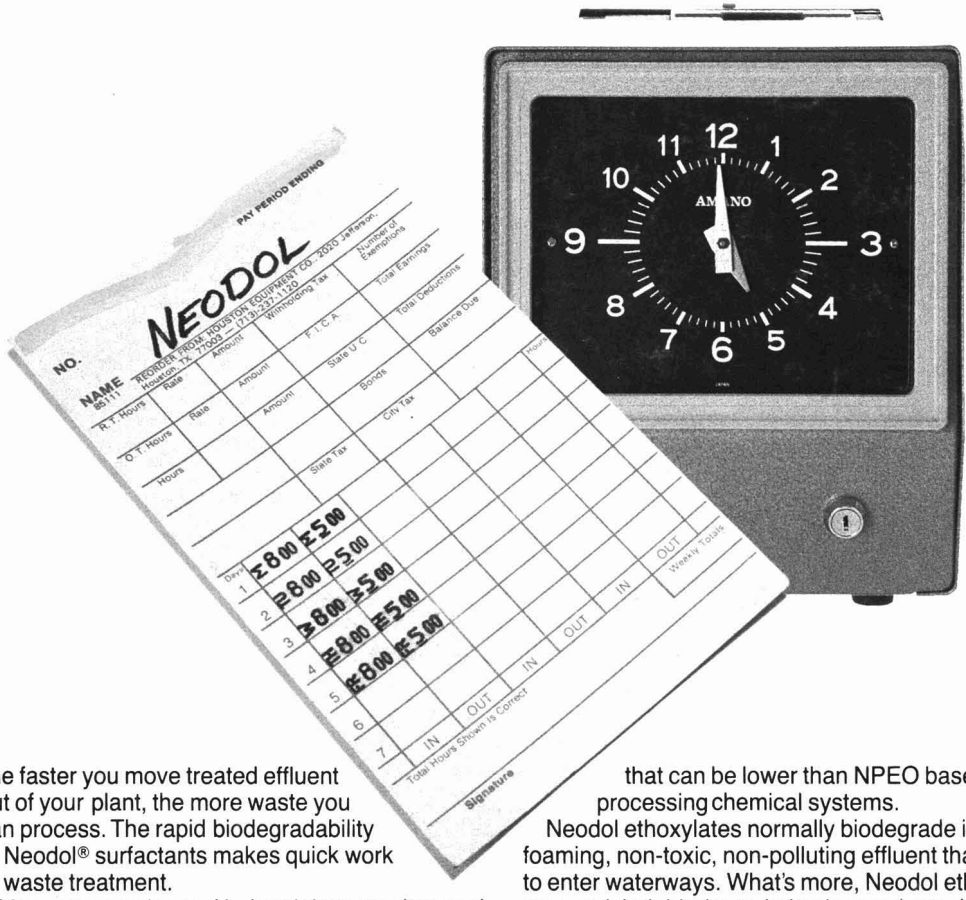

The faster you move treated effluent out of your plant, the more waste you can process. The rapid biodegradability of Neodol® surfactants makes quick work of waste treatment.

Many commonly used industrial processing products contain surfactants. Some surfactants, such as nonylphenol ethoxylates (NPEOs), biodegrade slowly. Their lengthy effluent processing time can limit a facility's treatment capacity and increase utility costs.

In contrast, processing products containing Neodol ethoxylates from Shell Chemical biodegrade much faster than those containing NPEOs, essentially increasing effluent treatment capacity without capital expenditures. And at a total processing cost that can be lower than NPEO based processing chemical systems.

Neodol ethoxylates normally biodegrade into non-foaming, non-toxic, non-polluting effluent that is safe to enter waterways. What's more, Neodol ethoxylates and their biodegradation by-products do not contain aromatic residues which react with chlorine in municipal treatment facilities to produce toxic, bioresistant compounds that can be harmful to aquatic life.

In waste treatment, time is more than money. It's also valuable treatment capacity. To find out more about time-saving, environmentally safe Neodol surfactants, write to: Shell Chemical Company, Manager Neodol Communications, P.O. Box 2463, One Shell Plaza, Houston, Texas 77252.

Shell Chemical Company